UNIVERSITÀ
DI PARMA

UNIVERSITÀ DEGLI STUDI DI PARMA

DOTTORATO DI RICERCA IN
"FISICA"

CICLO XXXII

ACCELERATED ADIABATIC QUANTUM CONTROL

Coordinatore:
Chiar.mo Prof. Stefano Carretta

Tutore:
Chiar.mo Prof. Sandro Wimberger

Dottorando: Francesco Petiziol

Anni 2016/2019

Francesco Petiziol

Accelerated adiabatic quantum control, © October 2019
Parma

ABSTRACT

The challenge to fully grasp and to harness the bizarre phenomena which take place in the quantum realm is crucially linked to the ability to engineer and manipulate quantum systems with high precision. The scientific progress in this direction is opening new routes for the investigation of fundamental quantum physics, and it is at the same time paving the way to the development of the first quantum technologies.

This thesis is dedicated to the search of strategies for high-fidelity and noise-tolerant quantum control. A versatile theoretical framework is set up for the design of optimized control protocols based on accelerated adiabatic processes. The benefits of the adiabatic dynamics, rooted in its intrinsic stability versus control imperfections, are released from the requirement of slow evolution: this is achieved thanks to the theoretical construction of accelerating control Hamiltonians which dynamically counteract deviations from the target dynamics. Our framework provides a methodical way to engineer these Hamiltonians by introducing fast modulations of the initially-available control parameters, and it results from the interplay between the theory of counterdiabatic fields and Floquet-Magnus average Hamiltonian theory. As compared to other shortcut-to-adiabaticity strategies, our control method keeps the system always close to the exact adiabatic path while not requiring the implementation of new Hamiltonian couplings. Moreover, the flexibility in the construction of the accelerating Hamiltonians offers a fertile ground for the hybridization with optimal control techniques.

The general setup is applied to exemplary control problems of relevance in quantum optics and quantum information processing. First, a protocol is designed for the generation of entanglement between effective two-level systems coupled through a transmission line, in the experimental context of circuit quantum electrodynamics. Second, an accelerated version of the widespread technique of stimulated Raman adiabatic passage is presented, which dramatically enlarges its range of applicability for implementations both in the optical and in the microwave regime.

The results strongly support the potential of the quantum control framework developed in this thesis. In particular, our methodology offers the opportunity to flank high fidelities and small error sensitivity with on-demand adaptability to experimental constraints and the flexibility for integrations with other control techniques. This makes it a valuable resource for applications in many branches of quantum science, with a natural outlet in quantum computation and simulation.

CONTENTS

ACRONYMS AND ABBREVIATIONS

AHT average Hamiltonian theory

BCD boundary cancellation driving

cd counterdiabatic

cd-STIRAP counterdiabatic STIRAP

cQED circuit quantum electrodynamics

ecd effective counterdiabatic

fmod frequency-modulated

fmod-STIRAP frequency-modulated STIRAP

fmod-fSTIRAP frequency-modulated fractional STIRAP

fSTIRAP fractional STIRAP

GKSL Gorini-Kossakowski-Sudarshan-Lindblad

LAD local adiabatic driving

LZMS Landau-Zener-Majorana-Stückelberg

RWA rotating wave approximation

STA shortcut(s) to adiabaticity

STIRAP stimulated Raman adiabatic passage

SQUID superconducting quantum interference device

TCQ tunable coupling qubit

tsl transitionless

1 INTRODUCTION

Despite almost one century has passed since the theory of quantum mechanics [116] was soundly established, the challenge to harness the unique features of the quantum domain and their potential technological implications are nowadays fueling a strong expansion of the research in quantum science. The counterintuitive behavior of quantum systems, as compared to the physics we are used to at human-size (energy) scales, has been longly promising the rise of a large-scale technological revolution. Indeed, genuinely quantum phenomena such as coherence or entanglement are expected to make possible, for instance, the implementation of new algorithms which would revolutionize modern computing [122, 128], high-precision sensors [47], simulators allowing to probe and predict the behavior of physical systems which are too complex to be efficiently simulated on classical computers [71]. The possibility to exploit this potential is ultimately bonded to the capability to actively manipulate quantum systems at will. In recent years, the great development of the experimental skills to engineer and control quantum systems has allowed to test in the laboratory quantum phenomena which were studied only theoretically before, and to construct the first quantum devices [128]. In the same days as this thesis is being written, the results of the first experiment claiming to have demonstrated quantum supremacy, i.e. the solution of a computational problem inaccessible to classical computers (with state-of-the-art algorithms and in a reasonable time), have been published [9]. Even though quantum computers are still arguably at a prototypical stage, other devices such as quantum sensors are already being exploited for cutting-edge applications [1]. Furthermore, great potential is foreseen in hybrid classical-quantum strategies, which are being also investigated quite intensively. For instance, the optimal calibration of quantum control tasks can benefit from hybrid feedback procedures: the simulation of the quantum dynamics is performed directly on a programmable quantum hardware, whose output data are rerouted to an optimization routine performed on a classical computer [55, 92, 179], which may also take advantage of machine learning techniques [151].

Time-dependent quantum control. With the increase of experimental capabilities, the call for new theoretical techniques for the design of efficient control protocols has flowed into the rapid growth of the theory of quantum control [41, 57]. This subject has attracted more and more attention from the scientific community, and has featured joint efforts from very diverse scientific backgrounds besides quantum physics, such as applied mathematics, electrical and systems engineering, and chemistry to name a few. Beyond its relevance for supporting the design of

experiments, quantum control theory is also providing new perspectives on the theory of quantum mechanics.

While reviewing the full branches of this field is a challenging task which goes beyond our scope here, it is possible to divide the different quantum control strategies into fairly general categories, which allow us to better frame the context of this thesis. A first distinction regards whether the physical processes which are exploited for control are coherent or incoherent, that is, if they can be fully described by unitary evolutions or if they involve non-unitary phenomena such as decay, measurements or thermalization. We will focus here strictly on the first case. Secondly, we will consider so-called open-loop control: this entails that the control procedure is calibrated once and for all upon preventive numerical simulations, before being operated on the system. An alternative is to use feedback strategies, in which the calibration is performed by updating, iteratively or "on-the-fly", the control parameters following test evolutions on the system.

Experimental progress has recently sparked much interest in the use of so-called pulse-shaping techniques, which aim at exploiting the ability to modulate the profile of the control fields in time. The possibility to engineer precise, smooth time-dependencies of the driving forces provides a further degree of freedom which can be used to develop optimized control strategies. This has, in turn, channeled much efforts in the study of the time evolution of systems with explicitly time-dependent Hamiltonians. The increase of complexity in solving the time-dependent Schrödinger equation for this kind of problems makes the prediction of the system's behavior a formidable task, which often requires the adoption of carefully selected approximation techniques [149]. A most widespread class of time-dependent control protocols is based on a phenomenon that can be understood under one of these approximations, and which was already described theoretically in the early development of quantum mechanics [21]. This is the so-called adiabatic theorem [2, 116, 137, 149].

Quantum adiabaticity. Let us consider a quantum system prepared in some eigenstate of the Hamiltonian. If one parameter λ in the Hamiltonian is varied in a continuous manner, for each of its values it is possible to diagonalize the "instantaneous" (or "snapshot") Hamiltonian $H(\lambda)$ and to obtain a new set of "instantaneous" eigenvectors. Unless the energy levels become degenerate for some value of the evolving parameter, for each initial eigenvector one can identify a continuous path in state space by joining the corresponding eigenvectors of the snapshot Hamiltonian for all values of λ. Loosely speaking, the adiabatic theorem states that, if the parameter variation occurs very slowly as compared to the characteristic timescales of the system, then the state of the system follows this path faithfully at all times. No excitations (or deexcitations) towards other (instantaneous) energy levels occur throughout the evolution. It is then immediate to formulate a control protocol based on this result [Figure 1.1]. Let us assume that the system is initially prepared in the eigenstate $|n(\lambda_i)\rangle$ of the Hamiltonian $H(\lambda_i)$ corresponding to the value λ_i of the control parameter. Let us further assume that the target state is

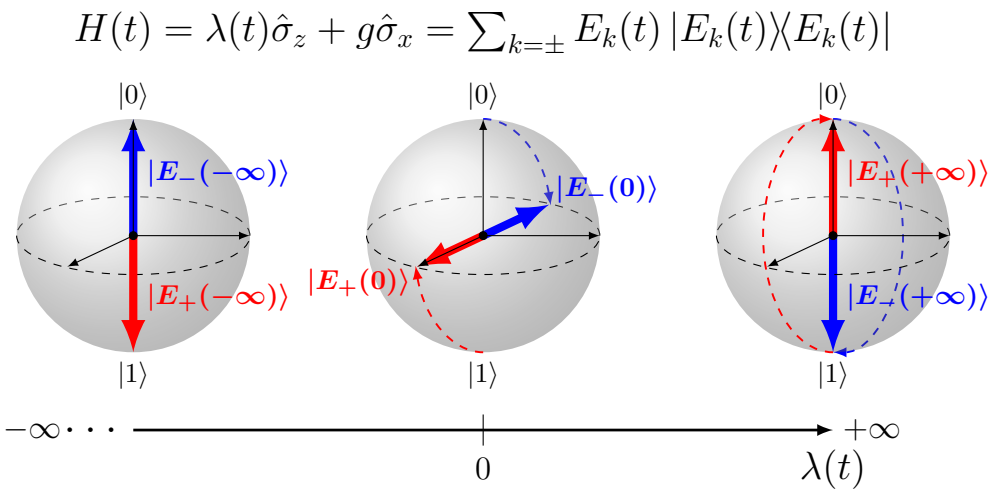

Figure 1.1: Bloch-sphere representation of the instantaneous eigenvectors of a driven two-level Hamiltonian. When the control parameter $\lambda(t) \to -\infty$, the eigenvectors of the two-state Hamiltonian $H(t) = \lambda(t)\hat{\sigma}_z + g\hat{\sigma}_x$, where $\hat{\sigma}_x$ and $\hat{\sigma}_z$ are the Pauli matrices, are eigenstates of $\hat{\sigma}_z$. The ground state coincides with state $|0\rangle$, while the excited state lies along $|1\rangle$. As the parameter is changed, reaching its zero value $\lambda(t) = 0$, the eigenvectors of $H(t)$ are those of $\hat{\sigma}_x$, i.e., the superpositions $(|0\rangle \pm |1\rangle)/\sqrt{2}$. Finally, when $\lambda(t) \to +\infty$, the instantaneous eigenstates are again eigenstates of $\hat{\sigma}_z$, but with exchanged eigenvalues as compared to the $-\infty$ case. An adiabatic variation of $\lambda(t)$ in this Hamiltonian, for the system prepared in the ground state at $\lambda(t) \to -\infty$ for instance, would then realize a population inversion between states $|0\rangle$ and $|1\rangle$.

the eigenstate $|n(\lambda_f)\rangle$ of the Hamiltonian $H(\lambda_f)$ corresponding to the value λ_f of the parameter. Then, by slowly varying $\lambda(t)$ from λ_i to λ_f, the adiabatic theorem guarantees that the system will reach the target state. Adiabatic drivings have the great advantage that they are by construction robust against imperfections in the implementation of the protocol (due to the absence of excitations). This model is at the base, or has contributed to the development, of many fields of research, such as the discovery of quantum geometric phases [14], adiabatic [2] and holonomic [175] quantum computation, quantum annealing [20], quantum critical dynamics [127] to name a few.

Despite the success and widespread diffusion of the adiabatic methods, the requirement of very slow evolutions is an extremely weak point for their use as control strategies. Indeed, time is, with very few exceptions, one the most precious resources for experiments in the quantum realm. This is especially due to the fact that every quantum system is inevitably affected, to some extent, by the interaction with the surrounding environment. The latter may induce decoherence, i.e. destruction of quantum superpositions, and dissipation, i.e. loss of energy, which impose a maximal lifetime within which the system exhibits quantum features or can be reliably manipulated. Moreover, the longer the time required for a single operation on the system, the more errors originating from uncontrollable sources accumulate. Even in the case in which these effects are not relevant at the

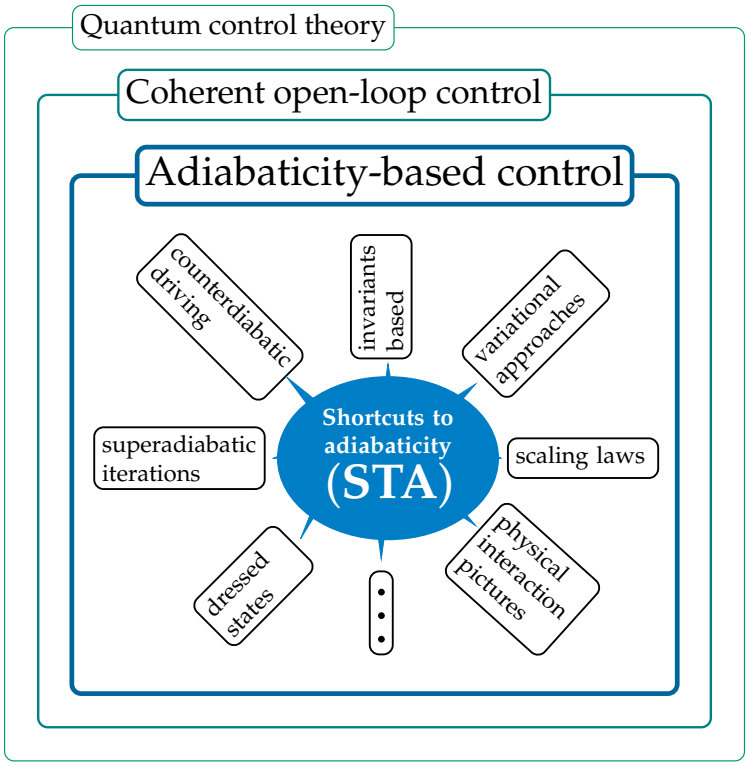

Figure 1.2: Field of research. Within the field of quantum control, we focus in this thesis on a set of coherent open-loop strategies, i.e., protocols for which control is achieved with a coherence-preserving process [57]. Moreover, these protocols do not adapt iteratively based on information acquired from the system, but realize "single-shot" state transfers calibrated on preventive simulations. Among the wide pool of methodologies in this area of research, we consider a class which is characterized by its connection with the concept of quantum adiabaticity, that is, of slowly driven evolutions. Going to further detail, we develop a theoretical framework for constructing accelerated adiabatic protocols, which can be framed within the field of shortcuts to adiabaticity [76].

single-operation level, one would like to be able to perform the largest possible number of operations on the system within the total available time window. This is essential, for instance, when a quantum algorithm is being implemented.

Shortcuts to adiabaticity. The attempt to maintain the characteristic benefits of adiabaticity whilst achieving fast operational times has opened an entire new field of research, now commonly known as "shortcuts to adiabaticity" (STA) [29, 76, 152]. A shortcut to adiabaticity is typically defined as a protocol which produces the same final conditions as those which would be given by an adiabatic variation of the control parameters, though in a shorter time [76]. For the purposes of the present thesis, we will also add the further characterization that shortcut methods do not rely on any form of adiabatic approximation. In other words, we distinguish shortcuts from "truly" adiabatic methods by the fact that the evolving system

state for the shortcuts is not, strictly speaking, an instantaneous eigenstate of the control Hamiltonian. This distinction implies that optimized adiabatic methods such as the local adiabatic and boundary cancellation drivings to be described in Section 2.2 fall into the class of adiabatic methods rather than shortcuts. Even though earlier work in this direction was already present in the literature [63, 154], the origin of the field is usually traced back to the works of Demirplak and Rice [48], and Berry [15], who independently pursued one common core idea. These authors developed a scheme, dubbed "counterdiabatic" (cd) [48] or "transitionless" driving [15] scheme, which, given an initial Hamiltonian $H(t)$, produces an exact tracking of the adiabatic states of $H(t)$ in arbitrarily short time. This is achieved by introducing a separate control Hamiltonian $H_{\mathrm{cd}}(t)$ which dynamically decouples those states. The growth and establishment of the STA field has then experienced a boost starting from 2010, when the term "shortcut to adiabaticity" was first introduced [34], and the first experimental verification of the cd framework was performed shortly afterwards [13]. Since then, many different STA frameworks have been developed theoretically, see [10, 27, 33, 34, 37, 46, 59, 82, 84, 113, 115, 124, 136, 143] for instance (see the reviews [29, 76, 152] for a more complete list), and a number of them has been realized in experiments, in a variety of platforms including superconducting circuits [104, 157, 169], trapped ions [5], colour centers [93, 174, 177], micromechanical oscillators [103, 114] and cold atoms [13, 58, 139]. They have been also applied in the context of quantum critical dynamics [30, 31], and quantum thermodynamics [28, 32]. As it is pointed out in Ref. [76], the strength of STA resides in the wide pool of methodologies which they offer to address one problem. This gives the opportunity to choose the best strategy for a given specific context.

The Hamiltonian $H_{\mathrm{cd}}(t)$, though guaranteeing perfect adiabatic tracking, turns out to be a tricky object. First, even if an explicit algorithm exists to determine it, this requires the full spectral properties of the original Hamiltonian $H(t)$, i.e. eigenvalues and eigenvectors, for all values of time. Although this is not a limitation for few-level quantum systems, or in cases in which information on a small subset of the spectrum is sufficient within the relevant dynamics, it becomes prohibitive in a many-body scenario. Second, and more importantly, it typically involves time-dependent control of matrix elements which are not within the set of initially accessible interactions, i.e., of the control parameters in the original $H(t)$. This feature makes the scheme hard to be implemented experimentally for most problems, even for few-level systems. Many STA are variants and extensions of the counterdiabatic scheme which try to circumvent either of these two difficulties. A general theme in these strategies is to find interaction-picture frames where the control Hamiltonian has entirely realizable components. If this is possible, then one can interpret the interaction picture as a new lab-frame physical process, and realize the latter rather than the counterdiabatic driving [10, 50, 82]. As a result, under suitable conditions on the boundary properties of the rotating-frame transformations, the system will match the initial and final state of the true adiabatic evolution, while deviating from the adiabatic path at intermediate times. In other words, the speed

up is achieved by allowing transitions during the evolution, provided initial and final states still match the desired ones.

These methods typically permit to realize arbitrarily-fast state transfers, in principle, but the initial concept of adiabaticity, i.e. the system being in an instantaneous eigenstate of the driven Hamiltonian, is lost. Hence, although the problem of time economy is solved, this might be at the price of losing stability against potential protocol errors. Moreover, in the laboratory, experimental constraints are typically present on the strength of the control Hamiltonian which can be implemented. These set a lower bound to the minimum timescale over which the total pulse area necessary for attaining a given state transfer can be reached, a problem also related to the concept of quantum speed limits [45]. These are bounds on the minimal time (or rate) over which a system is able to evolve. Given that one cannot accelerate the adiabatic process at very fast timescales, one may wonder if some degree of adiabaticity, and the related robustness, can be still exploited before resorting to fully-nonadiabatic shortcuts.

In this thesis. The work presented in this thesis attempts to complement the STA field with a method which, in a way, represents a smooth link between truly adiabatic methods and more traditional STA. More precisely, we introduce a framework for constructing a class of shortcuts which, on the one hand, do not demand the implementation of new controlled Hamiltonian couplings. On the other, it still produces a dynamics which approximates the adiabatic evolution closely at all times. By varying the total timescale of the evolution, for fixed shape of the drivings, it is possible to move smoothly from a quasi-adiabatic regime, in which the shortcut acts as a weak correction to the original Hamiltonian $H(t)$, to a fully fast-forward regime in which the shortcut is the dominant part of the system Hamiltonian. Besides, the latter case constitutes an efficient method also if $H(t)$ is completely absent. Therefore, depending on the available time resources in a hypothetical experiment, one can straightforwardly adapt the protocol for achieving the desired precision in the given time.

The fundamental idea behind our framework is that of using rapid modulations in the control parameters. When averaging over the fast timescale, these modulations produce effective time-dependent Hamiltonians that are forced to match the counterdiabatic Hamiltonian $H_{\mathrm{cd}}(t)$. For this reason, the method will be dubbed "effective counterdiabatic driving". By first studying the matrix structure of $H_{\mathrm{cd}}(t)$, it is shown by control-theoretic arguments that, for finite-dimensional systems, it is always possible to construct realizable shortcuts which approximate the dynamics generated by $H_{\mathrm{cd}}(t)$. The procedure for designing explicitly the shortcuts is based on the use of the Floquet-Magnus average Hamiltonian theory [23, 25, 74]. This is typically used to engineer synthetic Hamiltonians via fast periodic driving. Although the construction can be operated following a systematic procedure, the methodology maintains a large degree of flexibility, which allows one to tailor the protocol over the specific problem at hand.

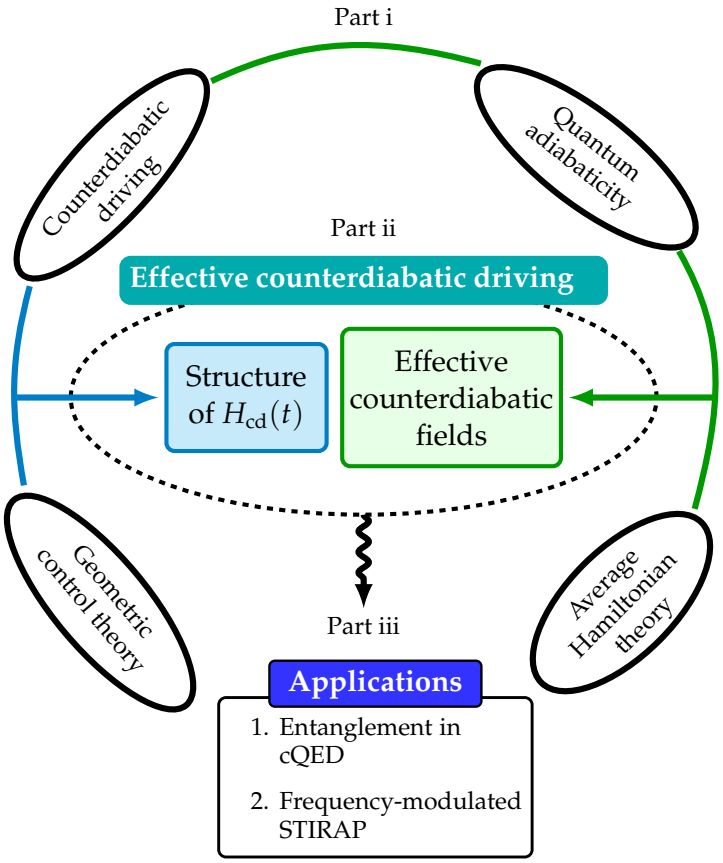

Figure 1.3: Map of the thesis. In Part i, we will introduce the concept of quantum adiabaticity, and the shortcut-to-adiabaticity method known as counterdiabatic driving. The latter will be then combined with geometric control theory in the order to assess general properties of the counterdiabatic Hamiltonian $H_{cd}(t)$ (—). After introducing average Hamiltonian theory, we will integrate such a tool with the theory of adiabaticity (—) for engineering effective counterdiabatic Hamiltonians which induce accelerated adiabatic evolution without requiring the implementation of new Hamiltonian couplings. This general theory, denoted as "effective counterdiabatic driving", will then be applied to real quantum control problems in Part ii.

Once the general theory is established, we discuss in detail two potential applications. Our strategy is used to find efficient shortcuts in problems which, we believe, may be of interest in various experimental setups. The first application concerns the construction of a protocol for entangling two qubits in the context of circuit quantum electrodynamics (cQED) [16, 75, 172]. The specific experimental setup which we consider is that of two superconducting qubits which are dispersively coupled to a waveguide and which interact thanks to the exchange of virtual photons through the waveguide. As a first step, an adiabatic sweep is designed such that the adiabatic path connects the initial separable states $|\uparrow\downarrow\rangle$ and $|\downarrow\uparrow\rangle$ of the two qubits with the final entangled states $(|\uparrow\downarrow\rangle \pm |\downarrow\uparrow\rangle)/\sqrt{2}$. In this context, we compare the performance of a variety of optimized adiabatic sweeps. Subsequently, these sweeps are accelerated and assisted through the addition of

an effective counterdiabatic Hamiltonian, which is implemented by making the qubit-cavity coupling to oscillate fast. As a result, high fidelities are achieved in competing timescales while maintaining stability against protocol imperfections and environmental noise.

The second application is the construction of an accelerated version of the widespread STImulated Raman Adiabatic Passage (STIRAP) technique [165]. The latter produces population transfers between two states of a three-level system which cannot be coupled by a direct transition, by coupling them to a common —often lossy— intermediate state via laser pulses. If the pulse sequence satisfies suitable criteria, the state transfer is achieved by tracking an adiabatic state which evolves only in the space spanned by the initial and target state. For this problem, the effective counterdiabatic field can be realized simply by introducing corrections to the main laser pulses on symmetric frequency sidebands, and it greatly enlarges the parameter space in which STIRAP returns large protocol fidelities. The shortcut is efficient also in the presence of dissipation and decoherence phenomena, both considering experimental implementations in the optical regime, namely a Rydberg excitation, and in the microwave regime, namely a superconducting circuit.

The structure of the thesis is as follows (Figure 1.3). In the Background part, Part i, the fundamental concepts of quantum adiabaticity are described (Chapter 2) and the foundations of average Hamiltonian theory are introduced (Chapter 3). Then, the general theory underpinning our STA framework is developed in Part ii, Chapter 4, where basic examples are also discussed. Part iii is dedicated to applications of the method in two contexts, namely the construction of the protocol entangling two qubits in cQED (Chapter 5) and of frequency-modulated STIRAP (Chapter 6). Each Chapter contains a final Section "Discussion" where an outlook regarding its specific contents is presented. In the final Chapter "Conclusion and perspectives", 7, we discuss ideas for future developments of the whole framework presented in this thesis. These will focus principally on possible extensions of our methodologies to the field of open quantum systems [22], but also on the use of quantum control techniques for testing and improving quantum simulation algorithms, a field which is attracting much interest in recent times (in this direction, see, e.g., Ref.s [77, 79, 89, 106, 107]).

Part I

BACKGROUND

2 QUANTUM ADIABATICITY

The concept of quantum adiabaticity is the central starting point of the work presented in this thesis. Its essence is contained in a result dubbed the "adiabatic" theorem of quantum mechanics [116], whose core concept can be summarized as follows. Let us considers a system being in an eigenstate of the initial Hamiltonian. If some microscopic parameter is modified continuously in time in a very slow manner, then the system is expected to remain at all times close to the corresponding instantaneous eigenvector of the time-dependent Hamiltonian. Starting from the seminal work of Berry on the geometric phase [14], it was recognized that adiabaticity is intimately related to geometric aspects of the state space of a quantum system [120], and hence it is nowadays often presented with emphasis on a geometric angle. We will follow this approach, to some extent, introducing the concept of adiabatic gauge potential [94], in Sec. 2.1. We will then overview a derivation of an adiabatic theorem in Sec. 2.1.2. This gives us the opportunity to introduce in a natural way many of the quantities which play a central role in this thesis, such as global and local adiabatic approximations and boundary cancellation methods (Sec. 2.2). The final goal of this Chapter is to present the counterdiabatic driving scheme [15, 48], i.e., a shortcut-to-adiabaticity methodology which produces exact adiabatic dynamics arbitrarily fast, in principle, by a 100% compensation of nonadiabatic effects.

2.1 ADIABATIC APPROXIMATION

2.1.1 Adiabatic gauge potential

A quantum system featuring some internal parameter $\lambda(t)$ which changes in time can be described by a Hamiltonian $H[\lambda(t)]$ which is explicitly time-dependent. One such system may be, for instance, a spin coupled to time-varying magnetic fields. Let us assume that the Hilbert space $\mathbb{H}$ of the system has dimension N. For each value of $\lambda(t)$, the so-called snapshot Hamiltonian $H(\lambda)$ can be instantaneously diagonalized leading to the spectral decomposition

$$H(\lambda) = \sum_{n=0}^{N-1} E_n(\lambda) \, |n_\lambda\rangle\langle n_\lambda| \, , \tag{2.1}$$

where $\{E_n(\lambda)\}_{n=0,\dots,N-1}$ are the instantaneous eigenenergies, which we assume to be never degenerate for any value of λ, while $\{|n_\lambda\rangle\}_{n=0,\dots,N-1}$ are the instantaneous eigenvectors, satisfying the eigenvalue equation

$$H(\lambda)\,|n_\lambda\rangle = E_n(\lambda)\,|n_\lambda\rangle\,. \tag{2.2}$$

The evolution in time of the quantum system is fully determined by the time-dependent Schrödinger equation. In terms of the evolution operator $U(\lambda)$, and by changing variable from t to $\lambda(t)$, this reads

$$i\hbar\frac{\partial U(\lambda)}{\partial\lambda} = \frac{1}{\dot\lambda}H(\lambda)U(\lambda), \qquad U(0)=\mathbb{1}, \tag{2.3}$$

where the dot denotes the time derivative, $\dot\lambda = \partial\lambda/\partial t$. We will not assume, for now, any specific time dependence for the parameter $\lambda(t)$ and, without loss of generality, we take it to vary in the interval $\lambda(t)\in[0,1]$. In many treatments of adiabaticity though, $\lambda(t)$ is chosen to represent a measure of the actual physical time t in units of a relevant global timescale of the evolution t_f, accordingly to $\lambda = (t-t_i)/t_f$, where t_i is the initial time. This may be a useful reference example for the reader, and we will resort to it often in the next Chapters.

Adiabaticity deals with studying the behavior of equation (2.3) in the asymptotic limit of slow driving, "$\dot\lambda\to 0$". For doing so, it is convenient to look at the system from a very specific "comoving" frame. This is defined, for each value of λ, by the basis of instantaneous eigenvectors $\{|n_\lambda\rangle\}$. The transformation which brings the initial "fixed" basis $|n_0\rangle$ to the comoving basis $|n_\lambda\rangle = U_\lambda\,|n_0\rangle$ is described by the unitary operator U_λ, reading

$$U_\lambda = \sum_{n=0}^{N-1}|n_\lambda\rangle\langle n_0|\,. \tag{2.4}$$

Like for all unitary transformations, it is possible to identify its corresponding generator. This is defined by

$$\mathcal{A}_\lambda = i\hbar\frac{\partial U_\lambda}{\partial\lambda}U_\lambda^\dagger. \tag{2.5}$$

This will be a most important quantity for all the following treatment, and it goes under the name of *adiabatic gauge potential* [94]. The nomenclature "gauge potential" is typically referred to generators of continuous translations in parameter space. Inserting equation (2.4) into (2.5), one finds that $\mathcal{A}_\lambda$ acts as the λ-derivative operator

$$\mathcal{A}_\lambda = i\hbar\sum_{n=0}^{N-1}|\partial_\lambda n_\lambda\rangle\,\langle n_\lambda| = i\hbar\partial_\lambda, \tag{2.6}$$

consistently with the fact that $\mathcal{A}_\lambda$ generates displacements associated with a variation of λ. Indeed, a small variation of λ induces a variation of the instantaneous eigenvectors as $|n_{\lambda+d\lambda}\rangle \simeq |n_\lambda\rangle - \frac{i}{\hbar}\mathcal{A}_\lambda\,|n_\lambda\rangle$. This can be better seen by taking the derivative of the diagonalization equation

$$U_\lambda^\dagger H(\lambda)U_\lambda = H_d(\lambda), \tag{2.7}$$

where $H_d(\lambda)$ is the diagonal matrix (in the initial $\lambda = 0$ basis)

$$H_d(\lambda) = \sum_{n=0}^{N-1} E_n(\lambda) \, |n_0\rangle\langle n_0| \, . \tag{2.8}$$

This way, after a few manipulations, one finds the relation [84]

$$\frac{\partial H(\lambda)}{\partial \lambda} = \frac{i}{\hbar}[H(\lambda), \mathcal{A}_\lambda] + \partial H_d(\lambda), \tag{2.9}$$

where $\partial H_d(\lambda) = U_\lambda H_d(\lambda) U_\lambda^\dagger$ is a diagonal matrix in the basis of instantaneous eigenvectors whose eigenvalues are the "generalized forces" [94] $\partial E_n(\lambda)/\partial\lambda$,

$$\partial H_d(\lambda) = \sum_{n=0}^{N-1} \frac{\partial E_n(\lambda)}{\partial \lambda} \, |n_\lambda\rangle\langle n_\lambda| \, . \tag{2.10}$$

equation (2.9) highlights the fact that a variation of $H(\lambda)$ resulting from changing λ is governed by two components: the variation of instantaneous eigenvalues, with the eigenbasis fixed, is generated by $\partial H_d(\lambda)$, while the variation of instantaneous eigenvectors is determined by $i[H(\lambda), \mathcal{A}_\lambda]/\hbar$, i.e., by the adiabatic gauge potential. Indeed, $\partial H_d(\lambda)$ commutes with $H(\lambda)$. By further taking, in equation (2.9), the commutator with $H(\lambda)$ on both sides, one obtains the relation

$$[H(\lambda), \partial_\lambda H(\lambda)] = \frac{i}{\hbar} \, [H(\lambda), [H(\lambda), \mathcal{A}_\lambda]] \, . \tag{2.11}$$

This expression can be used to formulate variational principles which allow one to derivate approximate adiabatic gauge potentials [94], and they are a particularly precious tool when the exact diagonalization of the Hamiltonian is hard. An explicit recipe for computing the adiabatic gauge potential $\mathcal{A}_\lambda$ starting from the system Hamiltonian can be obtained by first taking the derivative with respect to $\lambda$of the eigenvalue equation (2.2). After a few manipulations, and assuming that no degeneracies among the instantaneous levels occur at any time, one finds that

$$\langle m_\lambda | \partial_\lambda n_\lambda \rangle = \frac{\langle m_\lambda | \, \partial_\lambda H(\lambda) \, | n_\lambda \rangle}{E_n(\lambda) - E_m(\lambda)}, \tag{2.12}$$

if $n \neq m$. Combining with equation (2.6), we obtain the desired connection with $H(\lambda)$, namely

$$\mathcal{A}_\lambda = i\hbar \sum_n \langle n | \partial_\lambda n_\lambda \rangle \, |n_\lambda\rangle \, \langle n_\lambda| + i\hbar \sum_{n \neq m} |m_\lambda\rangle \, \frac{\langle m_\lambda | \, \partial_\lambda H(\lambda) \, | n_\lambda \rangle}{E_n(\lambda) - E_m(\lambda)} \, \langle n_\lambda| \, . \tag{2.13}$$

In the next section we will see that the adiabatic gauge potential is a core quantity in the context of quantum adiabaticity.

2.1.2 Adiabatic theorem

By moving to the frame defined by U_λ according to $U(\lambda) = U_\lambda U_1(\lambda)$, the Schrödinger equation (2.3) becomes

$$\begin{aligned} i\hbar\frac{\partial U_1(\lambda)}{\partial\lambda} &= U_\lambda^\dagger\left[\frac{1}{\dot\lambda}H(\lambda) - \mathcal{A}_\lambda\right]U_\lambda U_1(\lambda) \\ &= \left[\frac{\overline{H}(\lambda)}{\dot\lambda} - \bar{\mathcal{A}}_\lambda\right]U_1(\lambda), \end{aligned} \tag{2.14}$$

where we have used the unitarity of U_λ, i.e.,

$$U_\lambda^\dagger U_\lambda = U_\lambda U_\lambda^\dagger = \mathbb{1} \quad \Rightarrow \quad \frac{\partial U_\lambda^\dagger}{\partial\lambda}U_\lambda + U_\lambda^\dagger\frac{\partial U_\lambda}{\partial\lambda} = 0, \tag{2.15}$$

and we have indicated with a bar the rotating-frame quantities

$$\overline{H}(\lambda) = U_\lambda^\dagger H(\lambda)U_\lambda; \qquad \bar{\mathcal{A}}_\lambda = U_\lambda^\dagger\mathcal{A}_\lambda U_\lambda. \tag{2.16}$$

The term $\overline{H}(\lambda)$ is, by definition of U_λ, diagonal,

$$\overline{H}(\lambda) = H_d(\lambda). \tag{2.17}$$

The term $\bar{\mathcal{A}}_\lambda$ is a "centrifugal" term instead arising from the fact that we are looking at the dynamics from a moving frame.

The diagonal term $\overline{H}(\lambda)$ generates the *dynamical phase factors*, i.e., it provides each instantaneous eigenvector with a phase depending on the time-integral and the corresponding eigenenergy,

$$|n_\lambda\rangle \longrightarrow e^{-\frac{i}{\hbar}\int_{t_0}^t E_n(t')dt'}|n_\lambda\rangle\,. \tag{2.18}$$

In order to proceed in the derivation of an adiabatic theorem, it is convenient to adsorb these factors into the basis frame by means of a further transformation $U_1(\lambda) = U_d(\lambda)U_2(\lambda)$ with

$$U_d(\lambda) = \exp\left(-\frac{i}{\hbar}\int_0^\lambda\frac{\overline{H}(\lambda_1)}{\partial_t\lambda_1}d\lambda_1\right), \tag{2.19}$$

$$= \sum_{n=0}^{N-1}\exp\left(-\frac{i}{\hbar}\int_0^\lambda E_n(\lambda_1)\dot\lambda_1^{-1}d\lambda_1\right)|n_0\rangle\langle n_0|\,. \tag{2.20}$$

As a result, using also equations (2.20), equation (2.14) becomes

$$i\hbar\frac{\partial U_2(\lambda)}{\partial\lambda} = -\sum_{n,m=0}^{N-1}e^{i\omega_{nm}(\lambda)}\mathcal{A}_\lambda^{(n,m)}|n_0\rangle\langle m_0|\,U_2(\lambda), \tag{2.21}$$

where we have introduced the integrated transition frequencies

$$\omega_{nm}(\lambda) = \frac{1}{\hbar}\int_0^\lambda[E_n(\lambda_1) - E_m(\lambda_1)]\partial_t\lambda_1^{-1}d\lambda_1 \tag{2.22}$$

and the matrix elements of the adiabatic gauge potential in the basis of instantaneous eigenvectors,

$$\mathcal{A}_\lambda^{(n,m)} = \langle n_\lambda | \mathcal{A}_\lambda | m_\lambda \rangle ; \qquad \mathcal{A}_\lambda^{(n)} = \langle n_\lambda | \mathcal{A}_\lambda | n_\lambda \rangle , \tag{2.23}$$

which can be computed from (2.13). From a first inspection of the r.h.s. of equation (2.21), we see that, when $n \neq m$ and assuming that the eigenenergies $E_n(\lambda)$ and $E_m(\lambda)$ are distinct for all λ, the matrix elements are multiplied by phase factors which oscillate quickly if $\dot{\lambda} \ll 1$ for all times. Therefore, we can anticipate that, once integrated, one expects these terms to average out. This is not the case though for the diagonal elements, which are fully determined by the gauge potential $\mathcal{A}_\lambda$, since $\omega_{nn} = 0$. As for the case of the dynamical phases, we adsorb these elements into the basis frame with the transformation $[U_2(\lambda) = U_g(\lambda) U_3(\lambda)]$

$$U_g(\lambda) = \sum_{n=0}^{N-1} e^{i \int_0^\lambda \mathcal{A}_{\lambda'}^{(n)} d\lambda'} |n_\lambda\rangle\langle n_\lambda| . \tag{2.24}$$

The new basis vectors are then

$$|\psi_n(\lambda)\rangle = e^{i \int_0^\lambda \mathcal{A}_{\lambda'}^{(n)} d\lambda' - \frac{i}{\hbar} \int_0^\lambda E_n(\lambda')(\dot{\lambda}')^{-1} d\lambda'} |n_\lambda\rangle . \tag{2.25}$$

The transformation (2.24) leads to the Schrödinger equation

$$i\hbar \frac{\partial U_3(\lambda)}{\partial \lambda} = - \sum_{n \neq m} e^{i\omega_{nm}(\lambda) - i\gamma_{nm}(\lambda)} \mathcal{A}_\lambda^{(n,m)} |n_0\rangle\langle m_0| U_3(\lambda). \tag{2.26}$$

We have introduced the notation

$$\gamma_{nm}(\lambda) = \int_0^\lambda [\mathcal{A}_{\lambda'}^{(n)} - \mathcal{A}_{\lambda'}^{(m)}] d\lambda'. \tag{2.27}$$

We can now formally integrate equation (2.26) over the full variation of the parameter $\lambda(t) \in [0,1]$, given the initial condition $U_3(0) = \mathbb{1}$,

$$U_3(1) - \mathbb{1} = \frac{i}{\hbar} \sum_{n \neq m} |n_0\rangle\langle m_0| \int_0^1 e^{i\omega_{nm}(\lambda)} \mathcal{A}_\lambda^{(n,m)} U_3(\lambda) d\lambda. \tag{2.28}$$

Then, by considering the operator norm of the l.h.s., defined as

$$\|X\| = \sup\{\|X|\psi\rangle\| \, : \, |\psi\rangle \in \mathbb{H} \text{ and } \||\psi\rangle\| = 1\}, \tag{2.29}$$

we have that

$$\|U_3(1) - \mathbb{1}\| \leq \frac{1}{\hbar} \sum_{n \neq m} \left\| \int_0^1 e^{i\omega_{nm}(\lambda)} \mathcal{A}_\lambda^{(n,m)} U_3(\lambda) d\lambda \right\| . \tag{2.30}$$

Let us consider the integral in equation (2.28). Assuming that the energy levels never cross, we can rewrite

$$e^{i\omega_{nm}(\lambda)} = \frac{1}{i\partial_\lambda \omega_{nm}(\lambda)} \frac{\partial}{\partial\lambda} e^{i\omega_{nm}(\lambda)}, \tag{2.31a}$$

$$= \frac{-i\dot{\lambda}}{E_{nm}(\lambda)} \frac{\partial}{\partial\lambda} e^{i\omega_{nm}(\lambda)}, \tag{2.31b}$$

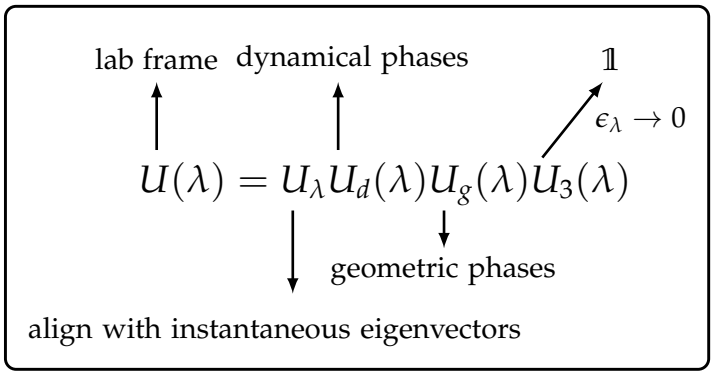

Figure 2.1: Sequence of convenient rotating-frame transformations in the derivation of the adiabatic theorem.

where we have used equation (2.22) and we have introduced the notation $E_{nm}(\lambda) = E_n(\lambda) - E_m(\lambda)$. Then, we can integrate by parts, obtaining

$$\int_0^1 e^{i\omega_{nm}(\lambda)} \mathcal{A}_\lambda^{(n,m)} U_3(\lambda) d\lambda = \left[\frac{-i\dot{\lambda} e^{i\omega_{nm}(\lambda)}}{E_n(\lambda) - E_m(\lambda)} e^{-i\gamma_{nm}(\lambda)} \mathcal{A}_\lambda^{(n,m)} U_3(\lambda) \right]_0^1 - \int_0^1 e^{i\omega_{nm}(\lambda)} \frac{\partial}{\partial\lambda} \left[\frac{\dot{\lambda} e^{-i\gamma_{nm}(\lambda)}}{iE_{nm}(\lambda)} \mathcal{A}_\lambda^{(n,m)} U_3(\lambda) \right] d\lambda. \quad (2.32)$$

Now, let us assume that $|d\lambda(t)/dt|$ is bounded by a small constant ϵ_λ for all times. Then we have

$$\left\| \int_0^1 e^{i\omega_{nm}(\lambda)} \mathcal{A}_\lambda^{(n,m)} U_3(\lambda) d\lambda \right\| \leq \epsilon_\lambda \left[\frac{|\mathcal{A}_0^{(n,m)}|}{|E_n(0) - E_m(0)|} + \frac{|\mathcal{A}_1^{(n,m)}|}{|E_n(1) - E_m(1)|} \right] + \epsilon_\lambda \left\| \int_0^1 e^{i\omega_{nm}(\lambda)} \frac{\partial}{\partial\lambda} \left[\frac{e^{-i\gamma_{nm}(\lambda)}}{iE_{nm}(\lambda)} \mathcal{A}_\lambda^{(n,m)} U_3(\lambda) \right] d\lambda \right\|. \quad (2.33)$$

Let us insert equation (2.33) into equation (2.30), and let us recall that the lab-frame propagator $U(\lambda)$ is related to $U_3(\lambda)$ by $U(\lambda) = U_\lambda U_d(\lambda) U_g(\lambda) U_3(\lambda)$ (this is summarized in Figure 2.1). By reverting the rotating-frame transformations U_λ, U_g and U_d, we have obtained the following version of the adiabatic theorem.

Theorem 1. (Adiabatic theorem) *Given a N-dimensional quantum system driven by a control parameter $\lambda(t)$ with Hamiltonian $H[\lambda(t)] = \sum_{n=0}^{N-1} E_n(\lambda) |n_\lambda\rangle\langle n_\lambda|$, if the instantaneous eigenvalues $E_n(\lambda)$ never cross for any value of λ and if $|d\lambda/dt| \leq \epsilon_\lambda$ for all times t, then the propagator satisfies*

$$U(\lambda) = \sum_{n=0}^{N-1} e^{-\frac{i}{\hbar}\int_0^\lambda d\lambda' E_n(\lambda')(\dot{\lambda}')^{-1} - \int_0^\lambda \langle n_{\lambda'} | \partial_{\lambda'} n_{\lambda'} \rangle d\lambda'} |n_\lambda\rangle\langle n_0| + O(\epsilon_\lambda). \quad (2.34)$$

Therefore, in the adiabatic limit the system instantaneously follows the states $|\psi_n(\lambda)\rangle$ of equation (2.25), which are thus called *adiabatic states*. The transformation (2.34) (negleting the $O(\epsilon_\lambda)$ term) is called *adiabatic transformation* instead. The phases

$$e^{i\int_0^\lambda \mathcal{A}_{\lambda'}^{(n)} d\lambda'} = e^{-\int_0^\lambda \langle n_{\lambda'}|\partial_{\lambda'} n_{\lambda'}\rangle d\lambda'} \tag{2.35}$$

are the so-called *geometric* (or *Berry*) *phases* [6, 14, 38]. Note that, when one incorporates these phases into the eigenvectors, by redefining

$$|n'_\lambda\rangle = e^{-\int_0^\lambda \langle n_{\lambda'}|\partial_{\lambda'} n_{\lambda'}\rangle d\lambda'} |n_\lambda\rangle , \tag{2.36}$$

then by taking the derivative with respect to λ, and projecting over $\langle n'_\lambda|$, we obtain

$$\langle n'_\lambda|\partial_\lambda n'_\lambda\rangle = 0. \tag{2.37}$$

Hence, the choice of phases (2.35) implies that the variation of eigenvector produced by a variation of the parameter λ is orthogonal to the eigenvector itself. Since this is the condition which defines parallel transport along a curve in a curved space [120], this choice of phases is known as *parallel transport gauge*. We now slightly refine equation (2.32) in order to obtain quantitative conditions for adiabaticity. Proceeding in the same way as in equation (2.32), integrating by parts the remain integral in the same manner, we find

$$\begin{aligned}
&\left[\frac{-i\dot\lambda e^{i\omega_{nm}(\lambda)}}{E_n(\lambda)-E_m(\lambda)} e^{-i\gamma_{nm}(\lambda)} \mathcal{A}_\lambda^{(n,m)} U(\lambda)\right]_0^1 \\
&- \left[\frac{\dot\lambda e^{i\omega_{nm}(\lambda)}}{E_{nm}(\lambda)} \frac{\partial}{\partial\lambda}\left(\frac{\dot\lambda e^{-i\gamma_{nm}(\lambda)}}{E_{nm}(\lambda)} \mathcal{A}_\lambda^{(n,m)} U(\lambda)\right)\right]_0^1 \\
&\qquad + \int_0^1 e^{i\omega_{nm}(\lambda)} \frac{\partial}{\partial\lambda}\left[\frac{\dot\lambda}{iE_{nm}(\lambda)} \frac{\partial}{\partial\lambda}\left(\frac{\dot\lambda e^{-i\gamma_{nm}(\lambda)}}{iE_{nm}(\lambda')} \mathcal{A}_\lambda^{(n,m)} U(\lambda)\right)\right] d\lambda.
\end{aligned} \tag{2.38}$$

Therefore, the leading ϵ_λ-order term is given only by the first term in (2.32). The norm of such term is

$$\left|\left[\frac{d\lambda}{dt}\right]_{\lambda=0}\right| \frac{|\mathcal{A}_0^{(n,m)}|}{|E_n(0)-E_m(0)|} + \left|\left[\frac{d\lambda}{dt}\right]_{\lambda=1}\right| \frac{|\mathcal{A}_1^{(n,m)}|}{|E_n(1)-E_m(1)|}. \tag{2.39}$$

Hence, deviations from adiabaticity are determined to the leading order by two quantities, namely the (matrix elements of the) adiabatic gauge potential and the energy gaps. As a rule of thumb, one can thus expect the system to evolve adiabatically if these terms are negligible. Using equation (2.13), and taking the first term in equation (2.39), one obtains the condition, for all $m \neq n$,

$$\max_\lambda \left|\frac{d\lambda}{dt}\right| \frac{|\langle m_\lambda| \partial_\lambda H(\lambda) |n_\lambda\rangle|}{|E_n(\lambda)-E_m(\lambda)|^2} \ll 1. \tag{2.40}$$

This is the so-called *global adiabatic condition*, stating that nonadiabatic transitions can be neglected if the nonadiabatic couplings divided by the corresponding squared

energy gaps are small quantities. In the next section, we will see how different perspectives on the adiabatic condition and more precise error estimates on the adiabatic perturbation expansion can be used to conceive optimized adiabatic drivings.

2.2 OPTIMIZED ADIABATIC SWEEPS

When one wants to exploit an adiabatic process for control, the central requirement is the choice of the exact time dependence of the driven parameter $\lambda(t)$, which encodes the variation of the system Hamiltonian. It is common practice to use the global adiabatic condition (2.39) as the standard criterium for designing adiabatic drivings, i.e., drivings which are slow enough to guarantee that the adiabatic theorem holds. However, when an economy of the total timing of the driven evolution becomes an important aspect, that condition may be, in some cases, too restrictive. An analysis of this limitation has lead to the development of local adiabatic drivings, i.e., controls which satisfy an instantaneous version of the adiabatic condition (2.39) at all instants of the evolution. On the other hand, given that the total evolution time is sufficiently large for equation (2.39) to be satisfied, one could still optimize the global adiabatic driving so to minimize nonadiabatic errors. In this direction, further inspection of the derivation of quantitative adiabatic theorems (i.e., which quantify the magnitude of the deviations) reveals that errors at order ϵ_λ^n are dependent on the n-th derivative of the Hamiltonian evaluated at the beginning and at the end of the evolution, $\partial_\lambda^n H(0)$ and $\partial_\lambda^n H(1)$. Hence, the level of approximation can be arbitrarily improved by choosing shapes of the driving with vanishing derivatives at the boundary up to the desired order. This eventually leads to error estimates which are exponentially small in the adiabatic parameter [2, 105].

We elaborate in this section on these two different approaches to the optimization of adiabaticity, which are typically referred to as local adiabatic drivings and boundary cancellation methods.

2.2.1 Local adiabatic driving (LAD)

In the context of adiabatic quantum computation [2], it was shown that, by selecting drivings which satisfy a "local-in-time" version of the adiabatic condition, much evolution time can be saved [134]. The idea comes from the observation that, since transitions grow quadratically with the inverse gap [equation (2.39)], undesired transitions are greatly enhanced in the vicinity of points in the time-dependent spectrum where energy levels get very close to one another. Therefore, even though the global adiabatic condition is determined by these points, and must be satisfied around them, for the majority of the dynamics such a condition is way too rigid. Rather than looking at the dynamics globally, one can then break the total time

window into smaller subintervals, and apply the adiabatic condition (2.39) to each of those. In the limit of infinitesimally small intervals, the condition (2.39) must be satisfied at all points, i.e.

$$\left|\frac{d\lambda}{dt}\right| \frac{|\langle m_\lambda|\,\partial_\lambda H(\lambda)\,|n_\lambda\rangle\,|}{|E_n(\lambda)-E_m(\lambda)|^2} \ll 1, \tag{2.41}$$

This condition is dubbed the *local* adiabatic condition. In Ref. [134], this idea was used to produce an adiabatic protocol realizing a quantum search algorithm with equivalent performance as the Grover algorithm [122]. The concept of local adiabatic driving was then also connected with geometric aspects of adiabaticity, being generalized to the idea of the quantum adiabatic brachistochrone [133].

2.2.1.1 *LAD 1 – à la Roland-Cerf*

For application in the next Sections, we use the principles of Sec. 2.2.1 in order to derive two different local adiabatic drivings (LADs) for a driven two-level system, as an example. With some caveats, these drivings can be directly used also for more-level problems, as we will do in Chapter 5. Let us consider a two-level system with Hamiltonian

$$H(t) = g\lambda(t)\hat{\sigma}_z + x_0\hat{\sigma}_x, \tag{2.42}$$

where $\hat{\sigma}_x$ and $\hat{\sigma}_z$ are the Pauli matrices,

$$\hat{\sigma}_x = \begin{pmatrix} 0 & 1 \\ 1 & 0 \end{pmatrix}, \qquad \hat{\sigma}_y = \begin{pmatrix} 0 & -i \\ i & 0 \end{pmatrix}, \qquad \hat{\sigma}_z = \begin{pmatrix} 1 & 0 \\ 0 & -1 \end{pmatrix}, \tag{2.43}$$

and where $g > 0$, $x_0 > 0$ and the dimensionless $\lambda(t)$ is assumed to vary smoothly from an initial value $\lambda_0 > 0$ to zero in a monotonic manner, i.e., $\lambda(t) \geq 0$ and $\partial_t\lambda(t) \leq 0$. Our purpose is to engineer the time-dependence of $\lambda(t)$ in such a way that the local adiabatic condition (2.41) is fulfilled. The Hamiltonian (2.42) has the instantaneous energy gap

$$\Delta E(\lambda) = 2g\sqrt{\lambda^2(t) + (x_0/g)^2}. \tag{2.44}$$

After computing the instantaneous eigenvectors, one finds the nonadiabatic coupling

$$|\langle 1_\lambda|\,\partial_\lambda H(\lambda)\,|0_\lambda\rangle| = \frac{x_0}{\sqrt{\lambda^2(t) + (x_0/g)^2}}. \tag{2.45}$$

The local adiabatic condition (2.41), fixing the error to ϵ, then produces the following differential equation,

$$\frac{dt}{d\lambda} = -\frac{x_0}{4\epsilon g^2[\lambda^2(t) + (x_0/g)^2]^{3/2}}. \tag{2.46}$$

By integrating both sides, one finds an expression for $t(\lambda)$ which can then be inverted in order to find $\lambda(t)$. The result is

$$\lambda(t) = \frac{x_0\lambda_0(1 - t/t_f)}{g\sqrt{(x_0/g)^2 + \lambda_0^2 \frac{t}{t_f}(2 - \frac{t}{t_f})}}, \tag{2.47}$$

where we have introduced the total time t_f, which is computed given $t(\lambda)$ and it reads

$$t_f = \frac{\lambda_0}{4\epsilon x_0\sqrt{\lambda_0^2 + (x_0/g)^2}}. \tag{2.48}$$

2.2.1.2 *LAD 2 – quantum adiabatic brachistochrone*

Since more precise adiabatic conditions typically depend on the norm of the Hamiltonian and its derivatives [2], Ref. [133] proposes the generalized local adiabatic condition

$$\left|\frac{d\lambda}{dt}\right| \frac{\|\partial_\lambda H(\lambda)\|}{\Delta E^2(\lambda)} < \epsilon, \tag{2.49}$$

with $\|M\| = \sqrt{\mathrm{tr}[MM^\dagger]}$ the Hilbert-Schmidt norm. Even if, for a two-level system, this condition is very similar to (2.41), it leads to a slightly different local adiabatic driving. For the Hamiltonian (2.42), equations (2.49) and (2.44) produce the differential equation

$$\frac{dt}{d\lambda} = -\frac{\sqrt{2}}{4\epsilon g[\lambda^2(t) + (x_0/g)^2]}. \tag{2.50}$$

Integration of the latter with the initial condition $t(\lambda_0) = 0$ gives the total time

$$t_f = \frac{\alpha}{2\sqrt{2}\epsilon x_0}, \tag{2.51}$$

where $\alpha = \arctan(g\lambda_0/x_0)$. Recalling that $\lambda_0 > 0$ and $g > 0$, the total time t_f is positive. The solution for $\lambda(t)$ is instead

$$\lambda(t) = \frac{x_0}{g}\tan[\alpha(1 - t/t_f)]. \tag{2.52}$$

2.2.2 Boundary cancellation driving (BCD)

Let us now consider equation (2.33), assuming that the adiabatic parameter ϵ_λ is sufficiently small for the expansion to converge. Since it holds that

$$|\mathcal{A}_\lambda^{(n,m)}| \leq \frac{\|\partial_\lambda H(\lambda)\|}{|E_{nm}(\lambda)|}, \tag{2.53}$$

we see from equation (2.39) that the leading order deviation from adiabaticity can be bounded to zero if

$$\|\partial_\lambda H(\lambda)\|_{\lambda=0} = 0, \quad \text{and} \quad \|\partial_\lambda H(\lambda)\|_{\lambda=1} = 0. \tag{2.54}$$

Analyzing the subsequent term in equation (2.38), at order ϵ_λ^2, one can show that it vanishes if $\left\|\partial_\lambda^2 H(\lambda)\right\|$ vanishes at the initial and final points. Pushing the expansion to higher orders in ϵ_λ reveals that order n in the adiabatic parameter can be set to zero by setting to zero the n-th time derivative of the Hamiltonian at the initial and final times [66]. In general, a function with n derivatives vanishing at the boundary can be obtained by interpolating a polynomial of sufficiently large degree. In the following analyses, we will use, for instance, a polynomial with three zero derivatives at the boundary, namely

$$\lambda(t) = \lambda_0 \left[1 - 35\left(\frac{t}{t_f}\right)^4 + 84\left(\frac{t}{t_f}\right)^5 - 70\left(\frac{t}{t_f}\right)^6 + 20\left(\frac{t}{t_f}\right)^7\right], \tag{2.55}$$

where t_f is the total time. A function whose derivatives can be easily set to zero to arbitrary order was introduced in Ref. [132]. This is

$$\Theta_k(x) = \frac{B_x(1+k, 1+k)}{B_1(1+k, 1+k)}, \tag{2.56}$$

where

$$B_x(a, b) = \int_0^x y^{a-1}(1-y)^{b-1} dy, \tag{2.57}$$

with $|x| \leq 1$, $\Re(a) > 0$, $\Re(b) > 0$ is the incomplete Beta function [119]. The function (2.56) has exactly k vanishing derivatives. Accordingly, we will consider the BCD

$$\lambda(t) = \lambda_0 \left[1 - \Theta_k\left(\frac{t}{t_f}\right)\right]. \tag{2.58}$$

In Chapter 5, we will compare the performance produced by all these different optimized adiabatic sweeps. Contextually, we will see that, in general, one cannot identify the best adiabatic driving in a univocal way. Rather, the best choice fundamentally depends on the specific timescale in which one wishes to operate the control protocol.

2.3 COUNTERDIABATIC DRIVING

The use of optimized adiabatic sweeps can improve the performance of global adiabatic drivings by far. Nonetheless, they often work over timescales which are still irremediably susceptible to decoherence and substantial noise accumulation. This has brought to birth and induced the rapid expansion of a new field of research, now widely recognized under the name of "shortcuts to adiabaticity". Its purpose is to develop new techniques for accelerating adiabatic processes, while possibly trying to maintain their intrinsic robustness. Whatever protocol producing the same final conditions as those given by an adiabatic variation of the control parameters can be classified as a *shortcut to adiabaticity* [76]. Alternatively, using a terminology adopted in other contexts [26], it can be called a *fast-forward* method.

The origin of this field can be traced back to the introduction of so-called *counter-diabatic* (cd) fields by Demirplak and Rice [48–50]. The same ideas were introduced afterwards and independently by Berry [15], under the name of *transitionless* (tsl) quantum driving. These authors fundamentally operated a change of perspective in the physical interpretation of the adiabatic gauge potential (2.5). Indeed, it was clear from earlier works that this quantity essentially governs the rate of nonadiabatic transitions, and as such it appears, in different forms, as a technical tool in many derivations of adiabatic theorems. The new perspective lies in the observation that it should be possible to completely cancel undesired transitions *exactly* if one is able to dynamically compensate the effect of the gauge potential at all times. Indeed, let us consider equation (2.14). If, in the rotating frame, $\bar{\mathcal{A}}_\lambda$ was absent, then the equation could be easily integrated, since $\overline{H}$ is diagonal, giving the adiabatic evolution exactly (in the parallel-transport gauge). In order to cancel $\bar{\mathcal{A}}_\lambda$, one can then formally add a *counterdiabatic* term in the initial lab-frame Hamiltonian,

$$H(\lambda) \to H_{\text{tsl}}(\lambda) = H(\lambda) + H_{\text{cd}}(\lambda), \tag{2.59}$$

such that, in the rotating frame, it exactly cancels $\bar{\mathcal{A}}_\lambda$. It is then easy to determine $H_{\text{cd}}(\lambda)$, since it must hold that

$$\frac{\overline{H}_{\text{cd}(\lambda)}}{\dot{\lambda}} - \bar{\mathcal{A}}_\lambda = 0. \tag{2.60}$$

The counterdiabatic Hamiltonian must be

$$H_{\text{cd}}(\lambda) = \dot{\lambda}\mathcal{A}_\lambda. \tag{2.61}$$

Therefore, $H_{\text{cd}}(\lambda)$ corresponds to the adiabatic gauge potential associated with a variation of the Hamiltonian in time. Hence, $H_{\text{cd}}(\lambda)$ trivially features all the interesting properties of the adiabatic gauge potential, explored in Sec. 2.1. From (2.6), we see that $H_{\text{cd}}(t)$ acts like the time-derivative operator. Moreover, by choosing the parallel-transport gauge for the instantaneous eigenvectors of $H(t)$ and using equation (2.13), it explicitly reads

$$H_{\text{cd}}(t) = i\hbar \sum_{n\neq m} \frac{|m_t\rangle\langle m_t| \, \partial_t H(t) \, |n_t\rangle\langle n_t|}{E_n(t) - E_m(t)}, \tag{2.62}$$

where we are implicitly assuming that no degenacies occur. Hence, it is purely off-diagonal in the basis of instantaneous eigenvectors.

As an example, we now derive the counterdiabatic Hamiltonian for a two-level system. To this end, let us consider the Hamiltonian

$$H(t) = u_x(t)\hat{\sigma}_x + u_z(t)\hat{\sigma}_z. \tag{2.63}$$

This can describe, for instance, a spin 1/2 driven by time-dependent magnetic fields. The instantaneous eigenstates of the Hamiltonian of equation (2.63) can be written in the parametrized form

$$|E_+(t)\rangle = -\sin\theta(t)\,|0\rangle + \cos\theta(t)\,|1\rangle\,, \tag{2.64a}$$
$$|E_-(t)\rangle = \cos\theta(t)\,|0\rangle + \sin\theta(t)\,|1\rangle\,, \tag{2.64b}$$

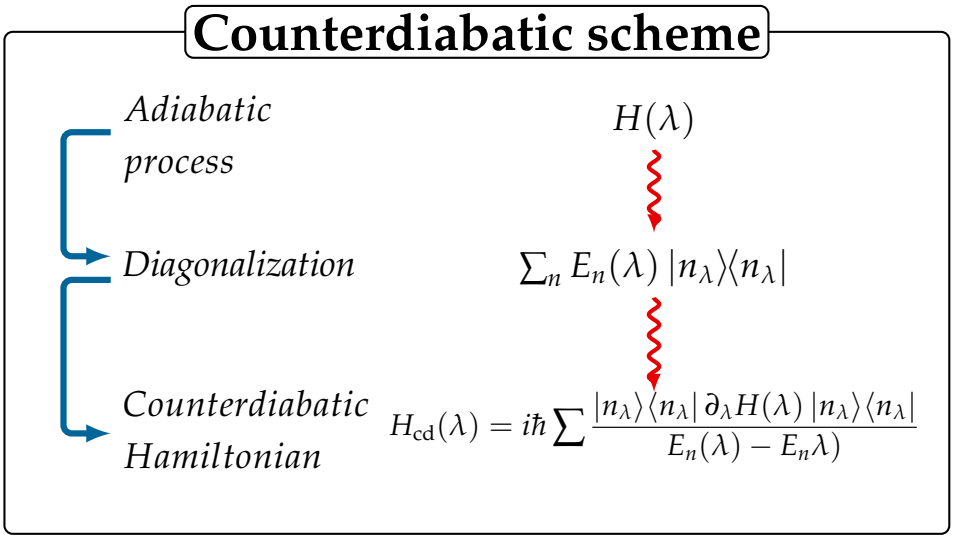

Figure 2.2: Algorithm for computing the counterdiabatic Hamiltonian. Given a Hamiltonian $H(\lambda)$ describing the adiabatic process to be accelerated, the cd scheme first requires diagonalization of $H(\lambda)$. Then, the spectral information, together with the derivative $\partial_\lambda H(\lambda)$, is used for computing the cd Hamiltonian $H_{\text{cd}}(\lambda)$.

where

$$2\theta(t) = \arctan\left[\frac{u_x(t)}{u_z(t)}\right] \tag{2.65}$$

is the mixing angle, which is also the azimuthal angle of the Hamiltonian vector from the "z" axis. Using these expressions, the counterdiabatic field can be computed using equation (2.62) or (2.5) [48], and it reads

$$H_{\text{cd}}(t) = \hbar\frac{\partial\theta(t)}{\partial t}\hat{\sigma}_y, \tag{2.66}$$

where

$$\frac{\partial\theta(t)}{\partial t} = \frac{1}{2}\frac{u_z(t)\partial_t u_x(t) - u_x(t)\partial u_z(t)}{u_x^2(t) + u_z^2(t)}. \tag{2.67}$$

Therefore, for a two-level system evolving with a real Hamiltonian having components along the Pauli matrices $\hat{\sigma}_x$ and $\hat{\sigma}_z$, the counterdiabatic correction evolves along $\hat{\sigma}_y$. This property will be explored in further detail in Chapter 4. Now we will discuss the counterdiabatic field for a class of problems of great relevance in the context of adiabaticity, related to the phenomenon of the avoided level crossing.

2.4 EXAMPLE 1: LANDAU–ZENER–MAJORANA–STÜCKELBERG MODEL

In this section, we discuss a prototypical example of adiabatic and nonadiabatic effects. This is the so-called Landau-Zener-Majorana-Stückelberg (LZMS) model [101,

111, 145, 148, 176]. The model represents the simplest description of a phenomenon which is ubiquitous in quantum physics, namely that of the avoided level crossing. Despite its simplicity, the model is able to capture many important aspects of adiabaticity locally in general spectra, which are then retrieved also in more complex scenarios. The formulation features a two-level system which is subject to the Hamiltonian

$$H(t) = \frac{\hbar\lambda(t)}{2}\hat{\sigma}_z + \frac{\hbar\Omega}{2}\hat{\sigma}_x. \tag{2.68}$$

with the time evolution starting far at negative times and $\lambda(t)$ linearly swept in time, $\lambda(t) = \Lambda t$ with $\lambda(t)$ now not being restricted to $[0, 1]$ only. For understanding the physics described by this Hamiltonian, let us first assume that the coupling is zero, $\Omega = 0$. In this case, the time evolution makes the two instantaneous energy levels $\pm\hbar\lambda(t)/2$ cross at time $t = 0$, the highest one exchanged with the lowest one and vice versa. The instantaneous eigenvectors are the stationary states $|0\rangle$ and $|1\rangle$, but the role of the ground and the excited state is exchanged together with the levels. If the system is initially prepared in an eigenstate, it will remain there for the whole evolution. When the coupling is turned on instead, $\Omega \neq 0$, the two instantaneous eigenvalues are $E_\pm(t) = \pm\frac{\hbar}{2}\sqrt{\lambda^2(t) + \Omega^2}$. These do not cross any more at time zero, but they rather repel each other, following hyperbolas which get closest at $t = 0$, with a value of the gap equal to $\hbar\Omega$ (Fig. 2.3). Because of this, the phenomenon is called avoided crossing or anticrossing. The instantaneous eigenvectors are now time dependent, and they can be written in the parametrized form of equation (2.64) with a mixing angle

$$\theta(t) = \frac{1}{2}\arctan\left[\frac{\Omega}{\lambda(t)}\right]. \tag{2.69}$$

Let us consider the situation of large negative and positive times, such that $|\lambda(t)| \gg \Omega$. If $\lambda(t)$ is negative, then the ground state is very close to the fixed basis vector $|0\rangle$ while the excited state is close to $|1\rangle$. For positive large times instead, the ground states tends to the state $|1\rangle$, while the excited state gets closer and closer to $|0\rangle$. At time equal to zero, the two instantaneous eigenstates are in a flat coherent superposition of the basis states, $|E_\pm(0)\rangle = (|0\rangle \pm |1\rangle)/\sqrt{2}$ (see Fig. 1.1 in the Introduction). If the rate of the evolution is sufficiently slow, the adiabatic theorem holds and the dynamics follows the instantaneous eigenstates. If this is the case, adiabatic passage can be used to prepare the system in interesting states. For instance, if the whole sweep is performed, a state-flip can be achieved, while, if one stops at the anticrossing time, a flat superposition can be produced. The LZMS model is of particular interest in the study of adiabaticity since it permits to characterize in an exact manner the deviations from the adiabatic regime. As such, it is a precious resource also for the investigation of complex phenomena [42, 43, 144]. Indeed, assuming that the system is initially in the ground state, it is possible to compute analytically the asymptotic $t \to \infty$ probability of nonadiabatic transition, i.e., the

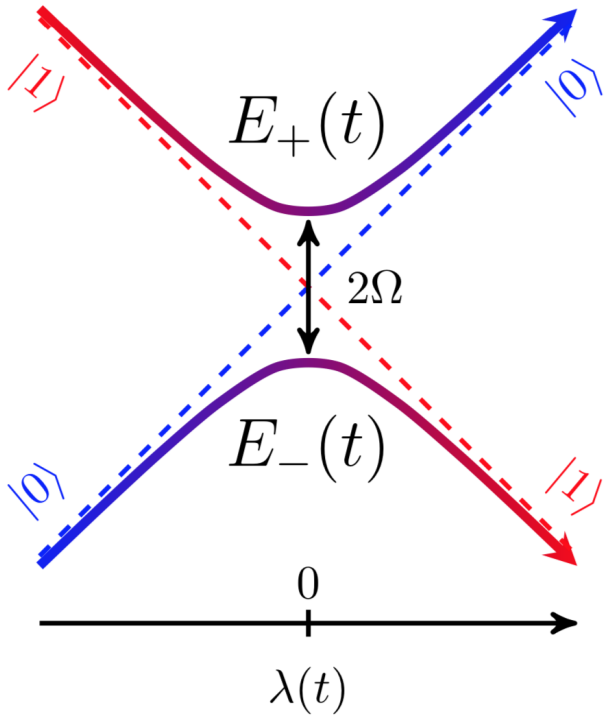

Figure 2.3: Avoided level crossing. Scheme of the time-dependent energy levels of the Hamiltonian (2.68). When the system is driven through the avoided crossing, the bare state $|0\rangle$ and $|1\rangle$ mix, so that the instantaneous ground state, matching $|0\rangle$ for $\lambda(t) \to -\infty$, is in a equally balanced superposition at the anticrossing time $\lambda(t) = 0$, and it matches state $|1\rangle$ asymptotically for $\lambda(t) \to +\infty$. Hence, in the limit of adiabatic driving, a system prepared in $|0\rangle$ evolves along the ground state adiabatic path and the protocol realizes a population inversion between the bare states.

probability that the system has jumped away from the instantaneous adiabatic states. With the condition that the sweep starts at $t \to -\infty$, such a probability is

$$P_{n.a.} = \exp\left(-\frac{\pi\Omega^2}{2\Lambda}\right). \tag{2.70}$$

Equation (2.70) is dubbed the Landau-Zener-Majorana-Stückelberg formula. It was derived by Landau [101] using semiclassical methods, by Zener [176] solving the time-dependent Schrödinger equation in terms of Parabolic Cylinder Functions [119], and by Majorana [111] who solved the equation using asymptotic methods (which produce an integral representation of the solution found by Zener). The LZMS formula (2.70) is exact in the asymptotic limit $t \to \infty$, but it is often used as an approximation for the finite-time dynamics. For studying the finite-time case, it is convenient to rewrite the LZMS Hamiltonian in a way which makes more transparent the role of the total duration of the protocol. For this purpose, let us consider a symmetric sweep of total duration t_f which starts at time $t_i = t_c - t_f/2$ and terminates at time $t_c + t_f/2$, where t_c is the anticrossing time. Let us call $\hbar\lambda_0 = \hbar\epsilon(t_i)$ the value of the gap at the initial (and also at the final) time t_i and

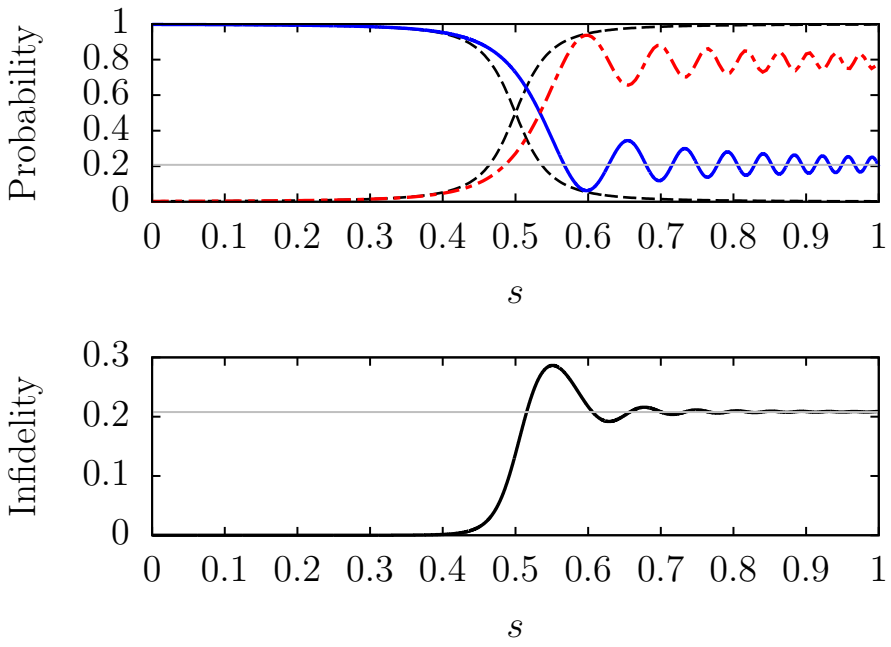

Figure 2.4: Dynamics of the finite-time LZMS model. In the upper panel, the population dynamics is shown for the system initially prepared in the ground state, as a function of the rescaled time. The —— line indicates the population of the ground state, while the red line (-·-·-) is the population of the excited state. The - - - line shows the populations corresponding to the exact adiabatic states. The energy sweep is too fast for the system to remain close to the instantaneous ground state during the evolution, and starts to deviate from the adiabatic dynamics after the anticrossing. This is further evidenced in the lower panel, where the instantaneous infidelity, i.e., the probability of nonadiabatic transition, is represented. The infidelity remains very close to zero until the avoided crossing is reached. It then experiences a jump followed by decaying oscillations around the value predicted by the LZMS formula (2.70), which is indicated with the thin gray line (——). The parameters used for the simulation are $\lambda_\Omega = 20$, $\tau_\Omega = 20$.

let us introduce the rescaled time $s = (t - t_i)/t_f$ which then varies in the interval $s \in [0,1]$. Further, we measure energy in units of the coupling $\hbar\Omega$ and the time in units in Ω^{-1}. Defining the dimensionless parameters $\lambda_\Omega = \lambda_0/\Omega$ and $\tau_\Omega = t_f\Omega$, the LZMS Schrödinger equation finally becomes in the dimensionless form

$$i\frac{\partial U(s)}{\partial s} = \tau_\Omega H_{\mathrm{LZMS}}(s)U(s), \tag{2.71}$$

where

$$H_{\mathrm{LZMS}}(s) = \left[\lambda_\Omega\left(s - \frac{1}{2}\right)\hat{\sigma}_z + \hat{\sigma}_x\right]. \tag{2.72}$$

In terms of the new dimensionless parameters, the LZMS formula is $P_{\mathrm{LZMS}} = \exp\left(-\pi\tau_\Omega/2\lambda_\Omega\right)$.

What happens in the finite-time case can be seen from the upper panel of Fig. 2.4, in which the evolution of populations over a finite interval of time are shown, being produced by numerical integration of the Schrödinger equation. One can see that the system does not experience substantial transitions until it passes through the anticrossing. This is the basis of the ideas presented in Secs. 2.2.1. The probability of transitions then jumps and starts to oscillate around the value predicted by the LZMS formula, with the oscillations decaying as time goes by. Finite-time LZMS problems have been longly studied from the theoretical point of view in the literature, see, for instance, Ref.s [161, 162]. A fundamental point regarding the LZMS formula is the fact that the probability of nonadiabatic transitions decays exponentially in the limit of slow dynamics, i.e, with respect to the total duration τ_Ω. This feature turns out to be a universal characteristic of nonadiabaticity [44, 60, 81].

Let us now focus on the counterdiabatic treatment for the LZMS problem. Using the explicit expressions for the instantaneous eigenvectors (equation (2.64)) the counterdiabatic Hamiltonian has the form of equation (2.66), namely

$$H_{\mathrm{cd}}(s) = f_{\mathrm{cd}}(s)\hat{\sigma}_y \tag{2.73}$$

with profile

$$f_{\mathrm{cd}}(s) = -\frac{1}{2\tau_\Omega}\frac{\lambda_\Omega}{\lambda_\Omega^2\left(s-\frac{1}{2}\right)^2+1}. \tag{2.74}$$

This function exhibits a Lorentzian profile with peak centered on the anticrossing. It is now evident that $f_{\mathrm{cd}}(s)$ decays like τ_Ω^{-1} for large durations. This is an interesting point: although the probability of nonadiabatic transitions, see the LZMS formula, is exponentially weak in τ_Ω, the counterdiabatic correction which compensates it behaves linearly in τ_Ω^{-1} [15]. The total transitionless Hamiltonian then reads

$$H_{\mathrm{tsl}}(s) = \tau_\Omega\left[\lambda_\Omega\left(s-\frac{1}{2}\right)\hat{\sigma}_z+\hat{\sigma}_x\right]+f_{\mathrm{cd}}(s)\hat{\sigma}_y. \tag{2.75}$$

2.5 EXAMPLE 2: SEQUENCE OF AVOIDED CROSSINGS

In the following, we will discuss a more complex situation, in which a three-level system is driven in time in such a way that its spectrum exhibits a sequence of avoided crossings. This problem was studied in Ref. [150]. The purpose of this example is first of all that of going beyond a simple two-level case. This allows us to test the features of the counterdiabatic construction in a more complex scenario. Furthermore, we will see how the complexity of the matrix structure of the counterdiabatic Hamiltonian $H_{\mathrm{cd}}(t)$ grows when the dynamical problem becomes more involved. This motivates the necessity of approximate methods for implementing $H_{\mathrm{cd}}(t)$, which is the central theme of this thesis.

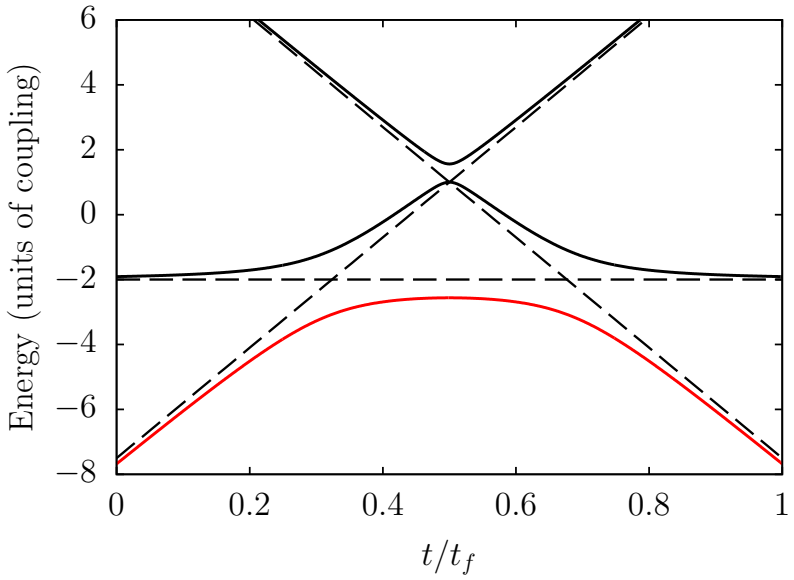

Figure 2.5: Time-dependent spectrum of the three-level system. Instantaneous energy levels of the Hamiltonian of equation (2.76) as a function of time. The instantaneous ground state and the instantaneous first excited state form a sequence of two avoided crossings arising from a direct coupling between states $|0\rangle$ and $|1\rangle$. A smaller anticrossing is instead present between the instantaneous first-excited and second-excited eigenstates $|E_0(t)\rangle$ and $|E_+(t)\rangle$, which is due to a second-order coupling between states $|1\rangle$ and $|2\rangle$.

The Hamiltonian we consider now is, in dimensionless form,

$$H(s) = \tau_\Omega \begin{pmatrix} d_\Omega + \lambda_\Omega \left(s - \frac{1}{2}\right) & 1 & 0 \\ 1 & -2d_\Omega & 1 \\ 0 & 1 & d_\Omega - \lambda_\Omega \left(s - \frac{1}{2}\right) \end{pmatrix}. \tag{2.76}$$

This Hamiltonian may describe an effective spin 1 system. For instance, it may describe a portion of the spectrum of a molecular nanomagnet driven by external magnetic fields [39], or of a nitrogen-vacancy colour center [56]. In this case, the diagonal driving term would be produced by the coupling to a latitudinal magnetic field linearly sweeping along the z direction, whilst the off-diagonal coupling would be produced by a longitudinal magnetic field along the x direction. Then, the parameters λ_Ω and $3d_\Omega$, in units of the x-field coupling, would correspond to the rate of variation of the latitudinal magnetic field and to the axial zero-field-splitting parameter [67], respectively. The time-dependent spectrum of the Hamiltonian of equation (2.76) is shown in Fig. 2.5. The three levels produce in time a sequence of three avoided crossings, which occur at times $s = 1/2 \pm d_\Omega/\lambda_\Omega$, $s = 1/2$. The one between the upper and the intermediate level is smaller than the other two, since it results from an effective coupling at second-order [150]. The counterdiabatic Hamiltonian is not accessible analytically for all times and values

of the parameters, but only in special cases such as $d_\Omega = 0$ or $s = 1/2$. In the $d_\Omega = 0$ case, the Hamiltonian (2.76) is a pure spin-1 Hamiltonian,

$$H(t) = \lambda_\Omega(s - 1/2)\hat{S}_z + \hat{S}_x, \tag{2.77}$$

where $\{\hat{S}_x, \hat{S}_y, \hat{S}_z\}$ are the spin-1 matrices. The counterdiabatic Hamiltonian is then similar in structure to the case of a two-level system. Indeed, it reads [150]

$$H_{\rm cd}^{(d_\Omega=0)}(s) = \frac{\partial\theta(s)}{\partial s}\hat{S}_y, \tag{2.78}$$

where $\tan\theta(s) = \frac{1}{\lambda_\Omega(s-1/2)}$. The case $s = 1/2$ leads instead to the counterdiabatic Hamiltonian

$$H_{\rm cd}(1/2) = \frac{i}{\sqrt{2}}\left.\frac{\partial\theta(t)}{\partial t}\right|_{s=1/2}\begin{pmatrix} 0 & 1 & -\sqrt{2}d_\Omega \\ 1 & 0 & -1 \\ \sqrt{2}d_\Omega & 1 & 0 \end{pmatrix}. \tag{2.79}$$

The eigenvalues at this time instant are instead

$$E_+(1/2) = -\frac{d_\Omega}{2} + \frac{1}{2}\sqrt{8 + 9d_\Omega^2}, \tag{2.80}$$

$$E_-(1/2) = -\frac{d_\Omega}{2} - \frac{1}{2}\sqrt{8 + 9d_\Omega^2}, \tag{2.81}$$

$$E_0(1/2) = d_\Omega. \tag{2.82}$$

Therefore, the smaller anticrossing at time $s = 1/2$ has width $\sqrt{8 + 9d_\Omega^2}$.

The general case (i.e., $d_\Omega \neq 0$ and s not fixed to $1/2$) is computed numerically, and $H_{\rm cd}(t)$ has the overall purely imaginary structure

$$H_{\rm cd}(t) = \begin{pmatrix} 0 & -if_{\rm cd}^{(01)} & -if_{\rm cd}^{(02)} \\ if_{\rm cd}^{(01)} & 0 & -if_{\rm cd}^{(12)} \\ if_{\rm cd}^{(02)} & if_{\rm cd}^{(12)} & 0 \end{pmatrix}, \tag{2.83}$$

with the time profile of the cd functions $f_{\rm cd}^{(ij)} = \langle i|\, H_{\rm cd}(t)\, |j\rangle$ shown in Fig. 2.6. The $\langle 2|\, H_{\rm cd}(t)\, |0\rangle$ matrix element is the one reaching maximal value at $s = 1/2$, which, from equation (2.79), is d_Ω. We immediately see that the realization of the Hamiltonian (2.83) necessitates independent control in time over all the imaginary off-diagonal elements.

It is interesting to study how the control elements inside $H_{\rm cd}(t)$ change as the separation between the avoided crossings, quantified by the parameter d_Ω/λ_Ω, is varied [150]. One finds that these typically decay like power laws for all values of d_Ω/λ_Ω and thus no definite decay scale can be defined. Hence, it is not possible to treat sequential anticrossing separately in an exact manner. The presence of adjacent anticrossings always influences the correcting control fields needed to suppress nonadiabatic transitions arising from the selected one. One can still resort to approximate methods: if the parameter d_Ω/λ_Ω is sufficiently large, one can

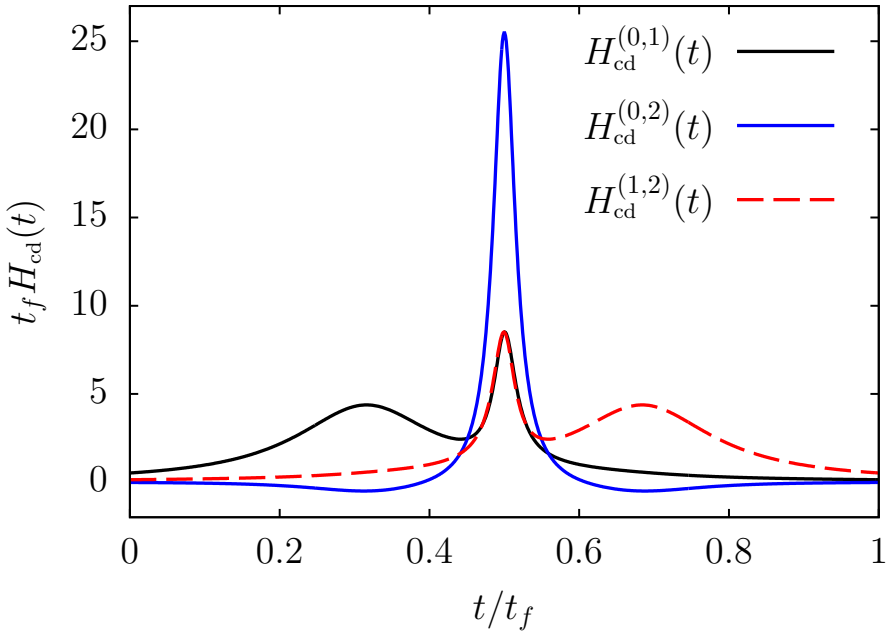

Figure 2.6: Sequential avoided crossings: elements of the counterdiabatic Hamiltonian. Temporal dependence of the matrix elements of the counterdiabatic Hamiltonian of equation (2.83) for the three-level system described by the Hamiltonian of equation (2.76), determined numerically using equation (2.62) for parameters $d_\Omega = 1$, $\lambda_\Omega = 17$, $\tau_\Omega = 1$.

benchmark numerically a separation threshold which allows to treat each avoided crossing separately while achieving at least some prefixed lower bound on the final fidelity [150]. Another simplification can be operated in the case in which one is interested in driving adiabatically only the ground state $|E_-(t)\rangle$. In this case, if the anticrossing between the upper levels occurs far in energy from the ground state ($d_\Omega \gg 1$), one may avoid to implement the $\langle 2| H_{\rm cd}(t) |0\rangle$ correction, since this does not compensate transitions originating directly from the ground state $|E_-(t)\rangle$. However, due to the non-complete separability of the avoided crossing problems, this procedure cannot lead to unit fidelity, and some transition probability always survives due to imperfect compensation. Moreover, the presence of level $|E_+(t)\rangle$, if neglected in the correcting Hamiltonian, prevents in general beneficial repopulation from state $|E_0(t)\rangle$ to the ground state $|E_-(t)\rangle$: the population loss due to diabatic transitions occurring at the first anticrossing cannot be recovered from inverse diabatic transitions at the third anticrossing, since it may be partially transferred to level $|E_+(t)\rangle$ during the $s = 1/2$ anticrossing. Both these approximation schemes still require the time-dependent control of new couplings not present in the original $H(t)$.

2.6 DISCUSSION

In this Chapter we have explored the concept of adiabaticity, its use for quantum control purposes, and its limitative requirement of long evolution timescales, quantified by adiabatic conditions (Section 2.1). We have seen in Section 2.2 that adiabatic drivings can be optimized following different criteria, such as by exploiting local adiabatic conditions (Section 2.2.1), or improved error bounds on adiabatic perturbative expansions (Section 2.2.2). Contextually, we have described in Section 2.3 the idea of shortcut to adiabaticity, introducing the scheme of counterdiabatic driving. This allows one to solve the problem of slow evolutions at the cost of introducing new control elements in the Hamiltonian. We have exemplified all these concepts by discussing the problem of adiabaticity breaking in the vicinity of avoided crossings in the time-dependent energy spectrum (Sections 2.4 and 2.5). These elements will be the central starting point for the development of the technique which will be discussed in Chapter 4. The core of this methodology is that of providing a framework for constructing shortcut-to-adiabaticity Hamiltonians which do not require an exceed of control resources. Moreover, the method provides a smooth connection between purely adiabatic and purely fast-forward strategies. The second ingredient for proceeding in this task is presented in the following Chaper 3, Average Hamiltonian Theory. This represents a means for constructing effective Hamiltonians given a limited set of control parameters, and it will provide us with the tools for developing the theory of effective counterdiabatic driving in Chapter 4.

3 AVERAGE HAMILTONIAN THEORY

In Chapter 2, we have discussed the case in which the driving Hamiltonian varies over timescales much larger than those characteristic of the driven system. In this Chapter instead, we will consider a situation in which control modulations are introduced that vary over timescales much faster than those of the system. We will see how this fast driving regime can be used to engineer effective "average" Hamiltonians, according to the so-called Floquet-Magnus average Hamiltonian theory [23, 25, 74]. First of all, in Section 3.1, we introduce some concepts from geometric control theory [41] which will be useful for the analysis in Chapter 4. Then, in Section 3.2 the concepts of Magnus and Floquet-Magnus expansions will be discussed. These provide the basis for the construction of approximate counterdiabatic fields in the following Chapter 4.

3.1 SOME CONCEPTS FROM (GEOMETRIC) CONTROL THEORY

Quantum control theory is often divided conceptually into two main branches. The first one concerns the mathematical study of the controllability of a given quantum system [41, 54]. This tries to answer questions such as the reachability—that is, which target states can be attained by a controlled evolution given a certain fixed set of control knobs on the system. This kind of analysis often return a yes/no answer to a target problem, without providing a constructive way to determine the actual control procedure. The second branch regards then the synthesis of controls, also called motion planning, which aims at designing suitable control sequences in practice.

While most of the content of this thesis can be categorized under to the second branch, it will be helpful for the forthcoming discussion to recall some concepts from controllability theory. It is important to remark that we will consider finite-dimensional systems, for which the theory is well established. It is first of all essential to formally rewrite the controlled Hamiltonian of the system in a general form which highlights how external control can affect its structure. Namely, we put the attention to the fact that the Hamiltonian of a controlled system can be first of all decomposed into two parts, namely a driven part —which is explicitly time dependent — and a time-independent, so-called drift, part. Secondly, the driven part can be further decomposed by taking into account which are the different matrix components whose coefficients can be tuned in time in an independent manner. The latter coefficients are the control parameters, which might describe the

coupling to an external field or simply the variation of some intrinsic parameter of the system. The decomposition then reads [41]

$$H[\boldsymbol{u}(t)] = H_0 + \sum_{k=1}^{M} u_k(t) H_k, \tag{3.1}$$

where H_0 represents the part of the Hamiltonian which cannot be externally influenced, called the *drift Hamiltonian*, while the matrices $\{H_k\}_{k=1,\ldots,M}$ represent the *control Hamiltonians*, whose strength is varied in time by means of the *control functions* $\boldsymbol{u}(t) = \{u_1(t), \ldots, u_M(t)\}$. The time-dependence intrinsic in $H(t)$ origins only from the functions $\boldsymbol{u}(t)$. We will use the following notation,

$$\boldsymbol{H} = \{H_0, H_1, \ldots, H_M\}, \tag{3.2}$$

for referring to the different matrix components of $H(t)$ according to the control decomposition (3.1).

For a quantum system of dimension N, Hamiltonians can be represented as $N \times N$ Hermitian matrices. Since the zero of the energy scale is arbitrary, these can always be redefined to be traceless by the transformation $H \to H - \mathrm{tr}(H)/N$. The set of traceless $N \times N$ skew-Hermitian matrices $-iH$ is the Lie algebra $\mathfrak{su}(N)$, which has dimension $N^2 - 1$ (the "-1" comes from the condition of zero trace). By matrix exponentiation, a "Hamiltonian" $-iH$, which belongs to the algebra $\mathfrak{su}(N)$, generates the evolution operator $U(t) = e^{-iHt}$, which is an element of $SU(N)$, the Lie group of all special unitary matrices (i.e., unitary matrices with unit determinant). The time-dependent Schrödinger equation (in units of $\hbar$)

$$i\frac{\partial U(t)}{\partial t} = H(t)U(t), \qquad U(0) = \mathbb{1}, \tag{3.3}$$

with the Hamiltonian (3.1), defines a right-invariant system of differential equations. This means that, because of the group property, the propagator $U(t)$ solving (3.3) does not depend on the choice of the initial state. This is important since it allows to lift the problem of controllability from the state space to the group. One can hence study which unitary transformations can be generated from the given control Hamiltonians, rather than focus on what vector states can be attained.

The set of all propagators $U_{\boldsymbol{u}}$ which can be obtained at time t as a solution of the Schrödinger equation

$$i\frac{\partial U_{\boldsymbol{u}}}{\partial t} = H(\boldsymbol{u})U_{\boldsymbol{u}}, \tag{3.4}$$

by tuning the control functions $\boldsymbol{u}(t)$, is called *the reachable set at time t*, denoted by $\mathfrak{R}_t$. The *reachable set* $\mathfrak{R}$ is then the union of the reachable sets at all positive times

$$\mathfrak{R} = \cup_{t \geq 0} \mathfrak{R}_t. \tag{3.5}$$

Given a controlled quantum system with the Hamiltonian (3.1), a central quantity in the study of controllability is the *dynamical Lie algebra* $\mathfrak{L}$ of the system. This

is defined as the set containing the matrices $-i\boldsymbol{H} = \{-iH_0, -iH_1, \ldots, -iH_M\}$, the commutators $[-iH_j, -iH_k]$ of matrices from $-i\boldsymbol{H}$, all nested commutators $[-iH_i, \ldots, -[iH_j, -iH_k]]$ of an arbitrary number of matrices, and all possible linear combinations of these elements. For determining $\mathfrak{L}$ in practice, one can operate an algorithmic procedure for constructing a basis of $\mathfrak{L}$. This works as follows. First, the commutator involving each possible pair of Hamiltonians in $-i\boldsymbol{H}$ is computed. For each new resulting matrix, one checks whether it can be expressed or not as a linear combination of matrices from the initial set. If this is the case, the new matrix is discarded, otherwise it is added to the basis set. Next, one considers the commutator of the new basis elements with the original ones and repeats the procedure. This is iterated, taking commutators of newly obtained matrices with all the basis elements determined up to the previous step, until no new linearly independent matrices are found. An explicit algorithm is provided, for instance, in Ref. [140].

The set of states which can be reached by the system through control is intimately related to the possible "directions" in state space along which the system can be stirred. These, in turn, are fundamentally determined by the set of Hamiltonian that can be realized. Indeed, each Hamiltonian can be thought of intuitively as a rotation vector. One then knows that new "directions" can be generated by combining rotations. For instance, Euler-angles decomposition of a three-dimensional rotation shows explicitly that whatever rotation in three dimensions can be obtained by combining rotations along only two orthogonal axes. Therefore, loosely speaking, the reachable set for a finite-dimensional system is characterized by the set of all possible combinations of "Hamiltonian rotations".

Mathematically, these concepts are rigorously expressed by the so-called Lie Algebra Rank Condition [41, 73] which states that the reachable set $\mathfrak{R}$ is equal to the connected Lie group generated by the dynamical Lie algebra $\mathfrak{L}$ of the system

$$\mathfrak{R} = e^{\mathfrak{L}}. \tag{3.6}$$

This result was first derived in Ref. [86], and it was first used for studying controllability properties of quantum systems in [80].

It is worth mentioning that the condition (3.6), even though it is a powerful criterium for finite-dimensional systems, does not hold for the case of infinite-dimensional, or open, quantum systems. This is due to the fact that, in the latter case, the control Hamiltonians may not generate a compact group [70]. Compactness of the Lie group is necessary for the reachability of "negative-time" propagators, $e^{iH_0 t}$, generated by some drift part H_0 of the control Hamiltonian. Indeed, if the Lie group is compact, then the quantum recurrence theorem holds [19], stating that

$$\forall \epsilon > 0,\ \exists\ T_R > 0\ :\ \left\| e^{-iH_0 T_R} - \mathbf{1} \right\| < \epsilon, \tag{3.7}$$

for a given matrix norm. This result means that for every propagator $U(t) = e^{-iHt}$ there exists some positive time T_R such that $U(t)$ gets arbitrarily close to the identity, i.e., is recurrent to the value $U(0)$. By virtue of equation (3.7), one can then reach

the propagator $e^{iH_0 t}$ by letting the system evolve sufficiently long to be t-close to recurrence, so that one can interpret

$$e^{iH_0 t} = e^{-iH_0(T_R - t)}. \tag{3.8}$$

The quantum recurrence theorem in general does not hold for systems with continuous energy spectra. A simple example in which the system Lie group is not compact is thus a free particle: the propagator generated by the momentum operator $\hat{p}$ in that case, $e^{-i\hat{p}t}$ is never recurrent to the identity for any $t > 0$. In the case of open quantum systems [22], recurrence is in general prevented since environment-induced noise introduces irreversibility in the dynamics of quantum systems. In the Markovian regime (see Section 5.1.2), this shows up mathematically in the fact that the dynamical maps form a semigroup, rather than a group (the implications for control theory are discussed, e.g., in Ref.s [64, 73, 90]).

In the study of controllability, it is important to characterize the properties and the structure of the system Lie algebra $\mathfrak{L}$. A useful tool in this direction is that of a Cartan decomposition [41]. This is a decomposition of $\mathfrak{L}$ into the form of a direct sum

$$\mathfrak{L} = \mathfrak{h} \oplus \mathfrak{p}, \tag{3.9}$$

with the property that $\mathfrak{h}$ is a subalgebra of $\mathfrak{L}$, and the following commutation relations hold

$$[\mathfrak{h}, \mathfrak{h}] \subseteq \mathfrak{h}, \qquad [\mathfrak{h}, \mathfrak{p}] \subseteq \mathfrak{p}, \qquad [\mathfrak{p}, \mathfrak{p}] \subseteq \mathfrak{h}. \tag{3.10}$$

The latter notation means that the commutator of any two distinct elements of $\mathfrak{h}$ belongs to $\mathfrak{h}$, the commutator of any two distinct elements of $\mathfrak{p}$ belongs to $\mathfrak{h}$ as well, but the commutator of an element of $\mathfrak{h}$ with an element of $\mathfrak{p}$ belongs to $\mathfrak{p}$ instead. Cartan decompositions have been used in different contexts for the study of controllability [41, 54, 88], and they will help us in Chapter 4 to better characterize how the matrix structure of the counterdiabatic Hamiltonian $H_{\mathrm{cd}}(t)$ is related to that of the original Hamiltonain $H(t)$.

3.2 FLOQUET–MAGNUS EXPANSION

In standard quantum mechanics courses, it is shown, in the framework of time-dependent perturbation theory, that the solution $U(t)$ of the time-dependent Schrödinger equation,

$$i\frac{\partial U(t)}{\partial t} = H(t)U(t), \tag{3.11}$$

can be formally written as a Dyson series [137, 149], involving a time-ordered exponential,

$$U(t) = \mathcal{T} e^{-i\int_{t_0}^{t} H(t')dt'}. \tag{3.12}$$

For many applications, it can however be convenient to use different formal representations of the propagator. One of these, which will be of our interest for the forthcoming discussion, has a (non time-ordered) exponential form, and is called the Magnus expansion [18, 109, 149]. We present here its main features and we refer to the Review [18] for proofs and further details, for instance concerning convergence properties. The Magnus expansion reads

$$U(t) = e^{-iH_{\text{eff}}(t)t}, \tag{3.13}$$

where the effective Hamiltonian $H_{\text{eff}}(t)$ is an infinite sum, $H_{\text{eff}} = H_{\text{eff}}^{(0)} + H_{\text{eff}}^{(1)} + H_{\text{eff}}^{(2)} + \dots$ whose first terms read

$$H_{\text{eff}}^{(0)}(t) = \frac{1}{t}\int_0^t dt_1 H(t_1), \tag{3.14a}$$

$$H_{\text{eff}}^{(1)}(t) = -\frac{i}{2!t}\int_0^t dt_1 \int_0^{t_1} dt_2 [H(t_1), H(t_2)], \tag{3.14b}$$

$$H_{\text{eff}}^{(2)}(t) = -\frac{1}{3!t}\int_0^t dt_1 \int_0^{t_1} dt_2 \int_0^{t_3} dt_3 \left([H(t_1), [H(t_2), H(t_3)]] + [H(t_3), [H(t_2), H(t_1)]]\right). \tag{3.14c}$$

Hence, the first term is essentially the time average of the driven Hamiltonian, while at following orders there appear combinations of nested commutators of $H(t)$. As compared to the more standard Dyson expansion (3.12), the Magnus expansion has a few properties which make it more appealing for our purposes. First of all, due to its exponential form and the fact that all terms are skew-hermitian, a truncation of the (exponent of the) expansion still returns a unitary operator. If this were not the case, it would have been harder to identify a proper effective Hamiltonian for the closed system, since the generator of the truncated operator might have been non-hermitian. In a different context, this property is of great interest in numerical analysis since it allows one to design norm-conserving numerical integrators [18]. Secondly, the explicit dependence on commutators of the Hamiltonian (at different times) puts in evidence which are the new elements of the system Lie algebra that are produced at each term of the expansion.

Now, let us consider the case in which the controlled Hamiltonian is periodic,

$$H(t+T) = H(t), \tag{3.15}$$

with a small period $T = 2\pi/\omega$. Then, it can be expressed as a Fourier series with terms oscillating at the (large) driving frequency ω and its harmonics $n\omega$ (n is an integer),

$$H(t) = \sum_n H_n e^{in\omega t}. \tag{3.16}$$

This form may describe a system driven by external magnetic fields or subject to shaken potentials. The Fourier components of $H(t)$ are thus defined by

$$H_n = \frac{1}{T}\int_0^T H(t)e^{-in\omega t}. \tag{3.17}$$

Since the H_n components may represent, or be proportional to, the amplitude (Rabi frequency) of a control field, we will also dub them control amplitudes. Inserting the expression (3.16) into equation (3.14), and considering the integration interval over a period of the fundamental frequency, $2\pi/\omega$, one obtains the explicit expressions for the effective Hamiltonian in terms of the Fourier components of $H(t)$ [117],

$$H_{\text{eff}}^{(0)} = H_0, \tag{3.18a}$$

$$H_{\text{eff}}^{(1)} = \sum_{k=1}\frac{[H_k, H_{-k}]}{k\omega} - \sum_{k\neq 0}\frac{[H_k, H_0]}{k\omega}e^{-ik\omega t_0}, \tag{3.18b}$$

$$\begin{aligned} H_{\text{eff}}^{(2)} = &\sum_{m\neq 0}\frac{[[H_{-m}, H_0], H_m]}{2m^2\omega^2} + \sum_{m\neq 0}\sum_{n\neq 0,m}\frac{[[H_{-m}, H_{m-n}, H_n]}{3mn\omega^2} \\ &- \sum_{m\neq 0}\frac{[[H_m, H_0], H_0]}{m^2\omega^2}e^{-im\omega t_0} - \sum_{m,n\neq 0}\frac{[[H_m, H_n], H_{-n}]}{3mn\omega^2}e^{-im\omega t_0} \\ &+ \sum_{m,n\neq 0}\frac{[[H_n, H_{-n}], H_m]}{3mn\omega^2}e^{-im\omega t_0} - \sum_{m\neq 0}\sum_{n\neq 0,m}\frac{[[H_n, H_{m-n}], H_0]}{2mn\omega^2}e^{-im\omega t_0} \\ &+ \sum_{m,n\neq 0}\frac{[[H_m, H_n], H_0]}{2mn\omega^2}e^{-i(m+n)\omega t_0} - \sum_{m,n\neq 0}\frac{[[H_m, H_0], H_n]}{2mn\omega^2}e^{-i(m+n)\omega t_0}. \end{aligned} \tag{3.18c}$$

Now, let us assume that the driving frequency ω is much larger than the frequency scales of the system. In this way, one may assume that the above expansion is perturbative with respect to small $1/\omega$. This high-frequency expansion is often termed *Floquet-Magnus* expansion [25]. If ω is sufficiently large, the system's dynamics features a fast oscillating *micromotion* that tracks around a global *macromotion* governed by the leading-order effective Hamiltonian. Hence, while the effective Hamiltonian does not encapsulate the full dynamical properties, it controls the *average* behaviour of the system.

We list here some further important properties of the Floquet-Magnus expansion, namely related to its time symmetry [23]

- $H(t)$ *is time-symmetric*: If $H(t)$ is symmetric over one period, i.e., $H(t) = H(T-t)$, then all odd-order terms in the Floquet-Magnus expansion vanish

$$H_{\text{eff}}^{(2n+1)} = 0, \qquad n = 0, 1, \ldots; \tag{3.19}$$

- $H(t)$ *is time-antisymmetric*: If $H(t)$ is anti-symmetric over one period, i.e., $H(t) = -H(T-t)$, then the full Floquet-Magnus expansion vanishes

$$H_{\text{eff}}^{(n)} = 0, \qquad \text{for all } n. \tag{3.20}$$

Symmetries Floquet-Magnus expansion	
Hamiltonian	Effective Hamiltonian
$H(t) = H(t-T)$	$H_{\text{eff}}^{(2n+1)} = 0, \quad n = 0, 1, 2, \dots$
$H(t) = -H(t-T)$	$H_{\text{eff}}^{(n)} = 0 \quad$ for all n
$[S, H(t)] = 0 \quad$ for all t	$[S, H_{\text{eff}}^{(n)}] = 0 \quad$ for all n

Table 3.1

Let us now derive a further symmetry. Let us suppose that a certain operator S commutes with the time-dependent Hamiltonian $H(t)$ at all times t. Then, having in mind the decomposition of equation (3.1), this means that S commutes with all the matrices $\boldsymbol{H}$. If this is the case, the Jacobi identity implies that S commutes with all elements of the system Lie algebra $\mathfrak{L}$ generated by the matrices $\boldsymbol{H}$.

Hence, in mathematical language, S belongs to the centralizer $\mathfrak{C}(\mathfrak{L})$ of the system Lie algebra $\mathfrak{L}$,

$$\mathfrak{C}(\mathfrak{L}) = \{s \text{ such that } [s, H_k] = 0 \text{ for all } H_k \in \mathfrak{L}\}. \tag{3.21}$$

If this is the case, since all terms in the Magnus expansion – and hence all orders of the effective Hamiltonian – generated by $H(t)$ are elements of $\mathfrak{L}$, then necessarily all order of the effective Hamiltonian must also commute with S,

$$[H_{\text{eff}}^{(n)}, S] = 0, \quad \text{for all } n. \tag{3.22}$$

This is important since it means that, whenever one targets some specific synthetic Hamiltonian, if this Hamiltonian does not share the symmetry S with $H(t)$ then it cannot be generated effectively by $H(t)$.

In order to engineer a target Hamiltonian, one needs to identify the lowest-order Magnus term which contains the desired algebraic structure. Then, assuming that the Fourier components of the Hamiltonian are freely controllable, these can be chosen so to make vanish terms at higher orders in ω and undesired terms at the same order. In this way, say that the desired Hamiltonian term appears at the n-th Magnus term, then the interaction will be suppressed by a factor ω^{-n}. In some cases, it is possible to counteract this effect by amplifying the control amplitudes in the Hamiltonian. When these become of the order of the driving frequency, more exotic effects may take place [25]. Indeed, if one Fourier component H_n gets multiplied by ω, for instance, then all Magnus terms containing products of k components H_n will be amplified by a factor ω^k, thus altering the perturbative expansion. In other words, the order in ω of the expansion would no more match the order of the Magnus term. This effect is a fundamental resource that can be exploited to bring higher-order terms to leading order, making the corresponding interaction dominant. A proper treatment for reestablishing the matching between the order in ω and the order of the Magnus terms would require to move to an interaction picture with respect to the amplified terms. This would correspond to

resumming all terms at the same ω-order in the lab-frame expansion. However, the exact computation of the interaction picture Hamiltonian is often unfeasible, in which cases the methodology must be applied with additional care in the original expansion.

3.3 DISCUSSION

In the beginning of this Chapter, in Section 3.1, we have introduced useful basic concepts from the mathematical theory of controllability. These will help us, in the next Chapter, to characterize on general grounds the matrix structure of the counterdiabatic Hamiltonian. Moreover, they will allow us to show that such a Hamiltonian can always be approximated, in principle, by modulating the initially available control Hamiltonians.

Starting from Section 3.2, we have discussed a methodology for constructing effective evolutions by means of external control. The general idea is that systems which are driven periodically with a large frequency, as compared to their natural frequency scales, tend to exhibit a dynamics which can be separated into two different timescales. These define an average behavior, that is exact if one looks at the evolution only at multiples of the fundamental driving period, and a microscopic motion surrounding the average one. The average evolution, in which we are interested in, is captured by the concept of an effective Hamiltonian. This Hamiltonian can be computed mathematically in an approximate way, using high-frequency expansions of the propagator. In particular, one can consider a Magnus expansion, introduced in Section 3.2, computed at the end of one oscillation period. This can be truncated, in the limit of large frequency, and the (approximate) effective Hamiltonian can be recovered from the leading-order term. In general, the effective Hamiltonian depends on the choice of the initial time (see equation (3.18)). Physically, this means that it depends on the choice of the global phases of the control fields. Let us point out that also different techniques can be used for estimating the average Hamiltonian. For instance, one may use the idea of (block) diagonalization of the Floquet quasienergy operator in the extended Floquet-Hilbert space (see Ref. [149] for a definition), which can be achieved, for instance, through degenerate perturbation theory [61], or using flow-equation approaches [159, 166] (see [87, 170, 171] and Section 4.1.2 for the concept of flow equation).

In the next Chapter, we are going to use Average Hamiltonian Theory for engineering approximate counterdiabatic fields.

Part II

EFFECTIVE COUNTERDIABATIC SCHEME

4 EFFECTIVE COUNTERDIABATIC DRIVING

In this Chapter, which constitutes the core of this thesis, we introduce the new methodology for constructing shortcuts to adiabaticity. This is based on the adaptations and use of the average Hamiltonian theory presented in Chapter 3 for designing approximate counterdiabatic fields. Our goal is to construct shortcuts which *(i)* enforce the dynamics to follow approximately the exact adiabatic dynamics, and *(ii)* realize this purpose without requiring the implementation of couplings which are absent in the original Hamiltonian $H(t)$. Our first step, in Section 4.1, is to study more in detail how the matrix struture of the counterdiabatic (cd) Hamiltonian $H_{\rm cd}(t)$ is related to that of $H(t)$. In particular, we will show that, in a certain sense, $H(t)$ always contains sufficient structure for being able to "simulate" $H_{\rm cd}(t)$. In Section 4.2 we will proceed by developing an explicit procedure for designing the shortcut Hamiltonians. This will be done by assuming the possibility to introduce fast oscillations in the control parameters of $H(t)$. The average (macromotion) dynamics produced by the oscillating controls will be determined by means of average Hamiltonian theory, see Chapter 3. The new control elements are then enforced to match the desired adiabatic dynamics at stroboscopic times. We will exemplify the procedure in a number of examples, concerning avoided crossing problems (Section 4.2.2) and the generation of entanglement (Section 4.3.2). In Section 4.4, we compare the performance of our method with the traditional adiabatic approximation (described in Section 2.1.2), better characterizing how the new protocol accelerates the reference adiabatic process. For probing the robustness of our methodology against control imperfections, a discussion regarding the effect of potential phase errors in the implementation of the rapidly modulated driving fields is addressed, in Section 4.5. In the final part of the Chapter, Section 4.6, we present a preliminary analysis which sets the ground for further extensions of the general theory introduced here to quantum many-body systems. This regards the construction of shortcuts under strict constraints on the locality of the driving fields, and the engineering of dominant many-body terms in the driving-induced effective Hamiltonian.

4.1 STRUCTURE OF THE COUNTERDIABATIC HAMILTONIAN

We have seen in Section 2.3 that counterdiabatic Hamiltonians can be designed to produce perfect adiabatic following, without transitions, in an arbitrarily small time. We have also seen that the counterdiabatic Hamiltonian $H_{\rm cd}(t)$ equals the adiabatic gauge potential with the varying parameter being the physical time (Section 2.1)

and, hence, it directly inherits all its properties, which were discussed in Section 2.1. In this Section, we will elaborate on the algebraic properties of $H_{\rm cd}(t)$. In particular, we will try to answer two fundamental questions:

1. How does $H_{\rm cd}(t)$ relate to the structure of the time-dependent system Hamiltonian?
2. Is it possible to "simulate" the action of $H_{\rm cd}(t)$ without introducing additional control components in the Hamiltonian?

For this purpose, we will exploit two different connections for the theory of counterdiabatic fields, one involving geometric control theory introduced in Section 3.1, the other one related to the theory of flow equations.

4.1.1 Control-theory perspective

For addressing these problems, we first of all adopt a decomposition of the Hamiltonian, assuming that the system's Hilbert space in finite-dimensional, from a control-theory perspective, as it was described in Section 3.1. In particular, the Hamiltonian can be written in the general form (3.1),

$$H(t) = H_0 + \sum_{n=1}^{M} u_n(t) H_n, \tag{4.1}$$

where H_0 is the drift Hamiltonian, $\{H_1, \dots, H_M\}$ are the hermitian control Hamiltonians (which are assumed to be linearly independent), while $\boldsymbol{u}(t) = \{u_1(t), \dots, u_M(t)\}$ are the real-valued control functions. As described in Section 3.1, this decomposition is motivated by the fact that, given a system driven by time-dependent external fields or by tuning some internal parameter, it is always possible to distinguish, first of all, the part of the Hamiltonian matrix which is not controllable, and which is hence time independent, from the time-dependent part. The latter can then be decomposed by identifying which are the different matrix components that can be controlled in time in an independent manner.

Our first result states that $H_{\rm cd}(t)$ always belongs to the dynamical Lie algebra $\mathfrak{L}$ of the system. This is important in our context especially for (at least) two reasons. First of all, it means that the evolution produced by the counterdiabatic Hamiltonian $H_{\rm cd}(t)$ can be emulated, to arbitrary precision, by suitably combining the initial control Hamiltonians. In other words, there exist control sequences achieving adiabatic dynamics approximately, which require tuning of the functions $\boldsymbol{u}(t)$ only. Therefore, no new control Hamiltonians are needed, contrary to the case of exact counterdiabatic driving.

Second, the result restricts the possible matrix structure of $H_{\rm cd}(t)$ before requiring its explicit computation. If the quantum system is fully controllable, then the dynamical Lie algebra $\mathfrak{L}$ coincides with the whole $\mathfrak{su}(N)$. If this is the case, then $-iH_{\rm cd}(t)$, being a traceless skew-Hermitian matrix, is obviously within $\mathfrak{L}$. For large systems which are not fully controllable though, the Lie algebra $\mathfrak{L}$ may have a much

smaller dimension than $\mathfrak{su}(N)$. In that situation, the number of new Hamiltonians needed to implement $H_{\text{cd}}(t)$ does not necessarily scale with the system size, and it can remain small. We formalize these findings in the following Theorem.

Theorem 2. *Let the Hamiltonian $H(t)$ of the driven finite-dimensional system be expressed in the form*

$$H(t) = H_0 + \sum_{n=1}^{M} u_n(t) H_n, \tag{4.2}$$

and let $\mathfrak{L}$ be the dynamical Lie algebra generated by the skew-hermitian matrices $\{-iH_k\}_{k=1,\dots,M}$. Then, the generator produced by the counterdiabatic Hamiltonian, $-iH_{cd}(t)$, corresponding to $H(t)$, belongs to $\mathfrak{L}$ for all times t.

Proof. Proving that a matrix H_x belongs to the Lie algebra $\mathfrak{L}$ of the system can typically be done via one of the two ways:

1. Show that the unitary propagator $U_x(t) = e^{-iH_x t}$ generated by H_x can be expressed as a concatenation of propagators generated by elements of $\mathfrak{L}$, thus of elements of the group $e^{\mathfrak{L}}$;

2. Show that H_x can be expressed as a linear combination of elements of $\mathfrak{L}$ —that is, of the control matrices $\{H_k\}_{k=1,\dots,M}$ and their possibly nested commutators.

Here we will follow the first strategy. The proof of the theorem is essentially a consequence of the adiabatic Theorem 1 of Section 2.1.2. Indeed, the adiabatic Theorem states that, in the asymptotic limit of slow evolution, the exact adiabatic dynamics can be achieved to arbitrary precision by varying the control functions in $H(t)$. The adiabatic dynamics differs in general from the one induced by $H_{\text{cd}}(t)$ by relative phase factors associated to each instantaneous eigenvector of $H(t)$. Let us fix one instant in time $t = \hat{t}$, and let us consider the "freezed" Hamiltonian $\hat{H}_{\text{cd}} = H_{\text{cd}}(\hat{t})$. Let U_{cd}(t) be the solution of the Schrödinger equation with Hamiltonian H_{cd}(t), i.e., in units of $\hbar$,

$$i\frac{\partial U_{\text{cd}}(t)}{\partial t} = H_{\text{cd}}(t) U_{\text{cd}}(t). \tag{4.3}$$

From equation (2.59), we have that $H_{\text{cd}}(t) = H_{\text{tsl}}(t) - H(t)$. Let $M_{\text{tsl}}(t)$ and $M(t)$ be the exponents of the Magnus expansions (see Section 3.2), produced by $H_{\text{tsl}}(t)$ and $H(t)$, respectively. Then, the solution of (4.3) can be written in the Magnus form

$$U_{\text{cd}}(t) = e^{M_{\text{tsl}}(t) - M(t) + R(t)}, \tag{4.4}$$

where

$$R(t) = -\frac{1}{2}\int_0^t dt_1 \int_0^{t_1} dt_2 \left([H_{\text{tsl}}(t_1), H(t_2)] + [H(t_1), H_{\text{tsl}}(t_2)]\right) + \dots \tag{4.5}$$

involves nested integrals of nested commutators containing both $H_{\text{tsl}}(t)$ and $H(t)$. We can estimate the strength of this term by formally expanding in Taylor series the

Hamiltonians in (4.5) for small t around the midpoint of the integration interval, $t^* = t/2$. One then obtains that $R(t) = O(t^3)$,

$$R(t) = -\frac{1}{12}\left([H_{\text{tsl}}^{[1]}, H^{[0]}] - [H_{\text{tsl}}^{[0]}, H^{[1]}]\right) t^3 + O(t^4), \tag{4.6}$$

where we used the notation

$$H_x^{[n]} = \frac{1}{n!}\frac{\partial^n H_x(t)}{\partial t^n}\bigg|_{t=t^*}. \tag{4.7}$$

Now, we can use an exponential decomposition known as Zassenhaus formula [109] to split $U_{\text{cd}}(t)$ as the product

$$U_{\text{cd}}(t) = U_{\text{tsl}}(t)U^\dagger(t)e^{-\frac{1}{2}[M_{\text{cd}}(t),M(t)]}e^{O(t^3)}. \tag{4.8}$$

Expanding again around the point t^*, one obtains the bound

$$-\frac{1}{2}[M_{\text{cd}}(t), M(t)] = O(t^2). \tag{4.9}$$

By the adiabatic Theorem 1, Section 2.1.2, the exact adiabatic evolution $U_{\text{tsl}}(t)$ can be obtained by a slow modulation of $H(t)$. We denote the adiabatic propagator of equation (2.34) as $U_{\text{ad}}(t)$: even though it matches the transitionless solution $U_{\text{tsl}}(t)$, we want to emphasize that they result from different dynamical processes (one involving only variations of control functions $\boldsymbol{u}(t)$, whilst the other requiring new Hamiltonian couplings). Therefore, we have that

$$U_{\text{cd}}(t) = U_{\text{ad}}(t)U^\dagger(t)e^{O(t^2)} + O(\epsilon_\lambda). \tag{4.10}$$

Next, we observe that we can rewrite

$$\hat{H}_{\text{cd}} = \frac{1}{t}\int_{\hat{t}}^{\hat{t}+t} H_{\text{cd}}(t_1)dt_1 + O(t). \tag{4.11}$$

By exponentiating, and by virtue of the Magnus expansion, we have that

$$e^{-i\hat{H}_{\text{cd}}t} = U_{\text{cd}}(\hat{t}+t, \hat{t})e^{O(t^2)} \tag{4.12}$$

By equation (4.10) we finally obtain

$$e^{-i\hat{H}_{\text{cd}}t} = U_{\text{ad}}(\hat{t}+t, \hat{t})U^\dagger(\hat{t}+t, \hat{t})e^{O(t^2)} + O(\epsilon_\lambda). \tag{4.13}$$

Hence, we find that the group element generated by the "freezed" counterdiabatic Hamiltonian at whatever time instant $\hat{t}$, can be approximated by combining two evolutions governed by $H(t)$: a "forward"-in-time adiabatic evolution and a "backward" finite-time one. □

The second result gives a sufficient condition for the counterdiabatic Hamiltonian $H_{\text{cd}}(t)$ to be always completely outside from the set of controllable matrices and their linear combinations. This, in some cases, allows one to determine the matrix structure of $H_{\text{cd}}(t)$ before proceeding to the diagonalization of $H(t)$. In particular,

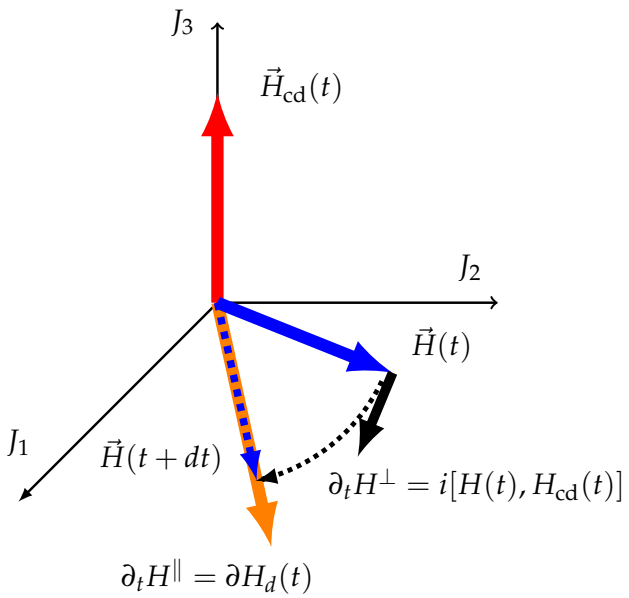

Figure 4.1: Structure of the counterdiabatic Hamiltonian. The Hamiltonian $H(t) = u_1(t)J_1 + u_2(t)J_2$, where $\{J_k\}_{k=,1,2,3}$ are angular momentum generators, $[J_j, J_k] = i\epsilon_{jk\ell}J_\ell$, can be represented as a vector $\vec{H}(t) = \{u_1(t), u_2(t), 0\}$ of length $\sqrt{u_1^2(t) + u_2^2(t)}$ evolving on the plane spanned by J_1 and J_2. Then, a variation of this vector with time can be decomposed into two components: a component $\partial_t H^{\parallel}$ parallel to $\vec{H}(t)$, i.e., a variation of length, which is generated by the matrix $\partial H_d(t)$ of equation (2.10), and a perpendicular component $\partial_t H^{\perp}$ generating rotations, which corresponds to a variation of the eigenvectors of $H(t)$. This is generated by $-iH_{\rm cd}(t)$, whose representative vector lies then orthogonally to the $\{J_1, J_2\}$ plane. (Figure adapted from [124])

we identify a class of Hamiltonians which, in a certain sense, generalizes that of real symmetric Hamiltonians. For the latter, it is easy to show that the corresponding $H_{\rm cd}(t)$, for whatever (allowed) time-dependence of $H(t)$, never has real components: it is purely imaginary, skew-symmetric. Indeed, if the Hamiltonian $H(t)$ has only real entries, then it can be diagonalized by a real orthogonal matrix $O(t)$. If that is the case, then the adiabatic gauge potential would be, according to definition (2.5), equal to $i\hbar\partial_t O(t)O^{\dagger}(t)$, and therefore it would be purely imaginary. Another simple example is that of the angular momentum algebra with the three generator $\{J_1, J_2, J_3\}$. Given $H(t)$ as a combination of two generators, say $H(t) = u_1(t)J_1 + u_2(t)J_2$, the cd field turns out to be proportional to the third one $H_{\rm cd}(t) \propto J_3$. This can be seen without calculating it explicitly, by recalling that $H_{\rm cd}(t)$ is orthogonal to both $H(t)$ and $\partial_t H(t)$ (as discussed in Section 2.3), and hence must lie outside the plane spanned by J_1 and J_2. An interesting visualization can be obtained from equation (2.9). Indeed, we can represent the three generators as a triad of orthogonal vectors in three dimensions, see Figure 4.1. The Hamiltonian $H(t)$ can be interpreted as a time-dependent vector $\vec{H}(t)$ whose length is equal to its larger eigenvalue, evolving on the plane spanned by J_1 and J_2. Then, by equation (2.9), one can see that $\partial H_d(t)$, by inducing a variation of eigenvalues, generates

the stretching of the Hamiltonian vector along its own direction. On the other hand, $H_{\text{cd}}(t)$ induces rotations on the plane, and can then be represented as a rotation vector orthogonal to that plane, i.e., lying along J_3. We now formulate these statements as a theorem, using the concept of Cartan decomposition introduced at the end of Section 3.1.

Theorem 3. *Let us suppose that the system Lie algebra $\mathfrak{L}$ admits a Cartan decomposition $\mathfrak{L} = \mathfrak{h} \oplus \mathfrak{p}$. Further, given the decomposition of the Hamiltonian in the form (4.1), suppose that the linear span $\text{span}\{-iH_k\}_{k=0,\dots,M} \in \mathfrak{p}$ and that also $-i\partial H_d(t) = -i\sum_n \partial_t E_n(t)\,|n_0\rangle\langle n_0| \in \mathfrak{p}$. Then, the counterdiabatic Hamiltonian belongs to the subalgebra $\mathfrak{h}$.*

Proof. If $\text{span}\{-iH_k\}_{k=0,\dots,M}$ belongs to $\mathfrak{p}$, then it means that both $-iH(t) \in \mathfrak{p}$ and $-i\partial_t H(t) \in \mathfrak{p}$. If $i\partial H_d(t) \in \mathfrak{p}$ as well, from Equation (2.9) and (2.61) we have that $[H(t), H_{\text{cd}}(t)] \in \mathfrak{p}$, since it can be written as a combination of $i\partial_t H(t)$ and $i\partial H_d(t)$. From the commutation relations (3.10) defining a Cartan decomposition, then it must hold that $-iH_{\text{cd}}(t) \in \mathfrak{h}$. □

For the case of fully-controllable real Hamiltonians, the system Lie algebra is $\mathfrak{L} = \mathfrak{su}(N)$ and the Cartan decomposition is $\mathfrak{su}(N) = \mathfrak{so}(N) \oplus \mathfrak{I}(N)$, where $\mathfrak{so}(N)$ is the algebra of $N \times N$ real skew-symmetric matrices, while $\mathfrak{I}(N)$, being the orthogonal complement of $\mathfrak{so}(N)$ in $\mathfrak{su}(N)$, is the set of purely imaginary symmetric matrices. In the next subsection we will use some results from the theory of flow equations [87, 170, 171] for showing that, under certain general conditions, the matrix structure of the counterdiabatic Hamiltonian can be found by considering a single commutator of the control Hamiltonians $\text{span}\{-iH_k\}_{k=0,\dots,M}$.

4.1.2 A connection with the theory of flow equations

In the context of many-body physics (or generally infinite-dimensional systems), the exact diagonalization of the system Hamiltonian may not be accessible, and approximate methods need to be used. The Hamiltonian is, for the moment, assumed to be independent of time. A successful technique in this direction, developed in the 90s [171], makes use of the idea of infinitesimal one-parameter unitary transformations. These transformations are constructed in such a way that, as the parameter ℓ "flows" from zero towards infinity, the unitarily-transformed Hamiltonian becomes closer and closer to a certain desired form, reaching it exactly in the asymptotic limit. This form can be strictly diagonal, in which case the flow gets rid of off-diagonal terms, or it can be a non-interacting representation of an initially interacting system, in which case the flow gets rid of the interaction part. Hence, a powerful aspect of this method is that, by truncating the flow at a finite parameter value, one still recovers approximate solutions to the problem. The Hamiltonian corresponding to the value ℓ of the *flowing parameter* is defined by

$$H(\ell) = U(\ell)H(0)U^{\dagger}(\ell). \tag{4.14}$$

By taking the derivative of equation (4.14), and introducing the generator

$$\eta(\ell) = \frac{dU(\ell)}{d\ell} U^{\dagger}(\ell), \tag{4.15}$$

one obtains the following differential equation which rules the variation of Hamiltonian induced by the flow,

$$\frac{dH(\ell)}{d\ell} = [\eta(\ell), H(\ell)]. \tag{4.16}$$

The system of differential equations described by (4.16) defines the set of so-called *flow equations*, which give name to this approach [87, 170, 171]. If these equations are solved, one is able to determine both the generator and the diagonalized/decoupled form of the Hamiltonian. For the unitary flow to induce diagonalization or decoupling, the fundamental point is the choice of this generator $\eta(\ell)$. This is such that, as ℓ increases, the undesired matrix elements of the given Hamiltonian decrease tending eventually to zero. The flowing Hamiltonian $H(\ell)$ can be decomposed into the form

$$H(\ell) = H_{\text{tg}}(\ell) + H_{\text{int}}(\ell), \tag{4.17}$$

where $H_{\text{tg}}(\ell)$ is target form of the Hamiltonian (diagonal, for example) while $H_{\text{int}}(\ell)$ is the interaction part which one wishes to eliminate. The necessary condition can be formulated, for instance, by imposing that the trace of $H^2_{\text{int}}(\ell)$ decreases with the flow, i.e.,

$$\frac{d}{d\ell} \text{tr}[H^2_{\text{int}}] \leq 0. \tag{4.18}$$

It can be proven [87] that the condition (4.18) can be satisfied by choosing the *canonical generator* (originally proposed by Wegner in Ref. [171])

$$\eta(\ell) = [H_{\text{tg}}(\ell), H_{\text{int}}(\ell)] = [H_{\text{tg}}(\ell), H(\ell)], \tag{4.19}$$

provided the following conditions on the flowing Hamiltonian hold,

$$\text{tr}\left[H_{\text{tg}}(\ell) H_{\text{int}}(\ell)\right] = 0, \tag{4.20a}$$

$$\text{tr}\left[\frac{dH_{\text{tg}}(\ell)}{d\ell} H_{\text{int}}(\ell)\right] = 0. \tag{4.20b}$$

The latter imply that both the diagonal/decoupled part of the flowing Hamiltonian $H_{\text{tg}}(\ell)$ and its derivative with respect to ℓ must be completely orthogonal, in the matrix sense of the Hilbert-Schmidt inner product, to the interaction Hamiltonian $H_{\text{int}}(\ell)$. Note that the conditions (4.20) are automatically satisfied in the case in which $H_{\text{tg}}(\ell)$ is diagonal and $H_{\text{int}}(\ell)$ is completely off-diagonal. If for some value of ℓ the generator (4.19) vanishes, then the flow reaches a stationary point in which $H_{\text{tg}}(\ell)$ and $H_{\text{int}}(\ell)$ commute. Although conditions (4.18) and (4.20) give a justification for the choice of the canonical generator (4.19), they still do not

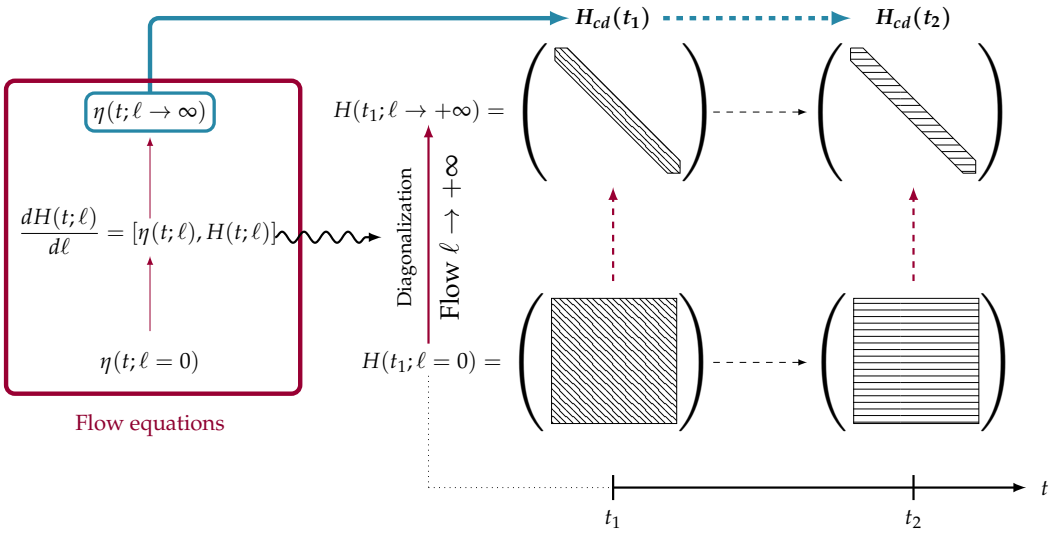

Figure 4.2: Flow equations and counterdiabatic driving. For each value t of time, the snapshot Hamiltonian $H(t)$ can be diagonalized through the flow-equations method: this introduces a family of continuous unitary transformations, generated by $\eta(t;\ell)$, which make the Hamiltonian "flow" towards its diagonal form. In the limit $\ell\to+\infty$, if diagonalization is achieved, the generator $\eta(t;\ell\to+\infty)$ matches the counterdiabatic generator at time t, $-iH_{\rm cd}(t)$.

guarantee success of the procedure. Hence, they rather imply that the canonical form is a good starting ansatz for the generator.

Let us now return to the theory of counterdiabatic fields, and consider the Hamiltonian of the system to be time-dependent again. For each value of time, the diagonalization procedure which defines the instantaneous counterdiabatic field $H_{\rm cd}(t)$ can in principle be operated by means of the flow-equations method. This requires to "freeze" the snapshot Hamiltonian $H(t)$ and to introduce the flowing Hamiltonian

$$H(t;\ell)=H_d(t;\ell)+H_{\rm int}(t;\ell), \tag{4.21}$$

with the corresponding generator $\eta(t;\ell)$. Then, since $H_{\rm cd}(t)$ is defined as (i times) the generator of the unitary transformation which diagonalizes $H(t)$, the generator of the flow $\eta(t;\ell)$ eventually matches $-iH_{\rm cd}(t)$ at the end of the flow

$$\eta(t;\ell)\overset{\ell\to\infty}{\longrightarrow}-iH_{\rm cd}(t). \tag{4.22}$$

First of all, in the spirit of flow-equations, this means that such a methodology can in principle be used for constructing approximate counterdiabatic corrections, by terminating the flow at intermediate steps. This procedure is reminiscent of the ideas used in the variational methods proposed in Ref.s [37, 143]. Second, we can apply the results on the structure of the generator of the flow $\eta(t;\ell)$ for probing

the structure of $H_{\rm cd}(t)$. Let us now consider the case in which the Hamiltonian of the system can be decomposed as follows

$$H(t) = \sum_n u_n(t) H_n + \sum_m \overline{u}_m(t) \overline{H}_m, \tag{4.23}$$

where the matrices $\{H_n\}$ are diagonal and their linear span is orthogonal to the linear span of the matrices $\{\overline{H}_m\}$,

$$\mathrm{tr}[H_n \overline{H}_m] = 0 \text{ for all } n, m. \tag{4.24}$$

Notice that, for instance, the two-level LZMS Hamiltonian of section (2.4) can be written in this form. If this is the case, then one can define the flowing Hamiltonian at fixed time t,

$$H(t;\ell) = H_d(t;\ell) + H_{\rm int}(t;\ell), \tag{4.25}$$

with

$$H_d(t;\ell) = \sum_n u_n(t;\ell) H_n; \qquad H_{\rm int}(t;\ell) = \sum_m \overline{u}_m(t;\ell) \overline{H}_m. \tag{4.26}$$

Hence, the flow maintains $H_d(t;\ell)$ within the span of the matrices $\{H_n\}$ and $H_{\rm int}$ within the span of the matrices $\{\overline{H}_m\}$. The flowing Hamiltonian (4.25) then satisfies the conditions of equation (4.20), and thus the ansatz generator of the flow can be taken to be of canonical form,

$$\eta(t;\ell) = [H_d(t;\ell), H_{\rm int}(t;\ell)], \tag{4.27a}$$

$$= \sum_{n,m} u_n(t;\ell) \overline{u}_m(t;\ell) [H_n, \overline{H}_m]. \tag{4.27b}$$

Equations (4.27)a-b, together with (4.22) give us an important result concerning the counterdiabatic Hamiltonian $H_{\rm cd}(t)$: in many case, a good initial ansatz for the structure of $H_{\rm cd}(t)$, under the conditions assumed here, is obtained by considering a single commutator of the independent matrix components of $H(t)$. This aspect is very interesting in view of the procedure which will be presented in the next section for constructing effective counterdiabatic Hamiltonians.

The results of this section give some criteria for restricting the possible matrix structure of the counterdiabatic Hamiltonian. However, they do not provide a systematic method for constructing approximate counterdiabatic corrections. A scheme for achieving this task is developed in the following Section, based on the design of time-dependent effective Hamiltonians via the average Hamiltonian theory introduced in Chapter 3.

4.2 EFFECTIVE COUNTERDIABATIC FIELDS

The results of Section 4.1 prove the theoretical possibility of achieving an approximate adiabatic dynamics by using only the initially available controls. What those

results do not show, is how to operate the construction of the controls in practice. Moreover, the Lie-algebraic controllability (Section 3.1) analysis is in general not concerned with the actual timescales for control. For instance, the validity of the Lie algebra rank condition (equation (3.6)) is based on the property of compactness of the system Lie group, which guarantees that, given sufficient time, evolutions get arbitrarily close to the starting point. This is essential since it provides an interpretation for "backward-in-time" evolutions. Although this can be taken as an explicit recipe for reaching the negative-time propagator e^{iHt}, the resulting protocol would be rather poorly performing, requiring an unreasonable time. The purpose of this section is to provide a systematic strategy to construct effective counterdiabatic Hamiltonians which can speed up the adiabatic state transfer. The methodology we introduce is based on average Hamiltonian theory (AHT), as presented in Chapter 3.

The general idea is the following. Given the original Hamiltonian $H(t)$, we complement it with a control Hamiltonian $H_{\text{ecd}}(t)$, such that the total system Hamiltonian is now $H(t) + H_{\text{ecd}}(t)$. The correction $H_{\text{ecd}}(t)$ is chosen to have the same matrix structure of $H(t)$, i.e., both Hamiltonians can be written in the form of equation (3.1) with the same control matrices $\boldsymbol{H}$ but different control functions $\boldsymbol{u}(t)$. The control functions in $H_{\text{ecd}}(t)$ are then chosen to be oscillating rapidly with respect to the dynamics induced by $H(t)$. In this way, the system is expected to respond to the average Hamiltonian produced by $H_{\text{ecd}}(t)$ as predicted by AHT. Our goal is then to tailor the control functions in such a way that this average Hamiltonian matches the counterdiabatic Hamiltonian $H_{\text{cd}}(t)$ in the limit of fast driving.

From Theorem 2, we know that, since $-iH_{\text{cd}}(t)$ is in the system Lie algebra $\mathfrak{L}$, the Hamiltonian $H_{\text{cd}}(t)$ can be expressed as a (in general unknown) combination of commutators of control matrices from $\boldsymbol{H}$. This suggests that it is convenient to adopt a Magnus representation, introduced in Section 3.2, of the propagator, since these commutators appear explicitly.

In the spirit of AHT, we consider a fully-controllable ansatz decomposition for $H_{\text{ecd}}(t)$, namely

$$H_{\text{ecd}}(t) = \sum_{k=1}^{M} u_k(t) H_k, \tag{4.28}$$

and we choose an ansatz for the control functions $\boldsymbol{u}(t)$ as a truncated Fourier series with N_h harmonics of a fundamental frequency $\omega = 2\pi/T$,

$$u_k(t) = \sum_{j=1}^{N_h} [c_{k,j} \cos(j\omega t) + s_{k,j} \sin(j\omega t)]. \tag{4.29}$$

The driving frequency ω, for AHT to work, will need to be much larger than the fundamental frequencies of the system. For instance, in the case of avoided crossing problems, ω needs to be much larger than the inverse minimal gap. With the explicit choice of equation (4.29), we can compute the Floquet-Magnus expansion

via equations (3.18). The 0-th order is zero, since there are no non-oscillating components in the functions (4.29), hence no zero Fourier components of the Hamiltonian,

$$H_{\text{eff}}^{(0)} = \frac{1}{T}\int_0^T H_{\text{ecd}}(t)dt = 0. \tag{4.30}$$

The first order is

$$H_{\text{eff}}^{(1)} = \frac{1}{2\omega}\sum_{k,j}^{1,N_h}\left(\sum_{n>0}(c_{k,n} - is_{k,n})(c_{j,n} + is_{j,n})\right)[H_k, H_j]. \tag{4.31}$$

One then has to go on with the calculation of higher orders until the matrix structure necessary to implement $H_{\text{cd}}(t)$ appears. As we will see, for many few-level problems this happens already at the first Magnus term, as suggested by the theory of flow equations discussed in Section 4.1.2. Once the desired structure is found, the amplitudes of the driving fields $\{c_{k,n}, s_{k,n}\}$ are used to enforce the effective Hamiltonian to be equal to $H_{\text{cd}}(t)$, at the end of one oscillation period, up to the largest possible order in large driving frequency ω^{-1}. In principle, the procedure should be repeated for each period of evolution, producing in general discontinuous field amplitudes $\{c_{k,n}, s_{k,n}\}$ in each interval. We will see though that, in all the cases which we will treat in this Chapter and in Part iii, an interpolation among different periods is straightforward and leads to smooth control functions $u_k(t)$.

4.2.1 Single-spin Lie algebra

For exemplifying the procedure, let us compute an effective counterdiabatic (ecd) field for a system whose dynamical Lie algebra is $\mathfrak{su}(2)$. This describes, for instance, a single spin driven by magnetic fields. Let us suppose that the control Hamiltonian of the system can contain only two of the three generators $\{\hat{\sigma}_x, \hat{\sigma}_y, \hat{\sigma}_z\}$. In other words, let us suppose that the experimenter is able to produce independent magnetic fields along two orthogonal directions only, say x and z. The ansatz form of the ecd control Hamiltonian is

$$H_{\text{ecd}}(t) = u_x(t)\hat{\sigma}_x + u_z(t)\hat{\sigma}_z. \tag{4.32}$$

For a Hamiltonian with this structure, the counterdiabatic field has the form $H_{\text{cd}}(t) = f_{\text{cd}}(t)\hat{\sigma}_y$, as discussed in Section 2.3. The Hamiltonian of equation (4.32), with the choice of functions (4.29), produces the following first-order average Hamiltonian, using equation (4.31),

$$H_{\text{eff}}^{(1)} = \frac{1}{\omega}\sum_{n>0}\frac{1}{n}\left(s_{x,n}c_{z,n} - c_{x,n}s_{z,n}\right)\hat{\sigma}_y. \tag{4.33}$$

It is thus evident that the first-order effective Hamiltonian has already the desired $\hat{\sigma}_y$ structure. Then, we need to equate the corresponding coefficients

$$\frac{1}{\omega}\sum_{n>0}\frac{1}{n}\left(s_{x,n}c_{z,n} - c_{x,n}s_{z,n}\right) = \frac{1}{T}\int_0^T f_{\text{cd}}(t)dt. \tag{4.34}$$

Since this is obtained by truncating the Magnus expansion of $H_{\mathrm{ecd}}(t)$ to order T, for comparing the average Hamiltonian H_{eff} with $H_{\mathrm{cd}}(t)$ order by order we also formally expand $H_{\mathrm{cd}}(t)$ in Taylor series for small T. This translates into expanding $f_{\mathrm{cd}}(t)$. In particular, it is technically convenient to expand $f_{\mathrm{cd}}(t)$ around the midpoint of the integration interval and then integrate term by term. This produces a higher level of approximation [$O(T^3)$] as compared to expanding at the end of the period [$O(T^2)$], due to time symmetry with respect to the integration period. Indeed,

$$\int_0^T dt f_{\mathrm{cd}}(t) = \sum_{n=0}^{\infty} \frac{1}{n!} \left.\frac{d^n f_{\mathrm{cd}}(t)}{dt^n}\right|_{t=T/2} \int_0^T dt \left(t - \frac{T}{2}\right)^n, \tag{4.35a}$$

$$= \sum_{n=0}^{\infty} \frac{1}{(2n+1)!} \left.\frac{d^{2n} f_{\mathrm{cd}}(t)}{dt^{2n}}\right|_{t=T/2} \left(\frac{T}{2}\right)^{2n+1}. \tag{4.35b}$$

Then, asking $H_{\mathrm{eff}}^{(1)}$ to be equal to H_{cd} to first order in T implies the following equation for the field amplitudes

$$-\frac{1}{\omega} \sum_{n=1}^{L} \frac{1}{n} \left(s_{x,n} c_{z,n} - c_{x,n} s_{z,n}\right) = f_{\mathrm{cd}}(T/2), \tag{4.36}$$

which gives

$$\sum_{n=1}^{L} \frac{1}{n} \left(s_{x,n} c_{z,n} - c_{x,n} s_{z,n}\right) = -\omega f_{\mathrm{cd}}(T/2). \tag{4.37}$$

A fundamental point which is evident from equation (4.37) is that, for the equality to be satisfied, the amplitudes need to be proportional to some power of ω, in such a way that their product is exactly proportional to ω. The reason for this is clear: while the counterdiabatic Hamiltonian H_{cd} acts at first order in ω^{-1} in its Magnus exponent, the average Hamiltonian $H_{\mathrm{eff}}^{(2)}$ comes into play at second order. Therefore, in order to have the dynamics produced by H_{eff} to be playing on exactly the same timescale as that produced by $H_{\mathrm{cd}}(t)$, the strength of the Hamiltonian H_{eff} need to be amplified by a factor ω. This can be somehow interpreted as realizing a "real-time" simulation of $H_{\mathrm{cd}}(t)$. However, the proportionality of the amplitudes to ω must be handled with great care. Indeed, if the strength of the Hamiltonian gets comparable with the perturbative parameter ω^{-1}, problems may arise with the Magnus expansion. This, for a start, may no longer converge, making the whole construction break down. More subtle effects can happen instead when only a subpart of H_{eff} is multiplied by some positive power of ω (e.g., just the $\hat{\sigma}_z$ in equation (4.32) term), as discussed in Section 3.2. If that is the case, the numbering of the Magnus addends may no more coincide with the corresponding order in T: some terms with the same order in T may appear inside different Magnus terms, so a truncation would no more be possible. In general, this issues should be treated by finding an appropriate interaction picture. This permits to formally re-sum all elements in the Magnus expansion with the same perturbative order.

Let us now simplify the problem by considering only one single harmonic, and by considering that only one oscillating function is used along each direction. Specifically, we choose $c_{k,n>1} = s_{k,n>1} = 0$ and $c_{z,1} = s_{x,1} = 0$. The control functions are now $u_x(t) = c_x \cos(\omega t)$ and $u_z(s) = s_z \sin \omega t$. Equation (4.37) then simplifies to

$$s_z c_x = \omega f_{\text{cd}}(T/2). \tag{4.38}$$

If we assume that $f_{\text{cd}}(t)$ is positive for all times t, then a possible solution of equation (4.38) is

$$s_z = c_x = \sqrt{\omega f_{\text{cd}}(T/2)}. \tag{4.39}$$

It is now straightforward to extend the solution to all periods: indeed, the method remains first-order in $1/\omega$ if we simply substitute $f_{\text{cd}}(T/2) \to f_{\text{cd}}(t)$. Finally, the corresponding effective counterdiabatic field is then

$$H_{\text{ecd}}(t) = \sqrt{\omega f_{\text{cd}}(t)}[\cos \omega t \hat{\sigma}_x + \sin \omega t \hat{\sigma}_z]. \tag{4.40}$$

4.2.2 Two-level LZMS problems

Let us consider the Landau-Zener-Majorana-Stückelberg (LZMS) model described in Section 2.4. This problem follows under the class treated in the previous Section, with the only caveat that, in this case, the profile of the cd field $f_{\text{cd}}(t)$, given in equation (2.74), is always negative for all times. Introducing the variable $s = (t - t_i)/t_f$, where t_i and t_f are the initial and final times, the Schrödinger equation, in dimensionless units, reads

$$i\frac{\partial U(s)}{\partial s} = \tau_\Omega [H_{\text{LZMS}}(s) + H_{\text{ecd}}(s)] U(s), \tag{4.41}$$

with τ_Ω defined before equation (2.71), $H_{\text{LZMS}}(s)$ as in equation (2.72) and $H_{\text{ecd}}(s)$ to be defined below. Using the results of Section 4.2.1, we take, as a solution of equation (4.38), the choice

$$c_x = -s_z = -\sqrt{\omega |f_{\text{cd}}(s)|}, \tag{4.42}$$

with $f_{\text{cd}}(s)$ given in equation (2.74) and where now ω is dimensionless. The resulting ecd Hamiltonian is then

$$H_{\text{ecd}}(s) = \sqrt{\omega |f_{\text{cd}}(s)|}[-\cos(\omega \tau_\Omega s)\hat{\sigma}_x + \sin(\omega \tau_\Omega s)\hat{\sigma}_z]. \tag{4.43}$$

The dynamics produced by this Hamiltonian is compared with the actual adiabatic dynamics in Figure 4.3. In this Figure, the evolution of the populations and of the instantaneous infidelity is shown, for the system initially prepared in the ground state. These results are obtained using the parameters $\lambda_\Omega = 20$, $\tau_\Omega = 20$, $\omega = 15$. As expected, the dynamics oscillates quickly around the target one, remaining

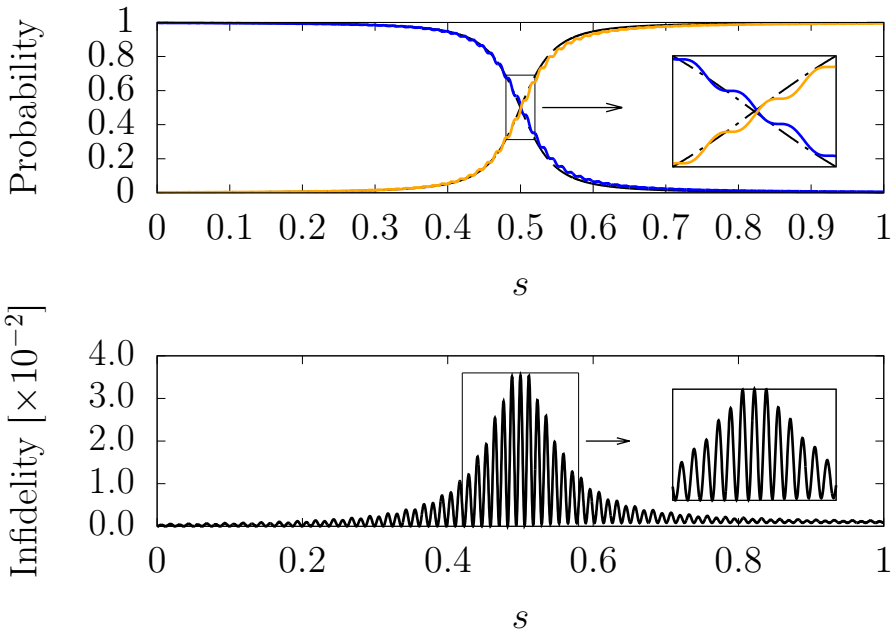

Figure 4.3: Effective counterdiabatic driving for the LZMS problem. The upper panel represents the evolution of the populations of states $|0\rangle$ (—) and $|1\rangle$ (—), with the system initialized in the instantaneous ground state (which almost coincides with $|0\rangle$) at time $s = 0$. In the lower panel, the evolution of the instantaneous probability of nonadiabatic transitions is depicted, which represents the deviation of the evolving system state from the instantaneous ground state. The inset highlights the rapidly oscillating character of the micromotion. The parameters used, in relation to equations (2.71), (2.72) and (4.43), are $\lambda_\Omega = 20$, $\tau_\Omega = 20$, $\omega = 15$. (Figure reproduced from [124])

always close. The envelope of the infidelity is proportional to $f_{\mathrm{cd}}(s)$ and exhibits thus a peak at the crossing time, while tending to zero at the beginning and at the end of the protocol. The latter effect is important, since it implies that errors due to the oscillation patterns get negligible when the sweep is complete.

4.3 FURTHER EXAMPLES

4.3.1 Three-level avoided crossings

Let us now construct an effective counterdiabatic field for the problem described in Section (2.5), involving a sequence of avoided crossings in a three-level system. For

this purpose, we start by choosing the following ansatz for the structure of the ecd Hamiltonian,

$$H_{\text{ecd}}(t) = \sqrt{\omega} \begin{pmatrix} u_3(t) & u_1(t) & 0 \\ u_1(t) & 0 & u_2(t) \\ 0 & u_2(t) & -u_3(t) \end{pmatrix}. \tag{4.44}$$

This Hamiltonian can be written more compactly in terms of the following Gell-mann matrices,

$$\hat{\lambda}_1 = \begin{pmatrix} 0 & 1 & 0 \\ 1 & 0 & 0 \\ 0 & 0 & 0 \end{pmatrix}, \qquad \hat{\lambda}_3 = \begin{pmatrix} 1 & 0 & 0 \\ 0 & -1 & 0 \\ 0 & 0 & 0 \end{pmatrix}, \tag{4.45}$$

$$\hat{\lambda}_6 = \begin{pmatrix} 0 & 0 & 0 \\ 0 & 0 & 1 \\ 0 & 1 & 0 \end{pmatrix}, \qquad \hat{\lambda}_8 = \frac{1}{\sqrt{3}} \begin{pmatrix} 1 & 0 & 0 \\ 0 & 1 & 0 \\ 0 & 0 & -2 \end{pmatrix}, \tag{4.46}$$

becoming

$$H_{\text{eff}}(t) = \sqrt{\omega} \left[u_1(t)\hat{\lambda}_1 + u_2(t)\hat{\lambda}_6 + u_3(t)\hat{S}_z) \right], \tag{4.47}$$

where $\hat{S}_z = (\hat{\lambda}_3 + \sqrt{3}\hat{\lambda}_8)/2$ is the spin-1 operator along z. Concerning the control functions, we make a choice which gives easily solvable constraint equations, namely we take

$$u_1(t) = c_{1,1}(t)\cos(\omega t) - c_{1,2}(t)\cos(2\omega t), \tag{4.48a}$$
$$u_2(t) = s_{2,1}(t)\sin(\omega t) - c_{2,3}(t)\cos(3\omega t), \tag{4.48b}$$
$$u_3(t) = s_{3,2}(t)\sin(2\omega t) + s_{3,3}(t)\sin(3\omega t). \tag{4.48c}$$

The reasoning behind this choice goes as follows. The necessary matrix terms for realizing the cd Hamiltonian are the Gell-mann matrices $\hat{\lambda}_2$, $\hat{\lambda}_5$ and $\hat{\lambda}_7$. These can be obtained as single commutators of the initial control matrices, indeed

$$\hat{\lambda}_2 = i[\hat{\lambda}_1, \hat{S}_z]; \quad \hat{\lambda}_5 = i[\hat{\lambda}_6, \hat{S}_z]; \quad \hat{\lambda}_7 = i[\hat{\lambda}_6, \hat{\lambda}_1]. \tag{4.49}$$

Then, the results on the two-level problem gives us immediately a strategy for producing the commutator dynamics at first order in ω^{-1}. Moreover, from the general theory, one knows that different harmonics of the fundamental driving frequency ω do not "interact" in the first term: this is why we choose a different harmonic for each commutator in the control functions. With the choice (4.48), the first-order constraint equations for the oscillation amplitude are

$$\frac{1}{4}c_{1,2}s_{3,2} = -f_{\text{cd}}^{(12)}(T/2), \tag{4.50a}$$
$$\frac{1}{6}c_{2,3}s_{3,3} = -f_{\text{cd}}^{(23)}(T/2), \tag{4.50b}$$
$$\frac{1}{2}c_{1,1}s_{2,1} = -f_{\text{cd}}^{(13)}(T/2). \tag{4.50c}$$

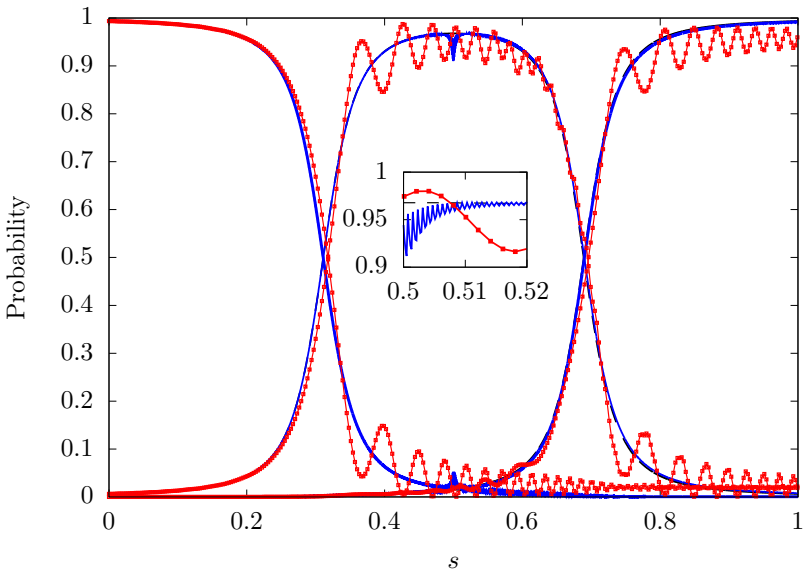

Figure 4.4: Effective counterdiabatic dynamics for a three-level system. The — line displays the ecd dynamics of the populations as a function of the rescaled time $s = t/t_f$. The populations stay always close to those of the adiabatic states with quick oscillations around it, as shown in the inset. The final infidelity is $\sim 10^{-4}$. This evolution is to be compared with the one produced by the simple LZMS-like sweep, represented with the —•— curve, which attains a final infidelity $\sim 10^{-2}$. (Figure reproduced from [124])

A possible solution, taking into account also the sign of the counterdiabatic functions, is

$$c_{1,1}(t) = -\mathrm{sgn}\left[f_{\mathrm{cd}}^{(13)}(t)\right]\sqrt{2|f_{\mathrm{cd}}^{(13)}(t)|}, \quad c_{1,2}(t) = s_{3,2}(t) = 2\sqrt{|f_{\mathrm{cd}}^{(12)}(t)|},$$
$$s_{2,1}(t) = \sqrt{2|f_{\mathrm{cd}}^{(13)}(t)|}, \quad c_{2,3}(t) = s_{3,3}(t) = \sqrt{6|f_{\mathrm{cd}}^{(23)}(t)|}, \tag{4.51}$$

where recall that the $f_{\mathrm{cd}}^{(ij)}(t)$ functions are determined numerically. The dynamics produced by the resulting ecd field is shown in Figure 4.4, for parameters $\tau_\Omega = 25$, $\lambda_\Omega = 40$, $d_\Omega = 5/2$. The solid blue line (—) represents the ecd evolution of the populations, as compared to the red curve (—•—) which represents the uncorrected dynamics. For a given final fidelity with these parameters, a speed up of around 2.5 times is attained.

4.3.2 Two-qubits entanglement

The power of quantum information processing is strongly connected to the manipulation of entanglement between single logical elements of a quantum computational architecture [122, 128]. Hence, since this is a hard task, the capability of producing entanglement is a central problem in quantum control.

In this section, we consider a prototypical system composed of two interacting qubits and we describe an adiabatic protocol for creating entanglement between

them. We then show how this protocol can be accelerated by using the effective conterdiabatic scheme developed in this Chapter. The Hamiltonian of the system is chosen as

$$H(s) = -B(s)\,[\hat{\sigma}_1^z + \hat{\sigma}_2^z] - g(s)\,[\hat{\sigma}_1^x\hat{\sigma}_2^x + \hat{\sigma}_1^z\hat{\sigma}_2^z]\,. \tag{4.52}$$

The variable $s \in [0,1]$ is the rescaled time t/t_f, where t_f is the total duration of the protocol. Accordingly, the Schrödinger equation is $i\partial_s U(s) = t_f H(s)U(s)$. The two qubits are thus driven by a latitudinal "magnetic" field $B(s)$, which modifies the energy gap of the bare qubits. Moreover, they are connected by an interaction of tunable strength $g(s)$. By rotating frame through the transformation $e^{i\pi/4[\hat{\sigma}_1^x+\hat{\sigma}_2^x]}$, we see that this interaction becomes $\hat{\sigma}_1^+\hat{\sigma}_2^- + \hat{\sigma}_1^-\hat{\sigma}_2^+$, i.e., it describes hopping of excitations between the rotated-frame basis vectors $[i\,|\psi_+\rangle \pm |\phi_-\rangle]/\sqrt{2}$ (up to global phases), where

$$|\psi_+\rangle = \frac{1}{\sqrt{2}}(|00\rangle + |11\rangle), \qquad |\phi_-\rangle = \frac{1}{\sqrt{2}}(|01\rangle - |10\rangle). \tag{4.53}$$

We identify, in the Hamiltonian of equation (4.52), the control matrices

$$H_1 = \hat{\sigma}_1^z + \hat{\sigma}_2^z, \tag{4.54a}$$
$$H_2 = \hat{\sigma}_1^x\hat{\sigma}_2^x + \hat{\sigma}_1^z\hat{\sigma}_2^z. \tag{4.54b}$$

When the local term H_1 is much stronger than the interaction H_2, that is, if $B \gg g$, then the system's eigenstates are tensor products of bare states of the two qubits. When the interaction is dominant instead, $g \gg B$, the eigenstates of the full Hamiltonian can be entangled states of the qubits. Therefore, an adiabatic evolution interpolating the first regime with the second one could be used to prepare the system in an entangled state. In particular, if one initially selects the separable state $|00\rangle$, this is adiabatically connected to the Bell state $(|00\rangle + |11\rangle)/\sqrt{2}$. For inspecting this scenario more in detail, we will assume a constant $g = 1$ interaction (this makes ε measured in units of $1/g$, and t_f measured in units of g), and an adiabatic linear ramp

$$B(s) = \varepsilon(1-s). \tag{4.55}$$

For constructing the ecd correcting Hamiltonian, we first need to determine the cd Hamiltonian. In this task, the results of Section 4.1 help us to find the matrix structure of $H_{\rm cd}(t)$. For a start, since $H_{\rm cd}(t)$ must be orthogonal to both $H(t)$ and the time derivative $\partial_t H(t)$ at all times, we find that $H_{\rm cd}(t)$ cannot have matrix components along H_1 and H_2. The control matrices $\{H_1, H_2\}$ generate a four-dimensional dynamical Lie algebra $\mathfrak{L}$ which is isomorphic to $\mathfrak{u}(2)$, the algebra of unitary two-by-two matrices. The other two basis elements can be taken to be:

$$H_3 = \hat{\sigma}_1^x\hat{\sigma}_2^y + \hat{\sigma}_1^y\hat{\sigma}_2^x, \tag{4.56a}$$
$$H_4 = \hat{\sigma}_1^x\hat{\sigma}_2^x - \hat{\sigma}_1^y\hat{\sigma}_2^y. \tag{4.56b}$$

Therefore, as it holds that $\mathfrak{L} \subset \mathfrak{su}(4)$ with strict sign, the system is not fully controllable. By Theorem 2, $H_{\rm cd}(t)$ must be searched within $\mathfrak{L}$ and thus one can conclude that it must be a combination of the remaining two basis elements of the Lie algebra, H_3 and H_4. For completing this analysis, we proceed in the explicit computation of $H_{\rm cd}(t)$. By means of an initial basis rotation, defined by the unitary

$$U_0 = |00\rangle\langle 00| + |\phi_+\rangle\langle 01| + |\phi_-\rangle\langle 10| + |11\rangle\langle 11|\,, \tag{4.57}$$

where $|\phi_+\rangle = (|01\rangle + |10\rangle)/\sqrt{2}$ and $|\phi_-\rangle$ is as in equation (4.53), it is possible to cast $H(s)$ in a partially-diagonalized form in which two levels are already decoupled from the remaining two. This is

$$U_0^\dagger H(s) U_0 = \begin{pmatrix} -1+2\varepsilon(s-1) & 0 & 0 & -1 \\ 0 & 0 & 0 & 0 \\ 0 & 0 & 2 & 0 \\ -1 & 0 & 0 & -1-2\varepsilon(s-1) \end{pmatrix}. \tag{4.58}$$

The two-by-two matrix defined by the four non-zero off-diagonal elements of equation (4.58) can then be diagonalized with another unitary $U_1(s)$. In conclusion, the overall diagonalizing matrix is $U(s) = U_1(s)U_0$ and the counterdiabatic field, using equation (2.5) and (2.61), is

$$H_{\rm cd}(s) = f_{\rm cd}(s) H_3, \tag{4.59}$$

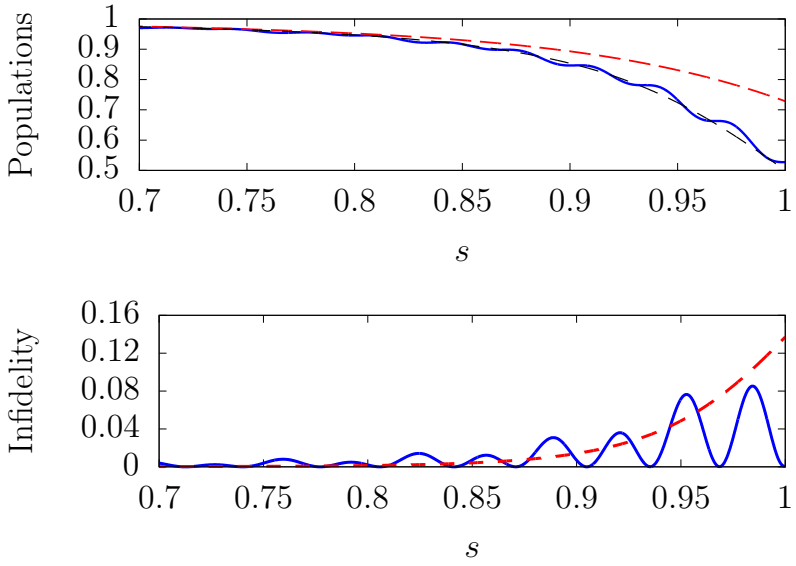

Figure 4.5: Two-qubit entanglement: populations and infidelity. In the top panel, the evolution of the occupation probability of the bare state $|00\rangle$ is depicted for the linear-ramp adiabatic sweep (- - -) and for the ecd protocol (—). The - - - indicates the exact adiabatic evolution. The lower panel is dedicated to the evolution of the infidelity between the system state and the instantaneous adiabatic state. (Figure reproduced from [124])

with

$$f_{\mathrm{cd}}(s) = \frac{1}{2t_f}\frac{\varepsilon}{1+4\varepsilon^2(s-1)^2}. \tag{4.60}$$

The counterdiabatic Hamiltonian (4.59) physically describes simultaneous excitation or de-excitation of the two qubits (as more evident by rewriting H_3 in the form $H_3 = -2i[\hat{\sigma}_1^- \hat{\sigma}_2^- + \hat{\sigma}_1^+ \hat{\sigma}_2^+]$). Moreover, it can be obtained from the commutator of the initial control matrices,

$$H_3 = 2i[H_1, H_2]. \tag{4.61}$$

Then, we now have all the elements to construct an ecd field. Indeed, proceeding as in Section 4.2.1, one obtains the ecd Hamiltonian

$$H_{\mathrm{ecd}}(s) = \sqrt{|f_{\mathrm{cd}}(s)|\omega}\left[-\cos(\omega s t_f)H_1 + \sin(\omega s t_f)H_2\right]. \tag{4.62}$$

By integrating the initial adiabatic driving with this correcting Hamiltonian, the adiabatic state transfer producing the entangled state can be greatly accelerated for a fixed target fidelity. For instance, using parameters $\varepsilon = 5$, $t_f = 5$, $\omega t_f = 20\pi$ and constraining the maximal strength of the ecd Hamiltonian to $\mathcal{S}(H_{\mathrm{ecd}}) \leq \mathcal{S}(H)/2$ [see the definition of strength $\mathcal{S}(\cdot)$ in equation (4.63)], one obtains an infidelity of 0.017. The evolution of the infidelity and of the population of state $|00\rangle$ for this example is shown in Figure 4.5. The same infidelity would be achieved by the adiabatic linear sweep in 12 times the same total duration.

4.4 COMPARISON WITH THE ADIABATIC APPROXIMATION

In order to further characterize the performance of the ecd method, it is interesting to compare its efficiency with that of the standard adiabatic approximation, with a focus on the resources used by the two protocols. In particular, it can be easily seen from the Schrödinger equation that a dilation of the total time can always be traded for a rescaling of the Hamiltonian. That is, the evolution time can be halved by doubling the "strength" of the Hamiltonian. Hence, a proper comparison of the temporal performance of two control protocols should be operated for fixed total "strength" of the involved control Hamiltonians. Here, we will use a general definition of the "strength" for performing this study, although the analysis can be tailored to more specific experimental constraints. The definition we use is the following,

$$\mathcal{S}(H_x) = \max_t \|H_x(t)\| \tag{4.63}$$

where $\|M\| = \mathrm{tr}\left[MM^\dagger\right]$ is the Frobenius norm. We then study the final infidelity attained by the protocols, in the case of the LZMS problem, as a function of the total duration τ_Ω, and for a fixed ratio of the corresponding strengths— namely, we impose the constraint

$$\mathcal{S}(H_{\mathrm{ecd}}) \leq k\mathcal{S}(H) \tag{4.64}$$

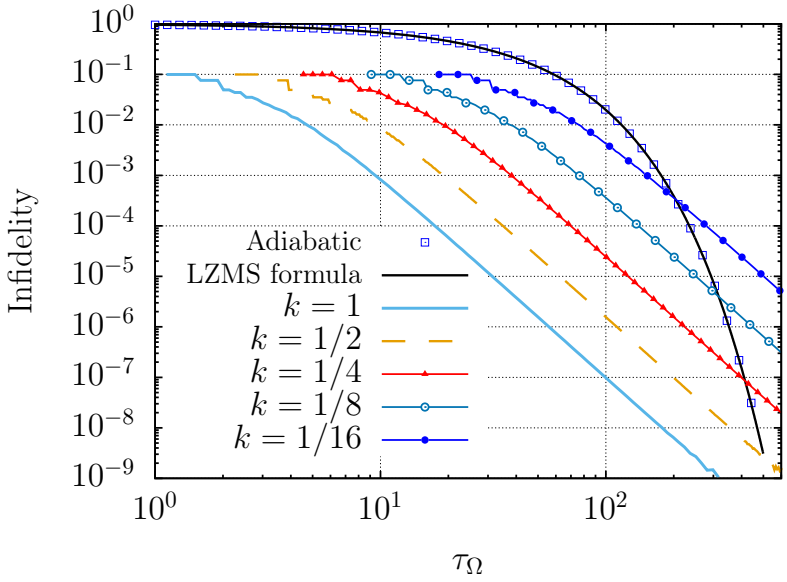

Figure 4.6: Comparison between ecd method and adiabatic approximation $\mathbf{1} - H_{\mathbf{ecd}}(t)$ alone. Log-log plot of the final protocol infidelity as a function of the total duration τ for a LZMS problem. The (□) squares represent the LZMS adiabatic (uncorrected) method, which is well described by the LZMS formula (2.70) [—]. Each other curve corresponds to the ecd approach for different ratios k between the strength of the ecd Hamiltonian and the LZMS Hamiltonian, as defined in equation (4.64). (Figure adapted from [124])

for different ratios k. For the case in which $H_{\text{ecd}}(t)$ as a standalone shortcut (and not $H(t) + H_{\text{ecd}}(t)$) is used, the results are shown in Figure 4.6. The exponential decay of the infidelity given by the LZMS driving is immediately evident, with the numerical data (□) well interpolated by the LZMS formula (2.70) (—). As predictable from the fact the ecd method is built upon a perturbative construction in large driving frequency, the decay in the infidelity for such a protocol is polynomial instead. As a consequence, when the adiabatic limit is well satisfied, the standard adiabatic method gives the best results. Crucially though, this is not the case for intermediate-range timescales, where the ecd method gives much higher fidelities at given durations. For instance, an ecd Hamiltonian with the same strength of the LZMS one [$k = 1$ in equation (4.64)] achieves fidelity 0.999 around twenty times faster than the adiabatic dynamics. Using less intense ecd Hamiltonians still produces consistent speed ups: for $k = 1/4$, a fidelity of 0.9999 requires a total time which is almost three times shorter than that needed using the LZMS sweep. Next, we consider the situation in which $H_{\text{ecd}}(t)$ is used as an adiabaticity-assisting term, rather than as a full shortcut—i.e., the total applied Hamiltonian is $H(t) + H_{\text{ecd}}(t)$. The corresponding results are displayed in Figure 4.7. Since the infidelity exhibits a fast varying behavior for different τ_Ω (—), the individual points shown represent an average of twenty surrounding points. For fixed ratio k, an initial temporal region emerges in which the ecd correction is not strong enough for efficiently canceling nonadiabatic transitions as wished. For larger durations, the infidelity behavior is

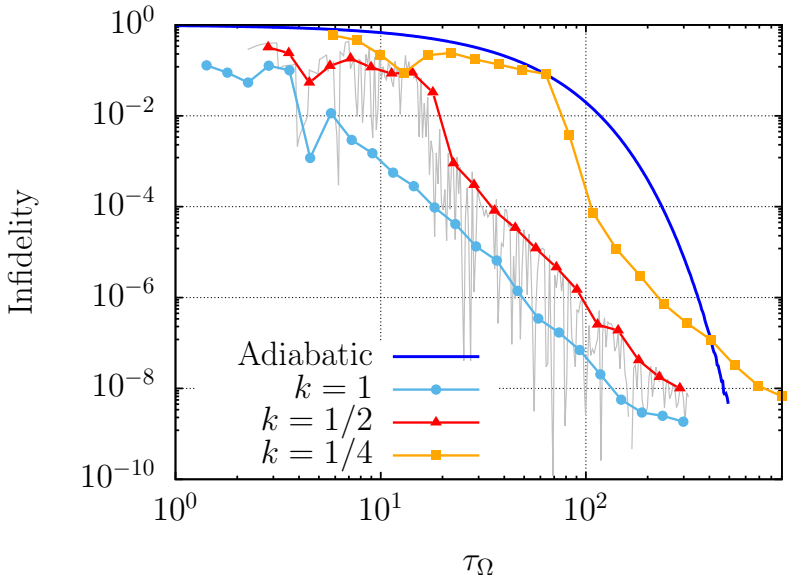

Figure 4.7: Comparison between ecd method and adiabatic approximation 2 – $H(t) + H_{\mathbf{ecd}}(t)$. Final infidelity, in log-log scale, for the application of the total shortcut Hamiltonian $H(t) + H_{\text{ecd}}(t)$, as a function of the total duration, for different strength of the correcting Hamiltonian (different ratios k in equation (4.64)). The — curve represents the standard adiabatic LZM protocol. (Figure adapted from [124])

similar to the one in Figure 4.6: a power-law decay which reaches smaller infidelities with respect to the adiabatic case. One can see that, even with rather weak ecd corrections, a great improvement is achieved. For instance, a correction with half the strength of the original Hamiltonian [$k = 1/2$ in equation (4.64)] produces a fidelity of 0.9999 with a speed up of around seven times, while a $k = 1/4$ correction needs less than a half the total time required by the LZMS sweep, for the same final fidelity. As a final analysis, we investigate the final infidelity obtained as a function of a different characterization of the strength. More specifically, we now take a fixed total duration equal to one and we study the infidelity produced by (i) the amplified Hamiltonian $\tau_\Omega H(t)$ when raising τ_Ω, and (ii) the Hamiltonian $H_{\text{ecd}}(t)$ when raising the driving frequency ω. As a figure of merit for the comparison, we take

$$\int_0^1 ds \, \|H_X(s)\| \,, \tag{4.65}$$

where the norm is chosen to be the Frobenius norm. The quantity in equation (4.65) can be understood, to a certain extent, as a measure of the total area of the control pulses. In this respect, it may be interpreted physically as the total amount of energy injected into the system by the driving. Moreover, it is connected to definitions of intrinsic quantum speed limits [94]. In Figure 4.8, the final infidelity as a function of the quantity in equation (4.65) is represented. We find a similar behavior as recognizable from Figure 4.7, with the curve representing the ecd method (—) decaying like a power law. The curve is always well below the curve corresponding

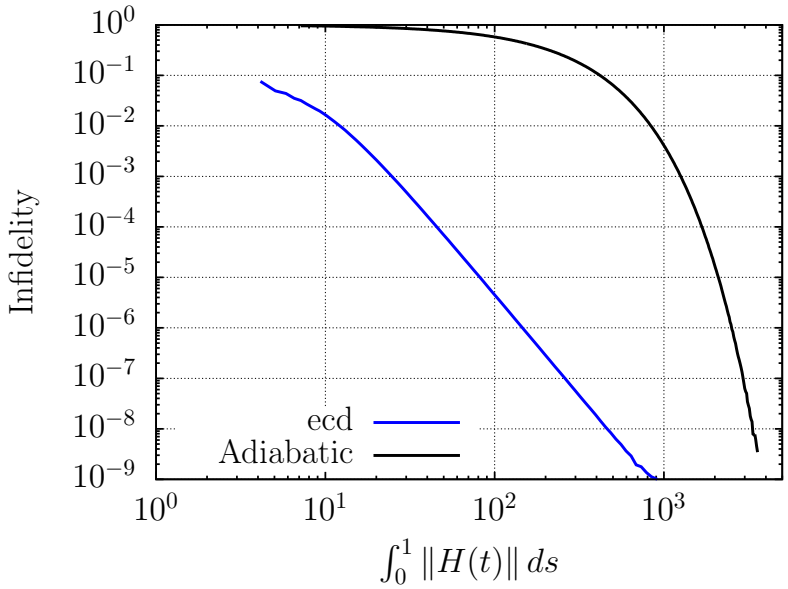

Figure 4.8: Performance vs generalized pulse area for the control Hamiltonians. Final infidelity as a function of the generalized pulse area defined in equation (4.65) for the ecd protocol (—), and for standard LZMS (—). (Figure adapted from [124])

to the adiabatic dynamics (—) within the region considered, proving that our protocol is efficient also with respect to the energetic resources used.

4.5 ROBUSTNESS AGAINST PHASE IMPERFECTIONS

In the procedure for constructing the effective counterdiabatic scheme, we assumed up to now that the oscillating fields have specific fixed phases. From the experimental point of view, it is extremely important to better characterize what is the response of the protocol to potential imperfections in these phases. Indeed, perfect phase relations are often challenging to be attained in the lab, and the experimenter might be suspicious on the practical performance of the ecd protocol. For this reason, in all the applications of the method to specific experimental problems which are discussed in Part iii, an *ad hoc* analysis is dedicated to the sensitivity of the protocol on phase errors in the control fields. Before treating these specific cases, in this Section we first discuss the problem from a general perspective.

4.5.1 Global phases

If a global phase $\phi \in [0, 2\pi)$ is added to all the control fields, it can always be reinterpreted as a variation in the choice of the initial time t_0 in the Magnus expansion. Indeed, if we consider the transformation $\omega t \longrightarrow \omega t + \phi$, where $\omega =$

$2\pi/T$ is the driving frequency, a change of integration variable in the Magnus expansion, equation (3.14), would produce a shift of the initial time

$$t_0 \longrightarrow t_0' = t_0 + \phi/\omega. \tag{4.66}$$

This in turn leads to a different effective stroboscopic Hamiltonian, which is unitarily equivalent to the initial one. In fact, one can notice that the stroboscopic propagator, given the new initial time $t_0' > t_0$, can always be related to the original one through the decomposition

$$U(T + t_0', t_0') = U(T + t_0', T + t_0)U(T + t_0, t_0)U^\dagger(t_0', t_0). \tag{4.67}$$

Due the periodicity of $U(t)$, $U(T + t) = U(t)$, this is equivalent to

$$U(T + t_0', t_0') = U(t_0', t_0)U(T + t_0, t_0)U^\dagger(t_0', t_0). \tag{4.68}$$

By writing the propagators $U(T + t_0', t_0')$ and $U(T + t_0, t_0)$ as exponentials, and using the fact that $U(t)e^{-iHt}U^\dagger(t) = e^{-itU(t)HU^\dagger(t)}$, we find

$$e^{-iTH_{\text{eff}}[t_0']} = e^{-iTU(t_0', t_0)H_{\text{eff}}[t_0]U^\dagger(t_0', t_0)}, \tag{4.69}$$

which confirms that the two effective Hamiltonians are related to each other by a unitary transformation,

$$H_{\text{eff}}[t_0'] = U(t_0', t_0)H_{\text{eff}}[t_0]U^\dagger(t_0', t_0). \tag{4.70}$$

Therefore, one can predict that the variation of the global phase may lead to undesired effective Hamiltonians, and consequently to the generation of evolutions which are different from what one sought. Nonetheless, one can see that the correction to the initial time induced by the variations of phase, see equation (4.66), decays like $1/\omega$. For very large driving frequency, the effective Hamiltonians tend to be the same.

Let us elaborate on this point for case of the ecd Hamiltonian. In all the examples we have seen so far, the matrix structure of the counterdiabatic Hamiltonian is achievable by means of a single commutator of some of the control Hamiltonians. Therefore, the desired matrix structure typically appears in the first-order term in the exponent of the Floquet-Magnus expansion (3.18b). From equation (3.18b) we see that such a term is produced by the "interaction" of Fourier components of the Hamiltonian at opposite frequencies, H_k and H_{-k}, and their interaction with the non-oscillating component H_0. By inspection of equation (3.18b), we see that, since the ecd Hamiltonian does not have any zero-frequency component, the dependence on the initial time t_0, and thus on the global phase, disappears from the first-order term. However, even if $H_0 = 0$, from equation (3.18c) we see that at the following order some t_0-dependent term still survives. Recalling that each Fourier component is proportional to $\sqrt{\omega}$ for these examples, we can conclude that variations of the global phase of the fields produce an error of $O(\omega^{-1/2})$ in the effective counterdiabatic Hamiltonian, which can be neglected consistently with the

initial level of approximation (in which $H_{\text{eff}}^{(2)}$ and the following terms are neglected). Hence, if the frequency is large enough for the scheme to work in the absence of imperfections in the global phase, then one should not expect substantial losses of performance if such imperfections are present.

4.5.2 Relative phases

Let us now discuss the effect of hypothetical errors in the relative phase among the different Fourier components. Again, let us focus on the case in which the matrix structure of $H_{\text{cd}}(t)$ appears at the first-order term in the Floquet-Magnus expansion.

From equation (3.18b), we see that phase offsets can have an effect at this level only if they take place between Fourier components with exactly opposite frequency. If this is not the case, then the error shows up at the following order and can be neglected as discussed for global phases. If it is the case instead, one should expect that the deviation from the desired effective Hamiltonian scales linearly with the phase offset which, in turn, translates into a quadratic dependence in the fidelity. Indeed, say that H_k and H_{-k} are shifted in phase by $\delta\phi$. Then, equation (3.18b) for small $\delta\phi$ would become

$$H_{\text{eff}}^{(1)} = \sum_{m=1}^{\infty} \frac{[H_{-m}, H_m]}{m\omega} e^{-im\delta\phi} \simeq \sum_{m=1}^{\infty} \frac{[H_{-m}, H_m]}{m\omega} + O(\delta\phi). \tag{4.71}$$

We thus see that the method is more sensitive to errors in the relative, rather than global, phase of the fields, provided these affect opposite-frequency Fourier components of the ecd Hamiltonian.

Let us now discuss these aspects more in detail with the help of a specific example.

4.5.3 A case study

The general discussion of Sections 4.5.1 and 4.5.2 has shown that the effective counterdiabatic construction is in general not much sensitive to errors in the global phase of the modulations, while it should suffer more from potential errors in the relative phase. Here we will make a quantitative analysis of these effects, using as a test ground the reference model of a two-level system. Specifically, let us consider the two-level problem described by the Hamiltonian

$$H(t) = \lambda(t)\hat{\sigma}_z + x_0\hat{\sigma}_x, \tag{4.72}$$

with the locally adiabatic sweep function $\lambda(t)$ derived in Section 2.2.1.2, equation (2.52), which varies from an initial value λ_0 to zero in a total time $t_f = 1$. Let us then consider the effective counterdiabatic field derived in Section 4.2.1,

$$H_{\text{ecd}}(t) = u_x(t)\hat{\sigma}_x + u_z(t)\hat{\sigma}_z, \tag{4.73}$$

where we also introduce phase shifts ϕ_g (global) and ϕ_r (relative) in the control functions, which then read

$$u_x(t) = X\sqrt{\omega}\cos(\omega t + \phi_g + \phi_r); \qquad u_z(s) = Z\sqrt{\omega}\sin(\omega t + \phi_g). \tag{4.74}$$

Let us denote with η_T the nonadiabatic coupling between the two instantaneous eigenvectors at time $T/2$, namely

$$\eta_T = \langle 0_t|\partial_t 1_t\rangle|_{t=T/2} = \left.\frac{\langle 0_t|\,\partial_t H(t)\,|1_t\rangle}{E_0(t) - E_1(t)}\right|_{t=T/2}. \tag{4.75}$$

In Appendix A, we derive the following expansion of the infidelity $\mathbb{I}_T$ at the end of the first period, up to order T^3,

$$\begin{aligned}\mathbb{I}_T = \eta^2(1-\cos\phi_r)^2T^2 + \frac{2}{\pi}\Big\{&(X\lambda\sin(\phi_g+\phi_r) + Zx_0\cos\phi_g)^2 \\ &+ \frac{\eta_T^2}{x_0^2+\lambda^2}\cos^2\phi_r\left(Xx_0\sin(\phi_g+\phi_r) - Z\lambda\cos\phi_g\right)^2\Big\}T^3.\end{aligned} \tag{4.76}$$

This expression allows us to grasp how the presence of the phases ϕ_g and ϕ_r affects the performance of the quantum control protocol.

Let us first analyze the dominant term which, in the limit of small T, is responsible for the global behavior of the infidelity when varying the relative phase ϕ_r. This term reaches its minimum when $\phi_r = 0$, in which case it vanishes. This corresponds to the choice of perfect $\pi/2$ phase offset between the control fields, as obtained in Sections 4.2.1 and 4.2.2. On the other hand, the term becomes maximal when the two control fields have a phase offset $\phi_r = \pi$. Let us remark that it is also symmetric with respect to the sign of ϕ_r. This implies that, if higher-order terms are negligible, values of ϕ_r different from zero always reduce the fidelity, $\mathbb{I}_T(\phi_r) \geq \mathbb{I}_T(0)$. It is then interesting to proceed analyzing the following term in equation (4.76). Unless $\phi_g + \phi_r = 0$, one can see that terms $\sin\phi_r$ are present, which make it asymmetric with respect to the sign of ϕ_r. Crucially, when ϕ_r is small, one can expect that some values exist for which the two terms in equation (4.76) compensate one another, leading to larger fidelities accidentally, as compared to the $\phi_r = 0$ case. A second important aspect is the explicit dependence on ϕ_g, which we can investigate by setting $\phi_r = 0$. What one learns from this is that, even though the relative phase is fixed, the global phase can be exploited to further minimize the infidelity. Finally, if ϕ_r becomes so small to be comparable with T, then the expression of equation (4.76) is not a useful perturbation expansion any more, since higher order terms might be larger than those at order T^2 and T^3 which are considered. Hence, one cannot predict in detail the behavior of the infidelity in this regime.

For exploring these properties in a quantitative manner, we resort to numerical tools, referring to the specific example of an avoided crossing problem (see Sec 2.4). In particular, we consider the effective counterdiabatic Hamiltonian of equation (4.40), with the locally adiabatic sweep function of equation (2.52). In the case of perfect phase relation ($\phi_r = 0$ in equation (4.74)), the evolution of the infidelity is shown in Figure 4.9, where the dynamics is also represented on the Bloch sphere.

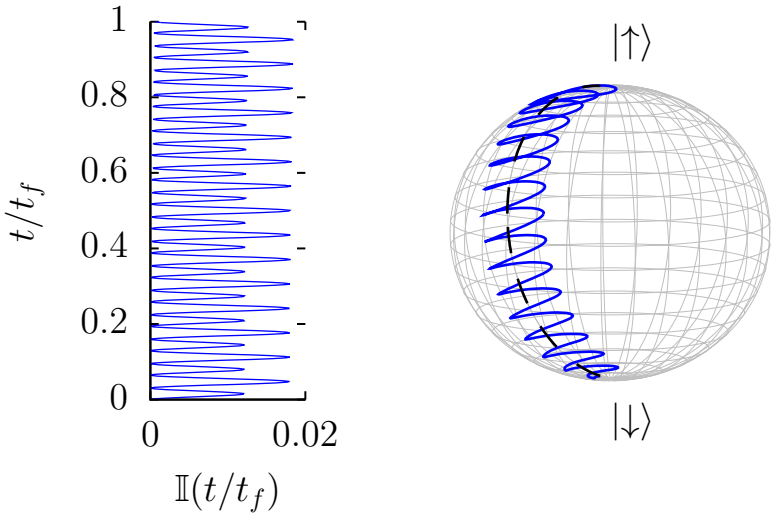

Figure 4.9: Effective counterdiabatic evolution of a two-level system. In the right panel, the evolution of the driven system is depicted on the Bloch sphere (—), where the black dashed line (- - -) represents the exact adiabatic path. The evolution of the infidelity for the same process can then be seen from the left panel, where time increases vertically. The parameters used are $\lambda_0 = 10$, $g = x_0 = 1$, $t_f = 1$, $\omega/2\pi = 15$. (Figure reproduced from [123])

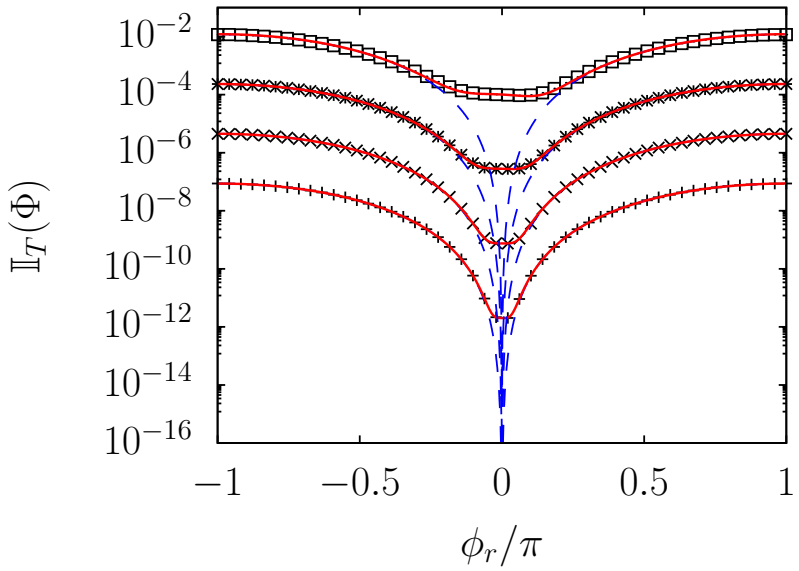

Figure 4.10: Infidelity vs relative phase offset between the control fields, see equation (4.74), in units of π. The symbols represent numerical results obtained for different time steps T, namely $T = 10^{-4}$ (+), 7×10^{-4} (×), 5×10^{-3} (∗), 4×10^{-2} (□). The blue dashed line (- - -) is produced from the first term of equation (4.76), while the red solid lines (—) are produced using all terms in (4.76). (Figure adapted from Ref. [123])

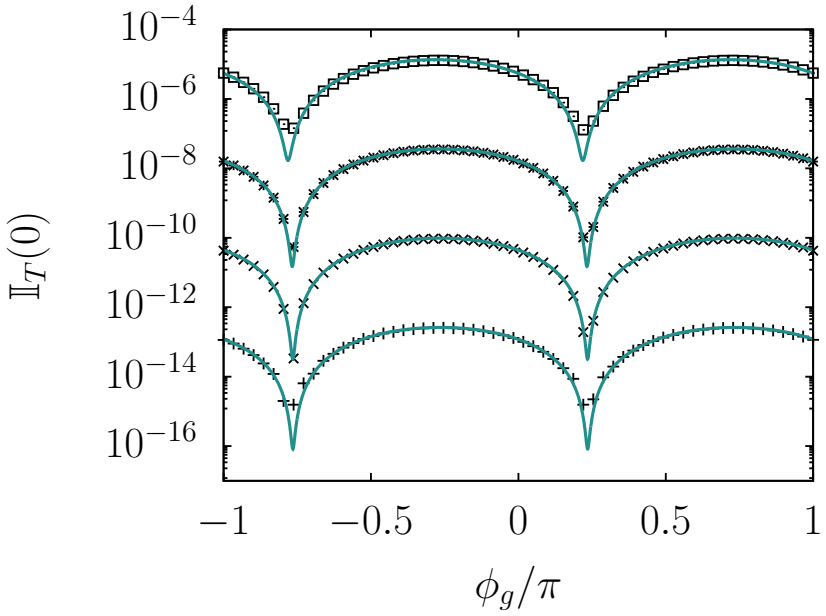

Figure 4.11: Dependence on the global phase. Infidelity at the end of one modulation period T, for zero relative phase ϕ_r between the control fields, as a function of the global phase, for different values of the period, namely $T = 10^{-4}$ (+), 7×10^{-4} (×), 5×10^{-3} (∗), 4×10^{-2} (□). The — curve represents the theoretical predictions according to equation (4.76) (Figure adapted from Ref. [123])

From Figure 4.10 we show that the first term of equation (4.76) describes very well the behaviour of the infidelity when a rather large relative phase offset $-\pi \leq \phi_r \leq \pi$ is present (with $\phi_g + \phi_r$ fixed to zero). For inspecting how the method is sensitive to this offset, and for highlighting the region close to zero, we report in this figure the values of the infidelity in semi-logarithmic scale, for different values of the time step T. The symbols represent numerical data, the blue dashed curves (- - -) are the prediction given by the first term in equation (4.76), whilst the red lines (—) are produced by considering all terms in equation (4.76). First of all, we point out that choosing $\phi_r \simeq \pm\pi$ can lead to a decrease in fidelity of more than two order of magnitude, and this effect is more stressed as the period T is diminished. While the leading-order term in (4.76) is a good description far from zero, it completely deviates from the numerical values in the vicinity of zero. This regime is well-captured instead by the following-order term.

The dependence of the infidelity on the global phase is depicted in Figure 4.11, by considering $\phi_r = 0$, which cancel the leading-order term of equation (4.76). Also in this case, the second term of (4.76) provides a good description. The asymmetry of such a term with respect to the sign of the global phase shift is reflected in the infidelity, which is not symmetric with respect to ϕ_g. Remarkably, minima in the infidelity do not actually lie at $\phi_g = 0$. It has been tested numerically that optimizing this values can produce an improvement up to one order of magnitude in the fidelity at the end of the whole protocol.

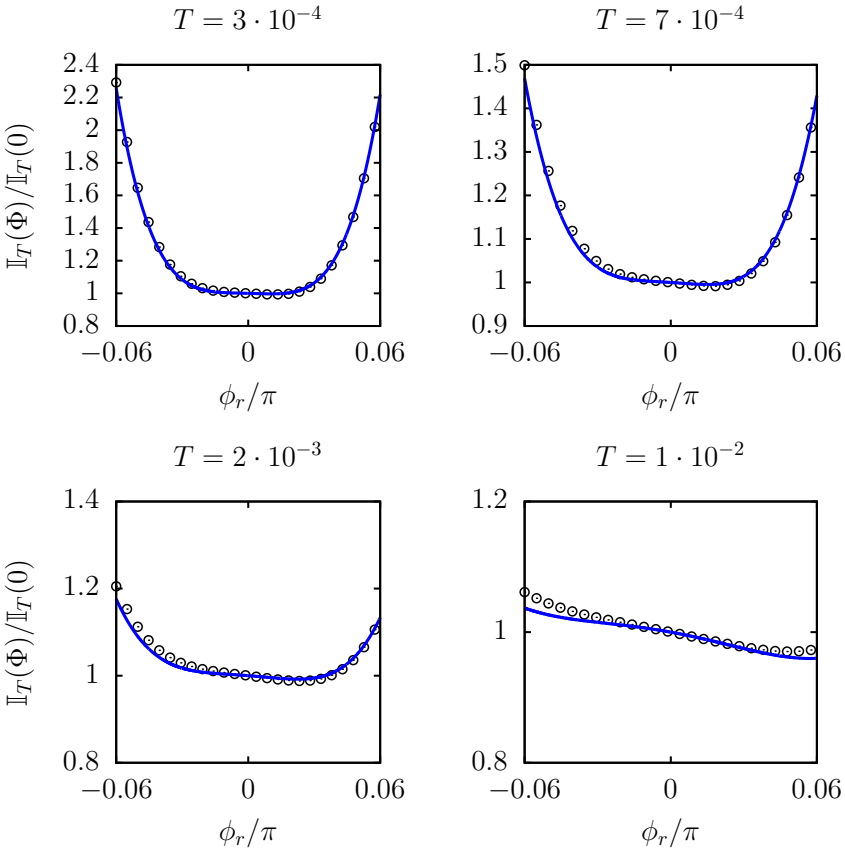

Figure 4.12: Ratio between the infidelity in the presence of relative phase shifts and the unperturbed value. Different panels correspond to different driving periods T. The symbols (○) indicate numerical data while the blue solid lines (—) indicate the prediction given by equation (4.76). (Figure adapted from Ref. [123])

Finally, Figure 4.12 reports the ratio between the infidelity as a function of ϕ_r and the unperturbed value $\mathbb{I}_T(0)$ for values of the relative phase ϕ_r in the vicinity of zero, and with different panels corresponding to different oscillation periods T. One can see that small asymmetries are present with respect to zero, witnessing the fact that small phase errors need not necessarily spoil the protocol. These asymmetries tend to disappear as the driving frequency is increased (i.e., as the period T becomes smaller).

4.6 LOCAL EFFECTIVE COUNTERDIABATIC DRIVING

In this Section, we report some preliminary analyses dedicated to a further potential development of the theory presented in this Chapter, whose investigation has begun towards the end of the PhD program. In particular, the results presented here may be useful for future applications of the ideas and methodologies introduced in this

thesis, which have been focused on few-level systems, to adiabatic problems in complex quantum many-body scenarios.

Throughout this Chapter, we have used the control fields for engineering effective counterdiabatic Hamiltonians. Importantly, the latter always originated entirely from the combination of the control modulations, rather than from the interplay between the modulations and the original Hamiltonian. For instance, in the cases we have discussed, the structure of the counterdiabatic Hamiltonian $H_{\rm cd}(t)$ could be found via the commutator of the initial control matrices, say H_1 and H_2. The commutator dynamics produced by $[H_1, H_2]$ was then reproduced effectively by introducing modulations both along H_1 and H_2. This construction has the advantage that the correcting Hamiltonian can be used as a shortcut even in the absence of the original Hamiltonian. As discussed at length in Section (4.4), this would correspond to the limit of purely fast-forward driving.

However, one may wonder whether the effective counterdiabatic scheme could be applied in situations where the control resources are more limited. With reference to our example involving H_1 and H_2, one may imagine to be able to control H_1 but not H_2. This is particularly relevant for many-body systems, where the implementation of the ecd scheme may require tuning many-body interactions, which is in general a hard request in most experimental setups. An immediate simple example of this situation is the two-qubit problem presented in Section 4.3.2: in that case, control over the two-body term $\hat{\sigma}_1^x\hat{\sigma}_2^x + \hat{\sigma}_1^z\hat{\sigma}_2^z$ was assumed. This raises the interesting question of whether effective counterdiabatic driving can be achieved by means of only local control.

For this purpose, in this Section we present two proof-of-principle analyses along these lines. The first one, in Section 4.6.1, shows that a shortcut protocol can be realized in a two-level system by only "local" ($\hat{\sigma}_z$) control. The second analysis, in Section 4.6.2, regards the construction of effective many-body interactions starting from fixed two-body terms and local control. This is relevant in view of more complex scenarios. In particular, we describe the construction of dominant three-body terms in a linear chain of qubits, which can be driven only by local fields. This investigation, though being relevant in our shortcut-to-adiabaticity framework, has also a much broader range of application, for instance in the field of quantum simulation (see, e.g., Ref.s [117, 142]).

4.6.1 Locally driven two-level system

We show the construction of a *local* effective counterdiabatic protocol for the LZMS two-level problem described in Section (2.4). We use the term "local" referring to the fact that we will assume that control can be operated only on the bare-level

spacing, and not on the coupling. The Hamiltonian of the control problem, as a function of the rescaled time $s = (t - t_i)/t_f \in [0, 1]$, is

$$H(s) = H_{\text{LZMS}}(s) + H_{\text{ecd}}(s) \tag{4.77a}$$

$$= \tau_\Omega \left\{ \left[\lambda_\Omega \left(s - \frac{1}{2} \right) + u(s) \right] \hat{\sigma}_z + \hat{\sigma}_x \right\}, \tag{4.77b}$$

where $H_{\text{LZMS}}(s)$ is the LZMS Hamiltonian with dimensionless parameters introduced in equation (2.72), while $H_{\text{ecd}}(s)$ is the correcting Hamiltonian which acts only along $\hat{\sigma}_z$,

$$H_{\text{ecd}}(s) = u(s)\hat{\sigma}_z. \tag{4.78}$$

We will assume the following ansatz for the control function $u(t)$,

$$u(s) = \sum_{k=1}^{L} u_k(s) \cos[k\omega s + \phi_k(t)]. \tag{4.79}$$

The variation of the amplitudes $u_k(s)$ and phase $\phi_k(s)$ is assumed to be slow as compared to the driving frequency ω, and we will thus assume that they can be treated as constant over a single period $T = 2\pi/\omega$. Our objective now is to construct the effective Hamiltonian produced by our driving scheme, and to tune it so to match the exact counterdiabatic Hamiltonian, according to the general principles of effective counterdiabatic driving introduced in Section 4.2. Since the control is expected to be the dominant term, and proportional to the driving frequency as it was the case in Section 4.2, it is convenient to do so in the frame which is comoving with the oscillating driving Hamiltonian. This transformation defines the so-called "toggling" frame,

$$U_\omega(s) = \exp\left(-i\tau_\Omega \int_0^s dt' u(t') \hat{\sigma}_z \right). \tag{4.80}$$

Let us recall that, at stroboscopic times $s_n = n\frac{2\pi}{\tau_\Omega \omega}$, $n = 1, 2, \ldots$, the time integral in equation (4.80) vanishes due to the oscillating character of $u(s)$. At those times, $U_\omega(s_n)$ is equal to the identity $\mathbb{1}$, ensuring matching between toggling-frame and laboratory-frame effective Hamiltonians. Moreover, let us point out that the effect of the transformation (4.80) on the computational states $|0\rangle$ and $|1\rangle$ is that of providing each of those states with rapidly oscillating phase factors. Therefore, their occupation probabilities are not affected by $U_\omega(t)$. If one tracks only those, no differences would be appreciable from the evolutions in the toggling and laboratory frame. This effect, in similar contexts, was exploited for instance in Ref.s [13, 58, 82], and it is reminiscent of strategies used, e.g. in [8]. The rotating-frame Hamiltonian obtained after the transformation (4.80) reads

$$H_\omega(s) = U_\omega^\dagger(s) H_{\text{LZMS}}(s) U_\omega(s), \tag{4.81a}$$

$$= \tau_\Omega \left[\lambda_\Omega \left(s - \frac{1}{2} \right) \hat{\sigma}_z + \cos\left(2\tau_\Omega \int_0^s dt' u(t') \right) \hat{\sigma}_x \right.$$
$$\left. - \sin\left(2\tau_\Omega \int_0^s dt' u(t') \right) \hat{\sigma}_y \right]. \tag{4.81b}$$

This Hamiltonian has components along all the three Pauli matrices. Let us then compute the 0-th order Floquet-Magnus term (Section 3.2) —that is, the time average of $H_\omega(t)$. Evaluation of the time integral of nested trigonometric functions can be expressed in terms of a generalized version of the Bessel functions of the first kind. These functions are introduced in Appendix B, and are denoted as $\mathcal{J}_n^{(L)}(\boldsymbol{z}, \boldsymbol{\Phi})$. The 0-th order effective Hamiltonian is then

$$H_\omega^{(0)}(s) = \tau_\Omega \left[\lambda_\Omega \left(\frac{s}{2} - \frac{1}{2} \right) \hat{\sigma}_z + \mathrm{Re}\mathcal{J}_0^{(L)}(\boldsymbol{z}, \boldsymbol{\Phi})\, \hat{\sigma}_x - \mathrm{Im}\mathcal{J}_0^{(L)}(\boldsymbol{z}, \boldsymbol{\Phi})\, \hat{\sigma}_y \right], \quad (4.82)$$

where $\boldsymbol{z}$ is the vector

$$\boldsymbol{z} = \left\{ \frac{2u_1\tau_\Omega}{\omega}, \frac{2u_2\tau_\Omega}{2\omega}, \ldots, \frac{2u_L\tau_\Omega}{L\omega} \right\}, \quad (4.83)$$

while $\boldsymbol{\Phi}$ is the vector of phases $\boldsymbol{\Phi} = \{\phi_1, \ldots, \phi_L\}$. Hence, $H_\omega^{(0)}$ features a LZMS-like Hamiltonian with a renormalized coupling $\mathrm{Re}\mathcal{J}_0^{(L)}(\boldsymbol{z}, \boldsymbol{\Phi})$ as compared to the original Hamiltonian, plus a $\hat{\sigma}_y$ term. Since, for whatever number of control harmonics L, it holds that $|\mathrm{Re}\mathcal{J}_0^{(L)}(\boldsymbol{z}, \boldsymbol{\Phi})| \leq 1$, the coupling renormalization can never increase the $\hat{\sigma}_x$ coupling. In the case in which one chooses only one harmonic, $L = 1$, and zero phase $\phi_1 = 0$, the $\hat{\sigma}_y$ term in (4.82) vanishes, since $\mathcal{J}_0^{(L)}(\boldsymbol{z}, \boldsymbol{\Phi}) = J_0(2u_k/\omega)$, and $H_\omega^{(0)}$ matches the original LZMS Hamiltonian $H_{\mathrm{LZMS}}(t)$. For non-zero phase, denoting $z_1 \equiv z$ and $\phi_1 \equiv \phi$, the effective Hamiltonian becomes

$$H_\omega^{(0)} = \left[\lambda_\Omega \left(\frac{s}{2} - \frac{1}{2} \right) \hat{\sigma}_z + \cos(z \sin\phi) J_0(z) \hat{\sigma}_x - \sin(z \sin\phi) J_0(z) \hat{\sigma}_y \right]. \quad (4.84)$$

Now we have enough free parameters and we can tune $z = z(s)$ and $\phi = \phi(s)$ so to change the prefactors of $\hat{\sigma}_x$ and $\hat{\sigma}_y$. This feature can then be exploited for having $H_\omega^{(0)}(t)$ to match the full counterdiabatic Hamiltonian of equations (2.73) and (2.74).

Since the squared sum of the prefactors is limited by $|\mathcal{J}_0^{(L)}(\boldsymbol{z}, \boldsymbol{\Phi})|^2 \leq 1$, for having nonzero $\hat{\sigma}_y$ component the $\hat{\sigma}_x$ component cannot be maximized to 1. Therefore, one cannot use $H_\omega^{(0)}$ for reproducing the conterdiabatic Hamiltonian exactly. Still, one can set the $\hat{\sigma}_x$ coupling to a lower value and have the $\hat{\sigma}_y$ component matching the corresponding cd correction. In other words, the driving would produce an effective Hamiltonian which describes a different LZMS process, characterized by a smaller minimal gap, with related dressed coupling g_{dr}, but which includes the cd correction. Then, one must verify numerically whether the approximately corrected process leads to higher fidelities. In general, one can anticipate that this may depend rather strongly on the specific choice of parameters. For instance, if the total duration is too short, the value of the counterdiabatic correction to be mimicked would become too large as compared to the maximal $\hat{\sigma}_y$ component achievable by tuning z and ϕ. On the other hand, if the duration is very large, one can expect that the basic adiabatic approximation performs well, as in the case of Section 4.4. In any case, we will show an example in which the shortcut protocol allows one to achieve a larger final fidelity.

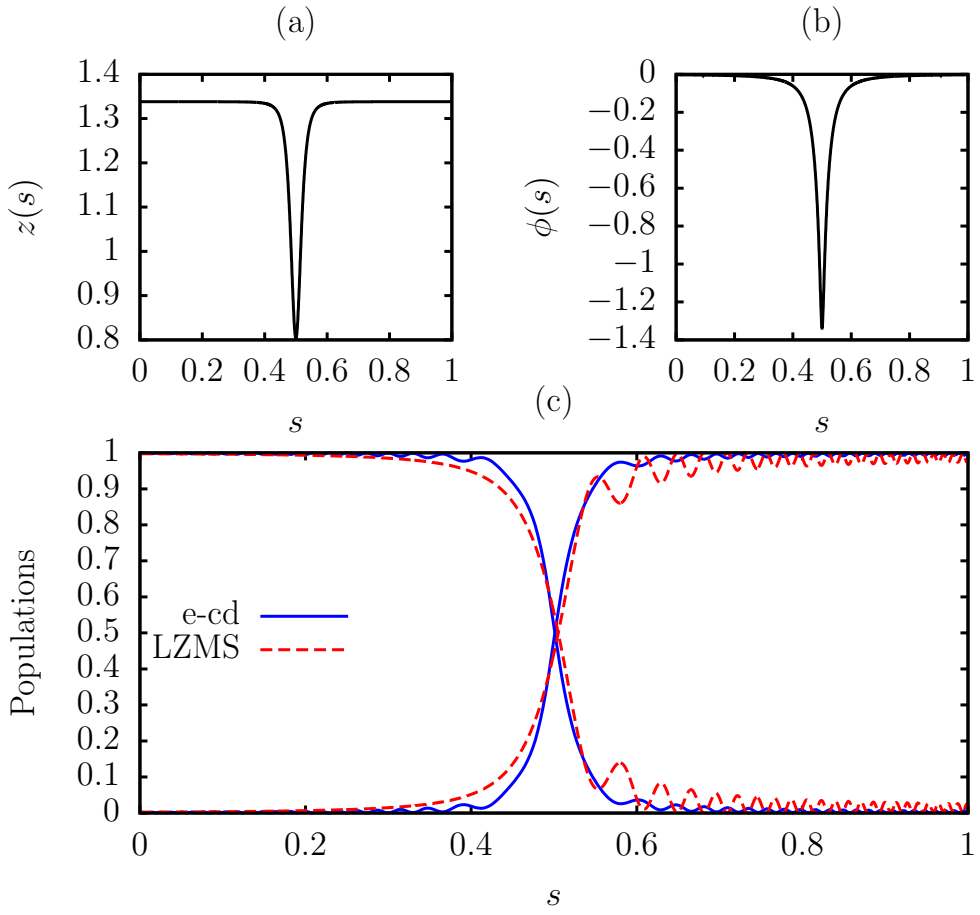

Figure 4.13: Local effective counterdiabatic driving for a two-level system. **(a)** Profile of the $z(s)$ function obtained by numerically solving equation (4.87), which is related to the time-dependent amplitude $u_1(t)$ of the driving field by equation (4.83) with $L = 1$. **(b)** Profile of the time-dependent phase $\phi(s)$ given by equation (4.86). **(c)** Populations of the bare states $|0\rangle$ and $|1\rangle$ of a LZMS process in the absence (- - -) and in the presence (—) of the local ecd correction. The value of the parameters considered are $\lambda_\Omega = 20$, $\tau = 28$, $g_{\rm dr} = 0.6$, $\omega\tau_\Omega = 2000$. In the first case, the fidelity reaches a value of ~ 0.976, while the shortcut produces a final fidelity of 0.998.

For a dressed gap $g_{\rm dr}$, this procedure and equation (4.84) give the equations

$$\cos[z(s)\sin\phi(s)]J_0[z(s)] = g_{\rm dr}, \tag{4.85a}$$

$$-\sin[z(s)\sin\phi(s)]J_0[z(s)] = f_{\rm cd}(s). \tag{4.85b}$$

Let us proceed with a possible solution of these equations. Inverting equation (4.85a), assuming that $z(s)$ and $J_0[z(s)]$ are different from zero for all t, we find the expression of $\phi(s)$ as a function of $z(s)$,

$$\phi(s) = \pm\arcsin\left[\frac{1}{z(s)}\arccos\left(\frac{g_{\rm dr}}{J_0[z(s)]}\right)\right]. \tag{4.86}$$

By taking the square of the two equations (4.85a) and (4.85b), and summing them up, we find an equation for $z(s)$:

$$J_0[z(s)] = \sqrt{g_{\rm dr}^2 + f_{\rm cd}^2(s)}. \tag{4.87}$$

The solution of equation (4.87) must be found numerically. Since $J_0[z(s)]$ needs to be positive for positive $g_{\rm dr}$ from Eq, (4.85a), and since for the LZMS problem the counterdiabatic correction $f_{\rm cd}(s)$ is negative, one finds that the sign of $\phi(s)$ in equation (4.86) must be chosen as negative. In Figure 4.13, we show the evolution of the populations of the bare states, together with the corresponding shape of $\phi(s)$ and $z(s)$. The parameters used are $\lambda_\Omega = 20$, $\tau_\Omega = 28$, $g_{\rm dr} = 0.6$, $\omega\tau_\Omega = 2000$. The protocol allows to achieve a final infidelity which is ten times larger than that produced by the basic adiabatic protocol. This proof-of-principle example shows that the effective counterdiabatic scheme can be efficiently used for constructing shortcuts also in the limit of local driving. This is a very promising first step for the applicability of the method in more complex situations, dealing eventually with quantum many-body problems. Further improvement of the protocol can be expected by performing a more refined parameter optimization. For instance, one can explore for different solutions for $z(s)$ and $\phi(s)$, or introduce further driving harmonics for having more freedom in the search of optimal solutions. The solution which we propose here requires a rather quick variation of $z(s)$ and $\phi(s)$ around the avoided crossing. This calls for a large driving frequency: it might be interesting to search for solutions which allow one to reduce its value as much as possible, for reducing also the strength of the modulation.

In the next section we will discuss a different development of these ideas. Specifically, we study the realizability of selected synthetic many-body terms through local control.

4.6.2 Synthesis of many-body interactions

In this section, we discuss the possibility of generating dominant many-body terms through local control in a chain of two-level systems. This problem is important in our context for investigating the possibility of constructing effective counterdiabatic fields in many-body quantum systems, and also for quantum simulation in a more general sense. Previous work in this direction, using techniques similar to those applied here, but aiming at the engineering of synthetic two-body terms only, has been pursued, e. g., in Ref. [97]. After discussing the general setup, we will show an explicit example in which non-trivial three-body interactions are constructed.

Let us consider a one-dimensional chain of N qubits, which interact with a two-body nearest-neighbors interaction, with open boundary conditions. The general form of this interaction is

$$H_{\rm int} = \sum_{k=1}^{N-1} \sum_{\alpha,\beta=x,y,z} J_{\alpha\beta} \hat{\sigma}_k^\alpha \hat{\sigma}_{k+1}^\beta, \tag{4.88}$$

where $J_{\alpha\beta}$ are the coupling constants. Now, let us introduce the time-dependent control Hamiltonian, which is assumed to contain only local terms. We assume that the local field on each site can vary along a fixed direction in three-dimensional space, which is identified by a unit vector $\boldsymbol{n}_k$. The Hamiltonian then reads

$$H_{\rm lc}(t) = \omega \sum_{k=1}^{N} b_k(t) \boldsymbol{n}_k \cdot \hat{\boldsymbol{\sigma}}, \tag{4.89}$$

where $\hat{\boldsymbol{\sigma}} = \{\hat{\sigma}_x, \hat{\sigma}_y, \hat{\sigma}_z\}$ is the vector of Pauli matrices. The local fields are assumed to be periodic with frequency $\omega = 2\pi/T$, involving a number L of harmonics, and they can be written, in units of ω, in the form

$$b_k(t) = \sum_{j=1}^{L} \Omega_{k,j} \cos(j\omega t + \phi_j). \tag{4.90}$$

Relevant quantities in the forthcoming analysis will be the time integrals (measured in units of the driving frequency) of the local fields (4.90), which we denote as

$$B_k(t) = \omega \int_0^t dt' b_k(t') = \sum_{j=1}^{L} \frac{\Omega_{k,j}}{j} \sin(j\omega t + \phi_{k,j}) - \sum_{k=1}^{L} \frac{\Omega_{k,j}}{j} \sin(\phi_{k,j}). \tag{4.91}$$

The choice of different initial times can be always recast into the form (4.91) by a suitable shift of the phases $\phi_{k,j}$. Since the control Hamiltonian (4.89) is the strongest interaction, it is convenient to move to the toggling frame comoving with the driving, via the transformation

$$U_\omega(t) = \exp\left(-i \int_0^t H_{\rm lc}(t') dt'\right). \tag{4.92}$$

Since $H_{\rm lc}(t) = H_{\rm lc}(t+T)$ is periodic, $U_\omega(t)$ is equal to the identity at stroboscopic times, guaranteeing that at those points the laboratory and toggling frames are matching. Hence, effective Hamiltonians computed in the toggling frame are valid also in the laboratory frame. Note that, if one would not assume the local oscillation direction $\boldsymbol{n}_k$ to be constant in time, the transformation (4.92) would not be in closed form in general. Since the control is local, the rotating-frame transformation amounts to compute local rotations of the Pauli matrices only. The toggling-frame Schrödinger equation, in units of $\hbar$, then reads

$$i\frac{\partial U(t)}{\partial t} = H_\omega(t) U(t), \tag{4.93}$$

with the Hamiltonian

$$H_\omega(t) = \sum_{k=1}^{N} \sum_{\xi,\eta=x,y,z} h^{(k)}_{\xi,\eta}(t) \sigma^\xi_k \sigma^\eta_{k+1}, \tag{4.94}$$

where

$$h^{(k)}_{\xi,\eta}(t) = \sum_{\alpha,\beta=x,y,z} J_{\alpha\beta} c^{(\alpha)}_{k,\xi}(t) c^{(\beta)}_{k+1,\eta}(t). \tag{4.95}$$

Therefore, $H_\omega(t)$ contains only two-body interactions. The quantities $c^{(\alpha)}_{k,\xi}$ represent the coefficient of the matrix $\hat{\sigma}^{\xi}_{k}$ resulting from the rotating-frame transformation of the matrix $\hat{\sigma}^{\alpha}_{k}$,

$$c^{(\alpha)}_{k,\xi} = \frac{1}{2}\mathrm{tr}\left[U^{\dagger}_{\omega}(t)\hat{\sigma}^{\alpha}_{k}U_{\omega}(t)\hat{\sigma}^{\xi}_{k}\right]. \tag{4.96}$$

Using the following "rotation relation" for the Pauli matrices [129],

$$\begin{aligned} e^{i\theta \boldsymbol{n}\cdot\hat{\boldsymbol{\sigma}}}\,\boldsymbol{a}\cdot\hat{\boldsymbol{\sigma}}\,e^{-i\theta \boldsymbol{n}\cdot\hat{\boldsymbol{\sigma}}} &= \cos 2\theta\, \boldsymbol{a}\cdot\hat{\boldsymbol{\sigma}} - (\boldsymbol{n}\times\boldsymbol{a})\cdot\hat{\boldsymbol{\sigma}}\sin 2\theta \\ &\quad + [1-\cos 2\theta](\boldsymbol{n}\cdot\hat{\boldsymbol{\sigma}})(\boldsymbol{n}\cdot\boldsymbol{a}), \end{aligned} \tag{4.97}$$

the coefficients $c^{(\alpha)}_{k,\xi}(t)$ can be given in a single expression as follows,

$$\begin{aligned} c^{(\alpha)}_{k,\xi}(t) &= [n^2_{k,\alpha} + (1-n^2_{k,\alpha})\cos 2B_k(t)]\delta_{\xi,\alpha} \\ &+ [n_{k,\alpha}n_{k,\alpha-1}(1-\cos 2B_k(t)) + n_{k,\alpha+1}\sin 2B_k(t)]\,\delta_{\xi,\alpha-1} \\ &\quad + [n_{k,\alpha}n_{k,\alpha+1}(1-\cos 2B_k(t)) - n_{k,\alpha-1}\sin 2B_k(t)]\,\delta_{\xi,\alpha+1}, \end{aligned} \tag{4.98}$$

where $\alpha-1$ and $\alpha+1$ indicate the preceding and successive elements of α in the cyclic set (x,y,z), respectively.

In the construction of the effective Hamiltonian, much care should be taken in the choice of the initial ansatz for the drivings. In particular, one should keep in mind the symmetry properties described in Section 3.2 (see Table 3.1 for a summary). For instance, the choice of a driving scheme leading to a toggling-frame Hamiltonian which is time-symmetric in the integration period would make all odd-order terms in the Floquet-Magnus expansion to vanish (see Table 3.1). Hence, this can be a great resource for selecting interactions which appear at even-order terms. Indeed, it would allow not only to simplify the problem by avoiding to deal with the minimization of odd-order terms, but it would also guarantee a higher level of approximation: for a given target $2n$-term, also the following $2n+1$ one would be zero by construction. If one plans instead to target interactions appearing at odd-order terms, time-symmetry must be avoided. Finally, one should keep in mind that effective Hamiltonians inherit from $H_\omega(t)$ all the "full-dynamics" symmetries, i.e. those arising from operators which commute with $H_\omega(t)$ at all times. Hence, effective Hamiltonians which do not posses these symmetries are not achievable with the present AHT scheme. In conclusion, the driving pattern must be conceived in such a way that $H_\omega(t)$ does not possess symmetries preventing the realization of desired interactions.

4.6.3 Computation of the effective Hamiltonian

Let us discuss some general aspects related to the computation of the Floquet-Magnus expansion for the Hamiltonian (4.94).

The 0-th order term contains two-body terms and involves the computation of the time average of the coefficients $h^{(k)}_{\xi,\eta}(t)$ of equation (4.95). This in turn requires

in general to compute time integrals of the product of two coefficients $c^{(\alpha)}_{k,\xi}(t)$ of equation (4.98), which involve trigonometric functions whose argument contain the Fourier summations (4.91). This type of integrals can be calculated and manipulated efficiently by using the generalized Bessel functions $\mathcal{J}^{(L)}_n(\boldsymbol{z}_k, \boldsymbol{\phi}_k)$ introduced in Appendix B. In particular, it turns out that one obtains expressions where the controllable terms depend on the generalized Bessel function of order $n = 0$ only. For optimizing the numerical evaluation of these functions, it is convenient to rewrite products of sines and cosines in the expressions $c^{(\alpha)}_{k,\xi}(t)$ as sines and cosines of the sum/difference of their arguments, e.g.,

$$\cos[2B_k(t)]\sin[2B_{k+1}(t)] = \frac{1}{2}\left(\sin[2(B_k(t)+B_{k+1}(t))] - \sin[2(B_k(t)-B_{k+1}(t))]\right). \tag{4.99}$$

This is helpful since the sum $2[B_k(t) \pm B_{k+1}(t)]$ can be simplified by noting that, for each harmonic $\ell\omega$ of the driving frequency appearing in $B_k(t)$ and $B_{k+1}(t)$ [equation (4.91)], one can find variables $z^{\pm}_k$ and Φ_k such that

$$\frac{2\Omega_{k,\ell}}{\ell}\sin(\ell\omega t + \phi_{k,\ell}) \pm \frac{2\Omega_{k+1,\ell}}{\ell}\sin(\ell\omega t + \phi_{k+1,\ell}) = z^{\pm}_{k,\ell}\sin(\ell\omega t + \Phi_{k,\ell}). \tag{4.100}$$

These variables are

$$z^{\pm}_{k,\ell} = \sqrt{\left(\frac{2\Omega_{k,\ell}}{\ell}\right)^2 + \left(\frac{2\Omega_{k+1,\ell}}{\ell}\right)^2 \pm 2\left(\frac{2\Omega_{k,\ell}}{\ell}\right)\left(\frac{2\Omega_{k+1,\ell}}{\ell}\right)\cos\left(\phi_{k+1,\ell} - \phi_{k,\ell}\right)}, \tag{4.101a}$$

$$\Phi_{k,\ell} = \mathrm{Arg}\left[\left(\frac{2\Omega_{k,\ell}}{\ell}\right)e^{i\ell\omega t + i\phi_{k,\ell}} \pm \left(\frac{2\Omega_{k+1,\ell}}{\ell}\right)e^{i\ell\omega t + i\phi_{k+1,\ell}}\right]. \tag{4.101b}$$

This eventually allows one to reduce the number of terms to be computed in the evaluation of the expression (B.4) for the functions $\mathcal{J}^{(L)}_n(\boldsymbol{z}_k, \boldsymbol{\phi}_k)$. The 0-th order effective Hamiltonian can then be used for creating effective two-body terms, as recently proposed in Ref. [97].

4.6.4 Example: construction of three-body interactions

As an example problem, we now discuss the construction of synthetic three-body terms starting from a chain with Ising-type interaction, namely, in units of the coupling,

$$H_{\mathrm{int}} = \sum_{k=1}^{N-1}\hat{\sigma}^z_k\hat{\sigma}^z_{k+1}. \tag{4.102}$$

Let us assume that all sites are driven by a transverse magnetic field along the x direction, so that the control Hamiltonian reads

$$H_{\mathrm{lc}}(t) = \omega\sum_{k=1}^{N} b_k(t)\hat{\sigma}^x_k, \tag{4.103}$$

with the local fields as in equation (4.90). Moving to the toggling frame (4.92), the Hamiltonian becomes

$$\begin{aligned} H_\omega(t) = \frac{1}{2}\sum_{k=1}^{N-1} \{ &[\cos[2(B_k(t)+B_{k+1}(t))] + \cos[2(B_k(t)-B_{k+1}(t))]]\,\hat{\sigma}_k^z\hat{\sigma}_{k+1}^z \\ &+ [\sin[2(B_k(t)+B_{k+1}(t))] - \sin[2(B_k(t)-B_{k+1}(t))]]\,\hat{\sigma}_k^z\hat{\sigma}_{k+1}^y \\ &+ [\sin[2(B_k(t)+B_{k+1}(t))] + \sin[2(B_k(t)-B_{k+1}(t))]]\,\hat{\sigma}_k^y\hat{\sigma}_{k+1}^z \\ &+ [\cos[2(B_k(t)-B_{k+1}(t))] - \cos[2(B_k(t)+B_{k+1}(t))]]\,\hat{\sigma}_k^y\hat{\sigma}_{k+1}^y \} , \end{aligned} \tag{4.104}$$

where the quantities $B_k(t)$ are the time integrals of the local fields $b_k(t)$ and were introduced in equation (4.91). The Hamiltonian (4.104) is the starting point for constructing the Floquet-Magnus expansion, whose first terms are analyzed in the following.

4.6.4.1 *Zero-th Floquet-Magnus term*

The 0-th term of the Floquet-Magnus expansion involves the time average of the Hamiltonian (4.104). The integrals of the trigonometric functions can be expressed in terms of the generalized Bessel function $\mathcal{J}_0^{(L)}(z,\mathbf{\Phi})$ (see Appendix B). The 0-th order effective Hamiltonian then reads

$$\begin{aligned} H_\omega^{(0)}(t) = \frac{1}{2}\sum_{k=1}^{N-1} \Big\{ &\mathrm{Re}\left[\mathcal{J}_0^{(L)}(z_k^+,\mathbf{\Phi}_k) + \mathcal{J}_0^{(L)}(z_k^-,\mathbf{\Phi}_k)\right]\hat{\sigma}_k^z\hat{\sigma}_{k+1}^z \\ &+ \mathrm{Im}\left[\mathcal{J}_0^{(L)}(z_k^+,\mathbf{\Phi}_k) - \mathcal{J}_0^{(L)}(z_k^-,\mathbf{\Phi}_k)\right]\hat{\sigma}_k^z\hat{\sigma}_{k+1}^y \\ &+ \mathrm{Im}\left[\mathcal{J}_0^{(L)}(z_k^+,\mathbf{\Phi}_k) + \mathcal{J}_0^{(L)}(z_k^-,\mathbf{\Phi}_k)\right]\hat{\sigma}_k^y\hat{\sigma}_{k+1}^z \\ &+ \mathrm{Re}\left[\mathcal{J}_0^{(L)}(z_k^-,\mathbf{\Phi}_k) - \mathcal{J}_0^{(L)}(z_k^+,\mathbf{\Phi}_k)\right]\hat{\sigma}_k^y\hat{\sigma}_{k+1}^y \Big\} , \end{aligned} \tag{4.105}$$

where the variables $z_k^\pm = \{z_{k,1}^\pm,\dots,z_{k,L}^\pm\}$ and $\Phi_k = \{\phi_{k,1},\dots,\phi_{k,L}\}$ were introduced in equation (4.101a) and (4.101b). Therefore, the 0-th effective Hamiltonian can be shaped in order to distort the two-body interaction. A interesting situation is that in which one would like to achieve dominant more-than-two–body interactions. In this case, one would like to make the 0-order become zero, for quenching the two-body terms. From equation (4.105), this implies the relations

$$\mathcal{J}_0^{(L)}(z_k^+,\mathbf{\Phi}_k) = 0, \qquad \mathcal{J}_0^{(L)}(z_k^-,\mathbf{\Phi}_k) = 0. \tag{4.106}$$

Let us then proceed to the computation of first-order effective Hamiltonian.

4.6.4.2 *First Floquet-Magnus term*

The first-order term of the Floquet-Magnus expansion can be written in the form:

$$\begin{aligned} H_\omega^{(1)} = \sum_{k=1}^{N-1} C_x^{(k)}\hat{\sigma}_k^x + \sum_{k=2}^{N-1} \Big[&C_{yxz}^{(k)}\hat{\sigma}_{k-1}^y\hat{\sigma}_k^x\hat{\sigma}_{k+1}^z + C_{zxy}^{(k)}\hat{\sigma}_{k-1}^z\hat{\sigma}_k^x\hat{\sigma}_{k+1}^y \\ &+ C_{yxy}^{(k)}\hat{\sigma}_{k-1}^y\hat{\sigma}_k^x\hat{\sigma}_{k+1}^y + C_{zxz}^{(k)}\hat{\sigma}_{k-1}^z\hat{\sigma}_k^x\hat{\sigma}_{k+1}^z \Big] . \end{aligned} \tag{4.107}$$

The explicit expressions for the coefficients $C_\alpha^{(k)}$ are quite lengthy, hence we discuss how they are obtained and report only two examples in Appendix C. The calculation of the integrals involved in this Floquet-Magnus terms, see equations (C.1) and (C.2) in Appendix C, are essentially linked to the calculations of integrals of the form

$$I_{\text{exp}}^{(1)} = \int_0^T dt_1 e^{(-1)^a 2i[B_k(t_1)\pm B_{k+1}(t_1)]} \int_0^{t_1} dt_2 e^{(-1)^b 2i[B_j(t_2)\pm B_{j+1}(t_2)]}. \tag{4.108}$$

These can be expressed in terms of generalized Bessel functions as follows

$$\begin{aligned} I_{\text{exp}}^{(1)} = \frac{2\pi}{\omega^2} \Big[& \pi \mathcal{J}_0^{(L)}\left(z_k^{\pm}, \mathbf{\Phi}_k\right) \mathcal{J}_0^{(L)}\left(z_{k+1}^{\pm}, \mathbf{\Phi}_{k+1}\right) \\ & - i \mathcal{J}_0^{(L)}\left(z_j^{\pm}, \mathbf{\Phi}_j\right) \sum_{n\neq 0}^{-\infty,\infty} \frac{1}{n} \mathcal{J}_n^{(L)}\left(z_k^{\pm}, \mathbf{\Phi}_k\right) \\ & + i \mathcal{J}_0^{(L)}\left(z_k^{\pm}, \mathbf{\Phi}_k\right) \sum_{n\neq 0}^{-\infty,\infty} \frac{1}{n} \mathcal{J}_n^{(L)}\left(z_j^{\pm}, \mathbf{\Phi}_j\right) \\ & - i \sum_{n\neq 0}^{-\infty,\infty} \frac{1}{n} \mathcal{J}_n^{(L)}\left(z_k^{\pm}, \mathbf{\Phi}_k\right) \mathcal{J}_{-n}^{(L)}\left(z_j^{\pm}, \mathbf{\Phi}_j\right) \Big]. \end{aligned} \tag{4.109}$$

These expressions are the starting point for the optimization procedure described in the next section.

4.6.4.3 *Effective three-body Hamiltonian*

Let us now discuss the explicit proof-of-principle procedure for constructing a non-trivial dominant three-body interaction on the chain of qubits. Given the expressions for the coefficients of the different interaction terms in the effective Hamiltonian (see equations C.1 and (C.2) in Appendix (C) for an example), we resort to a numerical optimization procedure for achieving the desired final effective Hamiltonian. In particular, we minimize, by means of a stochastic gradient algorithm, a cost function representing the distance from the target Hamiltonian, which is formulated in terms of the coefficients of the different terms appearing in $H_\omega^{(0)}$ and $H_\omega^{(1)}$. In particular, since we want to select a specific three-body term, this amounts to minimizing all the coefficients at the zero-th order (equation (4.106)), and all coefficients $C^{(k)}$ which correspond to undesired interactions at the first order. The amplitudes and phases of the control fields are the free parameters of this minimization. Our choice of target synthetic interaction is

$$H_{\text{tg}} = J \sum_{k=2}^{N-1} [\hat{\sigma}_{k-1}^y \hat{\sigma}_k^x \hat{\sigma}_{k+1}^y - \hat{\sigma}_{k-1}^z \hat{\sigma}_k^x \hat{\sigma}_{k+1}^z]. \tag{4.110}$$

Starting from the expressions for the coefficients in equation (4.107), it can be shown that this interaction appears when the local effective $\hat{\sigma}_k^x$ terms are set to zero, while the terms $\hat{\sigma}_{k-1}^z \hat{\sigma}_k^x \hat{\sigma}_{k+1}^z$ and $\hat{\sigma}_{k-1}^y \hat{\sigma}_k^x \hat{\sigma}_{k+1}^y$ are not individually tunable in this case. Running the optimization over the whole chain is of course impractical,

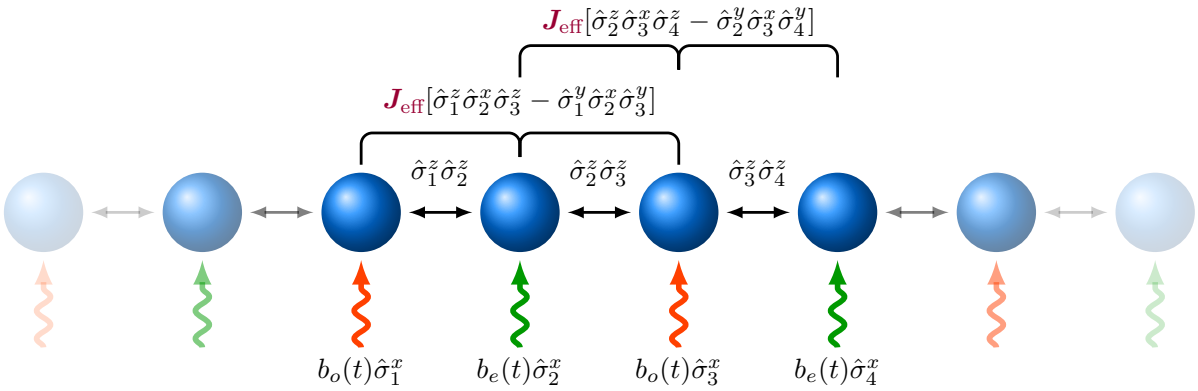

Figure 4.14: Driving scheme for constructing three-body terms. Even and odd sites are driven by different local fields. The driving parameters are determined following a numerical optimization, with the purpose of generating translational-invariant, dominant, three-body interaction terms.

and physical intuition also suggests that, since the target interaction is absolutely symmetric with respect to translations along the chain, also the driving scheme should somehow present a similar symmetry. In this spirit, we focus our numerical analysis on a chain of three qubits, labeled with $k = 1, 2, 3$, and we search for a sequence of two local driving fields $b_e(t)$ and $b_o(t)$ such that

1. drivings applied to odd sites are equal, $b_1(t) = b_3(t) = b_o(t)$, and different from those at the even site, $b_2(t) = b_e(t)$;
2. the driving sequence produces a dominant interaction of the form of equation (4.110) on the three qubits;
3. the control sequence obtained by exchanging the even-site driving with the odd-site one, $b_1(t) = b_3(t) = b_e(t)$ and $b_2(t) = b_o(t)$ produces the same interaction, with the same strength, as in point 2.

If these three conditions are satisfied, then the solution found can be directly extended to the whole chain. The driving scheme is depicted in Figure 4.14. Let us denote with H_{oeo} the effective Hamiltonian resulting from choice 1 of the drivings (truncated at the first Floquet-Magnus term), while H_{eoe} corresponds to choice 2. Different cost functions are being tested for ensuring the validity of these conditions. A possible choice, giving good results, is

$$\mathcal{F}(\{b_{k,l}\}, \{\phi_{k,l}\}) = \left\| \left\{ 1 - \frac{\text{tr}(H_{\text{oeo}} H_{\text{tg}})}{\|H_{\text{oeo}}\|}, 1 - \frac{\text{tr}(H_{\text{oeo}} H_{\text{eoe}})}{\|H_{\text{oeo}}\|} \right\} \right\| \tag{4.111a}$$

$$= \sqrt{\left(1 - \frac{\text{tr}(H_{\text{oeo}} H_{\text{tg}})}{\text{tr}(H_{\text{oeo}}^2)}\right)^2 + \left(1 - \frac{\text{tr}(H_{\text{oeo}} H_{\text{eoe}})}{\text{tr}(H_{\text{oeo}}^2)}\right)^2} \tag{4.111b}$$

The two elements of the vector appearing on the r.h.s. of Equation (4.111a) represent, respectively, the deviation from 1 of the normalized overlap between H_{oeo} and (i) the target Hamiltonian, (ii) the Hamiltonian H_{eoe}. As the number of harmonics

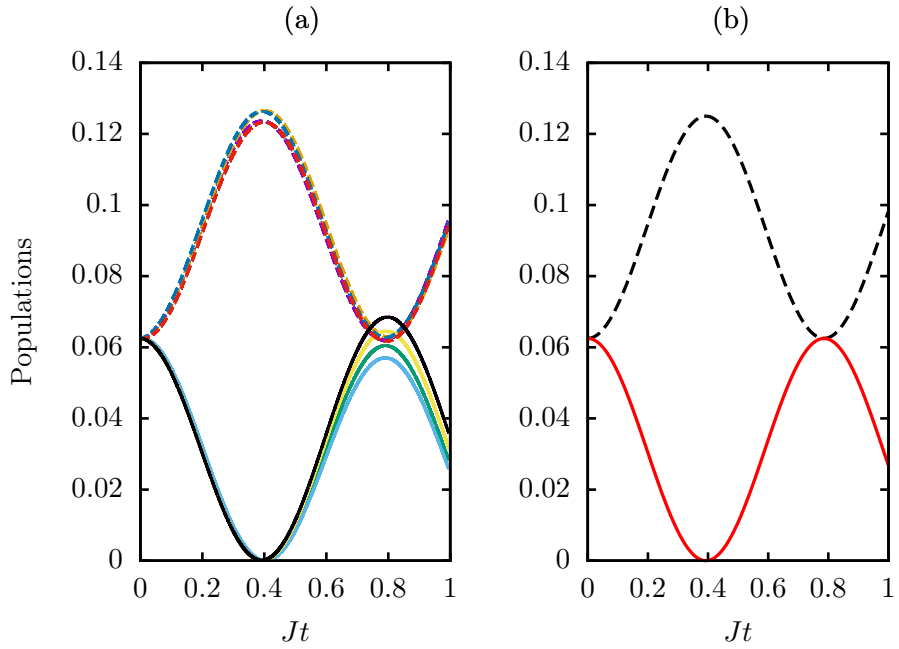

Figure 4.15: Effective three-body interaction. **(a)** Stroboscopic dynamics produced by the effective Hamiltonian on a chain of $N = 4$ qubits with the choice of driving amplitudes and phases of equation (4.112)a-e, for $\omega = 100$. **(b)** Exact evolution produced by the target Hamiltonian (4.110) with the same coupling strength $J = 1.58 \times 10^{-3}$ obtained in the effective Hamiltonian. In both panels, the dashed lines indicate the populations of the basis states $|0000\rangle$, $|1001\rangle$, $|0101\rangle$, $|1010\rangle$, $|0011\rangle$, $|1100\rangle$, $|1000\rangle$, $|0111\rangle$ (which result completely overlapped on the r.h.s., and almost overlapped in the l.h.s.), while the solid lines refer to the other eight basis states.

and different relative phases is raised, the number of free parameters grows fast. Therefore, a sampling of random initial conditions for the gradient-based minimization which is sufficiently large to span the relevant parameter space becomes rather time consuming. For this reason, we have first characterized a set of approximate solutions of equation (4.106), which requires less computational effort, and we then used this restricted set as a base for starting the random search. In Figure 4.15 we report the dynamics produced by one of the solutions found on a chain of four qubits. This solution is obtained by considering local fields of the form of equation (4.90) with $L = 2$ harmonics and $\omega = 100$. The numerical values for the parameters are

$$b_{1,1} = -1.838 \times 10^{-3}, \qquad b_{1,2} = 4.532, \tag{4.112a}$$
$$\phi_{1,1} = 0.4231, \qquad \phi_{1,2} = -0.5458, \tag{4.112b}$$
$$b_{2,1} = 1.9508 \times 10^{-3}, \qquad b_{2,2} = 4.4493, \tag{4.112c}$$
$$\phi_{2,1} = 1.6544, \qquad \phi_{2,2} = 2.0540, \tag{4.112d}$$
$$b_3(t) = B_1(t); \qquad b_4(t) = B_2(t). \tag{4.112e}$$

Figure 4.15a represents the effective stroboscopic dynamics starting with initial state

$$|\psi_0\rangle = |\psi_+\rangle \otimes |\psi_+\rangle \otimes |\psi_+\rangle \otimes |\psi_+\rangle\,, \tag{4.113}$$

where $|\psi_+\rangle = (|0\rangle + |1\rangle)/\sqrt{2}$, while Figure 4.15b corresponds to the exact evolution produced by the Hamiltonian (4.110) with $J = 1.5837 \times 10^{-3}$ equal to the corresponding value in the effective Hamiltonian. The initial state $|\psi_0\rangle$ is chosen in such a way that it allows to discriminate the desired interaction from the undesired ones present in equation (4.107). The results confirm that the effective Hamiltonian approximatively matches the target three body term, showing the efficiency of the general methodology. Further investigations are directed in the first place towards the search of solutions improving this matching, possibly by exploiting further harmonics in the driving fields. A second aspect regards the possibility of reaching a higher level of selectivity of the interaction in the example treated in this Section, by considering possible distortions of the direction of the local fields. These may allow to break the symmetries which prevent the individual addressability of terms like $\hat{\sigma}^z_{k-1}\hat{\sigma}^x_k\hat{\sigma}^z_{k+1}$ in the absence of effective local terms.

4.7 DISCUSSION

In this Chapter, we have introduced a framework for constructing shortcut-to-adiabaticity Hamiltonians, by combining two different ideas. The first one is that of counterdiabatic driving (described in Chapter 2, Section 2.3), i.e., of introducing correcting fields which dynamically prevent nonadiabatic transitions. The second one is that of engineering effective interactions by means of rapid modulations of the control parameters. This technique allows one to construct effective counterdiabatic Hamiltonians without the necessity of introducing new Hamiltonian couplings. The construction is made according to Floquet-Magnus average Hamiltonian theory (Chapter 3), which describes how to individuate effective Hamiltonians governing the average behavior of the system. We then exemplified the procedure in a number of different contexts (Sections 4.2.2 and 4.3), with particular attention to avoided crossing problems, which represent a primary example of (non)adiabatic physics.

The advantages of our methodology can be placed at different levels. First of all, the shortcuts can be operated in a wide regime of timescales, providing a smooth connection between truly adiabatic strategies and arbitrary-time fast-forward methods (see Section 4.4). Contextually, the methodology can be used both for constructing adiabaticity-assisting protocol, in which the driving acts as a weak perturbative correction to a reference adiabatic scheme, or as a standalone fast-forward method, in which the driving Hamiltonian represents the dominant interaction. For a given timescale of interest, this in general requires to adapt the values of the driving frequency and the strength of the driving (amplitude of the control fields).

The procedure for constructing the shortcut Hamiltonians leaves plenty of room for integration with optimal control strategies [73]. Indeed, the effective counterdiabatic Hamiltonian can be further shaped by taking into account possible optimization principles, such as the minimization of cost functions related to the use of certain experimental resources, or of some specific feature of the controlled dynamics. The optimization can then be carried out over the set of amplitudes of the control fields which act over different harmonics of the fundamental driving frequency. These general ideas were investigated, for instance, in Ref. [160], where polychromatic drivings were used for reducing the deviation produced by the micromotion dynamics.

The analysis from the point of view of control theory, in Section 4.1, provided interesting results regarding the characterization of the structure of the counterdiabatic Hamiltonian. The fact that the latter belongs to the dynamical Lie algebra of the system (Theorem 2, Section 4.1), despite being in a sense a direct consequence of the adiabatic theorem, is a powerful information. Indeed, it guarantees that our approximating scheme can be applied independently from the properties of controllability of the system. A second aspect of relevance comes from the connection with the theory of flow equations (Section 4.1.2). This allowed us to argue that, in many cases, the matrix structure of $H_{\mathrm{cd}}(t)$ can be found by taking a single commutator of the control Hamiltonians composing $H(t)$. The importance of this can be traced back to the following point: one can expect that it is sufficient to calculate only the first-order effective Hamiltonian in the Floquet-Magnus expansion (equations (3.18) in Section 3.2). It would be also interesting to elaborate on the use of flow equation approaches as a different route for constructing effective counterdiabatic fields. Indeed, since they can be used to produce partial diagonalization (by truncating the flow), and thus to approximate counterdiabatic Hamiltonians, they may be also used for constructing effective counterdiabatic fields without requiring the exact spectral properties of the Hamiltonian. We mention that these ideas seem to find quite a few similarities with the variational approaches proposed in Ref.s [37, 143]. This connection as well may be worth a further exploration.

A natural extension of this kind of analysis would regard infinite-dimensional systems. As discussed in Section 3.1, a number of technical problems arise when one tries to formally bring the counterdiabatic scheme to the infinite-dimensional setting. For instance, the concept of adiabatic state needs to be refined when continuous spectra are present. In this case, variations of the adiabatic theorem have been proposed in which the preservation of instantaneous eigensubspaces is related to continuous strips in the spectrum [108]. Another pathological situation is found when degeneracies occur. In this case, what one can aim at is the preservation of instantaneous degenerate eigensubspaces, when the degree of degeneracy is maintained during the evolution. No particular issues should be present instead when the infinite-dimensional spectrum involves only non-degenerate discrete levels. More generally, the whole machinery described in this Chapter can be safely applied whenever the quantum control problem involves only subparts of the spectrum of the system where the above-mentioned problems are not present.

Finally, the possibility of realizing local effective counterdiabatic driving (Section 4.6) is very appealing for the potential extension of the method to many-body quantum systems. The good preliminary results motivate further investigation in this direction. At the same time, the technique developed in Section 4.6.2 for the synthesis of dominant effective many-body terms can be of interest on its own, beyond the strict shortcut-to-adiabaticity framework, and it may develop towards a separate dedicated study.

The next Part, iii, of this thesis is dedicated to applications of the framework developed in this Chapter. The first application, presented in Chapter 5, deals with the problem of entanglement creation in a superconducting circuit, one of the most promising architectures for building quantum technologies. The second application covers the improvement of one of the most widespread adiabatic control techniques, namely the stimulated Raman adiabatic passage.

Part III

APPLICATIONS

5 ENTANGLEMENT PRODUCTION IN CIRCUIT QED

This Chapter is dedicated to the application of the methodology developed in Chapter 4 for quantum control in the field of circuit quantum electrodynamics (cQED), i.e., in the realm of superconducting circuits [17, 51, 75, 141, 172]. We will construct an accelerated adiabatic protocol whose purpose is to generate, with high precision and low noise sensitivity, entanglement between the fundamental computational units encoded in the system. This objective is of central importance for metrological applications [47] and for the implementation of entangling gates in quantum algorithms [122]. The present analysis also shows how our methodology can be efficiently applied to control an appropriately restricted subspace of a larger Hilbert space.

Superconducting qubits are, nowadays, one of the most rapidly expanding experimental platforms for building quantum technologies. At a more fundamental level, over the last ten years they have proven to be a precious resource for the progress of physical sciences, allowing to probe experimentally quantum effects which could not be addressed in the lab before. Indeed, since their first implementations [121], they have been largely involved, for instance, in the study of quantum computation, from algorithms [52, 147] to multiqubit entanglement [53] and quantum error correction [11, 131], quantum simulation [12, 35, 102], and quantum optics (e.g., Jaynes-Cummings physics [62]). A 53-qubit cQED hardware has been used in the first experiment claiming to have achieved quantum supremacy [9]. The appeal of cQED can be traced back also to the fact that it is ultimately based on electrical circuits, and it can be implemented on chips. This has proven, in the case of non-quantum technology, to be an easily scalable architecture.

The general context of cQED is presented in Section 5.1, where the relevant Hamiltonian of the system is introduced. We will also discuss the dynamical equations modeling the interaction of the system with the surrounding environment. This formulation will help us to analyze the stability of the protocol in realistic noisy situations, in Section 5.7. In Section 5.2, we describe the specific system that we will analyze, which consists of two driven qubits coupled to a common transmission line. As a first step towards the design of the final protocol, we define a reference adiabatic process. This is conceived in such a way that the adiabatic evolution connects separable states to entangled states. Moreover, we compare the performance produced by different choices of adiabatic sweep functions, which are chosen along the principles of Section 2.2. We will then proceed in the computation of the exact counterdiabatic (cd) Hamiltonian in Section 5.4, which turns out to require new couplings which cannot be realized in standard architectures. This motivates the introduction, in Section 5.5, of an effective counterdiabatic scheme

constructed according to the general theory described in Chapter 4. The results produced by the shortcut protocol are analyzed in Section 5.6, where we show that large fidelities can be attained in competitive evolution timescales, even in the presence of experimental constraints. We also compare the performance of shortcuts tailored over different original optimized adiabatic sweeps. We finally test, in Section 5.7, the robustness of the protocol against imperfections in amplitude, frequency and phase of the control modulations, and we show that promising results are maintained in the presence of environment-induced noise.

5.1 CIRCUIT QUANTUM ELECTRODYNAMICS

Superconducting circuits are, in essence, electric circuits composed of LC oscillators characterized by two quantum effects: superconductivity and the Josephson effect. These two ingredients make the circuit behave as a nonlinear quantum mechanical oscillator, that is, as a full-fledged artificial atom. Differently from other quantum computational candidates such as real atoms, ions, electrons or photons, superconducting qubits are macroscopic objects, of the order of few μm. They are typically divided into three categories, which are briefly named as charge, flux and phase qubits. Among these, a specific type of charge qubit, called the transmon [91], is becoming dominant, especially thanks to its long coherence times.

For building a full quantum device, superconducting qubits need of course to interact with each other. Years of development of cavity quantum electrodynamics, the field which describes the interaction of atoms with single photons confined within a cavity, have paved the way for a circuit implementation of the same setup. This allows one to achieve strong qubit-qubit interaction in an efficient way, and has given origin to the field of circuit quantum electrodynamics (cQED) [16, 167]. In this model, superconducting qubits are coupled to transmission line resonators. This architecture permits one to implement single-qubit operations, while having a switchable qubit-qubit interaction which is mediated by the exchange of virtual photons via the transmission line. In the next Section, we will present a full description of this model.

5.1.1 Jaynes-Cummings interaction

The purpose of this Section it to discuss the typical Hamiltonian describing a cQED system. The interaction of a set of N (artificial) atoms with a single mode of the quantized electromagnetic field can be described via the Hamiltonian

$$H = \hbar \sum_{k=1}^{\infty} \left[\omega_k \hat{b}_k^\dagger \hat{b}_k + \frac{\alpha_k}{2} \hat{b}_k^\dagger \hat{b}_k^\dagger \hat{b}_k \hat{b}_k \right] + \hbar \omega_r \hat{a}^\dagger \hat{a} + \hbar \sum_{k=1}^{N} g_k (\hat{b}_k + \hat{b}_k^\dagger)(\hat{a} + \hat{a}^\dagger). \quad (5.1)$$

The atoms are treated as anharmonic oscillators with bosonic field operators $\hat{b}_k$, $\hat{b}_k^\dagger$, transition frequencies ω_k and anharmonicity α_k. They are coupled with strength

$\hbar g_k$ to the electromagnetic field. The latter is characterized by field operators $\hat{a}$ and $\hat{a}^\dagger$ and has transition frequency ω_r. By performing a two-level approximation for the atoms, and setting $\hbar = 1$, the Hamiltonian of equation (5.1) simplifies to

$$H = \omega_r \hat{a}^\dagger \hat{a} + \sum_{k=1}^{2} \frac{\omega_k}{2} \hat{\sigma}_k^z + \sum_{k=1}^{2} g_k \left[\hat{\sigma}_k^+ \hat{a} + \hat{\sigma}_k^- \hat{a}^\dagger \right] + \sum_{k=1}^{2} g_k \left[\hat{\sigma}_k^+ \hat{a}^\dagger + \hat{\sigma}_k^- \hat{a} \right]. \quad (5.2)$$

Finally, let assume the rotating wave approximation (RWA) [112, 168]. This amount to neglecting terms oscillating at the sum of frequencies of the qubits and/or of the resonator, $\pm(\omega_{k_1} + \omega_{k_2})$ and/or $\pm(\omega_k + \omega_r)$, which are referred to as counter-rotating terms. These are produced by the doubly-exciting and doubly-annihilating combination of operators $\hat{\sigma}_k^+ \hat{a}^\dagger$ and $\hat{\sigma}_k^- \hat{a}$, for instance, as can be seen by moving to the interaction picture with respect to the noninteracting part of the Hamiltonian (5.2). The physical intuition behind this is that these terms oscillate at frequencies which are way larger then those arising from the corresponding differences, $\pm(\omega_{k_1} - \omega_{k_2})$ and $\pm(\omega_k - \omega_r)$, which are called rotating terms and are produced by the operators $\hat{\sigma}_k^+ \hat{a}$ and $\hat{\sigma}_k^- \hat{a}^\dagger$. Therefore, one expects that their effects average out if one considers phenomena which occur on timescales close to those set by the rotating terms. The consequence of the RWA is that the last summation term in equation (5.2) is neglected, and the Hamiltonian becomes

$$H_{\text{JC}} = \omega_r \hat{a}^\dagger \hat{a} + \sum_{k=1}^{2} \frac{\omega_k}{2} \hat{\sigma}_k^z + \sum_{k=1}^{2} g_k \left[\hat{\sigma}_k^+ \hat{a} + \hat{\sigma}_k^- \hat{a}^\dagger \right]. \quad (5.3)$$

This Hamiltonian thus features a Jaynes-Cummings interaction, a well-studied model of quantum optics [112, 168], which conserves the total number of excitations in the qubits-resonator system. Indeed, the Hamiltonian of equation (5.3) commutes with the operator $N = 1 + \hat{\sigma}_1^z/2 + \hat{\sigma}_2^z/2 + \sum_k \hat{a}^\dagger \hat{a}$ which counts the number of excitations.

The dispersive regime is identified by the condition that the detuning between the qubits' transition frequency and the transition frequency of the resonator is much larger than the coupling g. When this condition is fulfilled, and if the two qubits are brought in resonance with each other, a resonator-mediated coupling makes them interact. This originates from the transmission of a virtual photon through the resonator, and can be exploited in order to implement two-qubit operations [110]. In the rotating frame defined by the unitary transformation

$$U_1 = \exp\left[-\sum_{k=1}^{2} \frac{g}{\delta_k} (\hat{a}^\dagger \hat{\sigma}_k^- - \hat{a} \hat{\sigma}_k^+) \right], \quad (5.4)$$

where we have introduced the detuning $\delta_k = \omega_k - \omega_r$ between the k-th qubit and the resonator, the Hamiltonian (5.2), up to second order in g/δ_k, becomes

$$\begin{aligned} U_1 H U_1^\dagger =& \omega_r \hat{a}^\dagger \hat{a} + \sum_k \left[\frac{\omega_k}{2} + \frac{g^2}{2\delta_k}(2\hat{a}^\dagger \hat{a} + 1) \right] \hat{\sigma}_k^z \\ &+ \frac{1}{2} \sum_{k,\ell} \frac{g^2}{\delta_k} (\hat{\sigma}_\ell^- \hat{\sigma}_k^+ + \hat{\sigma}_\ell^+ \hat{\sigma}_k^-) + \sum_k g(\hat{a}^\dagger \hat{\sigma}_k^+ + \hat{a} \hat{\sigma}_k^-) \\ &+ \sum_k \frac{g^2}{\delta_k} [\hat{a}^2 + (\hat{a}^\dagger)^2] \hat{\sigma}_k^z + \sum_{k,\ell} \frac{g^2}{\delta_k} (\hat{\sigma}_\ell^- \hat{\sigma}_k^- + \hat{\sigma}_\ell^+ \hat{\sigma}_k^+). \end{aligned} \tag{5.5}$$

In the RWA, the last three terms are neglected. In the frame defined by U_1, we see that a hopping term between the two-qubits emerges (first term at the second line). When the qubits are at resonance, $\delta_1 = \delta_2 \equiv \delta$, within a subspace with fixed number of excitations $(n+1)$, an avoided crossings builds up between energy levels corresponding to the $\{|n \uparrow\downarrow\rangle, |n \downarrow\uparrow\rangle\}$ states. Here, n corresponds to the number of excitations of the electromagnetic field, while $\uparrow\downarrow$ refers to the states of the qubits. The width of such anticrossing (the minimal gap) is twice the qubit-qubit coupling, that is, from the perturbative Hamiltonian (5.5), $2g^2/\delta$. This phenomenon has been already exploited both for performing an $\sqrt{\text{i SWAP}}$ two-qubit gate [110], which is an entangling quantum gate [122]. Moreover, it has been used for studying Landau-Zener-Majorana-Stückelberg (LZMS) phenomena [130].

5.1.2 Model of dissipation and decoherence

Real quantum systems are always affected, to a variable extent, by the interaction with the external environment, whose effect is that of introducing noise in the system dynamics. This noise manifests itself into the dissipation of energy and into decoherence/dephasing processes, which imply the destruction of superpositions of energy eigenstates. These phenomena cannot be described by the standard time-dependent Schrödinger equation, since they cannot be the result of any unitary process. A proper description is provided by the theory of open quantum systems [22], and it requires the use of equations of motion for the density matrix of the system which extend the standard Heisenberg equation. When certain fairly general conditions on the system-environment interaction are satisfied, one can prove that these equations must have a specific structure, known as Gorini-Kossakowski-Sudarshan-Lindblad (GKSL) form. The set of typical physical approximations which allow one to derive equations of this form starting from a microscopic description of the combined system-environment pair are usually collected under the name of Born-Markov approximation. Let us denote with $\mathbb{H}_S$ the Hilbert space of the system and with $\mathbb{H}_E$ the Hilbert space of the environment. Let us further indicate with $\text{dens}(\mathbb{H})$ the set of density matrices defined on the Hilbert space $\mathbb{H}$. The Born approximation assumes that the coupling between system and environment is weak, such that, while the system is disturbed by the environment, the environment is not altered by the presence of the system. This allows to decompose the density matrix

$\hat{\rho}_{SE}(t) \in \text{dens}(\mathbb{H}_S \otimes \mathbb{H}_E)$ of the combined system in the separable form $\hat{\rho}_S(t) \otimes \hat{\rho}_E$ for all times, where $\hat{\rho}_S(t) \in \text{dens}(\mathbb{H}_S)$ describes the state of the system while $\hat{\rho}_E \in \text{dens}(\mathbb{H}_E)$ describes the state of the environment. The Markov approximation implies that (i) the time-variation of the state of the system at time t depends only on its current state $\hat{\rho}_S(t)$, and (ii) that the state of the system varies over timescales much longer than those characteristic of the environment. The resulting equations of motion are dubbed GKSL (often just Lindblad) Markovian master equations [22]. In the following, and also in Chapter 6, we make use of this formalism for studying the robustness of the effective counterdiabatic protocol against environment-induced noise.

The relevant incoherent processes which can occur in the superconducting circuit under analysis are spontaneous emission from the superconducting qubits, dephasing with respect to their bare states and photon leakage from the resonator. These phenomena can be included into the description of the system by means of the following GKSL master equation [17], which provides an evolution equation for the system density matrix $\hat{\rho}(t)$,

$$\frac{\partial \hat{\rho}(t)}{\partial t} = -\frac{i}{\hbar}[H(t), \hat{\rho}] + \kappa D[\hat{a}]\hat{\rho} + \sum_{k=1}^{2} \gamma_r^{(k)} D[\hat{\sigma}_k^-]\hat{\rho} + \sum_{k=1}^{2} \gamma_\phi^{(k)} D[\hat{\sigma}_k^z]\hat{\rho}, \tag{5.6}$$

where $\gamma_d^{(k)}$ and $\gamma_\phi^{(k)}$ are the relaxation and decoherence rates for qubit k, while κ is the damping rate of the resonator. The operator D, which is referred to as the Lindblad *dissipator* associated to a *collapse* (or *jump*) operator X, has the following explicit form,

$$D[x] = X\hat{\rho}X^\dagger - \frac{1}{2}\left\{XX^\dagger, \hat{\rho}\right\}.$$

5.2 ADIABATIC ENTANGLING PROTOCOL

Starting from the general model of equation (5.3), we now focus on the specific system over which we are going to concentrate our analysis. We consider an architecture composed of two superconducting qubits coupled to a coplanar transmission line resonator. The type of qubit which we choose is a so-called tunable coupling qubit (TCQ), as proposed in Ref. [65, 146]. A particular feature of the TCQ, as suggested by its name, is that not only its transition frequency can be tuned in time, but its coupling to the resonator as well. This high degree of controllability is achieved by connecting three superconducting island through superconducting quantum interference devices (SQUIDs). By changing the external magnetic flux applied to the SQUIDs, the dipole moment of the two pair of islands can be combined in a parallel or antiparallel way. The first case results in a strong coupling of the qubit with the resonator, while in the second case this coupling is quenched [65].

Let us take the dressed basis defined by the vectors $|n, \uparrow\downarrow, \uparrow\downarrow\rangle$, where n indicates the number of field excitations, while $\uparrow\downarrow$ refers to the bare state of each

qubit. Let us focus on a two-excitation manifold defined by the four basis states $\{|n-1,\uparrow\uparrow\rangle, |n,\uparrow\downarrow\rangle, |n,\downarrow\uparrow\rangle, |n+1,\downarrow\downarrow\rangle\}$. By considering a frame rotating at the resonator frequency ω_r, the Hamiltonian (5.3) can be rewritten like

$$H = \begin{pmatrix} \frac{\delta_1+\delta_2}{2} & g_2 & g_1 & 0 \\ g_2 & \frac{\delta_1-\delta_2}{2} & 0 & \sqrt{2}g_1 \\ g_1 & 0 & \frac{\delta_2-\delta_1}{2} & \sqrt{2}g_2 \\ 0 & \sqrt{2}g_1 & \sqrt{2}g_2 & -\frac{\delta_1+\delta_2}{2} \end{pmatrix}. \tag{5.7}$$

By considering the dispersive regime, this Hamiltonian features the formation of an avoided crossing between the intermediate states $|n\uparrow\downarrow\rangle$ and $|n\downarrow\uparrow\rangle$ when the two qubits are in resonance at the same frequency, $\delta_1 = \delta_2$, as discussed in Section 5.1.1. For simplicity, from now on we will consider a small total number of excitations, equal to 2, in which the system is in a fully quantum regime.

Our proposal is to exploit the emerging anticrossing for adiabatically preparing an entangled two-qubit state. This is possible by driving the qubits adiabatically from an initially large detuning, where the qubits are effectively decoupled, to the point where the avoided crossing occurs, which mixes the qubits bare basis into entangled states. If the system is initially prepared in a separable state $|\uparrow\downarrow\rangle$, by tracking the corresponding adiabatic state it will end up in an entangled singlet state $|\psi_s\rangle = (|\uparrow\downarrow\rangle - |\downarrow\uparrow\rangle)/\sqrt{2}$. Since the total duration of the resulting process turns out to be prohibitively long for realizing an efficient state-transfer protocol, we will combine the use of optimized adiabatic sweeps (see Section 2.2) with the ecd framework for achieving satisfactory fidelities in a short time, maintaining a strong stability against experimental protocol imperfections.

For simplicity, we will consider equal coupling $g_1 = g_2 \equiv g$ between the two qubits and the cavity. Nonetheless, the present analysis holds for unequal couplings as well. The central difference in that case is basically the relative position between the avoided crossing and the point where the system instantaneous eigenstate is the target state $|\psi_s\rangle$. For achieving the desired entangled state then, the final stop time of the adiabatic protocol should be reset to this new point.

Let us assume that the protocol takes place over a total time t_f. We then introduce the sweep function $f(t)$ describing the instantaneous half-detuning between the qubits in units of g,

$$f(t) = \frac{\delta_1 - \delta_2}{2g}. \tag{5.8}$$

During the adiabatic ramp, $f(t)$ varies from an initial value f_0 to zero. Introducing the dimensionless quantities $s = t/t_f$, $\tau = t_f g$, $\delta_g = (\delta_1 + \delta_2)/2g$, the Schrödinger equation reads

$$i\frac{\partial U}{\partial s}U(s) = \tau H(s)U(s), \tag{5.9}$$

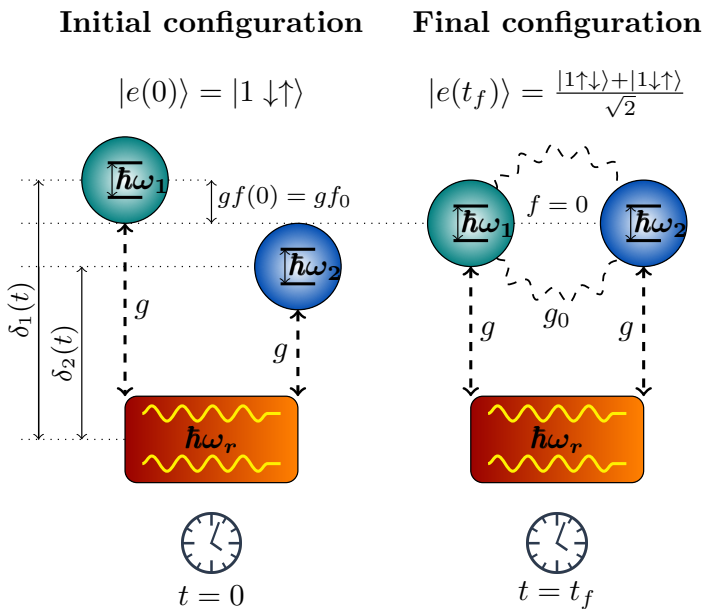

Figure 5.1: Sketch of the adiabatic entangling protocol. In the initial configuration (left), the two qubits, having transition frequencies ω_1 and ω_2, are detuned from each other by $2gf_0$, while being largely detuned by $\delta_1 \gg g$ and $\delta_2 \gg g$ from the resonators's transition frequency ω_r. They are coupled to the resonator with strength g. The system is in the first-excited state, which is the separable state $|\downarrow\uparrow\rangle$. The detuning between the two qubits is then adiabatically changed in time until the final configuration is reached (right). The two qubits are now in resonance with each other, and they interact via a resonator-mediated coupling g_0. In the adiabatic limit, the system follows the instantaneous excited state, reaching the entangled state $(|\uparrow\downarrow\rangle + |\downarrow\uparrow\rangle)/\sqrt{2}$ at the final time t_f. (Figure reproduced from [125])

with the rescaled Hamiltonian

$$H(s) = \begin{pmatrix} \delta_g & 1 & 1 & 0 \\ 1 & f(s) & 0 & \sqrt{2} \\ 1 & 0 & -f(s) & \sqrt{2} \\ 0 & \sqrt{2} & \sqrt{2} & -\delta_g \end{pmatrix}. \tag{5.10}$$

The whole setup is sketched in Figure 5.1. We will work with realistic experimental parameters within standard ranges, with reference to those used, for instance, in Ref.s [52, 110, 141]. In particular, we consider a resonator frequency $\omega_r/2\pi = 8.2$ GHz and qubit-cavity coupling $g/2\pi = 50$ MHz. The well-controllable transition frequencies of the qubits in the microwave range are instead varied from initial values $\omega_1/2\pi = 6.01$ GHz and $\omega_2/2\pi = 5.99$ to a final equal value 6.00 GHz. The avoided crossing for these parameters has width $2g_0 \simeq 14$ MHz. These are the values which will be used in the numerical simulations. In terms of the dimensionless quantities introduced in equation (5.10), these values translate into $\delta_g = -44$, $f_0 = 0.2$. The next step in our analysis is to choose an efficient adiabatic ramp.

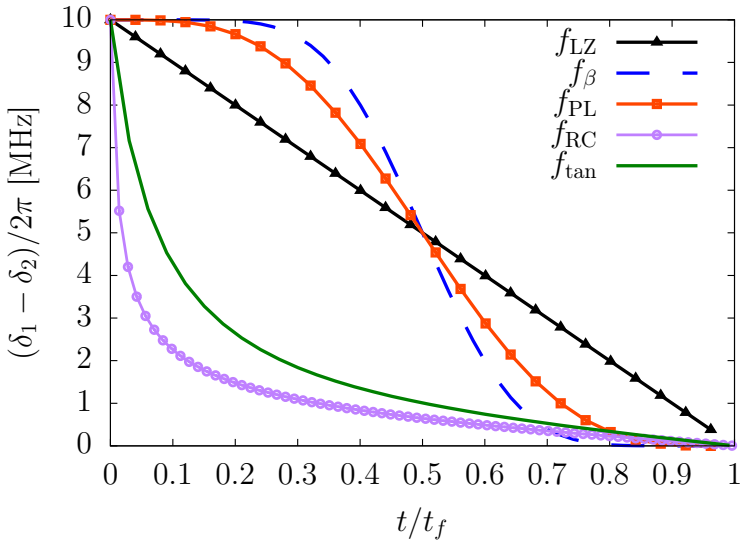

Figure 5.2: Adiabatic sweep functions. Temporal profile of the different adiabatic drivings under analysis. (Figure reproduced from [126])

5.3 OPTIMIZING THE ADIABATIC SWEEP

In Section 2.2, we discussed how the temporal profile of an adiabatic sweep can be optimized in order to achieve a satisfactory adiabatic approximation in finite time. In particular, we have introduced two different local adiabatic drivings (LADs), and two boundary-cancellation drivings (BCDs). Building on that discussion, we inspect now in detail how these sweeps perform in the present context, also in comparison with a simple linear ramp. In particular, we will study how the fidelity of the protocol is affected by that choice. Adapting to the system under analysis, the possible functional dependences which we consider are

1. Linear LZMS ramp,
$$f_{\rm LZ}(s) = f_0[1-s]; \tag{5.11}$$
2. [BCD] Regularized Beta function,
$$f_\beta(s) = [1-\Theta_k(s)] \tag{5.12}$$
where $\Theta_k(x)$ is defined in equation (2.56);
3. [BCD] Polynomial
$$f_{\rm pl}(s) = f_0[1-35s^4+84s^5-70s^6+20s^7] \tag{5.13}$$
with three time-derivatives vanishing at the boundary;
4. [LAD] Tangent,
$$f_{\rm tan}(s) = \frac{g_0}{g}\tan[\gamma(1-s)] \tag{5.14}$$
where $\gamma = \arctan(g f_0/g_0)$.

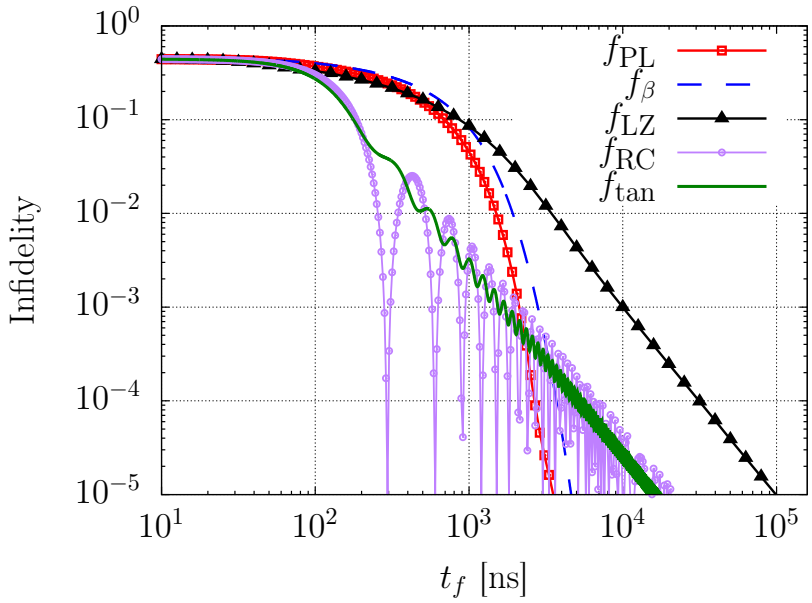

Figure 5.3: Final infidelity as a function of the total duration for different sweep functions. The use of optimized adiabatic sweeps greatly improves the protocol fidelity, at given total time, with respect to a basic linear LZMS ramp. The infidelity for BCDs follows initially the behavior of the LZMS curve, but when adiabatic timescales are reached, it decays exponentially fast both for f_{pl} and f_β. The infidelity for LADs, excluding accidental peaks, shows a behavior linearly decaying with the total time, which reaches fidelities between 0.9 and 0.999 faster than other methods, both for f_{RC} and $f_{\tan}$, before getting overcome by BCDs at around 1 μs. [Figure reproduced from [125]].

5. [LAD] Roland-Cerf-like,

$$f_{\mathrm{RC}}(s) = \frac{g_0 f_0 (1-s)}{g\sqrt{(g_0/g)^2 + f_0^2 s(2-s)}}. \tag{5.15}$$

The temporal profile of these functions, with the parameters of the problem treated in this Chapter, is shown in Figure 5.2. By numerically integrating the Schrödinger equation (5.9) for different total time τ, and using the different sweep functions just enumerated, one obtains a behavior of the final fidelity as reported in Figure 5.3. The function giving smaller fidelity, in general, for a given total time, is the linear ramp by far. The latter requires at least 10 μs for reaching a 0.999 fidelity. The BCDs initially follow the LZMS curve, but the fidelity then decays exponentially fast from around 700 ns, reaching 0.9999 in less than 3 μs. The global behavior for f_β and f_{pl} is basically the same, with the exponential-decay regime starting slightly earlier for f_{pl}. Finally, also the LADs share a common global trend, with f_{RC} presenting a rather large set of pronounced minima in the infidelity. Even though these can reach very small values, they are highly unstable with respect to the choice of the total time. Therefore, one expects that they cannot be exploited for a systematic optimization of the protocol. LADs make fidelities above 0.9 and 0.99 accessible from much

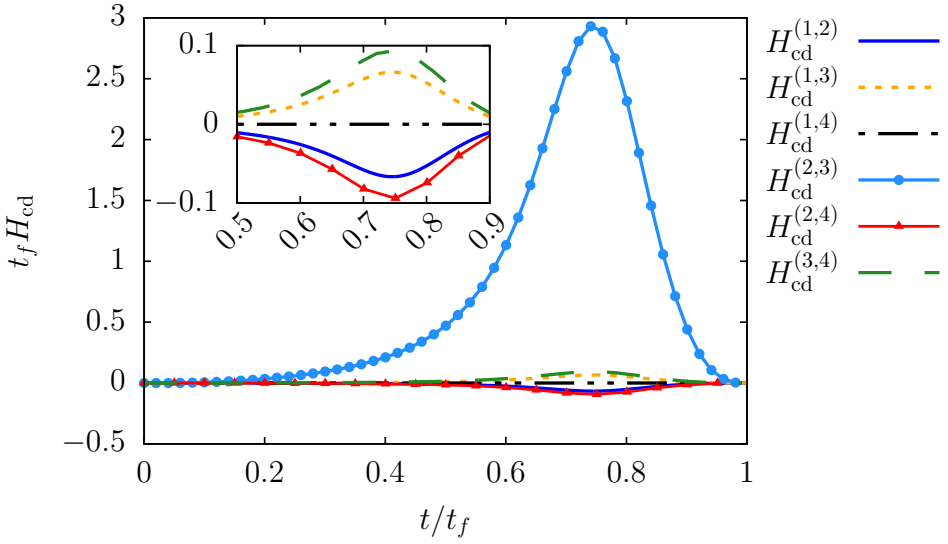

Figure 5.4: Imaginary part of the matrix entries of the $H_{\mathbf{cd}}(t)$ Hamiltonian[equation (5.16)]. The by far dominant matrix element of the counterdiabatic Hamiltonian $H_{\rm cd}(t)$ is $H_{\rm cd}^{(2,3)}(s)$ (and its complex conjugate), corresponding to a nonadiabatic coupling between state $|1\uparrow\downarrow\rangle$ and $|1\downarrow\uparrow\rangle$. (Figure adapted from [125]).

shorter times, around 200 ns and 400 ns respectively. However, neither $f_{\rm tan}$ nor $f_{\rm RC}$ can reach fidelities larger than 0.999 in less than one μs. In conclusion, excluding the linear ramp, we can identify two time regimes depending on whether LADs or BCDs achieve lower infidelities, but, still, the total protocol duration needed for interesting precision levels is too large for these adiabatic methods to be appealing in practice. The situation will get different instead, if the same adiabatic sweeps are supported by effective counterdiabatic driving fields, as we will analyze in the following Sections.

5.4 COUNTERDIABATIC HAMILTONIAN

Since the time-dependent Hamiltonian (5.10) cannot be diagonalized analytically, we resort to a numerical evaluation of the counterdiabatic field. First of all, the Hamiltonian is real-valued, hence the cd Hamiltonian $H_{\rm cd}(t)$ is fully imaginary (as discussed in Section 4.1). Considering the form 5.13 for the sweep function, the matrix entries

$$H_{\rm cd}^{(k,l)}(s) = \mathrm{Im}\,\langle k|H_{\rm cd}(s)|l\rangle\,, \tag{5.16}$$

with $\{|0\rangle, |1\rangle, |2\rangle, |3\rangle\} = \{|0\uparrow\uparrow\rangle, |1\uparrow\downarrow\rangle, |1\downarrow\uparrow\rangle, |2\downarrow\downarrow\rangle\}$, are depicted in Figure 5.4. It is immediately evident that the $H_{\rm cd}^{(2,3)}(t)$ component is largely dominant with respect to all the others. This component couples directly the two states $|1\uparrow\downarrow\rangle$ and $|1\downarrow\uparrow\rangle$ which, being those involved in the avoided crossing, also attain the smallest gap. Therefore, the global adiabatic condition (2.40) indicates that

nonadiabatic transitions are substantially determined by this term. For this reason, in the following we will neglect the other entries in the cd Hamiltonian and define a "partial" cd Hamiltonian

$$H_{\mathrm{p}}(s) = \frac{H_{\mathrm{cd}}^{(2,3)}(s)}{2}\left[\hat{\sigma}_1^x\hat{\sigma}_2^y - \hat{\sigma}_1^y\hat{\sigma}_2^x\right] \tag{5.17}$$

which we target to realize. If one is able to implement this coupling directly in the Hamiltonian, numerical inspection shows that fidelities above 99.999% would in principle be attainable at whatever timescale. However, due to the fact that $H_{\mathrm{cd}}(s)$ scales like $1/t_f$, the faster the protocol, the stronger the $H_{\mathrm{cd}}^{(2,3)}(s)$ component is. For instance, the Hamiltonian (5.17) would produce 0.99999 fidelity in 50 ns requiring a maximal value of $H_{\mathrm{cd}}^{(2,3)}$ around 10 MHz. By dividing the value depicted in Figure 5.4 by t_f, it is possible to extrapolate the maximal value of $H_{\mathrm{cd}}^{(2,3)}$ corresponding to different total times t_f.

5.5 EFFECTIVE COUNTERDIABATIC CONTROL

The matrix $\hat{\sigma}_1^x\hat{\sigma}_2^y - \hat{\sigma}_1^y\hat{\sigma}_2^x$ composing the counterdiabatic Hamiltonian (5.17) is in general not implementable directly in the experimental setup under analysis (see Section 5.2). Indeed, it would require time-dependent control of an imaginary qubit-qubit coupling. For this reason, we here proceed in the derivation of an effective counterdiabatic field which can be realized assuming fast tuneability of the coupling g in time.

We notice that the matrix structure of the partial counterdiabatic field, $\hat{\sigma}_1^y\hat{\sigma}_2^x - \hat{\sigma}_1^x\hat{\sigma}_2^y$, can be generated from the set of initial control matrices through the commutator of the matrices $\hat{C}_1, \hat{C}_2$ defined as

$$\hat{C}_1 = \begin{pmatrix} 0 & 1 & 0 & 0 \\ 1 & 0 & 0 & 0 \\ 0 & 0 & 0 & \sqrt{2} \\ 0 & 0 & \sqrt{2} & 0 \end{pmatrix}, \qquad \hat{C}_2 = \begin{pmatrix} 0 & 0 & 1 & 0 \\ 0 & 0 & 0 & 1 \\ \sqrt{2} & 0 & 0 & 0 \\ 0 & \sqrt{2} & 0 & 0 \end{pmatrix}. \tag{5.18}$$

Indeed, it holds that

$$\hat{\sigma}_1^y\hat{\sigma}_2^x - \hat{\sigma}_1^x\hat{\sigma}_2^y = 2i[\hat{C}_1, \hat{C}_2].$$

Following the general method described in Chapter 4, a simple ansatz for the ecd Hamiltonian is then

$$H_{\mathrm{ecd}}(t) = u_1(t)\hat{C}_1 + u_2(t)\hat{C}_2. \tag{5.19}$$

Using the previous results on the construction of the commutator dynamics (see Section 4.2.1), we choose the control functions to be

$$u_1(t) = A\sqrt{\omega}\sin(\omega t); \quad u_2(t) = B\sqrt{\omega}\cos(\omega t). \tag{5.20}$$

The exponent of the Magnus expansion (introduced in Section 3.2) generated by H_{ecd}, to the lowest order in $T = 2\pi/\omega$, is then equal to

$$\hat{M}_{\mathrm{ecd}}(T) = -iT\frac{AB}{4}\left[\hat{\sigma}_1^x\hat{\sigma}_2^y - \hat{\sigma}_1^y\hat{\sigma}_2^x\right] + O\left(T^{3/2}\right). \tag{5.21}$$

For obtaining the shortcut, this term needs to be equated to the Magnus exponent generated by $H_{\mathrm{p}}(t)$, which, once expanded in small T, reads

$$\hat{M}_{\mathrm{p}}(T) = -iT\frac{H_{\mathrm{cd}}^{(2,3)}(T/2)}{2}\left[\hat{\sigma}_1^x\hat{\sigma}_2^y - \hat{\sigma}_1^y\hat{\sigma}_2^x\right]. \tag{5.22}$$

The resulting equation for the control amplitudes is then $AB = 2H_{\mathrm{cd}}^{(2,3)}$. Since $H_{\mathrm{cd}}^{(2,3)}$ is positive at all times for the sweep function $f(s) = f_{\mathrm{pl}}(t)$, a straightforward solution is

$$A(t) = B(t) = \sqrt{2H_{\mathrm{cd}}^{(2,3)}(t)}, \tag{5.23}$$

which leads to the shortcut Hamiltonian

$$H_{\mathrm{ecd}}(t) = \sqrt{2\omega H_{\mathrm{cd}}^{(2,3)}(t)}\left[\sin(\omega t)\hat{C}_1 + \cos(\omega t)\hat{C}_2\right]. \tag{5.24}$$

Hence, the effective counterdiabatic Hamiltonian requires quick modulation of the qubit-resonator coupling.

5.6 RESULTS

Now that the shortcut Hamiltonian is determined, equation (5.24), we discuss its performance in terms of the final infidelity as a function of the total duration of the protocol. Besides, we correlate these results with constraints on the experimental realizability of the protocol. Specifically, since the ecd Hamiltonian requires control on the qubit-resonator couplings, we consider different ratios k between the maximal amplitude needed by the control functions and the initial coupling g, $k = \frac{\sqrt{\omega}A(t)}{g}$. Indeed, a too large coupling would break the strong coupling approximation, making the Jaynes-Cummings Hamiltonian (5.3) inappropriate for the description of the system. From equation (5.23), we see that this condition implies a bound on the maximal driving frequency utilizable, namely

$$\omega_{\max} = \frac{k^2g^2}{2\max_t\left|H_{\mathrm{cd}}^{(2,3)}(t)\right|}. \tag{5.25}$$

As a further constraint, we take into account the fact that a too large driving frequency ω can break the RWA as well (c.f. Section 5.1.1). For this reason, we also fix an overall maximal ceiling on the frequency, which is applied even if equation (5.25) is satisfied. The choice of the ceiling is arbitrary, but in general it should be such that no resonances with any transition occur and such that counterrotating

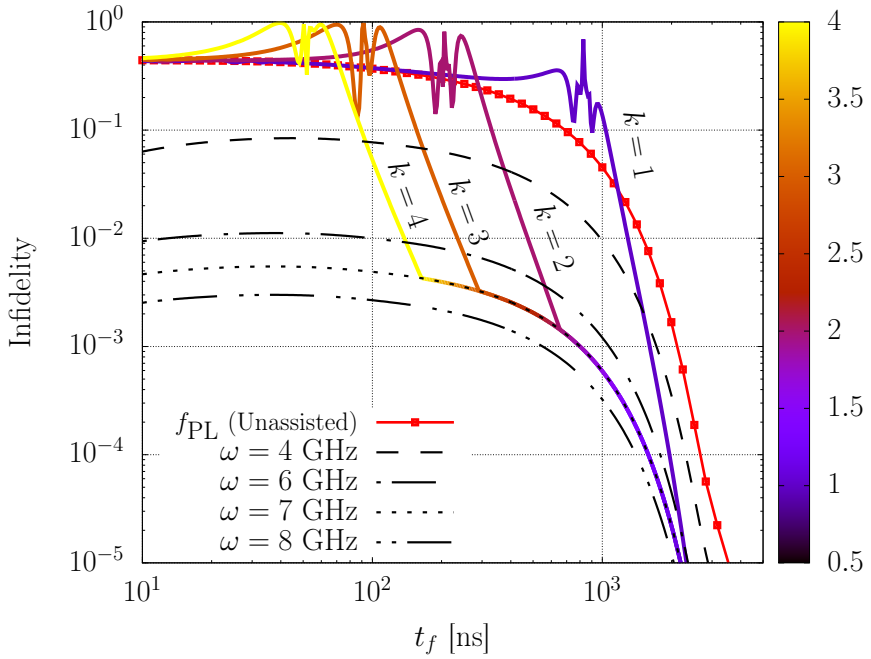

Figure 5.5: Final infidelity of the protocol as a function of the total duration for a polynomial BCD sweep. Broken curves correspond to the results of the ecd protocol (5.24) for an f_{pl} adiabatic drive and the fixed value of the driving frequency indicated in the legend, whilst the red curve (—■—) indicates those corresponding to the unassisted f_{pl} sweep. The colored curves represent the results for the ecd protocol when an upper bound is imposed to the maximal norm of the correcting Hamiltonian, as per equation (5.25) for different ratios k. The color scale indicates the maximal amplitude reached by the ecd fields in units of the coupling g. (Figure reproduced from [125])

terms are still at a rather large frequency. Here, we consider as main reference value $\omega_{\mathrm{max}}/2\pi = 7$ GHz, in which case terms neglected by the RWA oscillate at about $(\omega_r + \omega_{1,2})/2\pi = 14$ GHz at least. In any case, results for different ceilings between 4 and 8 GHz are still shown in the Figures below with broken black lines.

5.6.1 Accelerated BCD

In Figure 5.5, the results are shown for the case in which the ecd method is used to speed-up a boundary cancellation method, namely f_{pl} of equation (5.13). For $k = 1$, which implies an amplitude of the driving equal to g, an improvement is obtained with respect to the standard adiabatic method in a large-time regime. For instance, 0.999 fidelity is achieved with a 30% acceleration. However, since the total time still exceeds 2μs, stronger drivings would be preferable. Already for $k = 2$, the improvement is more net and fidelities above 0.999 start to become accessible from about $700 - 800$ ns.

Three regimes can be recognized from the colored curves: for fast timescales, $H_{\mathrm{cd}}^{(2,3)}$ is very large and the constraint on the maximal amplitude (5.25) strongly

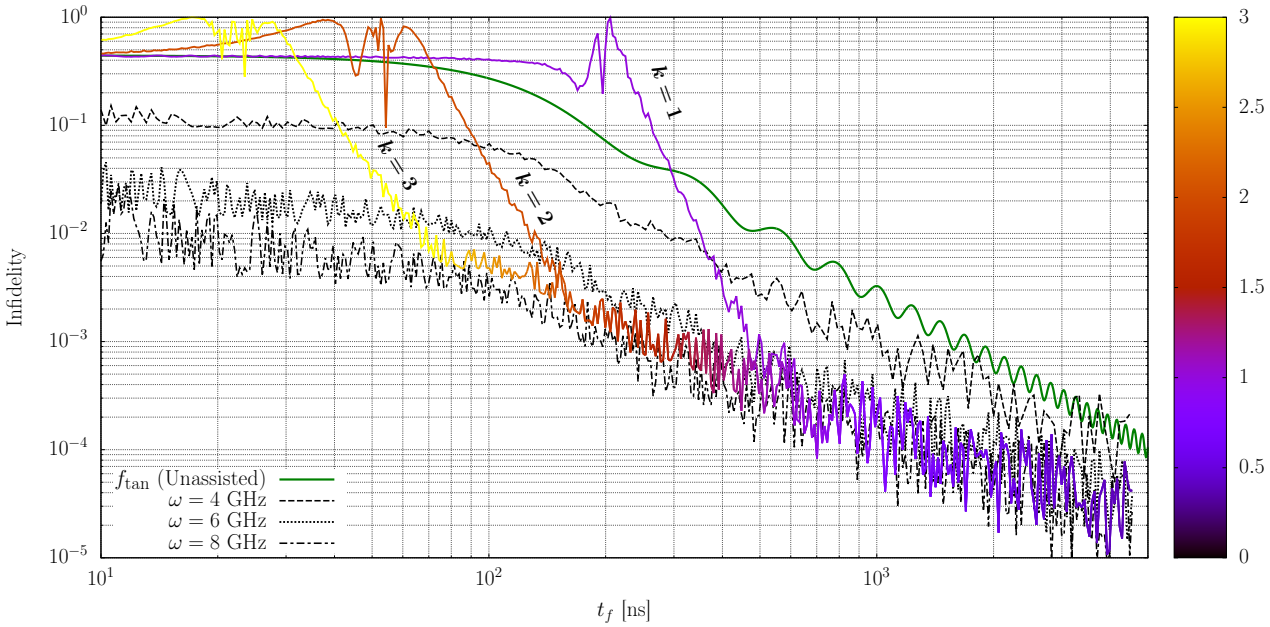

Figure 5.6: Final infidelity of the protocol as a function of the total duration for a LAD sweep. Results equivalent to those shown in Figure 5.5 for the choice of the reference adiabatic sweep $f_{\tan}$. The infidelity produced by the latter, in the absence of ecd correction, is represented by the (—) curve. (Figure reproduced from [125])

limits the maximal admissible driving frequency. The control is not sufficiently strong to compensate nonadiabatic transitions, and it becomes rather detrimental for the system dynamics. Then, for intermediate timescales, the method starts to be efficient and the infidelity decays polynomially with the timescale while the frequency is raised. Finally, the frequency reaches the 7 GHz ceiling, it remains constant at such value, and the infidelity decays exponentially. The choice of k determines how soon —that is, starting from which total time—the "7-GHz regime" is reached.

5.6.2 Accelerated LAD

The case in which a LAD is accelerated is represented in Figure 5.6. The sweep function considered is $f_{\tan}$, since it gives the best results in the unassisted case. We see immediately that lower infidelities are attained for a total time below one μs with respect to the BCD case of Section 5.6.1. Now, fidelities of at least 0.999 are obtained for $k = 1$ starting from around 500 ns. Fidelities of 0.99 can be obtained instead in around 65 ns with $k = 3$ and in 130 ns with $k = 1$. Hence, this protocol achieves the best results in the temporal regime in which we are interested in, and we will take it as the reference one for the following analyses.

5.6.3 Generalization to different parameters

All the results presented in this Chapter relate to the initial choice of system parameters made in Section 5.2. In this Section, let us discuss how these results generalize to different choices of these parameters. A central element in the whole analysis is the strength g of the coupling between each qubit and the resonator. If the value of g is increased, maintaining the qubit-resonator detunings δ_k fixed, then the global timescales for the protocol become shorter, for all possible choices of the sweep functions. This is easily explained in the light of a standard LZMS model: if g/δ increases, following an increase of g to the value $\bar{g} > g$, the avoided crossing between states $|\uparrow\downarrow\rangle$ and $|\downarrow\uparrow\rangle$ (see Section 5.1.1) becomes larger, $g^2/\delta \to \bar{g}^2/\delta$. From the point of view of adiabaticity, this is substantially equivalent to rescaling the duration by a factor $\bar{g}^2/g^2 > 1$. Hence, nonadiabatic transitions are reduced.

If the detuning $\delta_{\rm res}$ between the qubits (at the their resonant configuration) and the resonator is changed, two different effects must be taken into account. On the one hand, raising $\delta_{\rm res}$ diminishes the ratio $g/\delta_{\rm res}$ which is involved in the dispersive regime approximation. Making $g/\delta_{\rm res}$ smaller is in general beneficial since it further justifies the adiabatic elimination of states (belonging to the given excitation manifold) not involved in the protocol, i.e. $|2\downarrow\downarrow\rangle$ and $|0\uparrow\uparrow\rangle$. On the other hand, raising $\delta_{\rm res}$ also diminishes the ratio $g^2/\delta_{\rm res}$ which characterizes the width of the avoided crossing, thus leading to a dilation of the timescales necessary to attain the adiabatic regime. In conclusion, the values of g and $\delta_{\rm res}$ should be carefully balanced in such a way that the ratio $g/\delta_{\rm res}$ is minimized, while $g^2/\delta_{\rm res}$ is maximized.

A third important parameter is the gf_0, which quantifies the initial gap between the levels $|\uparrow\downarrow\rangle$ and $|\downarrow\uparrow\rangle$. The larger this value becomes, the faster the initial transient becomes in local adiabatic drivings, making those prevail in performance with respect to other methods. Of course, this is true provided the temporal rate of variation of the sweeps remains feasible experimentally. On the other hand, as gf_0 diminishes, all different sweep functions will tend to be well approximated by a simple linear (LZMS) ramp, giving then very similar results.

In the next Section, we will analyze how small variations of the parameters affect the overall performance of the protocol.

5.7 ROBUSTNESS

The results discussed in Section 5.6 bring evidence of the efficiency of the shortcut-to-adiabaticity method introduced in this Chapter. However, it is important to benchmark how the performance can be affected by the potential presence of unexpected errors in the protocol. First, we address here the effect of static shifts in the control parameters, namely frequency, amplitude and relative phase of the fields. Second, we take into account possible dissipative effects due to the interaction with

the environment. We perform these analysis using as a basis the ecd-LAD protocol discussed in Section 5.6.2, for driving frequency $\omega/2\pi = 7$ GHz.

5.7.1 Imperfections in the control parameters

Concerning parameter shifts, we introduce the perturbations $\boldsymbol{\epsilon} = \{\epsilon_\omega, \epsilon_\phi, \epsilon_A\}$ such that the parameter get distorted from their ideal values as

$$\omega \longrightarrow \omega[1+\epsilon_\omega], \tag{5.26a}$$

$$\cos(\omega t) \longrightarrow \cos(\omega t + \pi\epsilon_\phi), \tag{5.26b}$$

$$A(t) \longrightarrow A(t)[1+\epsilon_A]. \tag{5.26c}$$

We take the perturbations $\boldsymbol{\epsilon}$ to be random variables uniformly distributed over an interval $[-\epsilon_{\max}, \epsilon_{\max}]$, where we choose $\epsilon_{\max} = 5\%$. For quantifying the effect of these control errors on the system evolution, we study the average final infidelity produced over a number N_ϵ of realizations, which is

$$\left\langle \mathbb{I}_f(\boldsymbol{\epsilon}) \right\rangle_\epsilon = \frac{1}{N_\epsilon} \sum_\epsilon \mathbb{I}_f(\boldsymbol{\epsilon}). \tag{5.27}$$

We then study the relative error in the final infidelity due to the error, which, calling $\mathbb{I}_f^{(0)}$ the final infidelity for $\boldsymbol{\epsilon} = 0$, is

$$1 - \frac{\left\langle \mathbb{I}_f(\boldsymbol{\epsilon}) \right\rangle_\epsilon}{\mathbb{I}_f^{(0)}}. \tag{5.28}$$

This quantity is depicted in Figure 5.7 as a function of the total duration. An error bar is associated to each point, representing one standard deviation, defined as

$$\sigma\left(\mathbb{I}_f\right) = \sqrt{\left\langle \mathbb{I}_f^2(\boldsymbol{\epsilon}) \right\rangle_\epsilon - \left\langle \mathbb{I}_f(\boldsymbol{\epsilon}) \right\rangle_\epsilon^2}, \tag{5.29}$$

together with maximal and minimal values, indicated by asterisks and squares, respectively. The average values are typically lower than zero, indicating that, as expected, the method is spoiled by the presence of errors. However, the minimum values (asterisks) always lie at positive values. This means that sometimes small errors can accidentally lead to higher fidelities, as explained in detail in Section 4.5.

In the worst case, the infidelity increases by about 6 times with respect to the unperturbed value. On the other hand, the standard deviation always remains below 100%. This implies that, even if the infidelity fluctuates quite a lot in value if errors are present, it always increases by less than one order of magnitude. Therefore, since in typical quantum computation applications one targets a certain order of magnitude of the fidelity, we find that imperfections within 5% in the control parameter can be neglected to a good approximation. In order to elaborate on this feature, we report, in the lower panel of Figure 5.7, the average value of the logarithm of the infidelity,

$$\left\langle \log_{10} \mathbb{I}_f \right\rangle_\epsilon, \tag{5.30}$$

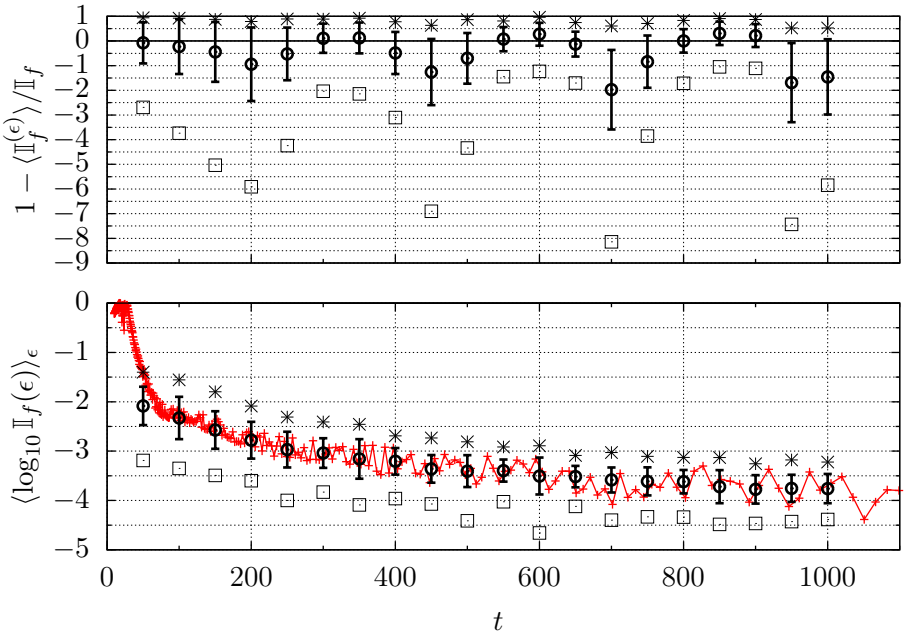

Figure 5.7: Two-qubit entanglement in cQED: robustness against protocol errors. Considering the accelerated LAD scheme of Section 5.6.2, the empty circles (○) in the upper panel represent the average relative error in the final infidelity as a function of the total protocol duration, for relative errors within 5% present in amplitude, frequency and relative phase of the ecd control fields [equations (5.26) and (5.27)]. The average logarithmic infidelity is depicted instead in the lower panel, where the red line reports the unperturbed results (—). The error bars represent one standard deviation, whilst asterisks (∗) and squared points (□) refer to maximal and minimal values, respectively (Figure reproduced from [126])

still as a function of the duration. Each point is accompanied by an error bar indicating one standard deviation, $\sigma(X) = \sqrt{\langle X^2 \rangle_\epsilon - \langle X \rangle_\epsilon^2}$ with $X = \log_{10}[\mathbb{I}_f(\boldsymbol{\epsilon})]$. One can see from Figure 5.7 that the infidelity in the presence of errors remains close to the unperturbed value, with the error bars always extending less than one order of magnitude. As an example, a fidelity larger than 0.999 can be obtained from 400 ns even with parameter imperfections.

5.7.2 Environment-induced noise

For analyzing the effect of dissipation and decoherence on the protocol, we make use of the GKSL master equation formalism introduced in Section 5.1.2. This takes into account photon leakage from the resonator, together with spontaneous emission and dephasing for the two qubits. We numerically solve the master equation for the full ecd Hamiltonian considering three photonic states of the cavity, assuming, for convenience, equal decay rates for the two qubits, $\gamma_r^{(1)} = \gamma_r^{(2)} \equiv \gamma$ and $\gamma_\phi^{(1)} = \gamma_\phi^{(2)} = \gamma/2$. Figure 5.8 reports a color map representing the final infidelity

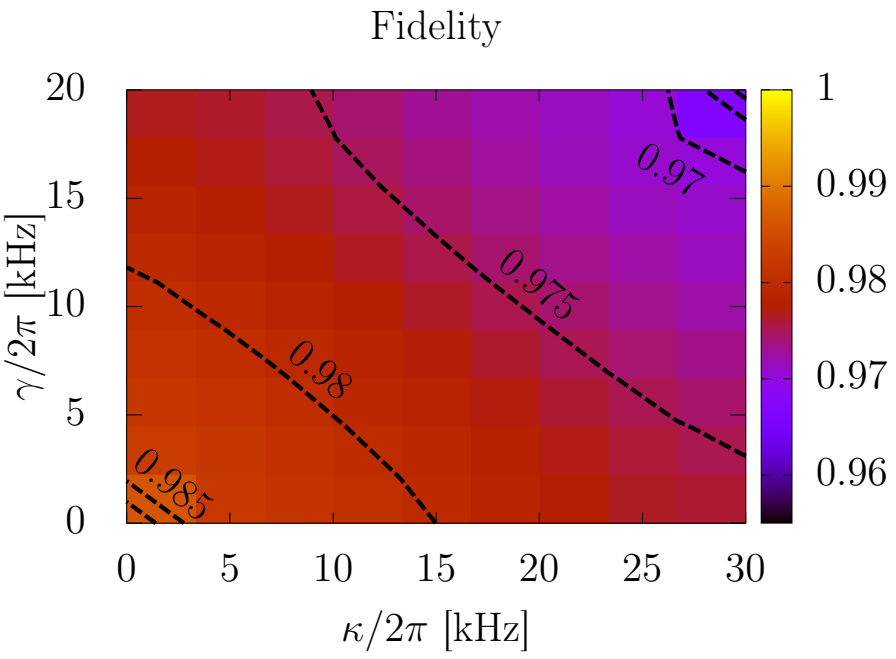

Figure 5.8: Final fidelity *vs* damping rates for the ecd entangling protocol. Results obtained from numerical solution of the master equation (5.6) for the tangent ecd-LAD protocol with $\omega/2\pi = 7$ GHz and total duration $t_f = 100$ ns. Three photonic states of the bosonic field and equal decay rates for the two qubits were considered. (Figure reproduced from [125])

as a function of the damping rate of the qubit γ and of the resonator κ. The fidelity maintains large values, remaining well above 98% for typical parameters, such as $\gamma/2\pi = 5$ kHZ and $\kappa/2\pi = 5$ kHz. Even for larger rates, around $10 - 15$ kHz, the fidelity never drops below 97%. In this context, we have also analyzed numerically the validity of the RWA approximation, both in the closed and open system setting. This has been done by using the full Hamiltonian of equation (5.2), again considering a truncation of the Fock Hilbert space to 3 photonic states. The corresponding dimension of the density matrix is 12×12. The outcome of the simulations confirm that the approximation is valid also in the presence of the driving. The major feature which is observed is the renormalization of the width of the avoided crossing induced by the presence of further levels of the spectrum. This phenomenon can produce a global improvement of the protocol due to the effect of the minimal anticrossing gap on the adiabatic dynamics described in Section 5.6.3. This can be explained by means of the following perturbative argument. Let us start with the Hamiltonian of equation (5.5), keeping also the counterrotating terms, and let us introduce the quantity $\Delta_k = \omega_k + \omega_r$. We then perform a unitary transformation whose aim is that of "removing" from the Hamiltonian the counterrotating term of order g, leaving only second-order terms. This transformation reads

$$U_2 = \exp\left[-\sum_{k=1}^{N} \frac{g}{\Delta_k}(\hat{\sigma}_k^- \hat{a} - \hat{\sigma}_k^+ \hat{a}^\dagger)\right]. \tag{5.31}$$

As a result, the Hamiltonian in this new frame reads

$$\begin{aligned} U_2U_1HU_1^\dagger U_2^\dagger =&\omega_r\hat{a}^\dagger\hat{a}+\sum_{k=1}^{N}\left\{\frac{\omega_k}{2}+\frac{1}{2}\left(\frac{g^2}{\delta_k}+\frac{g^2}{\Delta_k}\right)(2\hat{a}^\dagger\hat{a}+1)\right\}\hat{\sigma}_k^z \\ &+\frac{1}{2}\sum_{k,n=1}^{N}\left(\frac{g^2}{\delta_k}-\frac{g^2}{\Delta_k}\right)[\hat{\sigma}_k^+\hat{\sigma}_n^-+\hat{\sigma}_k^-\hat{\sigma}_n^+] \\ &+\sum_{k=1}^{N}\frac{g^2}{\delta_k}[\hat{a}^2+(\hat{a}^\dagger)^2]\hat{\sigma}_k^z+\sum_{k,n=1}^{N}\frac{g^2}{\delta_k}[\hat{\sigma}_k^-\hat{\sigma}_n^-+\hat{\sigma}_k^+\hat{\sigma}_n^+]. \end{aligned} \tag{5.32}$$

Inspecting the hopping interaction at the second line of equation (5.32), we see that one effect of not assuming the RWA shows up in terms of a renormalization of the coupling, which is modified according to

$$\frac{g^2}{\delta_k}\longrightarrow g^2\left(\frac{1}{\delta_k}-\frac{1}{\Delta_k}\right). \tag{5.33}$$

Interestingly, we see that the coupling strength can thus be either reduced or increased, depending on the sign of $\delta_k=\omega_k-\omega_r$, and hence on whether the transition frequency of the k-th qubit is larger or smaller than the resonator frequency ω_r, for a fixed detuning. If one chooses $\omega_k<\omega_r$, the coupling can be maximized (in absolute value) for our parameters to ≈ -8.2 MHz, while its minimal value is ≈ -5.5 MHz. This numbers match the numerical estimates. By maximizing the coupling strength, the global timescales of adiabaticity are reduced, as discussed in Section 5.6.3, leading to the desired fidelities even in a shorter time.

5.8 DISCUSSION

This Chapter has been dedicated to a first application of the framework introduced in Chapter 4 to a problem of relevance in the field of quantum control. This has featured the production of two-qubit entangled states in a model describing a typical architecture of superconducting circuits. Summarizing the analysis, we have first conceived a reference adiabatic protocol for achieving this task (Section 5.2). In this context, we have compared, in Section 5.3, different choices of optimized adiabatic sweep functions (whose general concepts were introduced in Section 2.2), by benchmarking the performance, in terms of final fidelity, for different total durations of the protocol (for a given set of realistic parameters). This has allowed us to individuate different temporal regimes according to the corresponding best-performing sweep function. We have then calculated numerically the exact counterdiabatic Hamiltonian in Section 5.4, according to the theory described in Chapter 2, Section 2.3, and we have ascertained that these corrections are not implementable in the architecture under analysis. We have then introduced shortcut corrections to the protocol, which produce an effective counterdiabatic field via rapid modulation of the qubit-resonator couplings. In the present experimental context, this procedure can be implemented provided one assumes that tunable-coupling qubits of the

type proposed, e.g., in Ref.s [65, 146] are used. Finally, we compared accelerated protocols associated to the different optimized adiabatic sweeps, keeping track of possible experimental constraints on the magnitude of amplitude and frequency of the modulation. We find that the performance hierarchy, at a given total timescale, among the different sweep functions is in general replicated for the corresponding accelerated protocols. In the temporal regime of interest for practical applications, the largest fidelity is attained by an accelerated local adiabatic driving (Section 5.4).

Interestingly, by operating a smart choice of the configuration of the transition frequencies of qubits and resonator, one can make the level shift induced by the presence of the full spectrum to be positive. The result of this is an enlargement of the avoided crossing exploited for creating entangled superposition states, which then translates into a global reduction of the total timescales needed for ensuring adiabatic tracking for all the choices of sweep.

Further investigation for this protocol can be directed towards the design of different modulation schemes realizing the same effective Hamiltonian. Indeed, having different control options which produce the same effective counterdiabatic correction would make the protocol more flexible with respect to the specific control resources available in the laboratory. A possibility can be that of trading modulations in the coupling with stronger modulations of the transition frequencies of the qubits. Stronger modulations are needed since the desired coupling would appear at higher-order terms in the Floquet-Magnus expansion in this case. One can predict though that, due to the strong driving, this procedure could lead to a shortcut protocol which is quite far from being adiabatic, hence arguably becoming more sensitive to external noise.

A separate interesting investigation, going beyond the topics covered in this thesis, would regard a detailed analysis of the effect of the driving scheme on dissipative effects. When including the presence of the environment in our model (Section 5.7), we have assumed a typical form of the dissipators well tested for the type of system considered. Although this is expected to give good qualitative information on what to expect in a realistic implementation, in the limit of strong driving further effects may be observed. For instance, decoherence phenomena may be distorted by the presence of the controls, in such a way that dressed states of the whole controlled qubit-resonator system may couple to the environment. We will extend this discussion in the final Chapter 7.

In the next Chapter, we will treat a different application, whose objective is that of realizing fast and robust population transfers in a three-level system and associated quantum gates. This is naturally implementable experimentally in the optical regime with atoms, as well as in the microwave regime of superconducting circuits described in this Chapter.

6 THREE-LEVEL ACCELERATED STATE TRANSFERS

In this Chapter we discuss a second application of the method developed in this thesis, whose purpose is that of optimizing the performance of one of the most widespread quantum control methodologies for few-level systems. In particular, the method is used for constructing an accelerated counterpart of the STimulated Raman Adiabatic Passage (STIRAP) [165] technique. Using the effective counter-diabatic (ecd) framework, we construct corrections to the standard control pulses of this protocol which allow one to strongly relax the conditions on the control parameters usually imposed by adiabaticity constraints. As a result, large fidelities become accessible in an extremely larger parameter space. We first introduce the basics of STIRAP in Section 6.1, and of the corresponding exact counterdiabatic (cd) correction in 6.2. The shortcut method is constructed in Section 6.3. Its realizability in explicit experimental platforms, in the optical and microwave regimes, is discussed in Section 6.3.2. The performance of the method is then analyzed in detail in Section 6.4, in terms of transfer fidelity, protocol speed and robustness against implementation errors and dissipative effects. Finally, a further application for the realization of quantum gates based on accelerated fractional-STIRAP [99, 163] is the subject of Section 6.5.

After the quantum computation application discussed in Chapter 5, this contributes a second example of a fundamental building block of a quantum circuit whose performance is enhanced by our method.

6.1 STIRAP

STIRAP is among the most diffused quantum control techniques [164, 165]. The fundamental model of STIRAP involves a three-level system driven by external laser fields. The purpose of the protocol is that of producing population transfer between two states $|0\rangle$ and $|2\rangle$ which cannot be coupled by a dipole-transition moment, while avoiding transient populations in potentially lossy intermediate states. This technique was first introduced in a series of works, Ref.s [68, 69, 96], being rather established with Ref. [69], and, since then, it has become a standard in many branches of physics and chemistry. The great success of STIRAP can be traced back to its robustness against moderate variations of the intrinsic parameters of the control sequence, and against population losses by spontaneous emission from other states involved in the process.

The protocol is realized by exploiting a laser coupling between each of the two states and an intermediate state $|1\rangle$. The three levels may lie in different

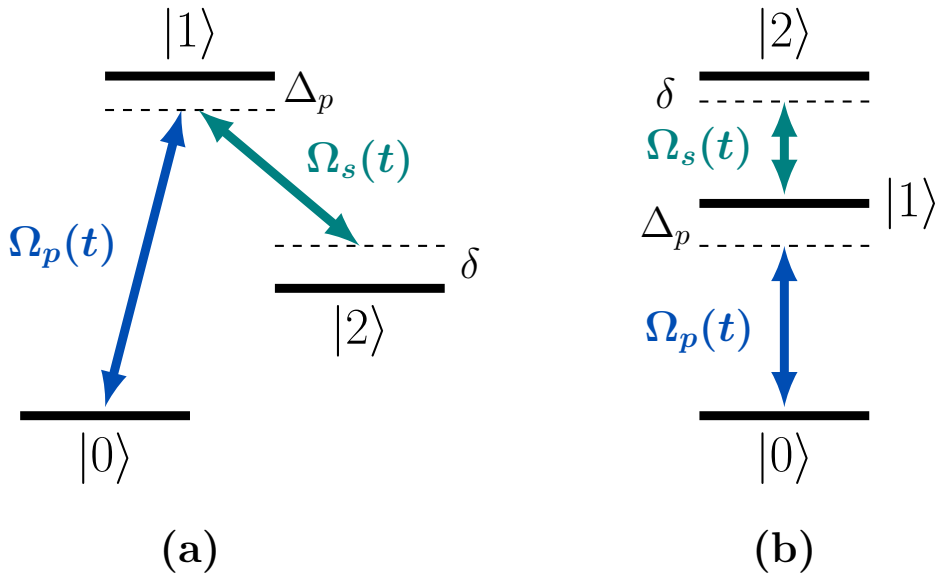

Figure 6.1: Level configurations for STIRAP. (a) Λ configuration; **(b)** ladder configuration.

configurations, such as the lambda (Λ) or the cascade/ladder (Figure 6.1). In the Λ scheme, the ordering of the energy levels corresponding to the three states is $E_1 > E_2$, $E_1 > E_0$, while in the ladder one the ordering is $E_2 > E_1 > E_0$. For simplicity, we will just consider the latter, even though all the following treatment can be straightforwardly adapted to the Λ case.

A central feature of STIRAP is that, despite the involvement of the third intermediate state, it does not induce population transients in such a state (in the ideal limit). Therefore, the method is highly robust against potential excitation losses from state $|1\rangle$. This is possible thanks to a so-called "counterintuitive" pulse sequence. The name originates from the fact that the first control laser, realizing the "Stokes" pulse, does not couple to the occupied state $|0\rangle$, but it rather couples the initially unoccupied states $|1\rangle$ and $|2\rangle$ instead. The second so-called "pump" pulse is then applied sequentially, and it couples states $|0\rangle$ and $|1\rangle$ completing the desired population transfer (see Figure 6.2). This procedure generates a time-dependent eigenvector of the driven Hamiltonian which evolves only in the subspace spanned by the $|0\rangle$ and $|2\rangle$ states. If the temporal features of the pulses are suitably designed, the system adiabatically follows this state and the desired population transfer is achieved.

In a frame rotating at the driving frequencies, and in the rotating-wave approximation, the Hamiltonian of STIRAP can be written as

$$H(t) = \frac{1}{2}\begin{pmatrix} 0 & \Omega_p(t) & 0 \\ \Omega_p(t) & 2\Delta_p & \Omega_s(t) \\ 0 & \Omega_s(t) & 2\delta \end{pmatrix}, \tag{6.1}$$

where Δ_p is the detuning of the pump laser from the $|0\rangle$-$|1\rangle$ transition, Δ_s is the detuning of the Stokes pulse from the $|0\rangle$-$|2\rangle$ transition, $\delta = \Delta_p + \Delta_s$ is the two-

photon detuning of the $|0\rangle$-$|2\rangle$ transition, $\Omega_p(t)$ and $\Omega_s(t)$ are the Rabi frequencies of the pump and Stokes pulses, respectively. For STIRAP to work, it is required that $\delta = 0$. Many different time profiles have been studied for these Rabi frequencies. A typical choice is to use Gaussian shapes. For definiteness, we use such pulses as well in the following, whose explicit form is

$$\Omega_p(t) = \Omega_{0,p} \exp\left[-\left(\frac{t-\tau}{T_w}\right)^2\right], \tag{6.2a}$$

$$\Omega_s(t) = \Omega_{0,s} \exp\left[-\left(\frac{t+\tau}{T_w}\right)^2\right]. \tag{6.2b}$$

In this way, the pulses have standard deviation $T_w/\sqrt{2}$ and their peaks are separated in time by $2\tau > 0$. We will assume equal peak values, i.e., $\Omega_{0,s} = \Omega_{0,p} \equiv \Omega_0$. It is further convenient to introduce dimensionless parameters, namely

$$t_w = t/T_w, \quad \Omega_{0w} = \Omega_0 T_w, \tau_w = \tau/T_w. \tag{6.3}$$

The Hamiltonian of (6.1) can be diagonalized exactly for all times [165]. Introducing the "adiabatic energy" $\overline{\Omega}(t) = \sqrt{\Omega_p^2(t) + \Omega_s^2(t)}$ [100], the instantaneous eigenvectors can be written in the parametrized form

$$|b_-(t)\rangle = \cos\phi(t)\,|b(t)\rangle - \sin\phi(t)\,|1\rangle\,, \tag{6.4a}$$

$$|b_+(t)\rangle = \sin\phi(t)\,|b(t)\rangle + \cos\phi(t)\,|1\rangle\,, \tag{6.4b}$$

$$|d(t)\rangle = \cos\theta(t)\,|0\rangle - \sin\theta(t)\,|2\rangle\,, \tag{6.4c}$$

where

$$|b(t)\rangle = \sin\theta(t)\,|0\rangle + \cos\theta(t)\,|2\rangle \tag{6.5}$$

will be dubbed the "bright state". The mixing angles $\theta(t)$ and $\phi(t)$ are defined by the relations

$$\tan\theta(t) = \frac{\Omega_p(t)}{\Omega_s(t)}; \quad \tan 2\phi(t) = \frac{\overline{\Omega}(t)}{\Delta_p}. \tag{6.6}$$

In the case of resonant STIRAP [$\Delta_p = 0$], the angle $\phi(t)$ simplifies to $\phi(t) = \pi/4$. The instantaneous eigenvalues are

$$E_\pm(t) = \frac{1}{2}\left[\Delta_p \pm \sqrt{\Delta_p^2 + \overline{\Omega}^2(t)}\right], \quad E_d(t) = 0. \tag{6.7}$$

The zero-energy state $|d(t)\rangle$ is known as the "dark" state [7] and, remarkably, it has no components along $|1\rangle$. Here lies the essence of STIRAP: if a system, initially prepared in $|0\rangle$, is driven adiabatically, then it will follow the instantaneous dark state ending up in the desired state $|2\rangle$ with no overlap over $|1\rangle$ during the evolution. In order to find what conditions need to be fulfilled by the pulses in order to induce adiabatic dynamics, we can use the adiabatic condition (2.40). The

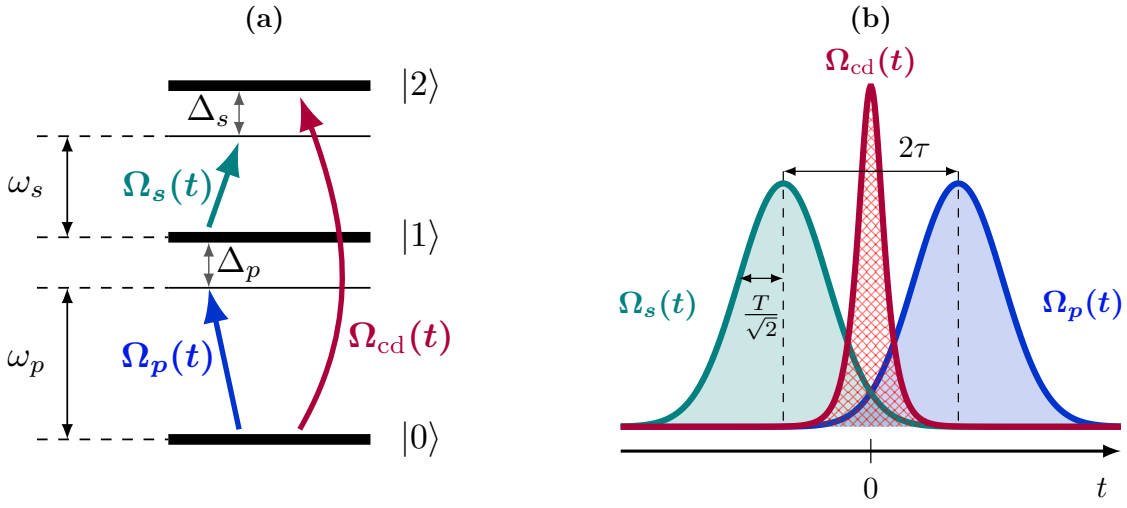

Figure 6.2: Ladder STIRAP configuration and sketch of the pulse sequence. (a) Scheme of the energy levels and of the laser couplings for STIRAP in ladder configuration. **(b)** temporal dependence of the Rabi frequencies of the pump, Stokes, and ideal counterdiabatic pulses. (Figure adapted from [126])

nonadiabatic coupling $\langle n|\partial_t m\rangle$ can be computed using the expressions (6.4), while the minimum gap is given by equations (6.7). At resonance [$\Delta_p = 0$], this leads to the condition

$$\max_t \frac{|\Omega_s(t)\partial_t\Omega_p(t) - \Omega_p(t)\partial_t\Omega_s(t)|}{\overline{\Omega}^2} \ll \min_t |\overline{\Omega}(t)|. \tag{6.8}$$

If relation (6.8) is satisfied, then one can expect the system to adiabatically follow the instantaneous dark state. Further details on different adiabatic conditions can be found in Ref. [165]. We will see in the next Sections that the adiabaticity constraint strongly reduces the space of parameters which can be used for implementing the protocol. This leaves room for the introduction of a shortcut technique which aims at enhancing STIRAP beyond this limitation.

6.2 COUNTERDIABATIC STIRAP

Direct application of the theory of transitionless quantum driving to STIRAP produces a counterdiabatic (cd) field which oddly requires time-dependent control of the $|0\rangle - |2\rangle$ transition [48]. Indeed, using the expressions (6.4) for the instantaneous eigenvector of the STIRAP Hamiltonian (6.1) together with equation (2.62), one finds the counterdiabatic Hamiltonian

$$H_{\rm cd}(t) = \frac{1}{2}\Omega_{cd}(t)\begin{pmatrix} 0 & 0 & i \\ 0 & 0 & 0 \\ -i & 0 & 0 \end{pmatrix}, \tag{6.9}$$

with

$$\Omega_{cd}(t) = 2\partial_t\theta(t) = 2\frac{\Omega_s(t)\partial_t\Omega_p(t) - \Omega_p(t)\partial_t\Omega_s(t)}{\overline{\Omega}^2(t)}. \tag{6.10}$$

For the case of Gaussian pulses as in equation (6.2a), the cd Rabi frequency $\Omega_{cd}(t)$ reads

$$\Omega_{cd}(t) = \frac{\Omega_{cd}^{\text{peak}}}{\cosh\left(\Omega_{cd}^{\text{peak}}t\right)}, \tag{6.11}$$

where $\Omega_{cd}^{\text{peak}} = 4\tau/T_w^2$ denotes its peak value. The time profile of $\Omega_{cd}(t)$ is sketched in Figure 6.2 in relation to the pump and Stokes pulses. It is always nonnegative (since we are considering $\tau > 0$) and it reaches its maximum at the time in which the STIRAP pulses cross. The shape of the counterdiabatic pulse for other time-dependencies of the STIRAP pulses can be found in Ref. [72]. Note again that the counterdiabatic Hamiltonian (6.9) is orthogonal to the STIRAP Hamiltonian, see the discussion in Section 4.1.

It is interesting, for the forthcoming analysis, to compute the protocol transfer time for cd driving. We define the latter as the time necessary for the system to evolve from an initial state characterized by an occupation $p_0^{(i)}$ of the atomic bare state $|0\rangle$ to a final state with occupation $p_2^{(f)}$ of state $|2\rangle$. In order to do so, we recall that cd-STIRAP makes the system follow the instantaneous dark state exactly. Therefore, given the parametrization (6.4c) in terms of the mixing angle $\theta(t)$ defined in equation (6.6), the instantaneous populations of the system are

$$p_0(t) = \cos^2\theta(t); \quad p_2(t) = \sin^2\theta(t). \tag{6.12}$$

One can then substitute the explicit expressions of the Gaussian Rabi frequencies, equation (6.2a), into the expression (6.6) of $\theta(t)$. After having plugged the result into equation (6.12), one can invert the resulting equations in order to get the time t at which the populations are p_0 and p_1, which reads

$$t(p_0) = \frac{1}{\Omega_{cd}^{\text{peak}}}\log\left[\sqrt{\frac{1-p_0}{p_0}}\right], \tag{6.13}$$

$$t(p_2) = \frac{1}{\Omega_{cd}^{\text{peak}}}\log\left[\sqrt{\frac{p_2}{1-p_2}}\right]. \tag{6.14}$$

Eventually, the total transfer time is the difference $\tau_{\text{cd}} = t\left(p_2^{(f)}\right) - t\left(p_0^{(i)}\right)$, which reads

$$\tau_{\text{cd}} = \frac{1}{\Omega_{cd}^{\text{peak}}}\log\left[\sqrt{\frac{p_2^{(f)}p_0^{(i)}}{\left(1-p_2^{(f)}\right)\left(1-p_0^{(i)}\right)}}\right]. \tag{6.15}$$

This quantity diverges in the limit $p_2^{(f)} \to 1$ or $p_0^{(f)} \to 1$, consistently with the fact that the dark state matches the bare states $|0\rangle$ and $|2\rangle$ only asymptotically for

infinitely large (negative and positive, respectively) time. Moreover, once initial and final populations are fixed, the transfer time is completely determined by the maximal Rabi frequency $\Omega_{cd}^{\text{peak}}$.

6.3 FREQUENCY-MODULATED STIRAP

6.3.1 Construction of the shortcut Hamiltonian

Let us now discuss the construction of an effective counterdiabatic field for STIRAP. The fundamental constraint which we require is that the shortcut Hamiltonian can be realized by simply adding dynamical corrections to the basic pump and Stokes pulses. In this way, direct implementability of the resulting protocol is guaranteed without needing substantial modifications, if any, of the experimental setup. For this reason, let us start by considering a shortcut Hamiltonian in the general form

$$H_{\text{fmod}} = \frac{1}{2}\begin{pmatrix} 0 & f(t) & 0 \\ f^*(t) & 0 & g(t) \\ 0 & g^*(t) & 0 \end{pmatrix}, \tag{6.16}$$

where $f(t)$ and $g(t)$ are polychromatic (i.e., multi-harmonic) drives. Accordingly, we write them as

$$f(t) = \sum_{k\neq 0}^{-\infty,+\infty} \Omega_{f,k}(t) e^{-ik\omega t}; \qquad g(t) = \sum_{k\neq 0}^{-\infty,+\infty} \Omega_{g,k}(t) e^{-ik\omega t}. \tag{6.17}$$

Now, let us consider the fundamental harmonic ω only, and let us compute the first average Hamiltonian terms using equations (3.18)a-b. Since we have excluded the non oscillating $k = 0$ term in equation (6.17) the zero-th order term in the Floquet-Magnus expansion vanishes by construction. The first order effective Hamiltonian reads instead

$$\begin{aligned} H_{\text{eff}}^{(1)} = \frac{1}{4\omega}\Big[& (|\Omega_{f,-1}|^2 - |\Omega_{f,1}|^2)[|0\rangle\langle 0| - |1\rangle\langle 1|] \\ & + (|\Omega_{g,-1}|^2 - |\Omega_{g,1}|^2)[|1\rangle\langle 1| - |2\rangle\langle 2|] \\ & + (\Omega_{f,-1}\Omega_{g,1} - \Omega_{f,-1}\Omega_{g,-1})\,|0\rangle\langle 2| \\ & + (\Omega_{f,-1}^*\Omega_{g,1}^* - \Omega_{f,1}^*\Omega_{g,-1}^*)\,|2\rangle\langle 0|\Big]. \end{aligned} \tag{6.18}$$

This Hamiltonians contains the terms necessary to build up H_{cd}, namely $|0\rangle\langle 2|$ and $|2\rangle\langle 0|$. However, also diagonal terms are present, differently from the case of the two-level system and the cQED one presented in Chapters 4 and 5. These physically correspond to ac-Stark shifts of the energy levels induced by the drivings, and need to be set to zero in order to have the effective Hamiltonian actually mimic the cd Hamiltonian.

For the Hamiltonian of equation (6.18) to match the counterdiabatic Hamiltonian, the following equations need to be solved:

$$|\Omega_{f,1}|^2 - |\Omega_{f,-1}|^2 = 0 \tag{6.19a}$$

$$|\Omega_{g,1}|^2 - |\Omega_{g,-1}|^2 = 0 \tag{6.19b}$$

$$\frac{1}{4\omega}\left[\Omega_{f,1}\Omega_{g,-1} - \Omega_{g,1}\Omega_{f,-1}\right] = i\frac{\Omega_{cd}(t)}{2} \tag{6.19c}$$

Since $\Omega_{cd}(t)$ is real and always non-negative with our choice of STIRAP pulses, a possible solution can be obtained by taking first

$$\Omega_{f,1} = \Omega_{f,-1}, \quad \Omega_{g,1} = -\Omega_{g,-1}. \tag{6.20}$$

Then, one can choose $\Omega_{f,1} = i\Omega_{g,-1} = \Omega_{\mathrm{d}}$, obtaining finally

$$\Omega_{\mathrm{d}}(t) = \sqrt{\omega\Omega_{cd}(t)}. \tag{6.21}$$

For the Gaussian pulses of equation (6.2a), the latter equation together with equation (6.11) gives

$$\Omega_{\mathrm{d}}(t) = \sqrt{\frac{\omega\Omega_{cd}^{\mathrm{peak}}}{\cosh\left(\Omega_{cd}^{\mathrm{peak}}t\right)}}. \tag{6.22}$$

It is interesting to note that, due to the proportionality to $\sqrt{\Omega_{cd}(t)}$, the Rabi frequency of the ecd control fields vanishes where $\Omega_{cd}(t)$ does. This is the case, importantly, at the beginning and at the end of the protocol. Therefore, not only the switching on and off of the ecd fields is smooth, but also the micromotion oscillations are suppressed at the final time, where measurements are performed. The effective counterdiabatic Hamiltonian, joining equations (6.16), (6.17) and (6.21), is thus

$$H_{\mathrm{ecd}}(t) = \Omega_{\mathrm{d}}(t)\begin{pmatrix} 0 & \cos(\omega t) & 0 \\ \cos(\omega t) & 0 & \sin(\omega t) \\ 0 & \sin(\omega t) & 0 \end{pmatrix}. \tag{6.23}$$

For testing the effect of potential phase variations in the control fields, we generalize the Hamiltonian (6.23) by introducing a global phase ϕ_G and a relative phase ϕ_R between them. The complete shortcut Hamiltonian we will analyze reads then as follows:

$$H_{\mathrm{fmod}}(t) = \Omega_{\mathrm{d}}(t)\Big\{\cos(\omega t + \phi_G)[|0\rangle\langle 1| + |1\rangle\langle 0|] + \sin(\omega t + \phi_G + \phi_R)[|1\rangle\langle 2| + |2\rangle\langle 1|]\Big\}. \tag{6.24}$$

We will call the latter fmod Hamiltonian. Physically, the Hamiltonian $H_{\mathrm{fmod}}(t)$ describes control over two frequency sidebands of the pump and Stokes pulses, detuned by $\pm\omega$ from the corresponding carriers. The symmetry in the action over each sideband produces symmetric light shifts, see equation (6.18), which compensate each other to the dominant order. This compensation is imposed, mathematically, by the constraint equations (6.19a) and (6.19b).

6.3.2 Possible experimental implementations

The fmod-STIRAP Hamiltonian of equation (6.24) can be realized experimentally by generating sidebands of the pump/Stokes STIRAP pulses at frequencies $\pm\omega$ for both transitions. These need then to be suitably combined in order to produce the proper phase relations producing the oscillating terms as in equation (6.24). We will see in Section 6.4.3, that the method is rather robust with respect to potential imperfection in the phase manipulation. In the limit of large detuning $\Delta_p \gg 1$, under which the state $|1\rangle$ can be eliminated, the shortcut Hamiltonian can be physically understood as describing a time-dependent two-photon transition between initial and target states, and in this sense it can be connected also to a different shortcut method introduced in Ref. [72] and implemented experimentally in [157]. In the forecoming analysis, we will consider two possible implementations, one in the optical and another in the microwave regime. The first one involves a Rydberg STIRAP excitation, as realized for example in Ref. [78], while the second one consists in a superconducting circuit as realized in Ref. [157]. In the case of the Rydberg excitation, the generation of the sidebands can be done using the same resources needed for STIRAP. In particular, an input laser intensity I_{in} is first equally divided between the two driven transitions, resulting in a Rabi frequency $\Omega_{\text{in}}/\sqrt{2}$ for each branch. Then, the two laser beams can be processed in order to generate the desired sidebands with a maximal carrier-sideband conversion efficiency of $\alpha_m = 0.9$ [36]. In the superconducting circuit setup, the sidebands can be produced separately by using specifically-dedicated microwave sources, as done in Ref. [157].

For convenience, we treat the perturbations arising from the interaction of the environment in a common framework for both the experimental platforms considered. Specifically, we use the following Gorini-Kossakowski-Sudarshan-Lindblad (GKSL) master equation (see the general introduction in Section 5.1.2) for the density matrix $\rho(t)$ of the three-level system [157],

$$\frac{\partial\rho(t)}{\partial t} = -i[H(t) + H_{\text{fmod}}(t), \rho(t)] + \sum_{k=1}^{2} \Gamma_{k-1,k} \left(C_k \rho(t) C_k^\dagger - \frac{1}{2} \left\{ C_k^\dagger C_k, \rho(t) \right\} \right), \quad (6.25)$$

where the collapse operators C_k are defined as $C_k = |k\rangle\langle k+1|$. The master equation (6.25) describes population losses within the three levels involved in STIRAP. Therefore, strictly speaking, it would not be entirely correct for the treatment of the Rydberg excitation, because in such a system losses are often towards external energy levels. Nonetheless, since we are considering a ladder STIRAP configuration and we are interested in being in the upper level $|2\rangle$, equation (6.25) is a bona fide approximation. This is also confirmed by numerical tests. Concerning the decay parameters Γ_{01} and Γ_{12}, we will use the values of Ref. [40] for a Rydberg excitation, namely $\Gamma_{01}T_w = 7$ and $\Gamma_{12}T_w = 0.003$, and those of Ref. [157] for the superconducting circuit, namely $\Gamma_{01}T_w = 0.017$ and $\Gamma_{12}T_w = 0.023$.

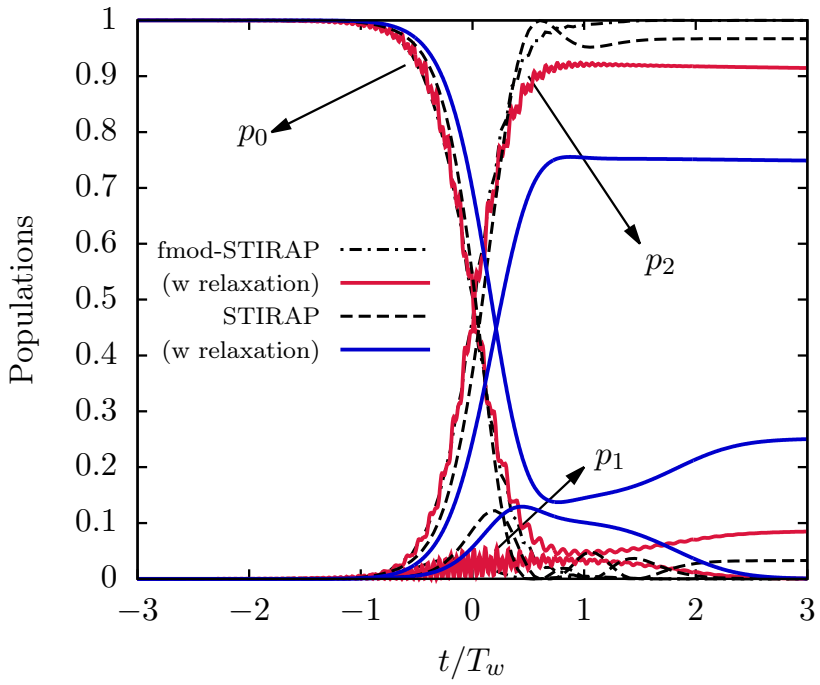

Figure 6.3: Dynamics of the populations for STIRAP and fmod-STIRAP. The broken lines indicate the evolution of the occupation probabilities in the absence of dissipation, for STIRAP (- - -) and fmod-STIRAP (-·-·), with parameters $\Omega_{0w} = 12$, $\tau_w = 0.7$, $\omega T_w = 60$. The colored curves (— for STIRAP and — for fmod-STIRAP) report the results in the presence of dissipative effects, obtained by numerical integration of the GKSL master equation (6.25) assuming the decay parameters of a Rydberg excitation described in Section 6.3.2, namely $\Gamma_{01} T_w = 7$, $\Gamma_{12} T_w = 0.003$. (Figure reproduced from [126])

A separate analysis is performed for potential applications in systems with strong decoherence effects, such as color centers implanted in solid-state materials. For taking into account this phenomenon, we introduce, in equation (6.25), artificial decoherence channels modeled by the collapse operators $\overline{C}_k = \sqrt{\gamma_k}\,|k\rangle\langle k|$, with $k = 0, 1, 2$. The rates γ_k are taken to vary within a few order of magnitudes larger than $\Gamma_{12} = 0.003$.

6.4 PROTOCOL FEATURES

6.4.1 Population transfers

First of all, we compare the final fidelity produced by the fmod-STIRAP protocol with that obtained using STIRAP. For the system initially prepared in STIRAP's dark state at the initial time $t = -6T_w$, the evolution of the populations is shown in Figure 6.3 in a temporal window $t/T = [-3T_w, 3T_w]$, for parameters $\tau = 0.7T_w$, $\Omega_0 T_w = 12$, $\omega T_w = 60$. The black broken curves (- - - for STIRAP and -·-· for

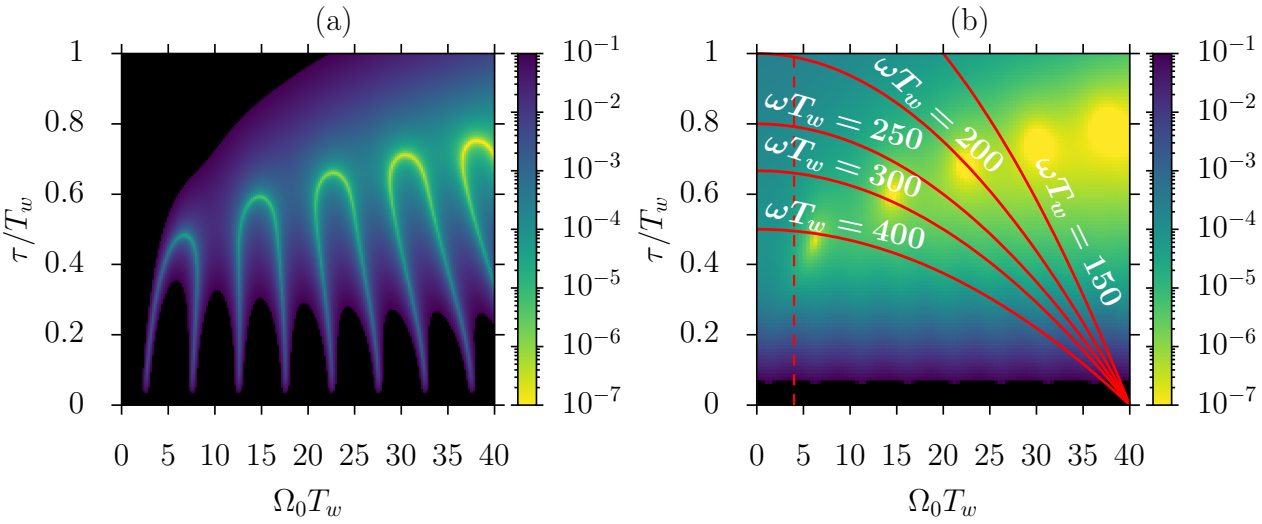

Figure 6.4: Final infidelity for STIRAP and fmod-STIRAP as a function of the parameters of the STIRAP pulses. (a) Infidelity produced by STIRAP at the final time $t = 4T_w$ with system initialized in the instantaneous STIRAP dark state at time $t = -8T_w$. **(b)** Final infidelity produced by fmod-STIRAP in the same time interval as for panel (a) for driving frequency $\omega T_w = 60$. For the experimental setup described in Section 6.3.2, a fixed maximal laser intensity limits the maximal intensity which can be dedicated to the sidebands and, consequently, it limits the maximal implementable driving frequency (see equations (6.26) and (6.27) in the main text and related discussion). The red solid lines (—) indicate the boundary below which the corresponding driving frequency is achievable, while the red dashed line (- - -) signals the minimal $\Omega_0 T_w$ achievable assuming maximal carrier-sideband conversion efficiency $\alpha_m = 0.9$. In both panels, the black regions indicate parameter sets for which the final fidelity does not reach 0.9. (Figure adapted from [126])

fmod-STIRAP) indicate results in the ideal case, i.e., in the absence of dissipative effects. On the other hand, colored solid curves (— for STIRAP and — for fmod-STIRAP) indicate results in the presence of dissipation for the decay parameters of a Rydberg excitation $\Gamma_{01} T_w = 7$, $\Gamma_{12} T_w = 0.003$ introduced in Section 6.3.2. In the ideal case, fmod-STIRAP produces a fidelity getting monotonically very close to one, while STIRAP settles on values slightly above 0.95. When dissipative effects are taken into account, the performance of STIRAP further diminishes as compared to the shortcut: the fidelity drops to values around 0.75 whereas fmod-STIRAP still remains above 0.9. This example not only shows that the shortcut protocol is very efficient in the ideal situation, but also that it maintains its efficiency against environmental disturbances. For making a more thorough comparison, we explore a wide range of parameter values in Figure 6.4. In order to do so, we consider different realistic values of the maximal Rabi coupling Ω_{0w} of the pump and Stokes pulses and of the pulse-shift τ_w. The infidelity at time $t/T_w = 4$, for the system initialized in the $|0\rangle$ state at time $t/T_w = -8$, is shown in Figure 6.4 using a logarithmic color scale. In both panels, the black areas indicate parameter

regions where the final fidelity is below 0.9. It is immediate to see that STIRAP (6.4a) gives fidelities above 0.9 in a restricted region. On the other hand, fmod-STIRAP achieves high fidelities (6.4b) almost everywhere, reaching peak values of 0.999999 in substantially extended sectors. Therefore, the shortcut protocol first of all improves the STIRAP state transfer for a fixed total time. Moreover, it greatly enlarges the range of applicability of STIRAP to parameter domains which where not usable before. It is interesting to note that STIRAP and fmod-STIRAP give their best results for similar parameters. For what concerns the oscillations around the target adiabatic path during the evolution, we show in Figure 6.5 how their peak value behaves as the driving frequency is raised, for different values of the temporal separation τ/T_w of the pump and Stokes pulses. The peak goes down rapidly with a power-law decay, witnessing that the dynamics produced by fmod-STIRAP is always very close to the instantaneous dark state. This is exactly the great advantage of our method.

Let us now discuss what is the effect of potential constraints on the power resources necessary to realize the fmod control fields. If an upper bound is imposed on the Rabi frequency $\Omega_{\mathrm{d}}^{\mathrm{peak}}$, according to equation (6.21), it translates into an upper

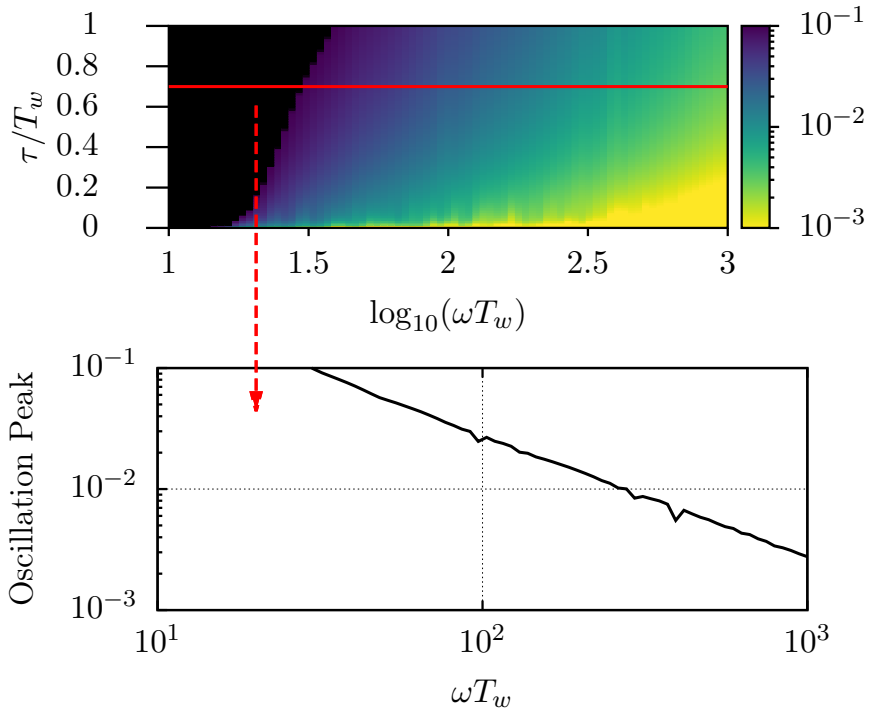

Figure 6.5: fmod-STIRAP: peak of the oscillations around the adiabatic path. In the upper panel, the peak of the oscillations in the time-dependent infidelity is shown, for varying pulse separation τ/T_w and driving frequency ωT_w. A latitudinal profile taken at $\tau/T_w = 0.7$ is reported in the lower panel. The black area excludes those points where the fidelity is below 0.9. (Figure adapted from [126])

bound on the driving frequency which can be used. If the latter becomes too small, the modulation is no more quick enough to effectively counteract nonadiabatic transition, and the whole shortcut construction is no more efficient. For instance, let us focus on the experimental setup discussed in Section 6.3.2 involving a Rydberg excitation. Let us assume that a maximal carrier intensity Ω_{in}^2 for each transition can be used, and that the sidebands are generated starting from this same carrier (as discussed in 6.3.2). Then, the maximal Rabi frequencies of the main STIRAP pulse, Ω_0, and of the two $\pm\omega$ sidebands, $\Omega_{\mathrm{d}}^{\mathrm{peak}}$, are constrained by the relation

$$\Omega_0^2 + 2(\Omega_{\mathrm{d}}^{\mathrm{peak}})^2 \leq \Omega_{in}^2. \tag{6.26}$$

Using equation (6.22), equation (6.26) then becomes

$$\frac{\tau}{T_w} \leq \frac{\Omega_{in}^2 - \Omega_0^2}{8\omega}. \tag{6.27}$$

This inequality implies a reduction of the parameter space which can be explored when using the fmod protocol for the given driving frequency ω. For $\Omega_{in}T_w = 40$ and for different driving frequencies, the boundaries defined by (6.27) are represented in Figure (6.4)b (—). If a limitation of 90% is taken on the efficiency of the carrier-sideband conversion, a further bound $\Omega_0 \geq 10\%\Omega_{in}$ must be taken into account: this is depicted with a - - - in Figure 6.4b. For all the choices of driving frequencies considered in the latter Figure, one can still select (Ω_{0w}, τ_w) points where the protocol gives optimal fidelity. This shows that the method can be used with great benefit also under strict experimental constraints.

For testing the robustness against dissipative and decoherence effects, the same results of Figure 6.4b are reproduced in Figure 6.6 when the system is open. Figure 6.6 is obtained using the GKSL master equation (6.25), with the decay parameters of a Rydberg excitation in (a), while using the decay parameters of a superconducting circuit in (b). In the case of the optical implementation, state $|2\rangle$ is very stable, and fidelities above 95% can be obtained even in the presence of environmental disturbance at the final time $t/T_w = 4$. The superconducting circuit presents a larger decay rate from state $|2\rangle$ and consequently the final fidelity is lower. Still, also in this case it remains above 0.9 for basically all sets of parameters for $\tau/T_w \geq 0.2$.

For systems with strong decoherence, we can individuate two different situations. First of all, dephasing processes involving the intermediate state $|1\rangle$ of the STIRAP process have little effect on the performance of the protocol, since this state is almost never populated during the evolution, thanks to the construction of the adiabatic process exploited. This type of decoherence is present, for instance, in the nitrogen-vacancy centre system studied in Ref. [178], even though in a Λ (rather than ladder) level configuration.

Secondly, for addressing the situation of dephasing affecting our "computational" basis $|0\rangle$ and $|2\rangle$ in a quantitative way, we consider the addition to the master equation of the jump operators $\overline{C}_0$ and $\overline{C}_2$ as described in Section 6.3.2.

The relaxation rate from state $|1\rangle$ which we have used in Figure 6.6a, $\Gamma_{01}T_w = 7$, is very strong, hence we judge that choosing an even stronger decoherence rate

would not be meaningful for realistic contexts. Therefore, we take as a reference point the relaxation rate of state $|2\rangle$, namely $\Gamma_{12}T_w = 0.003$, and we study the final infidelity for different ratios of this value and the artificial dephasing rates γ_0 and γ_2, with the same other parameters of Figure 6.6a. The results are reported in the panels (c)-(d) of Figure 6.6 for rates $\gamma_0 T_w = \gamma_2 T_w = 0.03$ [in 6.6c] and $\gamma_0 T_w = 0.3$, $\gamma_2 T_w = 0$ [in 6.6d]. The results for $\gamma_0 T_w = 0.3$, $\gamma_2 T_w = 0$ are equivalent to those in 6.6d. One can see that, even for decoherence rates a hundred times larger than Γ_{01} over one of the two states, the fidelity above 0.9 can be obtained for a wide set of control parameters. This supports the interest in our protocol also for systems with strong dephasing effects.

6.4.2 Protocol speed

For characterizing how fast the target state transfer can be performed, given a limited amount of resources, we compare in this section the total transfer time for the different protocols. Specifically, we measure the time elapsed from the state being with probability $p_0^{(i)}$ in state $|0\rangle$ to being in state $|2\rangle$ with probability $p_2^{(f)}$. We will choose $p_0^{(i)} = p_2^{(f)} = 0.99$.

As a first benchmark, we consider the transfer time for a "π"-pulse linking state $|0\rangle$ and $|2\rangle$ directly with Rabi frequency Ω(which is not realizable in the experimental contexts under analysis). In the two-level subspace, this saturates the quantum speed limit [45]. The Hamiltonian realizing this pulse is

$$H_\pi = i\Omega/2[|2\rangle\langle 0| - |0\rangle\langle 2|]. \tag{6.28}$$

Considering an initial state $|\psi_i\rangle$ and a final state $|\psi_f\rangle$ which are separated by an angle $\Theta_{f,i}$ in the subspace they span, the transfer time between these two is [45]

$$\tau_\pi = \frac{2\Theta_{f,i}}{\Omega} = \frac{2\arccos|\langle\psi_f|\psi_i\rangle|}{\Omega}. \tag{6.29}$$

If we parametrize the initial and final states as $|\psi_k\rangle = \cos\theta_k|0\rangle + e^{i\phi_k}\sin\theta_k|2\rangle$, the populations of the bare states $|0\rangle$ and $|2\rangle$ can be written like $p_0^{(i)} = \cos^2\theta_i$ and $p_2^{(f)} = \sin^2\theta_f$. Then one has that $\Theta_{f,i} = \theta_f - \theta_i$, leading eventually to the following expression of the transfer time as a function of the populations $p_0^{(i)}$ and $p_2^{(f)}$:

$$\tau_\pi = \frac{2}{\Omega}\left[\arcsin\sqrt{p_2^{(f)}} - \arccos\sqrt{p_0^{(i)}}\right]. \tag{6.30}$$

The total pulse area is simply

$$\int_{t_i}^{t_f}\Omega dt = \Omega\tau_\pi. \tag{6.31}$$

Using equation (6.30) with $p_0^{(i)} = p_2^{(f)} = 0.99$, we find the numerical transfer time

$$\tau_\pi = 2.74/\Omega. \tag{6.32}$$

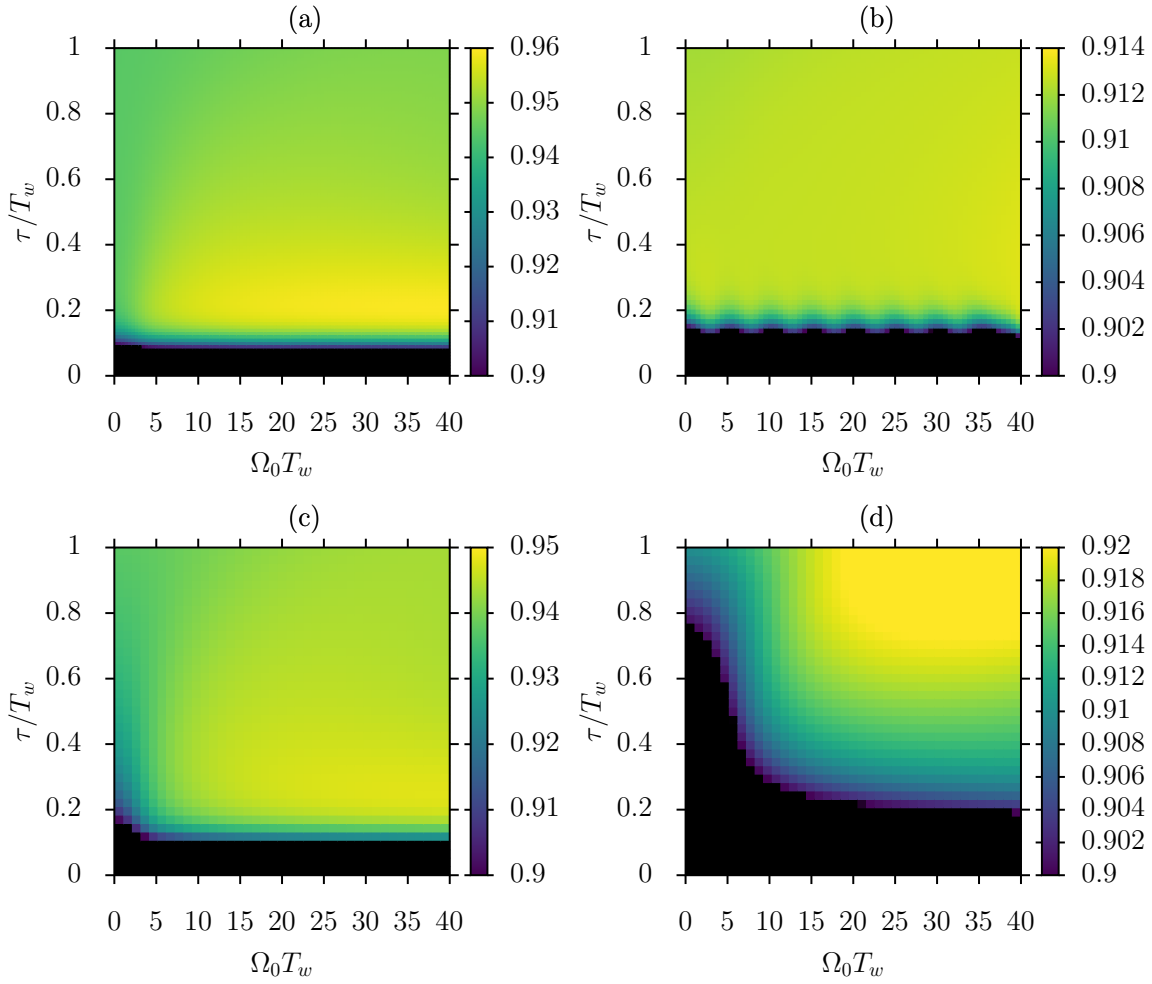

Figure 6.6: Final infidelity for STIRAP and fmod-STIRAP as a function of the parameters of the STIRAP pulses. (a) Infidelity produced by fmod-STIRAP in the presence of relaxation for the Rydberg excitation discussed in Section 6.3.2. The master equation (6.25) with decay parameters $\Gamma_{01}T_w = 7$, $\Gamma_{12}T_w = 0.003$ has been used, with the final time $t = 4T_w$ and with the system initialized in the instantaneous STIRAP dark state at time $t = -8T_w$. The driving frequency used is $\omega T_w = 120$. **(b)** The same quantity of panel (a), obtained using the decay parameters of the superconducting circuit discussed in Section 6.3.2, namely $\Gamma_{01}T_w = 0.017$, $\Gamma_{12}T_w = 0.023$, and using the driving frequency $\omega T_w = 35$. In both panels, the black regions indicate parameter sets for which the final fidelity does not reach 0.9. **(c)-(d)** The same results shown in (a) with the introduction of artificial decoherence channels $\overline{C}_0$ and $\overline{C}_2$ (see the last paragraph in Section 6.3.2) for dephasing rates $\gamma_0 T_w = \gamma_2 T_w = 0.03$ in (c), and $\gamma_0 T_w = 0.3$, $\gamma_2 T_w = 0$ in (d). [Panels (a) and (b) adapted from [126]]

The case of STIRAP was analyzed in detail in Ref. [72], where numerical simulations produce a transfer time

$$\tau_{st} = 7.05/\Omega_0 \tag{6.33}$$

for pulses with optimized parameters $T_w = 3.00$ and $\tau = 0.175 T_w$. The case of cd-STIRAP can be obtained from equation (6.15). This, for our choice of initial and final occupations, gives the numerical value

$$\tau_{\mathrm{cd}} = 4.59(5)/\Omega_{cd}^{\mathrm{peak}}. \tag{6.34}$$

It is not immediate to compute the transfer time for fmod-STIRAP, because of the quickly oscillating character of the dynamics of the populations. In order to obtain an estimate, we first perform a fit of the evolution of the populations using a sigmoid fit function of the form

$$p(t|\mu,\nu) = \frac{e^{\mu t+\nu}}{1+e^{\mu t+\nu}}. \tag{6.35}$$

By inverting the latter equation, the estimate for the time at which the population p_n of state $|n\rangle$ is $p_n = p$, at given fit parameters μ_n and ν_n, is

$$t(p_n = p) = \frac{1}{\mu_n}\left[\log\left(\frac{p}{1-p}\right) - \nu_n\right]. \tag{6.36}$$

Then, the transfer time for the fmod protocol is estimated as $\tau_{\mathrm{fmod}} = t\left(p_2^{(f)}\right) - t\left(p_0^{(i)}\right)$, which gives

$$\tau_{\mathrm{fmod}} = \frac{1}{\alpha_2}\left[\log\left(\frac{p_2^{(f)}}{1-p_2^{(f)}}\right) - \beta_2\right] - \frac{1}{\alpha_0}\left[\log\left(\frac{p_0^{(i)}}{1-p_0^{(i)}}\right) - \beta_0\right]. \tag{6.37}$$

Since fmod-STIRAP aims at reproducing the same evolution as that given by the exact counterdiabatic Hamiltonian, in the limit of infinite driving frequency we expect the fmod transfer time to match that of the cd scheme. This is confirmed by the results shown in Figure 6.7a: for a fixed maximal Rabi coupling of the cd field $\Omega_{cd}^{\mathrm{peak}}$, as the driving frequency is raised the transfer time gets closer and closer to τ_{cd} (— curve in logarithmic scale). Also, it gets closer and closer to the quantum speed limit given by τ_π of equation (6.30), as visible from the red dashed curve (- - -), whose values are depicted on the right vertical axis (in red color). However, due to the proportionality of the fmod Rabi coupling with the square root of the driving frequency ω [equation (6.21)], the maximal amplitude of the control fields also increases together with ω. As a consequence, the total pulse area required becomes larger as well. This is shown in Figure 6.7b, where the total pulse area of the control fields on the sidebands, divided by that of the π-pulse, is depicted.

6.4.3 Robustness with respect to phase errors

A possible argument against the use of shortcut-to-adiabaticity protocols in the context of STIRAP is the fact that these protocols require very specific phase relations among the control fields [165]. Imperfections arising in experimental implementations may then spoil the theoretical efficiency of the shortcuts. In order

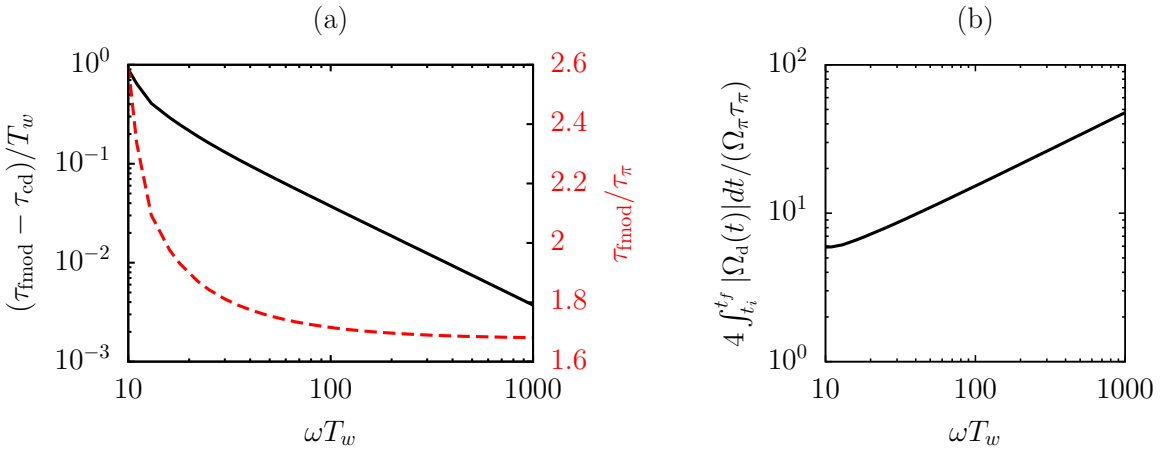

Figure 6.7: Transfer time for the fmod-STIRAP protocol. (a) In black (———), with reference to the l.h.s. axis, difference between the transfer time achieved by fmod-STIRAP (equation 6.37) and the transfer time of cd-STIRAP (equation (6.15)), in units of T. In red (- - -), and with reference to the r.h.s. axis, ratio between the transfer time of fmod-STIRAP and that of a π-pulse, given by equation (6.30). **(b)** Ratio between the total pulse area of the fmod-STIRAP pulses along the pump/Stokes sidebands and the area of a π pulse. In both panels, the parameters used are $\Omega_{0w} = 10$, $\tau_w = 0.7$, and the transfer time has been computed considering initial occupation $p_0^{(i)} = 0.99$ of state $|0\rangle$ and final occupation $p_2^{(f)} = 0.99$ of the target state $|2\rangle$. (Figure adapted from [126])

to rule out this potential criticism to the present fmod-STIRAP protocol, we analyze its performance when variations of the phases ϕ_G and ϕ_R, defined in equation (6.24), occur. First of all, we study the effect of the global phase ϕ_G on the final fidelity of the state transfer. This is represented in Figure 6.8a for different values of the driving frequency ω. One can see that the fidelity does not decrease below 0.999, thus signaling a very good stability of the method. The minima in the infidelity may not lie at the $\phi_G = 0$ value, even though, as the frequency is raised, this value gets closer and closer to being a minimum. Indeed, as ω^{-1} in increased, the truncation of the Floquet-Magnus effective Hamiltonian (introduced in Section 3.2) becomes a better and better approximation, thus making the higher-order effects negligible. With them, also the displacement of the minima vanishes. For not-large-enough frequencies instead, this analysis is useful for selecting an optimized value of the global phase. In Figure 6.8b, we report the infidelity as a function of the relative phase ϕ_R, in units of π. Phase errors of magnitude up to $10\%\pi$ still do not reduce the fidelity below 0.999. Moreover, for very small values, a small improvement can be found, which can be traced back to the effects explained in Section 4.5, i.e., to the "destructive interference" between the leading-order term and higher orders in the Floquet-Magnus expansion. This is possible in the regime in which the errors are comparable in magnitude with the modulation period. In agreement with the general treatment of Section 4.5, we find that errors in the global phase hardly affect the performance of the protocol. Although large relative-phase shifts can

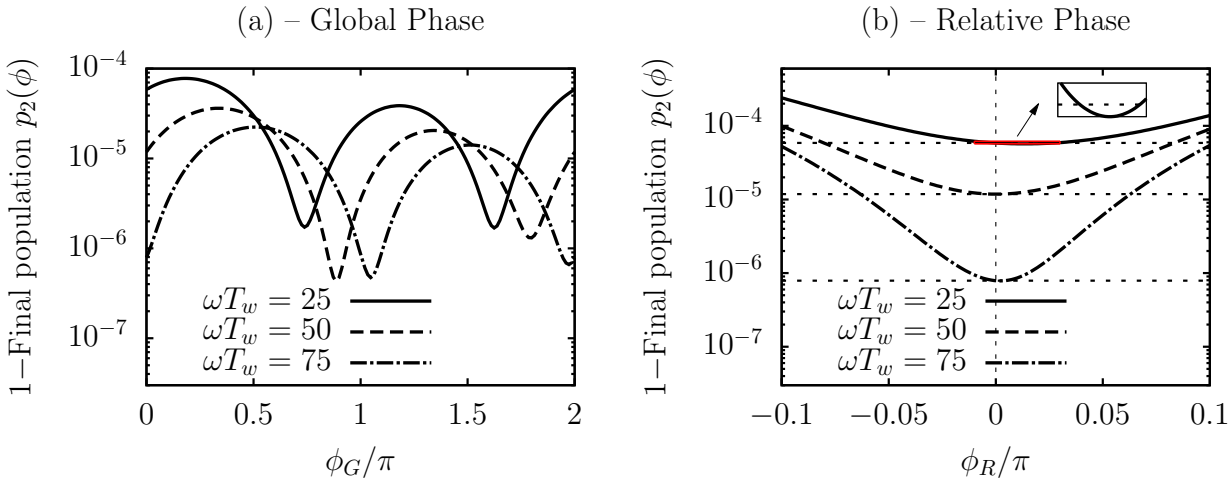

Figure 6.8: fmod-STIRAP: phase dependence of the final infidelity. (a) Final infidelity of the fmod-STIRAP protocol as a function of the global phase ϕ_G of the control fields. **(b)** Final infidelity as a function of the relative phase ϕ_R between the control fields, for $\phi_G = 0$. The inset shows that, for very small phase imperfections, small accidental improvements can be obtained. (Figure adapted from [126])

strongly reduce the final fidelity, if one assumes small errors the protocol does not suffer relevant limitations arising from this type of imperfections, and this is a very interesting feature for experimental implementations.

In the next Section, we will extend the fmod-STIRAP protocol to a modified version of STIRAP which aims at the realization of quantum gates, that is, the fundamental logical operations at the base of quantum algorithms. This application also complements Chapter 5 in the study of protocols useful for quantum information processing.

6.5 ACCELERATED QUANTUM GATES

6.5.1 fractional STIRAP and single-qubit gates

The basic STIRAP can be modified in order to efficiently construct protocols realizing quantum gates [98, 99, 135, 156]. One of these protocols exploits the idea of fractional-STIRAP (fSTIRAP) [163]. This aims at producing an arbitrary superposition of the $|0\rangle$ and $|2\rangle$ atomic states, i.e., it produces the state transformation

$$|\psi(t_i)\rangle = |0\rangle \quad \overset{\text{fSTIRAP}}{\longrightarrow} \quad |\psi(t_f)\rangle = \cos\eta\,|0\rangle - e^{-i\xi}\sin\eta\,|2\rangle\,, \tag{6.38}$$

with arbitrary ξ and η. This is achieved by maintaining the pump/Stokes sequence of STIRAP, though using different envelopes for the pulses, namely [163]

$$\Omega_p^{(\mathrm{f})}(t) = \Omega_0 \sin(\eta) e^{-i\xi} e^{-\left(\frac{t-\tau}{T_w}\right)^2}, \tag{6.39a}$$

$$\Omega_s^{(\mathrm{f})}(t) = \Omega_0 e^{-\left(\frac{t+\tau}{T_w}\right)^2} + \Omega_0 \cos(\eta) e^{-\left(\frac{t-\tau}{T_w}\right)^2}. \tag{6.39b}$$

Differently from STIRAP, even if the Stokes pulse still precedes the pump pulse, now the two pulses vanish simultaneously as t grows to $+\infty$. For better understanding how fSTIRAP works, let us recall that, in the limit of true adiabatic driving, the system remains in the instantaneous dark state [equation (6.4c)]. The mixing angle $\theta(t)$ of equation (6.6), for the pulses in (6.39), satisfies the following relations,

$$\tan\theta(t) \overset{t\to-\infty}{\longrightarrow} 0, \qquad \tan\theta(t) \overset{t\to+\infty}{\longrightarrow} \tan\eta, \tag{6.40}$$

thus confirming the transfer of equation (6.38). If fSTIRAP is applied to an initial state $|2\rangle$, then the system would follow an instantaneous eigenstate which is different from the dark state. Let us consider the non-resonant case $\Delta_p \neq 0$, and let us assume a large detuning $\Delta_p T_w \gg 1$. In this case, the intermediate state $|1\rangle$ can be adiabatically eliminated [24] and, using equations (6.4), the system follows the state $|b(t)\rangle$ of equation (6.5). The state transformation would thus be

$$|2\rangle \quad \overset{\text{fSTIRAP}}{\longrightarrow} \quad e^{-i\Phi_b}[e^{i\xi}\sin\eta\,|0\rangle + \cos\eta\,|2\rangle]. \tag{6.41}$$

Since the instantaneous eigenvectors $|b(t)\rangle$ has non-zero eigenvalue, differently from the dark state, such a state also acquires during the evolution a dynamical phase Φ_b which, using equations (6.7), reads

$$\Phi_b = \frac{1}{2}\int_{-\infty}^{+\infty} dt \left[\Delta_p - \sqrt{\Delta_p^2 + \overline{\Omega}^2(t)}\right]. \tag{6.42}$$

In the basis $\{|0\rangle, |2\rangle\}$ then, for $t \to +\infty$ the fSTIRAP adiabatic dynamics produces the propagator

$$\begin{aligned} U_f(\eta,\xi) &= |D(+\infty)\rangle\langle 0| + e^{-i\Phi_b}|X(+\infty)\rangle\langle 2|, \\ &= \begin{pmatrix} \cos\eta & e^{i\xi}e^{-i\Phi_b}\sin\eta \\ -e^{-i\xi}\sin\eta & e^{-i\Phi_b}\cos\eta \end{pmatrix}. \end{aligned} \tag{6.43}$$

If the dynamical phase Φ_b could be eliminated, this matrix would describe an arbitrary single-qubit quantum gate. This is not possible within the single-fSTIRAP framework. Nonetheless, it is possible to achieve this objective by suitably combining two fSTIRAPs in sequence [99]. Let us in fact consider a "reversed" fSTIRAP process, having the pulses of equation (6.39) swapped and substituting τ with $-\tau$, i.e.,

$$\Omega_p^{(\mathrm{rf})}(t) = \Omega_0 e^{-\left(\frac{t-\tau}{T_w}\right)^2} + \Omega_0 \cos(\eta) e^{-\left(\frac{t+\tau}{T_w}\right)^2}, \tag{6.44a}$$

$$\Omega_s^{(\mathrm{rf})}(t) = \Omega_0 \sin(\eta) e^{-i\xi} e^{-\left(\frac{t+\tau}{T_w}\right)^2}. \tag{6.44b}$$

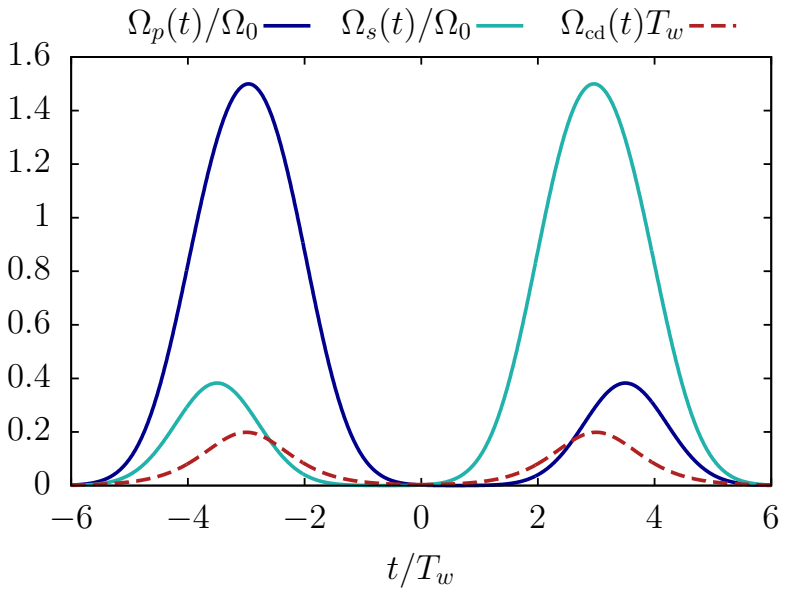

Figure 6.9: fSTIRAP-based quantum gates: shape of the pulses. Temporal profile, in dimensionless units, of the pump/Stokes pulses and of the corresponding cd Rabi frequency $\Omega_{cd}(t)$ for realizing a quantum gate based on a sequence of two fSTIRAPs, as per equation (6.48). The parameters used are $\chi = 0$, $\eta = \pi/8$. (Figure adapted from [126])

Now, the mixing angle $\theta(t)$ satifies

$$\tan\theta(t) \overset{t\to-\infty}{\longrightarrow} \text{cotan}\eta, \qquad \tan\theta(t) \overset{t\to+\infty}{\longrightarrow} +\infty, \tag{6.45}$$

and the instantaneous eigenvectors at $t \to -\infty$ are thus $|D(-\infty)\rangle = \sin\eta\,|0\rangle - \cos\eta\,|2\rangle$ and $|b(-\infty)\rangle = \cos\eta\,|0\rangle + \sin\eta\,|2\rangle$, while at $t \to \infty$ they are $|D(+\infty)\rangle = |2\rangle$ and $|b(+\infty)\rangle = |0\rangle$. The dynamical phase acquired by state $|b(t)\rangle$ is the same as for fSTIRAP. Accordingly, the propagator for the "reversed" fSTIRAP then reads

$$\begin{aligned} U_{rf}(\eta,\xi) &= |2\rangle\langle D(-\infty)| + e^{-i\Phi_b}\,|0\rangle\langle b(-\infty)|\,, \\ &= \begin{pmatrix} e^{-i\Phi_b}\cos\eta & e^{-i\Phi_b}\sin\eta \\ \sin\eta & -\cos\eta \end{pmatrix}. \end{aligned} \tag{6.46}$$

Therefore, we finally see that, by performing in sequence one reversed fSTIRAP and one fSTIRAP, the total propagator becomes

$$\begin{aligned} R(2\eta,\xi) =& U_f(\eta,\xi)U_{rf}(\eta,\xi), \\ =& e^{-i\Phi_b}\begin{pmatrix} \cos 2\eta & e^{i\xi}\sin 2\eta \\ -e^{-i\xi}\sin 2\eta & \cos 2\eta \end{pmatrix}. \end{aligned} \tag{6.47}$$

Up to a negligible global phase $e^{-i\Phi_b}$, the propagator $R(2\eta,\xi)$ realizes an arbitrary single-qubit rotation of angles 2η and ξ and, by choosing η and ξ, it can then be used for implementing an arbitrary single-qubit quantum gate. In practice, the

combined pulses which need to be applied for realizing the whole sequence are [99]

$$\Omega_p^{(g)}(t) = \Omega_p^{(\mathrm{rf})}(t + t_d/2) + \Omega_p^{(\mathrm{f})}(t - t_d/2), \tag{6.48a}$$
$$\Omega_s^{(g)}(t) = \Omega_s^{(\mathrm{rf})}(t + t_d/2) + \Omega_s^{(\mathrm{f})}(t - t_d/2), \tag{6.48b}$$

where we have introduced the delay time t_d between the two fSTIRAPs. The temporal profile of these pulses is depicted in Figure 6.9.

6.5.2 Accelerated Hadamard gate

We now develop an effective counterdiabatic scheme for speeding up the adiabatic transfer associated with the fSTIRAP quantum gate described in Section 6.5.1. Since the matrix structure of the original STIRAP Hamiltonian does not change, the only feature of the exact counterdiabatic Hamiltonian (6.9) which must be varied is the Rabi frequency $\Omega_{cd}(t)$, by adapting it to the new pump and Stokes pulses. Consequently, also the structure of the effective counterdiabatic Hamiltonian (6.24) needs not to be changed: it is sufficient to modify $\Omega_{\mathrm{d}}(t)$. Before doing so, let us emphasize that, strictly speaking, the realization of the full fSTIRAP quantum gate is not entirely adiabatic, even in the limit of infinite time. Indeed, when the switch between the first and the second fSTIRAP occurs, the system does not follow the same instantaneous eigenvector of the system. This is evident by comparing the expressions for the instantaneous eigenstates at the end of the first fSTIRAP with those at the beginning of the second fSTIRAP. For instance, let us consider the case $\eta = \pi/2$, $\xi = 0$ and initial state $|0\rangle$. During the first fSTIRAP, the system follows the dark state $|d(t)\rangle$ ending up in state $|2\rangle$. Then, during the second fSTIRAP, the system follows the bright state $|b(t)\rangle$ instead, ending up eventually in the superposition state $e^{-i\Phi_b}(|0\rangle + |2\rangle)/2$. Although the change of instantaneous eigenvector does not have an appreciable effect in terms of nonadiabatic transitions in practice, it may lead to confusing results in the calculation of the exact cd-fSTIRAP. In fact, if one tries to compute the Rabi frequency $\Omega_{cd}(t)$ starting from the combined pulses of equation (6.48), the result would exhibit a very pronounced and sharp peak around the switch time $t = 0$. This peak would be very hard to be realized in an experiment, and its presence would actually not produce an appreciable improvement of the protocol. In conclusion, the Rabi frequency $\Omega_{cd}(t)$ must be computed separately for the two fSTIRAPs using equations (6.39) and (6.44), and then summed up. The resulting pulse shape is represented in Figure 6.9, in relation to the global pump and Stokes pulses. Once $\Omega_{cd}(t)$ is determined, the fmod Rabi frequency $\Omega_{\mathrm{d}}(t)$ is straightforwardly obtained from equation (6.21). In Figure 6.10 we report numerical results on the evolution of the occupation probabilities for the realization of a Hadamard gate [122], which requires $\eta = \pi/8$ and $\xi = 0$ in equation (6.47). These results were obtained using the parameters $\Omega_0 T_w = 15$, $\tau_w = 1/2$, $t_d = 6T_w$, $\Delta_p = 35T_w$, $\omega T_w = 100$. The blue dot-dashed lines (-·-·-) indicate the populations for the fSTIRAP protocol, which leads to a final fidelity of

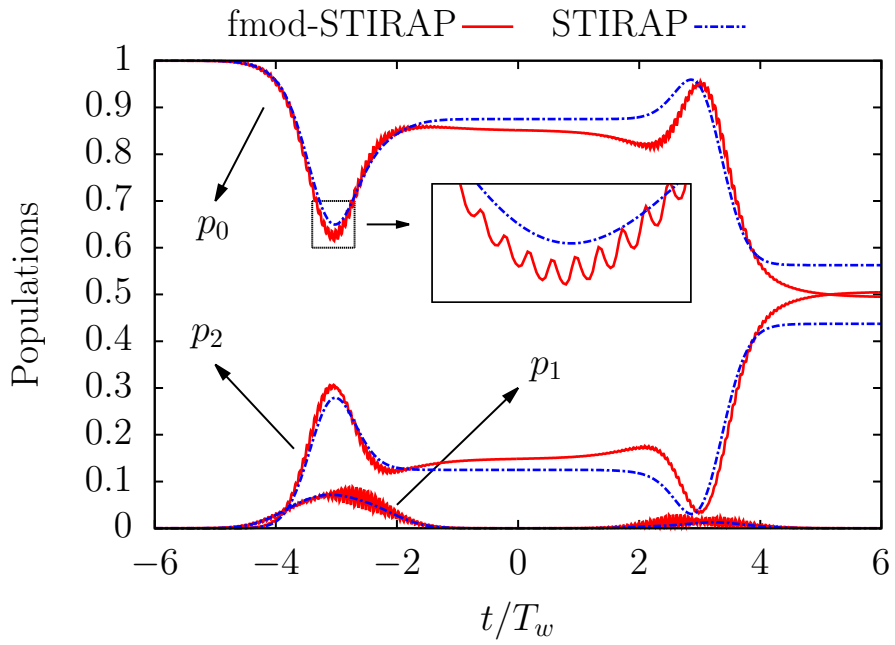

Figure 6.10: Evolution of the populations for a Hadamard gate. The system is initialized in state $|0\rangle$ and undergoes a sequence of two fSTIRAP processes which realizes an Hadamard gate as per equation (6.47) with $\eta = \pi/8$ and $\xi = 0$. The other parameters used are $\Omega_0 T_w = 15$, $\tau_w = 1/2$, $t_d = 6T_w$, $\Delta_p = 35T_w$, $\omega T_w = 100$. The standard fSTIRAP (-·-·-) produces a final fidelity of 0.998. If the fmod correction is added, the final fidelity reaches 0.99998 (——). (Figure adapted from [126])

0.998. The frequency-modulated fractional STIRAP (fmod-fSTIRAP) (——) produces a final fidelity of 0.99998, therefore achieving a much more precise state transfer. This example shows that the shortcut protocol has an interesting potential for applications in quantum computation problems, as well as in quantum simulation.

6.5.3 Gate robustness

Let us now investigate the behavior of the accelerated Hadamard gate with respect to different choices of the parameters and the presence of low-frequency dynamical noise. For the first case, we report in Figure 6.11 a study of the final infidelity of the protocol when the fundamental parameters Ω_0 and τ are changed, as it was done for the complete population transfer in Figure 6.4. The driving frequency used in producing Figure 6.11b is $\omega T_w = 100$ and the integration time was fixed to $t/T_w \in [-8, 8]$. These results show that, also in the case of the implementation of a quantum gate, the shortcut maintains a great robustness with respect to the choice of control parameters, achieving fidelities above in almost all the parameter space considered.

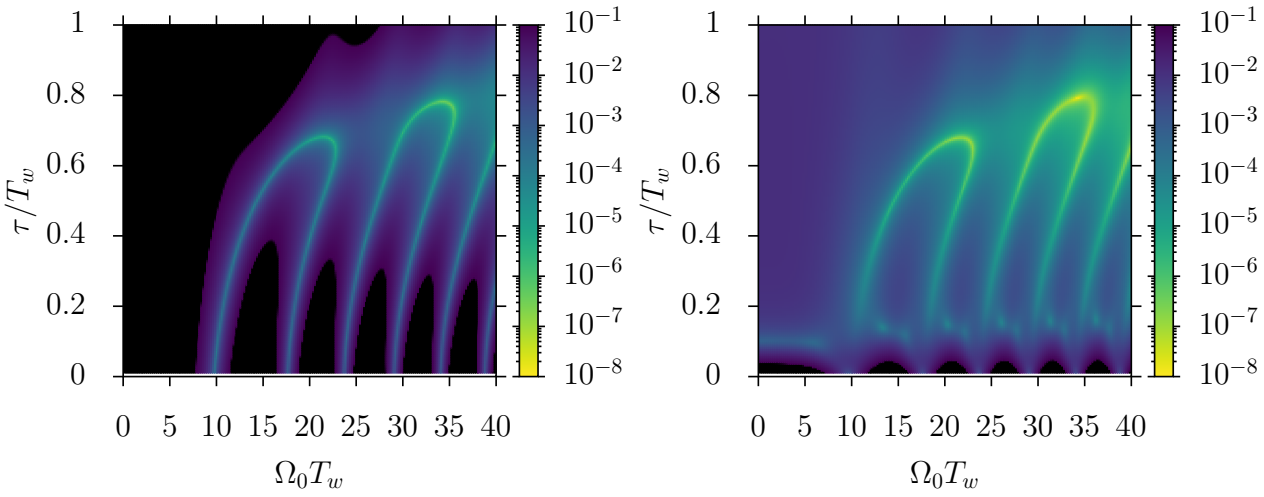

Figure 6.11: Hadamard gate: infidelity for different control parameters. Final infidelity produced by the fSTIRAP-based gate (left panel) and by the corresponding accelerated protocol (right panel), as a function of the pulse peak and pulse separation of the two fSTIRAP processes involved. The driving frequency used is $\omega T_w = 100$, and the integration time is $t \in [-8T_w, 8T_w]$. (Figure adapted from [126])

Concerning potential dynamical noise, we test the protocol against the presence of slowly varying imperfections in the time-dependent amplitude of the ecd control fields. This amounts to modify, in equation (6.24), the Rabi frequency as

$$\Omega_{\mathrm{d}}(t) \longrightarrow \Omega_{\mathrm{d}}(t)[1 + \delta\Omega_{\mathrm{d}}(t)]. \tag{6.49}$$

The variation $\delta\Omega_{\mathrm{d}}(t)$ is chosen of the form

$$\delta\Omega_{\mathrm{d}}(t) = \sum_{k=1}^{5} \left[\alpha_k \cos(\overline{\omega}_k t) + \beta_k \sin(\overline{\omega}_k t)\right], \tag{6.50}$$

where the constant α_k, β_k are drawn from a uniform distribution in $[0, 0.05]$, while the frequencies $\overline{\omega}_k$ are taken to be randomly distributed in $[0, 2\pi)$. Hence, maximal fluctuations from the ideal value of $\Omega_d(t)$ can introduce up to a 5% relative error. This is a rather pessimistic level of precision on the Rabi frequency for the experimental setups considered in Section (6.3.2). For the parameters of Figure 6.10, we run a large number of realizations of the process, and we compare the resulting final fidelity $\mathbb{F}_f^{(\mathrm{noise})}$ with the fidelity in the absence of noise $\mathbb{F}_f^{(0)}$ through the following error quantity,

$$\mathcal{E} = 1 - \frac{\mathbb{F}_f^{(\mathrm{noise})}}{\mathbb{F}_f^{(0)}}. \tag{6.51}$$

In figure 6.12, the unnormalized distribution of errors obtained from a sequence of 10000 runs is shown. This distribution exhibits a strong peak in the vicinity of zero, decaying fast with the error $\mathcal{E}$. The number of counts drops below 10% of the

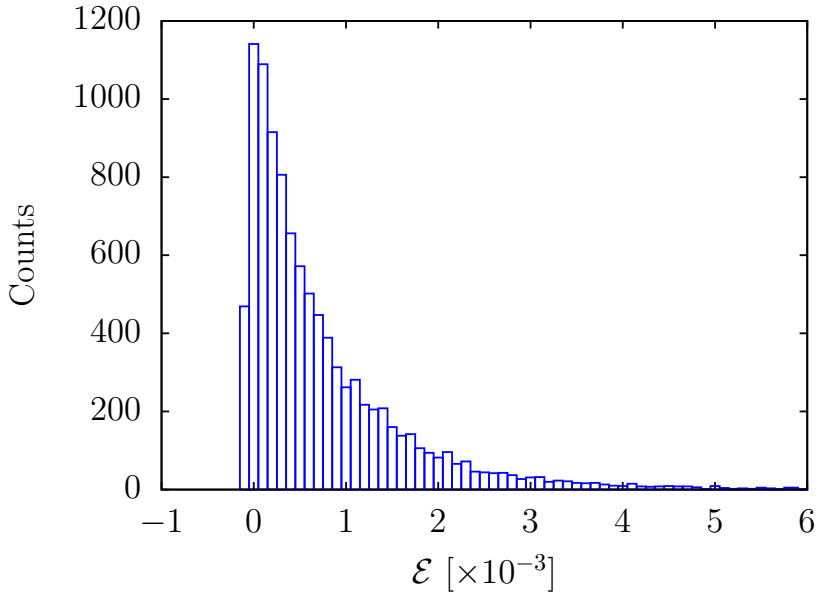

Figure 6.12: **Hadamard gate: distribution of the errors in the final fidelity due to dynamical amplitude noise**. Histogram of the errors $\mathcal{E}$, defined by equation (6.51), arising from dynamical noise in the accelerated Hadamard gate, which are modeled via equations (6.49) and (6.50). The histogram has been produced from 10000 runs with the control parameters of Figure 6.10

maximum peak for relative deviations larger than 0.002. Therefore, one can expect the fidelity to remain above 0.998 also in the presence of noise. Let us also observe that there are a few cases in which the protocol becomes slightly improved, as witnessed by the bin at negative values. These results suggest a strong robustness of the protocol, giving a further confirmation of its potential as a tool for the implementation of quantum algorithms.

6.6 DISCUSSION

In this chapter we have discussed how the shortcut-to-adiabaticity methodology introduced in Chapter 4 can contribute to the extension and improvement of one of the most widespread adiabatic quantum control techniques, the stimulated Raman adiabatic passage (STIRAP). Specifically, the integration of the STIRAP pulses with shortcut corrections opens the route to the applicability of this method to parameter regimes where it was not usable before, while keeping its highly praised robustness against protocol imperfections. The latter aspect has been investigated in detail, testing the sensitivity of the shortcut protocol against potential phase errors in the control fields (Section 6.4.3), and also against dissipative and dephasing effects in specific experimental contexts (Section 6.3.2 and 6.4.1). Further features of the protocol have been also analyzed in Section 6.4, besides the transfer fidelity, such as the transfer time and the response to possible experimental constraints.

A crucial point is that the shortcut is expected to be easily implementable in typical experimental setups. Indeed, it needs (i) the capability to create two symmetric sidebands for the two main pump/Stokes laser pulses, and (ii) the ability to control their Rabi frequency in time. As discussed in Section 6.3.2, these two requirement should not represent a prohibitive overhead of experimental resources: for instance, they can be achieved by a suitable modulation of the main pulses in an optical Rydberg excitation, and by dedicated additional microwave sources in a superconducting circuit. If sidebands at a larger frequency are still produced, these can be either exploited or compensated for in order not to limit the efficiency. Indeed, in the case in which their Rabi frequency can be controlled independently from that of the fundamental harmonic, they are a precious resource, as discussed in the outlook below. If they are not controllable in an independent manner instead, one can adapt the construction of the effective Hamiltonian described in Section 6.3.1 in order to harness their effect: this would lead in general to a modified choice of the Rabi frequency $\Omega_d(t)$.

We have shown in Section 6.5.2 that the same methodology can be straightforwardly adapted to assist STIRAP variations implementing quantum gates. This prototypical example gives a glimpse of interesting applications of our method in the context of quantum computation and simulation.

There are a number of directions along which the present methodology can be further developed. For instance, the main target of our analysis has been that of maximizing the final fidelity. It may be interesting to focus also on different figures of merit, tailored upon more specific experimental constraints. These may regard the smoothening of the oscillatory character of the dynamics, reducing either the maximal deviation from the adiabatic path or the instantaneous deviation of the micromotion. Alternatively, one could be interested in channeling and confining these deviations within the $|0\rangle - |2\rangle$ subspace, so to further reduce population transients in the (hypothetically lossy) state $|1\rangle$. In general, the simultaneous optimization of different aspects of the protocol would require the introduction of further degrees of control. Those can be introduced within our scheme by generating controlled sidebands at larger frequency. The amplitudes (and phases) of these additional modulations constitute new free parameters which can be used for carrying on on-demand optimization tasks.

Part IV

CONCLUSION

7 CONCLUSION AND PERSPECTIVES

7.1 SUMMARY

We have discussed the development of a theoretical framework for designing reliable, high-precision protocols for the control of quantum systems. A systematic scheme was introduced for generating efficient shortcuts to adiabaticity (STA), in Part ii, which allows one to produce approximate adiabatic evolutions in an accelerated manner, while satisfying criteria of experimental realizability. We believe that our method constitutes a precious added value to the variety of techniques offered by the expanding field of STA. This belief is supported by the promising results obtained in the study of the realistic applications described in Part iii, which also exemplify the suitability of our methods to diverse experimental platforms, such as atoms or superconducting circuits. In particular, effective counterdiabatic (ecd) protocols produce high-fidelity state transfers in short timescales. At the same time, they exhibit a strong robustness both against potential imperfections in the control parameters and against noise arising from the interaction of the controlled quantum system with the surrounding environment.

The construction procedure of ecd protocols is conceived in such a way that no additional matrix structure (time-dependent couplings) is needed with respect to the Hamiltonian $H(t)$ of the adiabatic process to be accelerated. The necessity of new interactions is traded for the introduction of fast-oscillating drivings in the initial control parameters. As compared to other shortcuts which are also realizable without new terms, our methods induce accurate tracking of the instantaneous eigenstates of $H(t)$ during the whole evolution, rather than matching those only at initial and final times. Therefore, a connection with the original idea of adiabaticity is maintained: even though, in the limit of very fast evolutions, the shortcut is the dominant Hamiltonian, in the opposite limit of quasi-adiabatic driving, one can achieve the speedup with a moderately weak ecd correction.

In this sense, our framework represents a bridge between purely fast-forward and purely adiabatic methodologies, inheriting some beneficial effects from both strategies —especially, time-efficiency of the first and robustness of the second. Consequently, it should be remarked that the best performance of the protocol, and its natural operational regime, is found over the wide range of timescales in between these two extreme situations. As discussed at length throughout the thesis (see, for instance, Chapters 4, 5 and 6), these limits can be quantified by studying the fidelities that can be attained, for a given total duration, once constraints are imposed on "strength"-measures of the control Hamiltonian (which may be the norm, or the peak value of the amplitudes of the control fields, or the total pulse

area)—see Sections 4.4 , 5.6 and 6.4.1. This analysis in general shows that, if the available time is sufficient for the adiabatic approximation to hold with good precision, then adiabatic methods give larger fidelities for a fixed "strength" of the Hamiltonian. On the other hand, it is known that quantum speed limits are attained by constant pulses with maximized coupling, which, however, are typically rather unstable when control errors occur. For all intermediate timescales instead, effective counterdiabatic driving represents an important candidate for jointly optimizing time, fidelity and reliability of the protocol.

The flexibility in the construction of our shortcuts leaves much room for adaptations to specific experimental contexts and control setups, and for the selective optimization of experimental resources or protocol features, as discussed in Section 4.7. In this direction, one can easily incorporate, within the general framework of Chapter 4, optimal control strategies [73]. An example might be the use of polychromatic drivings for minimizing micromotion oscillations [160], which in our context may allow one to reduce cumulative deviations from the adiabatic path instantaneously, rather than stroboscopically. Alternatively, one may integrate successful error-mitigating algorithms in the derivation of the effective counterdiabatic field, such as stochastic gradient learning methods [173], with the purpose of specializing the protocol robustness to particular types of noise.

7.2 OUTLOOK

7.2.1 Beyond finite-dimensional problems

The quantum control framework presented in this thesis has been developed for isolated finite-dimensional systems, and was focused mainly on few-levels problems. However, we have seen in Chapter 5 that, also in large systems, our strategies can be directly applied to selected subspaces of the full Hilbert space without modifications of the general theoretical setup. This kind of subspace-control is a situation of great interest for many applications in quantum information, for instance, and thus motivates our attention on small system sizes.

A first direction for extending these results is to address the case of general infinite-dimensional systems, as it was anticipated in Section 4.7. In this situation, a number of complications may arise requiring a suitable adaptation of the method. Let us point out first that no issues are expected for systems with discrete spectra, such as the prototypical example of the quantum harmonic oscillator. For that system, counterdiabatic corrections were already computed, using an analogy from classical mechanics [84] or directly using the counterdiabatic (cd) scheme recipe [118] (i.e., by the computation of spectral properties). This was possible even though the latter has been originally formulated only for finite-dimensional state spaces in Ref.s [15, 48]. Technical problems may occur for systems with continuous or degenerate spectra. These would require, first of all, an extension of the theory of cd driving which underpins our method, whose starting point would

be the adiabatic theorem itself, as discussed, for instance, in Ref. [108]. It would be further interesting to explore how the control-theoretic results on the structure of cd Hamiltonian described in Chapter 4 need to be modified in this context. Indeed, the Lie algebra of operators would not generate a compact Lie group any more. As a consequence, the concept of recurrence may be lost (see Section 3.1), and with it the Lie Algebra Rank Condition, which is at the base of our study of controllability, would hold no more in general [70].

7.2.2 Open quantum systems

A second direction to explore is the use of the ideas presented here for the control of open quantum systems [22, 90]. For the moment, the interaction with the environment was taken into account "passively", by studying how its presence spoils the efficiency of the protocol, reducing the final fidelity. However, information about the specific system-environment interaction can be used to actively optimize the protocol. The concept of adiabaticity itself becomes somehow fuzzier in an open-systems setting. This can be traced back to different interpretations of this concept. Indeed, one might study how the presence of the environment induces deviations from the isolated adiabatic evolution, i.e., from the tracking of instantaneous eigenstates of the isolated system. Alternatively, one may try to generalize the idea of the formation of dynamically invariant eigensubspaces. The first case has lead to the development of approximate methods for counteracting quantum noise, see, for instance, Ref. [4, 85]. The second case requires a new formulation since, for open quantum systems, the set of eigenstates of a Lindbladian is not univocally defined in general. However, it was recognized in [138] that a role similar to the close-system eigensubspaces is played by adiabatic Jordan blocks of the Lindbladian. The extension of the counterdiabatic scheme to this situation was then pursued in Ref. [155], where it was observed though that the resulting cd correction might not be hermitian, or might not even generate a completely positive map. The ecd framework can be, for instance, combined with strategies for mitigating environmental disturbance. For instance, reverse-engineering techniques have been recently proposed for correcting the average "direction" of a spin which is distorted by decoherence [83]. Similarly to the case of cd driving, the reverse-engineered Hamiltonian correction, which generates "dissipationless" solutions, may require control of further couplings which are hardly implementable. These could be produced effectively, following the ecd strategy, and included into the same accelerating field.

Another research direction is based on a different class of recent results. It has been shown [3] that, if a system weakly coupled to the environment is driven in a slow manner, under suitable conditions, then decoherence instantaneously projects toward the basis of adiabatic eigenvectors of the driven system, rather than in the fixed bare basis. In these cases, decoherence might act in support to adiabaticity, by preventing the system from escaping the adiabatic path. Under the hypothesis that the adiabatic driving is slightly accelerated, this effect is expected to break down.

An interesting question is whether ecd corrections can be designed for dynamically restoring this phenomenon, producing a beneficial combination of coherent control and environment-induced stabilization.

At a more fundamental level, it would be important to study how the presence of the fast oscillating ecd corrections influences dissipative effects when the driving is rather strong or when the coupling to the environment is not weak. For weak coupling, it is reasonable that Markovian master equations, as used here (see Sections 5.1.2 and 6.3.2), provide a good description of the system even in the presence of ecd driving. On the other hand, if the coupling and the driving are stronger, this description is most probably not accurate enough, and other techniques should be used. In this context, one should firstly derive valid equations of motion for the system, and secondly check whether the ecd framework can be adapted in order to work also in these regimes.

Concerning the robustness of the protocols against implementation imperfections, we principally considered potential static shifts of some characteristic parameter. Elaborating in this direction, it would be interesting to explore systematically the effect of (classical) dynamical noise, with different peculiarities, on the same parameters, extending and specializing the type of analysis performed in Chapter 6, Section 6.5.3. Our study has put in evidence the fact that, in most cases, small imperfections can produce small improvements, as discussed in Chapter 4, 5 and 6 in different contexts, due to an accidental cancellation effect produced at higher-order terms of the Floquet-Magnus expansion (see Section 4.5). Hence, it is worth investigating whether the protocol can be calibrated in such a way that the presence of a small degree of noise may be harnessed so to obtain improved average performance. Indeed, once the driving frequency is large enough for the method to work, (slightly-)noisy phases of the control fields might stabilize the micromotion dynamics, contributing to reduce the average error.

7.2.3 Quantum simulation

A third research direction can be oriented towards the optimization of quantum simulation algorithms. Average Hamiltonian theory techniques are being routinely used for designing analog quantum simulations. In this context, the ideas presented in Section 4.6.2, for the construction of effective many-body interactions, may find a broad interest, e.g., for applications towards the engineering of exotic many-body states or the simulation of fermionic systems, whose anticommutativity properties makes them particularly hard to be simulated both on classical and quantum computers [12, 153].

From a different angle, it may be interesting to explore possible hybridizations between ideas from time-dependent quantum control and digital simulation strategies, which go beyond the improvement of single digital gates. This could be done at different levels. For example, one can try to conceive single gates slightly distorted via time-dependent control. This distortion, which might be thought of as

a sort of "controllable error", could then be exploited to compensate errors arising from the digital combination of single gates.

Mathematically, this is motivated by the parallel between the structure of higher-order terms in the Magnus expansion of a driven system and the form of error estimates in digitalization procedures, which are typically computed by means of Baker-Campbell-Hausdorf exponential formulae such as the Trotter-Suzuki formula.

Part V

APPENDIX

A INFIDELITY EXPANSION FOR LARGE DRIVING FREQUENCY

In this Appendix, we derive the first terms of an expansion of the infidelity produced by the ecd control protocol in large driving frequency. We focus specifically on the two-level problem described in Section 4.5.3. More general results in this direction can be found in Ref. [123]. The expansion allows one to quantify precisely the errors to be expected when the system evolves under imprecise effective counterdiabatic driving. This helps us to derive estimates of the errors arising from phase imperfections in the control fields, in Section 4.5.3.

The problem is described by the total Hamiltonian

$$H(t) + H_{\text{ecd}}(t), \tag{A.1}$$

where $H(t)$ is the adiabatically driven Hamiltonian

$$H(t) = \lambda_x(t)\hat{\sigma}_x + \lambda_z(t)\hat{\sigma}_z, \tag{A.2}$$

while $H_{\text{ecd}}(t)$ is the effective counterdiabatic correction of explicit form

$$H_{\text{ecd}}(t) = X\sqrt{\omega}\cos(\omega t + \phi_g) + Z\sqrt{\omega}\sin(\omega t + \phi_g + \phi_r), \tag{A.3}$$

which is taken as in equation (4.73). Note that potential phase shifts ϕ_g and ϕ_r are included.

Let us start this analysis with the Schrödinger equation in the adiabatic frame defined by the transformation (2.34), which reads

$$i\frac{\partial \overline{U}(t)}{\partial t} = [\overline{H}_{\text{ecd}}(t) - \bar{\mathcal{A}}_t]\overline{U}(t), \tag{A.4}$$

where $\overline{H}_{\text{ecd}}$ is the rotated-frame ecd correcting Hamiltonain while $\bar{\mathcal{A}}_t$ is the rotated-frame adiabatic gauge potential defined in Eq. (2.5),

$$\overline{H}_{\text{ecd}}(t) = U_{\text{ad}}^{\dagger}(t)H_{\text{ecd}}(t)U_{\text{ad}}(t), \qquad \bar{\mathcal{A}}_t(t) = U_{\text{ad}}^{\dagger}(t)\mathcal{A}_t(t)U_{\text{ad}}(t). \tag{A.5}$$

By computing the first terms of the Floquet-Magnus expansion (see Section 3.2) generated by (A.4), one finds a decomposition of the adiabatic-frame propagator $\overline{U}(t)$ as

$$\overline{U}(t) = \exp\left(\frac{M_{\text{ecd}}^{(1)} + M_{\bar{\mathcal{A}}}^{(0)}}{\omega} + \frac{M_{\text{ecd}}^{(0)} + M_{\text{ecd}}^{(2)}}{\omega^{3/2}} + o(\omega^{-2})\right). \tag{A.6}$$

where $M^{(k)}_{\text{ecd}}$ indicates the k-th term of the Magnus expansion generated by $\overline{H}_{\text{ecd}}(t)$ at the end of one modulation period $T = 2\pi/\omega$, while $M^{(k)}_{\bar{\mathcal{A}}}$ is that generated by $\bar{\mathcal{A}}_t$. These Magnus terms explicitly reads

$$M^{(0)}_{\text{ecd}} = \frac{4\pi i}{\omega^{3/2}}[X\lambda_z \sin(\phi_g + \phi_r) + Z\lambda_x \cos\phi_g]\hat{\Sigma}_2, \tag{A.7a}$$

$$M^{(1)}_{\text{ecd}} = \frac{2\pi i}{\omega} XZ \cos\phi_r \hat{\Sigma}_2, \tag{A.7b}$$

$$\begin{aligned} M^{(2)}_{\text{ecd}} = &\frac{4\pi i}{\omega^{3/2}} \frac{XZ}{\sqrt{\lambda_x^2 + \lambda_z^2}}[(X \sin(\phi_g + \phi_r)\lambda_z + Z\cos\phi_g\lambda_x)\hat{\Sigma}_3 \\ &+ (X\sin(\phi_g + \phi_r)\lambda_x - Z\cos\phi_g\lambda_z)\hat{\Sigma}_1]\cos\phi_r, \end{aligned} \tag{A.7c}$$

$$M_{\bar{\mathcal{A}}}(T) = \frac{2\pi i}{\omega}\eta_T \hat{\Sigma}_2. \tag{A.7d}$$

where η_T is the nonadiabatic coupling computed at the end of one period,

$$\eta_T = \langle 0_t(T)|\partial_t 1_t(T)\rangle = \frac{\langle 0_t(T)|\,\partial_t H(T)\,|1_t(T)\rangle}{E_0(T) - E_1(T)}, \tag{A.8}$$

and where we have introduced the following matrices, which are the Pauli matrices in the basis of the zero-time instantaneous eigenvectors $|0_0\rangle$ and $|1_0\rangle$,

$$\hat{\Sigma}_1 = |0_0\rangle\langle 1_0| + |1_0\rangle\langle 0_0|\,, \tag{A.9a}$$

$$\hat{\Sigma}_2 = -i[|0_0\rangle\langle 1_0| - |1_0\rangle\langle 0_0|], \tag{A.9b}$$

$$\hat{\Sigma}_3 = |0_0\rangle\langle 0_0| - |1_0\rangle\langle 1_0|\,. \tag{A.9c}$$

Let us now focus on the infidelity at the end of one time step. Assuming that the system is initially prepared in an instantaneous eigenstate $|\psi_0\rangle$, this can be expressed as

$$\mathbb{I}_T = 1 - |\langle\psi_0(T)|\,\overline{U}(T)\,|\psi_0(T)\rangle\,|^2. \tag{A.10}$$

Then, let us insert equation (A.6) into (A.10). At this point, one can expand $\overline{U}(T)$ in power series: this allows one to compute the expectation value $\langle\psi_0|\cdot|\psi_0\rangle$ term by term. Computing the modulus squared, one obtains, up to order T^3, the expression

$$\begin{aligned} \mathbb{I}_T = &-\text{Re}\,\langle\psi_0|\left(M^{(1)}_{\text{ecd}} + M^{(0)}_{\mathcal{A}}\right)^2|\psi_0\rangle\, T^2 \\ &- \left[\text{Re}\,\langle\psi_0|\left(M^{(0)}_{\text{ecd}} + M^{(2)}_{\text{ecd}}\right)^2|\psi_0\rangle + \text{Im}^2\,\langle\psi_0|\,M^{(2)}_{\text{ecd}}\,|\psi_0\rangle\right] T^3. \end{aligned} \tag{A.11}$$

Inserting equations (A.7) into (A.11), we arrive at the desired infidelity expansion for our problem,

$$\begin{aligned} \mathbb{I}_T = \eta_T^2(1 - \cos(\phi_r))^2 T^2 + \frac{2}{\pi}\Big\{&(X\lambda_z\sin(\phi_g + \phi_r) + Z\lambda_x\cos\phi_g)^2 \\ &+ \frac{\eta_T^2\cos^2\phi_r}{\lambda_x^2 + \lambda_z^2}(X\lambda_x\sin(\phi_g + \phi_r) - Z\lambda_z\cos\phi_g)^2\Big\}\, T^3. \end{aligned} \tag{A.12}$$

This formula is at the base of the analysis of Section (4.5.3). Indeed, it helps us to see explicitly how the deviations from the exact adiabatic dynamics depend on the global and relative phase of the ecd modulations, and hence to study the stability of the whole procedure with respect to potential unpredicted shifts in their values.

B GENERALIZED BESSEL FUNCTIONS

In Chaper 4, Section 4.6, we have discussed the construction of effective Hamiltonians in the "toggling" frame defined by strong external periodic driving. The Floquet-Magnus expansion (defined in Section 3.2) can be applied, requiring the evaluation of Fourier components of the toggling-frame Hamiltonian. Because of the rapidly varying fields, the latter already contains rapidly varying components. These leads to the necessity of evaluating integrals of nested trigonometric functions. In the simplest case of a monochromatic control field, these result in standard Bessel functions [119]. When more harmonics are involved, the evaluation of these integrals becomes more complicated. In this Appendix we describe a generalization of the Bessel functions (of the first kind) $J_n(z)$ which allows one to conveniently evaluate and treat those integrals. Such a generalization is formulated in order to be convenient for the treatment of Sec. 4.6, and is adapted from similar analyses, see [158].

b.1 DEFINITION

We define the generalized Bessel functions $\mathcal{J}_n^{(L)}(\boldsymbol{z}, \boldsymbol{\Phi})$ via the following generating-function relation:

$$\exp\left(i \sum_{l=1}^{L} z_l \sin(lt + \phi_l) - i \sum_{l=1}^{L} z_l \sin(\phi_l) \right) = \sum_{n=-\infty}^{n=\infty} \mathcal{J}_n^{(L)}(\boldsymbol{z}, \boldsymbol{\Phi})\, e^{int}, \tag{B.1}$$

where L is the number oh harmonics involved, $\boldsymbol{z}$ is the vector of oscillation amplitudes $\boldsymbol{z} = \{z_1, \ldots, z_L\}$, whilst $\boldsymbol{\Phi}$ is the vector of the corresponding phases $\boldsymbol{\Phi} = \{\phi_1, \ldots, \phi_L\}$.

Hence, by extracting the Fourier coefficients from the above series, one immediately obtains the integral representation

$$\mathcal{J}_n^{(L)}(\boldsymbol{z}, \boldsymbol{\Phi}) = e^{-i\sum_{l=1}^{L} z_l \sin\phi_l} \frac{1}{2\pi} \int_{-\pi}^{\pi} dt\, e^{\sum_{l=1}^{L} z_l \sin(lt+\phi_l)} e^{-int}. \tag{B.2}$$

This representation can then be used for computing a useful expansion for $\mathcal{J}_n^{(L)}(\boldsymbol{z}, \boldsymbol{\Phi})$, which reduces its evaluation to the calculation of standard Bessel functions. Indeed, one can expand the exponentials in equation (B.2) according to the generating-function relation of standard Bessel functions [119],

$$e^{\frac{z}{2}(t-t^{-1})} = \sum_{n=-\infty}^{+\infty} J_n(z) t^n. \tag{B.3}$$

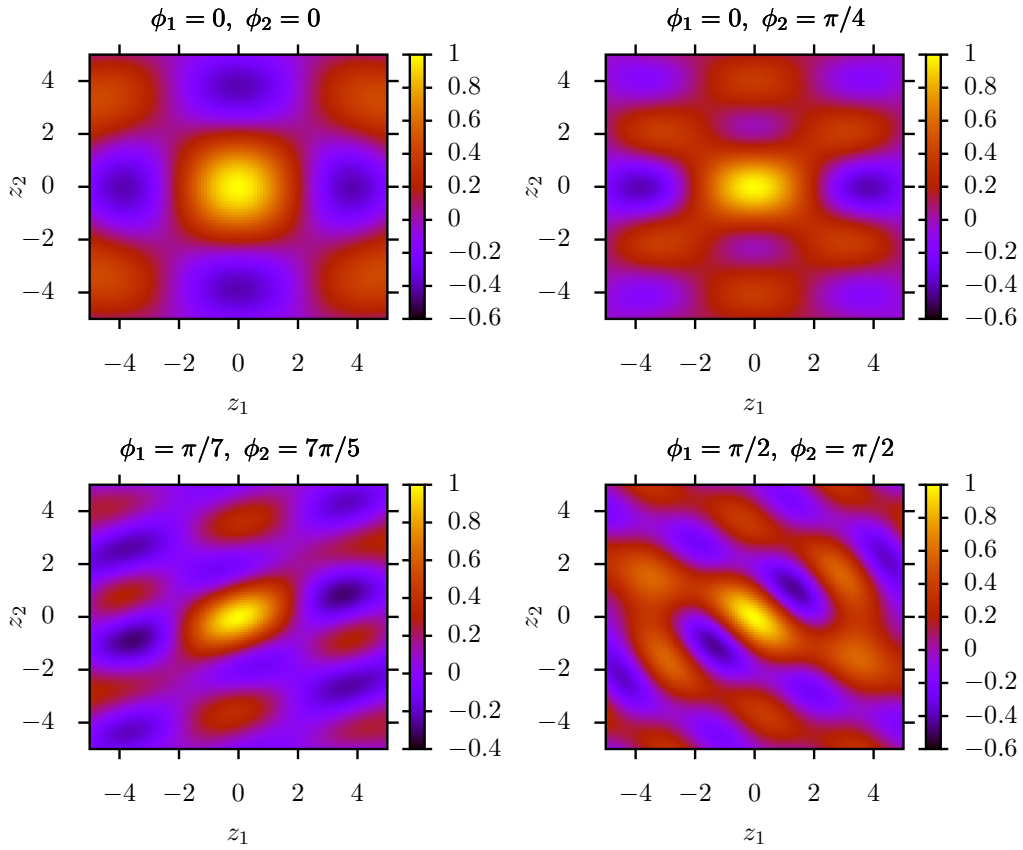

Figure B.1: Generalized Bessel function with 2 harmonics. The four panels show the real part of the generalized Bessel function $\mathcal{J}_0^{(2)}(\{z_1, z_2\}, \{\phi_1, \phi_2\})$, defined in equation (B.4), as a function of the arguments z_1 and z_2, for different fixed values of the phases ϕ_1 and ϕ_2.

The integral in (B.2) then becomes an integral of simple exponential functions. After some manipulations, one finally obtains the expansion

$$\mathcal{J}_n^{(L)}(\boldsymbol{z}, \boldsymbol{\Phi}) = e^{-i\sum_{l=1}^{L} z_l \sin(\phi_l)} \sum_{n_1=-\infty}^{\infty} \cdots \sum_{n_L=-\infty}^{\infty} J_{n_1}(z_1) J_{n_2}(z_2) \cdot \ldots \cdot J_{n_L}(z_L)\, e^{i\sum_l^L n_l \phi_l} \delta_{\sum_l^L l n_l, n}. \tag{B.4}$$

From the expression (B.4), one can see that standard Bessel functions are recovered in the limit of single harmonic ($L = 1$) with zero phase, $\phi_1 = 0$. In the case of $L = 2$, $\mathcal{J}_n^{(2)}(\boldsymbol{z}, \boldsymbol{\Phi})$ can be connected to the two-dimensional Bessel functions studied in Ref. [95]. A representation of the real part of $\mathcal{J}_0^{(2)}(\{z_1, z_2\}, \{\phi_1, \phi_2\})$ is shown in Figure B.1.

B.2 NUMERICAL EVALUATION

As one can intuitively expect from the r.h.s. of equation (B.4), numerical evaluation of $\mathcal{J}_n^{(L)}(\boldsymbol{z}, \boldsymbol{\Phi})$ turns out to be rather time consuming. For doing this in a reasonable time, one needs to first address two different aspects

1. find a satisfactory truncation scheme for the infinite sums;
2. optimize the generation of the indices involved in the sum, which are selected by the Kronecker delta in equation (B.4).

Let us first discuss point 2, assuming for the moment that point 1 is solved. A naive implementation of equation (B.4), in which one generates all sets of possible indices (within the selected truncation scheme), checks if they satisfy the condition imposed by the delta function, and then computes the corresponding product of Bessel functions, is a poorly performing methodology. It is rather convenient to generate and store the set of indices once and for all in the first place, and then compute the summations by drawing the indices from the precomputed set.

Turning now to point 1, it is first of all important to stress that, for our applications, the arguments z of these Bessel functions are in general not small. Therefore, expansions for small argument are not a viable strategy for simplifying the expressions. However, the Bessel functions $J_n(z)$ remain close to zero for a larger and larger region of values of z starting from zero as the order n is augmented. In the limit of large n, the following asymptotic expansion holds [119],

$$J_n(z) \overset{n\to+\infty}{\sim} \frac{1}{\sqrt{2\pi n}} \left(\frac{ez}{2n}\right)^n . \tag{B.5}$$

Hence, for a given z, there always exists a sufficiently large n which makes $J_n(z)$ small. This property allows one to truncate the infinite sums in equation (B.4). Let us call N_{Bess} the truncation threshold. Although equation (B.5) justifies this procedure, it does not provide an accurate estimate of N_{Bess} for a target error threshold, which must thus be probed numerically. An example of this is given in Figure B.2a. In that Figure, we show the convergence of the value of $\mathcal{J}_3^{(2)}(\boldsymbol{z}, \boldsymbol{\Phi})$ as a function of the threshold value N_{Bess}, for the variables $\{z_1, z_2\} = \{5, 5\}$ and for phases $\{\phi_1, \phi_2\} = \{0, 0\}$. Still, equation (B.5) can be used to refine the truncation criterion. In fact, when choosing N_{Bess} one takes into account that, in the case in which all $J_n(z_k)$ but one have maximal value 1 (which occurs when all $\{n_1, \ldots, n_L\}$ and all z_k are zero), this needs to be large enough for the remaining non-unit $J_n(z)$ to be below the prefixed error threshold. However, combinations of many Bessel functions having large order are in this way included in the summation even though they would be absolutely negligible. A qualitative condition on the product terms in (B.4) for avoiding this (without needing the evaluation of the product first), can be obtained by using equation (B.5). Let us suppose that, in a product term, there are at least $M \leq L$ non-zero indices. If these indices are large, and assuming

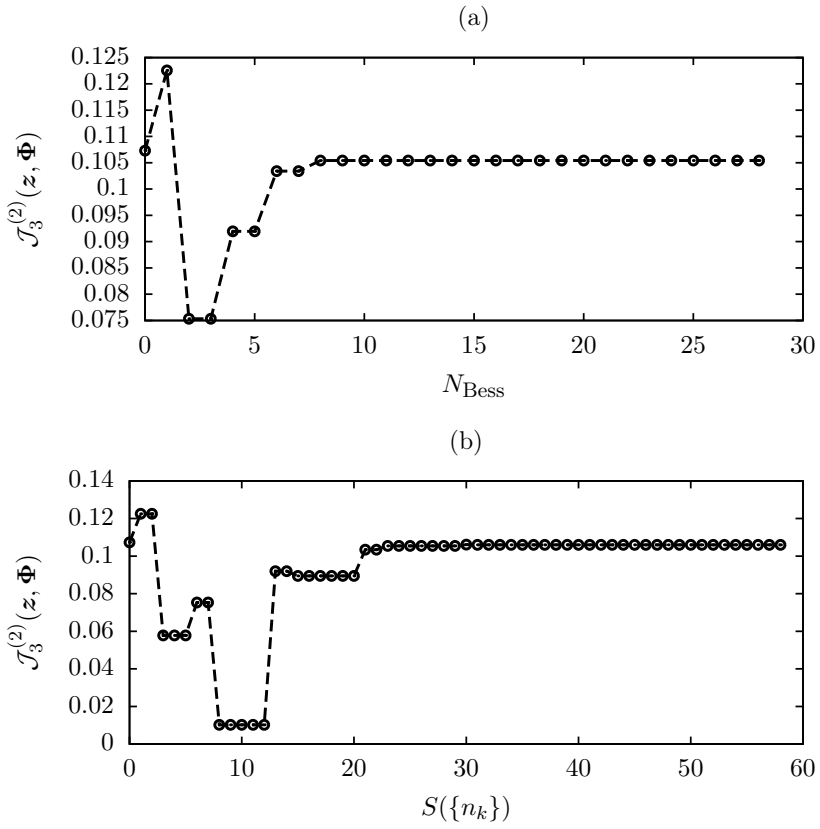

Figure B.2: Convergence of generalized Bessel functions. (a) Behavior of $\mathcal{J}_3^{(2)}(z,\mathbf{\Phi})$, for variables $z = \{5,5\}$ and $\Phi = \{0,0\}$, as a function of the maximal order N_{Bess} of the standard Bessel functions to which the summations in equation (B.4) are truncated, for $S(\{n_k\})$ of equation (B.9) fixed to 30. **(b)** Behavior $\mathcal{J}_3^{(2)}(z,\mathbf{\Phi})$, with the variables as in panel (a) and $N_{\text{Bess}} = 15$, as a function of the quantity $S(\{n_k\})$ of equation (B.9).

that they are all positive for simplicity, we can expand all the corresponding Bessel functions according to equation (B.5), so for the whole product we have

$$\frac{1}{(2\pi n)^{M/2}} \prod_{k=1}^{M} \left(\frac{ez}{2n_k}\right)^{n_k}. \tag{B.6}$$

Since the factors n^{-n} in equation (B.5) are those which dominate the decay in the limit of large n, we can roughly estimate the behavior of the quantity in (B.6) with

$$\prod_{k=1}^{M} \left(\frac{1}{n_k}\right)^{n_k} = e^{-\sum_k^M n_k \log n_k}. \tag{B.7}$$

Let us now introduce

$$S(\{n_k\}) = \sum_{k}^{M} n_k \log n_k, \tag{B.8}$$

where we use the notation S since the r.h.s. expression is reminiscent of an entropy measure. For the quantity in equation (B.7) to be small, we obtain the condition

$$S(\{n_k\}) \gg 1. \tag{B.9}$$

This condition can be used as a criterion for further thinning the set of indices, with the precise bound investigated again numerically. In Figure B.2b we report an example of this investigation.

C COEFFICIENTS OF THREE-BODY TERMS: AN EXAMPLE

The purpose of this Appendix is to introduce exemplary expressions of the coefficients appearing in equation (4.107) of Section 4.6.4. That equation describes the first-order effective Hamiltonian derived for the construction of synthetic dominant three-body interactions. The expressions derive from considering the (double) integral of the commutator of the driving Hamiltonian of equation (4.104) at different times, according to equation (3.14b) of Section 3.2. From the Hamiltonian (4.104), we see that this produces in general summations involving products of trigonometric functions, each featuring as argument terms like $B_k(t_j) \pm B_{k+1}(t_j)$. The quantities $B_k(t_j)$ are defined in equation (4.91), and they represent the time integrals of the local driving fields. The sums of these products can be rewritten more compactly in terms of the real and imaginary parts of product of exponentials: this allows one to obtain more compact expressions. Two examples of the resulting coefficients are as follows.

$$
\begin{aligned}
C^{(k)}_{yxz} = \frac{1}{4T}\int_0^T dt_1 \int_0^{t_1} dt_2 \Big\{ & \operatorname{Re}\left[e^{2i[B_k(t_1)-B_{k+1}(t_1)]}e^{-2i[B_{k-1}(t_2)+B_k(t_2)]}\right] \\
& + \operatorname{Re}\left[e^{2i[B_k(t_1)+B_{k+1}(t_1)]}e^{-2i[B_{k-1}(t_2)+B_k(t_2)]}\right] - \operatorname{Re}\left[e^{2i[B_k(t_1)-B_{k+1}(t_1)]}e^{2i[B_{k-1}(t_2)-B_k(t_2)]}\right] \\
& - \operatorname{Re}\left[e^{2i[B_k(t_1)+B_{k+1}(t_1)]}e^{2i[B_{k-1}(t_2)-B_k(t_2)]}\right] - \operatorname{Re}\left[e^{2i[B_{k-1}(t_1)+B_k(t_1)]}e^{-2i[B_k(t_2)+B_{k+1}(t_2)]}\right] \\
& + \operatorname{Re}\left[e^{2i[B_{k-1}(t_1)-B_k(t_1)]}e^{2i[B_k(t_2)-B_{k+1}(t_2)]}\right] - \operatorname{Re}\left[e^{2i[B_{k-1}(t_1)+B_k(t_1)]}e^{-2i[B_k(t_2)-B_{k+1}(t_2)]}\right] \\
& + \operatorname{Re}\left[e^{2i[B_{k-1}(t_1)-B_k(t_1)]}e^{2i[B_k(t_2)+B_{k+1}(t_2)]}\right] \Big\}, \qquad \text{(C.1)}
\end{aligned}
$$

$$
\begin{aligned}
C^{(k)}_{zxz} = \frac{1}{4T}\int_0^T dt_1 \int_0^{t_1} dt_2 \Big\{ & \operatorname{Im}\left[e^{2i[B_k(t_1)-B_{k+1}(t_1)]}e^{2i[B_{k-1}(t_2)-B_k(t_2)]}\right] \\
& + \operatorname{Im}\left[e^{2i[B_k(t_1)+B_{k+1}(t_1)]}e^{2i[B_{k-1}(t_2)-B_k(t_2)]}\right] - \operatorname{Im}\left[e^{-2i[B_k(t_1)+B_{k+1}(t_1)]}e^{2i[B_{k-1}(t_2)+B_k(t_2)]}\right] \\
& - \operatorname{Im}\left[e^{-2i[B_k(t_1)-B_{k+1}(t_1)]}e^{2i[B_{k-1}(t_2)+B_k(t_2)]}\right] - \operatorname{Im}\left[e^{-2i[B_{k-1}(t_1)+B_k(t_1)]}e^{2i[B_k(t_2)-B_{k+1}(t_2)]}\right] \\
& - \operatorname{Im}\left[e^{2i[B_{k-1}(t_1)-B_k(t_1)]}e^{2i[B_k(t_2)-B_{k+1}(t_2)]}\right] - \operatorname{Im}\left[e^{-2i[B_{k-1}(t_1)+B_k(t_1)]}e^{2i[B_k(t_2)+B_{k+1}(t_2)]}\right] \\
& - \operatorname{Im}\left[e^{2i[B_{k-1}(t_1)-B_k(t_1)]}e^{2i[B_k(t_2)+B_{k+1}(t_2)]}\right] \Big\}. \qquad \text{(C.2)}
\end{aligned}
$$

The numerical evaluation of this kind of formulae proceeds as described in the main text of Section 4.6.4, by means of the generalized Bessel functions defined in Appendix B.

BIBLIOGRAPHY

[1] J. et al. Aasi. "Enhanced sensitivity of the LIGO gravitational wave detector by using squeezed states of light." In: *Nature Photonics* 7 (), pp. 613–619. DOI: 10.1038/nphoton.2013.177.

[2] T. Albash and D. A. Lidar. "Adiabatic quantum computation." In: *Rev. Mod. Phys.* 90 (1 2018), p. 015002. DOI: 10.1103/RevModPhys.90.015002.

[3] T. Albash, S. Boixo, D. A Lidar, and P. Zanardi. "Quantum adiabatic Markovian master equations." In: *New Journal of Physics* 14.12 (2012), p. 123016. DOI: 10.1088/1367-2630/14/12/123016.

[4] S. Alipour, A. Chenu, A. T. Rezakhani, and A. del Campo. "Shortcuts to Adiabaticity in Driven Open Quantum Systems: Balanced Gain and Loss and Non-Markovian Evolution." In: *arXiv:1907.07460* (2019). DOI: arXiv:1907.07460v1.

[5] S. An, D. Lv, A. del Campo, and K. Kim. "Shortcuts to adiabaticity by counterdiabatic driving for trapped-ion displacement in phase space." In: *Nature Comm* 7 (2016), p. 12999. DOI: 10.1038/ncomms12999.

[6] J. Anandan. "The geometric phase." In: *Nature* 360 (1992), pp. 307–313. DOI: 10.1038/360307a0.

[7] E. Arimondo. "Coherent Population Trapping in Laser Spectroscopy." In: ed. by E. Wolf. Vol. 35. Progress in Optics. Elsevier, 1996, pp. 257–354. DOI: 10.1016/S0079-6638(08)70531-6.

[8] E. Arimondo, D. Ciampini, A. Eckardt, M. Holthaus, and O. Morsch. "Chapter 10 - Kilohertz-Driven Bose-Einstein Condensates in Optical Lattices." In: *Advances in Atomic, Molecular, and Optical Physics*. Ed. by P. Berman, E. Arimondo, and C. Lin. Vol. 61. Advances In Atomic, Molecular, and Optical Physics. Academic Press, 2012, pp. 515 –547. DOI: https://doi.org/10.1016/B978-0-12-396482-3.00010-7.

[9] F. Arute et al. "Quantum supremacy using a programmable superconducting processor." In: *Nature* 574.7779 (2019), pp. 505–510. DOI: 10.1038/s41586-019-1666-5.

[10] A. Baksic, H. Ribeiro, and A. A. Clerk. "Speeding up Adiabatic Quantum State Transfer by Using Dressed States." In: *Phys. Rev. Lett.* 116 (23 2016), p. 230503. DOI: 10.1103/PhysRevLett.116.230503.

[11] R. Barends et al. "Superconducting quantum circuits at the surface code threshold for fault tolerance." In: *Nature* 508.7497 (2014), pp. 500–503. DOI: 10.1038/nature13171.

[12] R. Barends et al. "Digital quantum simulation of fermionic models with a superconducting circuit." In: *Nature Communications* 6.1 (2015), p. 7654. DOI: 10.1038/ncomms8654.

[13] M. G. Bason, M. Viteau, N. Malossi, P. Huillery, E. Arimondo, D. Ciampini, R. Fazio, V. Giovannetti, R. Mannella, and O. Morsch. "High-fidelity quantum driving." In: *Nature Phys.* 8.147 (2012). DOI: 10.1038/nphys2170.

[14] M. V. Berry. "Quantal phase factors accompanying adiabatic changes." In: *Proceedings of the Royal Society of London. A. Mathematical and Physical Sciences* 392.1802 (1984), pp. 45–57. DOI: 10.1098/rspa.1984.0023.

[15] M. V. Berry. "Transitionless quantum driving." In: *J. Phys. A* 42.36 (2009), p. 365303. DOI: 10.1088/1751-8113/42/36/365303.

[16] A. Blais, R.-S. Huang, A. Wallraff, S. M. Girvin, and R. J. Schoelkopf. "Cavity quantum electrodynamics for superconducting electrical circuits: An architecture for quantum computation." In: *Phys. Rev. A* 69 (6 2004), p. 062320. DOI: 10.1103/PhysRevA.69.062320.

[17] A. Blais, J. Gambetta, A. Wallraff, D. I. Schuster, S. M. Girvin, M. H. Devoret, and R. J. Schoelkopf. "Quantum-information processing with circuit quantum electrodynamics." In: *Phys. Rev. A* 75 (3 2007), p. 032329. DOI: 10.1103/PhysRevA.75.032329.

[18] S. Blanes, F. Casas, J. A. Oteo, and J. Ros. "The Magnus expansion and some of its applications." In: *Physics Reports* 470.5 (2009), pp. 151 –238. DOI: 10.1016/j.physrep.2008.11.001.

[19] P. Bocchieri and A. Loinger. "Quantum Recurrence Theorem." In: *Phys. Rev.* 107 (2 1957), pp. 337–338. DOI: 10.1103/PhysRev.107.337.

[20] S. Boixo, T. Albash, F. M. Spedalieri, N. Chancellor, and D. A. Lidar. "Experimental signature of programmable quantum annealing." In: *Nature Communications* 4.May (2012), pp. 1–8. DOI: 10.1038/ncomms3067.

[21] M. Born and V. Fock. "Beweis des Adiabatensatzes." German. In: *Zeitschrift für Physik* 51.3-4 (1928), pp. 165–180. DOI: 10.1007/BF01343193.

[22] H.-P. Breuer and F. Petruccione. *The Theory of Open Quantum Systems*. Oxford: Oxford University Press, 2007, p. 656. DOI: 10.1093/acprof:oso/9780199213900.001.0001.

[23] A. Brinkmann. "Introduction to average Hamiltonian theory. I. Basics." In: *Concepts in Magnetic Resonance Part A* 45A.6 (2016), e21414. DOI: 10.1002/cmr.a.21414.

[24] E. Brion, L. H. Pedersen, and K. Mølmer. "Adiabatic elimination in a lambda system." In: *Journal of Physics A: Mathematical and Theoretical* 40.5 (2007), pp. 1033–1043. DOI: 10.1088/1751-8113/40/5/011.

[25] M. Bukov, L. D'Alessio, and A. Polkovnikov. "Universal high-frequency behavior of periodically driven systems: from dynamical stabilization to Floquet engineering." In: *Advances in Physics* 64.2 (2015), pp. 139–226. DOI: 10.1080/00018732.2015.1055918.

[26] M. Bukov, D. Sels, and A. Polkovnikov. "Geometric Speed Limit of Accessible Many-Body State Preparation." In: *Phys. Rev. X* 9 (1 2019), p. 011034. DOI: 10.1103/PhysRevX.9.011034.

[27] A. del Campo. "Shortcuts to Adiabaticity by Counterdiabatic Driving." In: *Phys. Rev. Lett.* 111 (10 2013), p. 100502. DOI: 10.1103/PhysRevLett.111.100502.

[28] A. del Campo, J. Goold, and M. Paternostro. "More bang for your buck: Super-adiabatic quantum engines." In: *Scientific Reports* 4 (2014), p. 6208. DOI: 10.1038/srep06208.

[29] A. del Campo and K. Kim. "Focus on Shortcuts to Adiabaticity." In: *New Journal of Physics* 21.5 (2019), p. 050201. DOI: 10.1088/1367-2630/ab1437.

[30] A. del Campo, M. M. Rams, and W. H. Zurek. "Assisted Finite-Rate Adiabatic Passage Across a Quantum Critical Point: Exact Solution for the Quantum Ising Model." In: *Phys. Rev. Lett.* 109 (11 2012), p. 115703. DOI: 10.1103/PhysRevLett.109.115703.

[31] A. del Campo and K. Sengupta. "Controlling quantum critical dynamics of isolated systems." In: *The European Physical Journal Special Topics* 224.1 (2015), pp. 189–203. DOI: 10.1140/epjst/e2015-02350-4.

[32] A. del Campo, A. Chenu, S. Deng, and H. Wu. "Friction-Free Quantum Machines." In: *Thermodynamics in the Quantum Regime: Fundamental Aspects and New Directions*. Ed. by F. Binder, L. A. Correa, C. Gogolin, J. Anders, and G. Adesso. Cham: Springer International Publishing, 2018, pp. 127–148. DOI: 10.1007/978-3-319-99046-0_5.

[33] Xi Chen and J. G. Muga. "Engineering of fast population transfer in three-level systems." In: *Phys. Rev. A* 86 (3 2012), p. 033405. DOI: 10.1103/PhysRevA.86.033405.

[34] Xi Chen, I. Lizuain, A. Ruschhaupt, D. Guéry-Odelin, and J. G. Muga. "Shortcut to Adiabatic Passage in Two- and Three-Level Atoms." In: *Phys. Rev. Lett.* 105 (12 2010), p. 123003. DOI: 10.1103/PhysRevLett.105.123003.

[35] Yu Chen et al. "Digitized adiabatic quantum computing with a superconducting circuit." In: *Nature* 534.7606 (2016), pp. 222–226. DOI: 10.1038/nature17658.

[36] D. Ciampini and E. Arimondo. Private communication.

[37] P. W. Claeys, M. Pandey, D. Sels, and A. Polkovnikov. "Floquet-Engineering Counterdiabatic Protocols in Quantum Many-Body Systems." In: *Phys. Rev. Lett.* 123 (9 2019), p. 090602. DOI: 10.1103/PhysRevLett.123.090602.

[38] E. Cohen, H. Larocque, F. Bouchard, F. Nejadsattari, Y. Gefen, and E. Karimi. "Geometric phase from Aharonov-Bohm to Pancharatnam-Berry and beyond." In: *Nature Rev. Phys.* 1 (2019), pp. 437–449. DOI: 10.1038/s42254-019-0071-1.

[39] D. Collison et al. "Magnetic and Optical Studies on an S = 6 Ground-State Cluster [Cr12O9(OH)3(O2CCMe3)15]: Determination of, and the Relationship Between, Single-Ion and Cluster Spin Hamiltonian Parameters." In: *Inorg. Chem.* 42.17 (2003), pp. 5293–5303. DOI: 10.1021/ic034541b.

[40] T. Cubel, B. K. Teo, V. S. Malinovsky, J. R. Guest, A. Reinhard, B. Knuffman, P. R. Berman, and G. Raithel. "Coherent population transfer of ground-state atoms into Rydberg states." In: *Phys. Rev. A* 72.2 (2005), p. 023405. DOI: 10.1109/QELS.2005.1548834.

[41] D. D'Alessandro. *Introduction to Quantum Control and Dynamics*. Chapman & Hall/CRC Applied Mathematics & Nonlinear Science. CRC Press, 2007.

[42] B. Damski. "The Simplest Quantum Model Supporting the Kibble-Zurek Mechanism of Topological Defect Production: Landau-Zener Transitions from a New Perspective." In: *Phys. Rev. Lett.* 95 (3 2005), p. 035701. DOI: 10.1103/PhysRevLett.95.035701.

[43] B. Damski and W. H. Zurek. "Adiabatic-impulse approximation for avoided level crossings: From phase-transition dynamics to Landau-Zener evolutions and back again." In: *Phys. Rev. A* 73 (6 2006), p. 063405. DOI: 10.1103/PhysRevA.73.063405.

[44] J. P. Davis and P. Pechukas. "Nonadiabatic transitions induced by a time-dependent Hamiltonian in the semiclassical/adiabatic limit: The two-state case." In: *The Journal of Chemical Physics* 64.8 (1976), pp. 3129–3137. DOI: 10.1063/1.432648.

[45] S. Deffner and S. Campbell. "Quantum speed limits: from Heisenberg uncertainty principle to optimal quantum control." In: *Journal of Physics A: Mathematical and Theoretical* 50.45 (2017), p. 453001. DOI: 10.1088/1751-8121/aa86c6.

[46] S. Deffner, C. Jarzynski, and A. del Campo. "Classical and Quantum Shortcuts to Adiabaticity for Scale-Invariant Driving." In: *Phys. Rev. X* 4 (2 2014), p. 021013. DOI: 10.1103/PhysRevX.4.021013.

[47] C. L. Degen, F. Reinhard, and P. Cappellaro. "Quantum sensing." In: *Rev. Mod. Phys.* 89 (3 2017), p. 035002. DOI: 10.1103/RevModPhys.89.035002.

[48] M. Demirplak and S. A. Rice. "Adiabatic Population Transfer with Control Fields." In: *J. Phys. Chem. A* 107.46 (2003), pp. 9937–9945. DOI: 10.1021/jp030708a.

[49] M. Demirplak and S. A. Rice. "Assisted Adiabatic Passage Revisited." In: *J. Phys. Chem. B* 109.14 (2005), pp. 6838–6844. DOI: 10.1021/jp040647w.

[50] M. Demirplak and S. A. Rice. "On the consistency, extremal, and global properties of counterdiabatic fields." In: *J. Chem. Phys.* 129.15 (2008), p. 154111. DOI: 10.1063/1.2992152.

[51] M. H. Devoret and R. J. Schoelkopf. "Superconducting Circuits for Quantum Information: An Outlook." In: *Science* 339.6124 (2013), pp. 1169–1174. DOI: 10.1126/science.1231930.

[52] L. DiCarlo et al. "Demonstration of two-qubit algorithms with a superconducting quantum processor." In: *Nature* 460.7252 (2009), pp. 240–244. DOI: 10.1038/nature08121.

[53] L. DiCarlo, M. D. Reed, L. Sun, B. R. Johnson, J. M. Chow, J. M. Gambetta, L. Frunzio, S. M. Girvin, M. H. Devoret, and R. J. Schoelkopf. "Preparation and measurement of three-qubit entanglement in a superconducting circuit." In: *Nature* 467.7315 (2010), pp. 574–578. DOI: 10.1038/nature09416.

[54] G. Dirr and U. Helmke. "Lie Theory for Quantum Control." In: *GAMM-Mitteilungen* 31.1 (2008), pp. 59–93. DOI: 10.1002/gamm.200890003.

[55] B. Dive, A. Pitchford, F. Mintert, and D. Burgarth. "In situ upgrade of quantum simulators to universal computers." In: *Quantum* 2 (2018), p. 80. DOI: 10.22331/q-2018-08-08-80.

[56] M. W. Doherty, N. B. Manson, P. Delaney, F. Jelezko, J. Wrachtrup, and Lloyd C.L. Hollenberg. "The nitrogen-vacancy colour centre in diamond." In: *Phys. Rep.* 528.1 (2013), pp. 1 –45. DOI: https://doi.org/10.1016/j.physrep.2013.02.001.

[57] D. Dong and I. R. Petersen. "Quantum control theory and applications: a survey." In: *IET Control Theory and Applications* 4 (12 2009), pp. 2651 –2671. DOI: 10.1049/iet-cta.2009.0508.

[58] Y.-X. Du, Z.-T Liang, Y.-C. Li, Q.-X. Yue X.-X.and Lv, W. Huang, X. Chen, H. Yan, and S.-L. Zhu. "Experimental realization of stimulated Raman shortcut-to-adiabatic passage with cold atoms." In: *Nature Comm.* 7 (5 2016), p. 12479. DOI: 10.1038/ncomms12479.

[59] C. W. Duncan and A. del Campo. "Shortcuts to adiabaticity assisted by counterdiabatic Born–Oppenheimer dynamics." In: *New Journal of Physics* 20.8 (2018), p. 085003. DOI: 10.1088/1367-2630/aad437.

[60] A. M. Dykhne. "Adiabatic Perturbation of Discrete Spectrum States." In: *Sov. Phys. JETP* 14.4 (1962), p. 941.

[61] A. Eckardt and E. Anisimovas. "High-frequency approximation for periodically driven quantum systems from a Floquet-space perspective." In: *New Journal of Physics* 17.9 (2015), p. 093039. DOI: 10.1088/1367-2630/17/9/093039.

[62] J. M. Fink, M. Göppl, M. Baur, R. Bianchetti, P. J. Leek, A. Blais, and A. Wallraff. "Climbing the Jaynes-Cummings ladder and observing its nonlinearity in a cavity QED system." In: *Nature* 454.7202 (2008), pp. 315–318. DOI: 10.1038/nature07112.

[63] M. Fleischhauer, R. Unanyan, B. W. Shore, and K. Bergmann. "Coherent population transfer beyond the adiabatic limit: Generalized matched pulses and higher-order trapping states." In: *Phys. Rev. A* 59 (5 1999), pp. 3751–3760. DOI: 10.1103/PhysRevA.59.3751.

[64] G. Dirr and U. Helmke and I. Kurniawan and T. Schulte-Herbrüggen. "Lie-semigroup structures for reachability and control of open quantum systems: kossakowski-lindblad generators form lie wedge to markovian channels." In: *Reports on Mathematical Physics* 64.1 (2009), pp. 93 –121. DOI: https://doi.org/10.1016/S0034-4877(09)90022-2.

[65] J. M. Gambetta, A. A. Houck, and A. Blais. "Superconducting Qubit with Purcell Protection and Tunable Coupling." In: *Phys. Rev. Lett.* 106 (3 2011), p. 030502. DOI: 10.1103/PhysRevLett.106.030502.

[66] L. M. Garrido and F. J. Sancho. "Degree of approximate validity of the adiabatic invariance in quantum mechanics." In: *Physica* 28.6 (1962), pp. 553 –560. DOI: https://doi.org/10.1016/0031-8914(62)90109-X.

[67] D. Gatteschi, R. Sessoli, and J. Villain. *Molecular Nanomagnets*. Oxford University Press, New York, 2007, 2007.

[68] U. Gaubatz, P. Rudecki, M. Becker, S. Schiemann, M. Külz, and K. Bergmann. "Population switching between vibrational levels in molecular beams." In: *Chemical Physics Letters* 149.5 (1988), pp. 463 –468. DOI: https://doi.org/10.1016/0009-2614(88)80364-6.

[69] U. Gaubatz, P. Rudecki, S. Schiemann, and K. Bergmann. "Population transfer between molecular vibrational levels by stimulated Raman scattering with partially overlapping laser fields. A new concept and experimental results." In: *The Journal of Chemical Physics* 92.9 (1990), pp. 5363–5376. DOI: 10.1063/1.458514.

[70] M. G. Genoni, A. Serafini, M. S. Kim, and D. Burgarth. "Dynamical Recurrence and the Quantum Control of Coupled Oscillators." In: *Phys. Rev. Lett.* 108 (15 2012), p. 150501. DOI: 10.1103/PhysRevLett.108.150501.

[71] I. M. Georgescu, S. Ashhab, and F. Nori. "Quantum simulation." In: *Rev. Mod. Phys.* 86 (1 2014), pp. 153–185. DOI: 10.1103/RevModPhys.86.153.

[72] L. Giannelli and E. Arimondo. "Three-level superadiabatic quantum driving." In: *Phys. Rev. A* 89 (3 2014), p. 033419. DOI: 10.1103/PhysRevA.89.033419.

[73] S. J. Glaser et al. "Training Schrödinger's cat: quantum optimal control." In: *The European Physical Journal D* 69.12 (2015), p. 279. DOI: 10.1140/epjd/e2015-60464-1.

[74] N. Goldman and J. Dalibard. "Periodically Driven Quantum Systems: Effective Hamiltonians and Engineered Gauge Fields." In: *Phys. Rev. X* 4 (3 2014), p. 031027. DOI: 10.1103/PhysRevX.4.031027.

[75] X. Gu, A. F. Kockum, A. Miranowicz, Y. Liu, and F. Nori. "Microwave photonics with superconducting quantum circuits." In: *Physics Reports* 718-719 (2017), pp. 1 –102. DOI: https://doi.org/10.1016/j.physrep.2017.10.002.

[76] D. Guéry-Odelin, A. Ruschhaupt, A. Kiely, E. Torrontegui, S. Martínez-Garaot, and J. G. Muga. "Shortcuts to adiabaticity: Concepts, methods, and applications." In: *Rev. Mod. Phys.* 91 (4 2019), p. 045001. DOI: 10.1103/RevModPhys.91.045001.

[77] M. Heyl, P. Hauke, and P. Zoller. "Quantum localization bounds Trotter errors in digital quantum simulation." In: *Science Advances* 5.4 (2019). DOI: 10.1126/sciadv.aau8342.

[78] G. Higgins, F. Pokorny, C. Zhang, Q. Bodart, and M. Hennrich. "Coherent Control of a Single Trapped Rydberg Ion." In: *Phys. Rev. Lett.* 119 (22 2017), p. 220501. DOI: 10.1103/PhysRevLett.119.220501.

[79] E. T. Holland, K. A. Wendt, K. Kravvaris, X. Wu, E. Ormand, J. L. DuBois, S. Quaglioni, and F. Pederiva. "Optimal Control for the Quantum Simulation of Nuclear Dynamics." In: *arXiv:1908.08222v1* (2019).

[80] G. M. Huang, T. J. Tarn, and J. W. Clark. "On the controllability of quantum-mechanical systems." In: *Journal of Mathematical Physics* 24.11 (1983), pp. 2608–2618. DOI: 10.1063/1.525634.

[81] J.-T. Hwang and P. Pechukas. "The adiabatic theorem in the complex plane and the semiclassical calculation of nonadiabatic transition amplitudes." In: *The Journal of Chemical Physics* 67.10 (1977), pp. 4640–4653. DOI: 10.1063/1.434630.

[82] S. Ibáñez, Xi Chen, E. Torrontegui, J. G. Muga, and A. Ruschhaupt. "Multiple Schrödinger Pictures and Dynamics in Shortcuts to Adiabaticity." In: *Phys. Rev. Lett.* 109 (10 2012), p. 100403. DOI: 10.1103/PhysRevLett.109.100403.

[83] F. Impens and D. Guéry-Odelin. "Fast quantum control in dissipative systems using dissipationless solutions." In: *Scientific Reports* 9 (2019), p. 4048. DOI: 10.1038/s41598-019-39731-z.

[84] C. Jarzynski. "Generating shortcuts to adiabaticity in quantum and classical dynamics." In: *Phys. Rev. A* 88 (4 2013), p. 040101. DOI: 10.1103/PhysRevA.88.040101.

[85] J. Jing, M. S. Sarandy, D. A. Lidar, D.-W. Luo, and L.-Ao Wu. "Eigenstate tracking in open quantum systems." In: *Phys. Rev. A* 94 (4 2016), p. 042131. DOI: 10.1103/PhysRevA.94.042131.

[86] V. Jurdjevic and H. J. Sussmann. "Control systems on Lie groups." In: *Journal of Differential Equations* 12.2 (1972), pp. 313 –329. DOI: 10.1016/0022-0396(72)90035-6.

[87] S. Kehrein. *The Flow Equation Approach to Many-Particle Systems*. Springer-Verlag, Berlin, Heidelberg, 2006. DOI: 10.1007/3-540-34068-8.

[88] N. Khaneja and S. J. Glaser. "Cartan decomposition of SU(2n) and control of spin systems." In: *Chemical Physics* 267.1 (2001), pp. 11 –23. DOI: 10.1016/S0301-0104(01)00318-4.

[89] G. C. Knee and W. J. Munro. "Optimal Trotterization in universal quantum simulators under faulty control." In: *Phys. Rev. A* 91 (5 2015), p. 052327. DOI: 10.1103/PhysRevA.91.052327.

[90] C. P. Koch. "Controlling open quantum systems: tools, achievements, and limitations." In: *Journal of Physics: Condensed Matter* 28.21 (2016), p. 213001. DOI: 10.1088/0953-8984/28/21/213001.

[91] J. Koch, T. M. Yu, J. Gambetta, A. A. Houck, D. I. Schuster, J. Majer, A. Blais, M. H. Devoret, S. M. Girvin, and R. J. Schoelkopf. "Charge-insensitive qubit design derived from the Cooper pair box." In: *Phys. Rev. A* 76 (4 2007), p. 042319. DOI: 10.1103/PhysRevA.76.042319.

[92] C Kokail et al. "Self-verifying variational quantum simulation of lattice models." In: *Nature* 569.7756 (2019), pp. 355–360. DOI: 10.1038/s41586-019-1177-4.

[93] J. Kölbl, A. Barfuss, M. S. Kasperczyk, L. Thiel, A. A. Clerk, H. Ribeiro, and P. Maletinsky. "Initialization of Single Spin Dressed States using Shortcuts to Adiabaticity." In: *Phys. Rev. Lett.* 122 (9 2019), p. 090502. DOI: 10.1103/PhysRevLett.122.090502.

[94] M. Kolodrubetz, D. Sels, P. Mehta, and A. Polkovnikov. "Geometry and non-adiabatic response in quantum and classical systems." In: *Physics Reports* 697 (2017), pp. 1 –87. DOI: 10.1016/j.physrep.2017.07.001.

[95] H. J. Korsch, A. Klumpp, and D. Witthaut. "On two-dimensional Bessel functions." In: *Journal of Physics A: Mathematical and General* 39.48 (2006), pp. 14947–14964. DOI: 10.1088/0305-4470/39/48/008.

[96] J. R. Kuklinski, U. Gaubatz, F. T. Hioe, and K. Bergmann. "Adiabatic population transfer in a three-level system driven by delayed laser pulses." In: *Phys. Rev. A* 40 (11 1989), pp. 6741–6744. DOI: 10.1103/PhysRevA.40.6741.

[97] O. Kyriienko and A. S. Sørensen. "Floquet Quantum Simulation with Superconducting Qubits." In: *Phys. Rev. Applied* 9 (6 2018), p. 064029. DOI: 10.1103/PhysRevApplied.9.064029.

[98] X. Lacour, N. Sangouard, S. Guérin, and H. R. Jauslin. "Arbitrary state controlled-unitary gate by adiabatic passage." In: *Phys. Rev. A* 73 (4 2006), p. 042321. DOI: 10.1103/PhysRevA.73.042321.

[99] X. Lacour, S. Guérin, N. V. Vitanov, L. P. Yatsenko, and H. R. Jauslin. "Implementation of single-qubit quantum gates by adiabatic passage and static laser phases." In: *Opt. Comm.* 264.2 (2006), pp. 362 –367. DOI: https://doi.org/10.1016/j.optcom.2006.01.059.

[100] T. A. Laine and S. Stenholm. "Adiabatic processes in three-level systems." In: *Phys. Rev. A* 53 (4 1996), pp. 2501–2512. DOI: 10.1103/PhysRevA.53.2501.

[101] L. D. Landau. In: *Phys. Z. Sowjetunion* 2.46 (1932).

[102] N. K. Langford, R. Sagastizabal, M. Kounalakis, C. Dickel, A. Bruno, F. Luthi, D. J. Thoen, A. Endo, and L. DiCarlo. "Experimentally simulating the dynamics of quantum light and matter at deep-strong coupling." In: *Nature Communications* 8.1 (2017), p. 1715. DOI: 10.1038/s41467-017-01061-x.

[103] A. Le Cunuder, I. A. Martínez, A. Petrosyan, D. Guéry-Odelin, E. Trizac, and S. Ciliberto. "Fast equilibrium switch of a micro mechanical oscillator." In: *Applied Physics Letters* 109.11 (2016), p. 113502. DOI: 10.1063/1.4962825.

[104] M. Li, X. Tan, K. Dai, P. Zhao, H. Yu, and Y. Yu. "Demonstration of superadiabatic population transfer in superconducting qubit." In: *Chinese Physics B* 27.6 (2018), p. 063202. DOI: 10.1088/1674-1056/27/6/063202.

[105] D. A. Lidar, A. T. Rezakhani, and A. Hamma. "Adiabatic approximation with exponential accuracy for many-body systems and quantum computation." In: *Journal of Mathematical Physics* 50.10 (2009), p. 102106. DOI: 10.1063/1.3236685.

[106] G. H. Low and I. L. Chuang. "Optimal Hamiltonian Simulation by Quantum Signal Processing." In: *Phys. Rev. Lett.* 118 (1 2017), p. 010501. DOI: 10.1103/PhysRevLett.118.010501.

[107] G. H. Low, T. J. Yoder, and I. L. Chuang. "Methodology of Resonant Equiangular Composite Quantum Gates." In: *Phys. Rev. X* 6 (4 2016), p. 041067. DOI: 10.1103/PhysRevX.6.041067.

[108] M. Maamache and Y. Saadi. "Adiabatic Theorem and Generalized Geometrical Phase in the Case of Continuous Spectra." In: *Phys. Rev. Lett.* 101 (15 2008), p. 150407. DOI: 10.1103/PhysRevLett.101.150407.

[109] W. Magnus. "On the exponential solution of differential equations for a linear operator." In: *Communications on Pure and Applied Mathematics* 7.4 (1954), pp. 649–673. DOI: 10.1002/cpa.3160070404.

[110] J. Majer et al. "Coupling superconducting qubits via a cavity bus." In: *Nature* 449.7161 (2007), pp. 443–447. DOI: 10.1038/nature06184.

[111] E. Majorana. "Atomi orientati in campo magnetico variabile." In: *Nuovo Cimento* 9.2 (1932), pp. 43–50. DOI: 10.1007/BF02960953.

[112] L. Mandel and E. Wolf. *Optical Coherence and Quantum Optics*. Cambridge University Press, 1995. DOI: 10.1017/CBO9781139644105.

[113] S. Martínez-Garaot, E. Torrontegui, Xi Chen, and J. G. Muga. "Shortcuts to adiabaticity in three-level systems using Lie transforms." In: *Phys. Rev. A* 89 (5 2014), p. 053408. DOI: 10.1103/PhysRevA.89.053408.

[114] I. A. Martínez, A. Petrosyan, D. Guéry-Odelin, E. Trizac, and S. Ciliberto. "Engineered swift equilibration of a Brownian particle." In: *Nature Physics* 12 (2016), p. 843. DOI: 10.1038/nphys3758.

[115] J. M. Martinis and M. R. Geller. "Fast adiabatic qubit gates using only σ_z control." In: *Phys. Rev. A* 90 (2 2014), p. 022307. DOI: 10.1103/PhysRevA.90.022307.

[116] A. Messiah. *Quantum Mechanics*. Dover Publications, New York, 1961.

[117] T. Mikami, S. Kitamura, K. Yasuda, N. Tsuji, T. Oka, and H. Aoki. "Brillouin-Wigner theory for high-frequency expansion in periodically driven systems: Application to Floquet topological insulators." In: *Phys. Rev. B* 93 (14 2016), p. 144307. DOI: 10.1103/PhysRevB.93.144307.

[118] J. G. Muga, Xi Chen, S. Ibáñez, I. Lizuain, and A. Ruschhaupt. "Transitionless quantum drivings for the harmonic oscillator." In: *Journal of Physics B: Atomic, Molecular and Optical Physics* 43.8 (2010), p. 085509. DOI: 10.1088/0953-4075/43/8/085509.

[119] *NIST Digital Library of Mathematical Functions*. http://dlmf.nist.gov/, Release 1.0.23 of 2019-06-15. F. W. J. Olver, A. B. Olde Daalhuis, D. W. Lozier, B. I. Schneider, R. F. Boisvert, C. W. Clark, B. R. Miller and B. V. Saunders, eds.

[120] M. Nakahara. *Geometry, topology and physics*. 2003.

[121] Y. Nakamura, C. D. Chen, and J. S. Tsai. "Spectroscopy of Energy-Level Splitting between Two Macroscopic Quantum States of Charge Coherently Superposed by Josephson Coupling." In: *Phys. Rev. Lett.* 79 (12 1997), pp. 2328–2331. DOI: 10.1103/PhysRevLett.79.2328.

[122] M. A. Nielsen and I. L. Chuang. *Quantum Computation and Quantum Information*. Cambridge University Press, 2010. DOI: 10.1017/CBO9780511976667.

[123] F. Petiziol and S. Wimberger. "Effect of Phase Errors on a Quantum Control Protocol Using Fast Oscillations." In: *Condens. Matter* 4 (2019), p. 34. DOI: 10.3390/condmat4010034.

[124] F. Petiziol, B. Dive, F. Mintert, and S. Wimberger. "Fast adiabatic evolution by oscillating initial Hamiltonians." In: *Phys. Rev. A* 98 (4 2018), p. 043436. DOI: 10.1103/PhysRevA.98.043436.

[125] F. Petiziol, B. Dive, S. Carretta, R. Mannella, F. Mintert, and S. Wimberger. "Accelerating adiabatic protocols for entangling two qubits in circuit QED." In: *Phys. Rev. A* 99 (4 2019), p. 042315. DOI: 10.1103/PhysRevA.99.042315.

[126] F. Petiziol, E. Arimondo, L. Giannelli, F. Mintert, and S. Wimberger. "Optimal three-level state transfers based on modulated optical excitations." In: *submitted to Sci. Rep. (17-09-2019)* (2019).

[127] A. Polkovnikov. "Universal adiabatic dynamics in the vicinity of a quantum critical point." In: *Phys. Rev. B* 72 (16 2005), p. 161201. DOI: 10.1103/PhysRevB.72.161201.

[128] J. Preskill. "Quantum Computing in the NISQ era and beyond." In: *Quantum* 2 (2018), p. 79. DOI: 10.22331/q-2018-08-06-79.

[129] R. R. Puri. *Mathematical Methods in Quantum Optics*. Springer-Verlag Berlin Heidelberg, 2007, 2001. DOI: 10.1007/978-3-540-44953-9.

[130] C. M. Quintana, K. D. Petersson, L. W. McFaul, S. J. Srinivasan, A. A. Houck, and J. R. Petta. "Cavity-Mediated Entanglement Generation Via Landau-Zener Interferometry." In: *Phys. Rev. Lett.* 110 (17 2013), p. 173603. DOI: 10.1103/PhysRevLett.110.173603.

[131] M. D. Reed, L. DiCarlo, S. E. Nigg, L. Sun, L. Frunzio, S. M. Girvin, and R. J. Schoelkopf. "Realization of three-qubit quantum error correction with superconducting circuits." In: *Nature* 482.7385 (2012), pp. 382–385. DOI: 10.1038/nature10786.

[132] A. T. Rezakhani, A. K. Pimachev, and D. A. Lidar. "Accuracy versus run time in an adiabatic quantum search." In: *Phys. Rev. A* 82 (5 2010), p. 052305. DOI: 10.1103/PhysRevA.82.052305.

[133] A. T. Rezakhani, W.-J. Kuo, A. Hamma, D. A. Lidar, and P. Zanardi. "Quantum Adiabatic Brachistochrone." In: *Phys. Rev. Lett.* 103 (8 2009), p. 080502. DOI: 10.1103/PhysRevLett.103.080502.

[134] J. Roland and N. J. Cerf. "Quantum search by local adiabatic evolution." In: *Phys. Rev. A* 65 (4 2002), p. 042308. DOI: 10.1103/PhysRevA.65.042308.

[135] B. Rousseaux, S. Guérin, and N. V. Vitanov. "Arbitrary qudit gates by adiabatic passage." In: *Phys. Rev. A* 87 (3 2013), p. 032328. DOI: 10.1103/PhysRevA.87.032328.

[136] Saberi, H. and Opatrný, T. and Mølmer, K. and del Campo, A. "Adiabatic tracking of quantum many-body dynamics." In: *Phys. Rev. A* 90 (6 2014), p. 060301. DOI: 10.1103/PhysRevA.90.060301.

[137] J. J. Sakurai and J. Napolitano. *Modern Quantum Mechanics*. 2nd ed. Cambridge University Press, 2017. DOI: 10.1017/9781108499996.

[138] M. S. Sarandy and D. A. Lidar. "Adiabatic approximation in open quantum systems." In: *Phys. Rev. A* 71 (1 2005), p. 012331. DOI: 10.1103/PhysRevA.71.012331.

[139] J. F. Schaff, X. L. Song, Capuzzi P., Vignolo P., and G. Labeyrie. "Shortcut to adiabaticity for an interacting Bose-Einstein condensate." In: *Europhysics Letters* 93.2 (2011), p. 23001. DOI: 10.1209/0295-5075/93/23001.

[140] S. G. Schirmer, H. Fu, and A. I. Solomon. "Complete controllability of quantum systems." In: *Phys. Rev. A* 63 (6 2001), p. 063410. DOI: 10.1103/PhysRevA.63.063410.

[141] R. J. Schoelkopf and S. M. Girvin. "Wiring up quantum systems." In: *Nature* 451.7179 (2008), pp. 664–669. DOI: 10.1038/451664a.

[142] C. Schweizer, F. Grusdt, M. Berngruber, L. Barbiero, E. Demler, N. Goldman, I. Bloch, and M. Aidelsburger. "Floquet approach to $\mathbb{Z}_2$ lattice gauge theories with ultracold atoms in optical lattices." In: *Nature Phys.* (2019). DOI: 10.1038//s41567-019-0649-7.

[143] D. Sels and A. Polkovnikov. "Minimizing irreversible losses in quantum systems by local counterdiabatic driving." In: *Proceedings of the National Academy of Sciences* 114.20 (2017), E3909–E3916. DOI: 10.1073/pnas.1619826114.

[144] K. Sengupta, D. Sen, and S. Mondal. "Exact Results for Quench Dynamics and Defect Production in a Two-Dimensional Model." In: *Phys. Rev. Lett.* 100 (7 2008), p. 077204. DOI: 10.1103/PhysRevLett.100.077204.

[145] S. N. Shevchenko, S. Ashhab, and F. Nori. "Landau-Zener-Stückelberg interferometry." In: *Physics Reports* 492.1 (2010), pp. 1 –30. DOI: 10.1016/j.physrep.2010.03.002.

[146] S. J. Srinivasan, A. J. Hoffman, J. M. Gambetta, and A. A. Houck. "Tunable Coupling in Circuit Quantum Electrodynamics Using a Superconducting Charge Qubit with a *V*-Shaped Energy Level Diagram." In: *Phys. Rev. Lett.* 106 (8 2011), p. 083601. DOI: 10.1103/PhysRevLett.106.083601.

[147] L. Steffen, Y. Salathe, M. Oppliger, P. Kurpiers, M. Baur, C. Lang, C. Eichler, G. Puebla-Hellmann, A. Fedorov, and A. Wallraff. "Deterministic quantum teleportation with feed-forward in a solid state system." In: *Nature* 500.7462 (2013), pp. 319–322. DOI: 10.1038/nature12422.

[148] E. C. G. Stückelberg. "Theory of Inelastic Collisions between Atom." In: *Helv. Phys. Acta* 5.369-423 (1932).

[149] D. Tannor. *Introduction to Quantum Mechanics: A Time-Dependent Perspective*. University Science Books, Sausalito, 2007.

[150] M. Theisen, F. Petiziol, S. Carretta, P. Santini, and S. Wimberger. "Superadiabatic driving of a three-level quantum system." In: *Phys. Rev. A* 96 (1 2017), p. 013431. DOI: 10.1103/PhysRevA.96.013431.

[151] G. Torlai et al. "Integrating Neural Networks with a Quantum Simulator for State Reconstruction." In: *arXiv:1904.08441v2* (2019). DOI: https://arxiv.org/abs/1904.08441.

[152] E. Torrontegui, S. Ibáñez, S. Martínez-Garaot, M. Modugno, A. del Campo, D. Guéry-Odelin, A. Ruschhaupt, Xi Chen, and J. G. Muga. "Shortcuts to Adiabaticity." In: *Adv. At., Mol. Opt. Phys.* 62 (2013), pp. 117 –169. DOI: 10.1016/B978-0-12-408090-4.00002-5.

[153] M. Troyer and U.-J. Wiese. "Computational Complexity and Fundamental Limitations to Fermionic Quantum Monte Carlo Simulations." In: *Phys. Rev. Lett.* 94 (17 2005), p. 170201. DOI: 10.1103/PhysRevLett.94.170201.

[154] R. G. Unanyan, L. P. Yatsenko, K. Bergmann, and B. W. Shore. "Laser-induced adiabatic atomic reorientation with control of diabatic losses." In: *Optics Communications* 139.1 (1997), pp. 48 –54. DOI: https://doi.org/10.1016/S0030-4018(97)00099-0.

[155] G. Vacanti, R. Fazio, S. Montangero, G. M. Palma, M. Paternostro, and V. Vedral. "Transitionless quantum driving in open quantum systems." In: *New Journal of Physics* 16.5 (2014), p. 053017. DOI: 10.1088/1367-2630/16/5/053017.

[156] A. Vepsäläinen, S. Danilin, and G. S. Paraoanu. "Optimal superadiabatic population transfer and gates by dynamical phase corrections." In: *Quantum Science and Technology* 3.2 (2018), p. 024006. DOI: 10.1088/2058-9565/aaa640.

[157] A. Vepsäläinen, S. Danilin, and G. S. Paraoanu. "Superadiabatic population transfer in a three-level superconducting circuit." In: *Science Advances* 5.2 (2019). DOI: 10.1126/sciadv.aau5999.

[158] A. Verdeny. "Optimally driven quantum systems." In: *Physics PhD theses*. Imperial College London (UK), 2016.

[159] A. Verdeny, A. Mielke, and F. Mintert. "Accurate Effective Hamiltonians via Unitary Flow in Floquet Space." In: *Phys. Rev. Lett.* 111 (17 2013), p. 175301. DOI: 10.1103/PhysRevLett.111.175301.

[160] A. Verdeny, Ł. Rudnicki, C. A. Müller, and F. Mintert. "Optimal Control of Effective Hamiltonians." In: *Phys. Rev. Lett.* 113 (1 2014), p. 010501. DOI: 10.1103/PhysRevLett.113.010501.

[161] N. V. Vitanov. "Transition times in the Landau-Zener model." In: *Phys. Rev. A* 59 (2 1999), pp. 988–994. DOI: 10.1103/PhysRevA.59.988.

[162] N. V. Vitanov and B. M. Garraway. "Landau-Zener model: Effects of finite coupling duration." In: *Phys. Rev. A* 53 (6 1996), pp. 4288–4304. DOI: 10.1103/PhysRevA.53.4288.

[163] N. V. Vitanov, K.-A. Suominen, and B. W. Shore. "Creation of coherent atomic superpositions by fractional stimulated Raman adiabatic passage." In: *Journal of Physics B: Atomic, Molecular and Optical Physics* 32.18 (1999), pp. 4535–4546. DOI: 10.1088/0953-4075/32/18/312.

[164] N. V. Vitanov, M. Fleischhauer, B. W. Shore, and K. Bergmann. "Coherent manipulation of atoms and molecules by sequential laser pulses." In: *Advances in Atomic Molecular and Optical Physics* 46 (2001), pp. 55–190. DOI: 10.1016/S1049-250X(01)80063-X.

[165] N. V. Vitanov, A. A. Rangelov, B. W. Shore, and K. Bergmann. "Stimulated Raman adiabatic passage in physics, chemistry, and beyond." In: *Rev. Mod. Phys.* 89 (1 2017), p. 015006. DOI: 10.1103/RevModPhys.89.015006.

[166] M. Vogl, P. Laurell, A. D. Barr, and G. A. Fiete. "Flow Equation Approach to Periodically Driven Quantum Systems." In: *Phys. Rev. X* 9 (2 2019), p. 021037. DOI: 10.1103/PhysRevX.9.021037.

[167] A. Wallraff, D. I. Schuster, A. Blais, L. Frunzio, J. Majer, M. H. Devoret, S. M. Girvin, and R. J. Schoelkopf. "Approaching Unit Visibility for Control of a Superconducting Qubit with Dispersive Readout." In: *Phys. Rev. Lett.* 95 (6 2005), p. 060501. DOI: 10.1103/PhysRevLett.95.060501.

[168] D. F. Walls and G. J. Milburn. *Quantum Optics*. Springer-Verlag, Berlin, Germany, 2008.

[169] T. Wang et al. "The experimental realization of high-fidelity 'shortcut-to-adiabaticity' quantum gates in a superconducting Xmon qubit." In: *New Journal of Physics* 20.6 (2018), p. 065003. DOI: 10.1088/1367-2630/aac9e7.

[170] F. J. Wegner. "Flow equations for Hamiltonians." In: *Nuclear Physics B - Proceedings Supplements* 90 (2000), pp. 141 –146. DOI: https://doi.org/10.1016/S0920-5632(00)00911-7.

[171] F. Wegner. "Flow-equations for Hamiltonians." In: *Annalen der Physik* 506.2 (1994), pp. 77–91. DOI: 10.1002/andp.19945060203.

[172] G. Wendin. "Quantum information processing with superconducting circuits: a review." In: *Reports on Progress in Physics* 80.10 (2017), p. 106001. DOI: 10.1088/1361-6633/aa7e1a.

[173] R.-B. Wu, H. Ding, D. Dong, and X. Wang. "Learning robust and high-precision quantum controls." In: *Phys. Rev. A* 99 (4 2019), p. 042327. DOI: 10.1103/PhysRevA.99.042327.

[174] K. Xu, T. Xie, F. Shi, Z.-Y. Wang, X. Xu, P. Wang, Y. Wang, M. B. Plenio, and J. Du. "Breaking the quantum adiabatic speed limit by jumping along geodesics." In: *Science Advances* 5.6 (2019), eaax3800. DOI: 10.1126/sciadv.aax3800.

[175] P. Zanardi and M. Rasetti. "Holonomic quantum computation." In: *Physics Letters A* 264.2 (1999), pp. 94 –99. DOI: 10.1016/S0375-9601(99)00803-8.

[176] C. Zener. "Non-Adiabatic Crossing of Energy Levels." In: *Proc. R. Soc. A* 137.833 (1932), pp. 696–702. DOI: 10.1098/rspa.1932.0165.

[177] J. Zhang et al. "Experimental Implementation of Assisted Quantum Adiabatic Passage in a Single Spin." In: *Phys. Rev. Lett.* 110 (24 2013), p. 240501. DOI: 10.1103/PhysRevLett.110.240501.

[178] B.B. Zhou, A. Baksic, H. Ribeiro, C.G. Yale, F.J. Heremans, P.C. Jerger, A. Auer, G. Burkard, A.A. Clerk, and D.D. Awschalom. "Accelerated quantum control using superadiabatic dynamics in a solid-state lambda system." In: *Nature Physics* 13 (2017), p. 330. DOI: 10.1038/nphys3967.

[179] L. Zhou, S.-T. Wang, S. Choi, H. Pichler, and M. D. Lukin. "Quantum Approximate Optimization Algorithm: Performance, Mechanism, and Implementation on Near-Term Devices." In: *arXiv:1812.01041* (2018). DOI: arXiv:1812.01041v1.